

SIMPLE AND COMPLEX MODELS FOR NONLINEAR SEISMIC RESPONSE
OF REINFORCED CONCRETE STRUCTURES

by

Mehdi Saiidi

and

Mete A. Sozen

A Report to the
NATIONAL SCIENCE FOUNDATION
Research Grant PFR-78-16318

Any opinions, findings, conclusions
or recommendations expressed in this
publication are those of the author(s)
and do not necessarily reflect the views
of the National Science Foundation.

University of Illinois
at Urbana-Champaign
Urbana, Illinois
August, 1979



ACKNOWLEDGMENT

The study presented in this report was part of a continuing experimental and analytical study of the earthquake response of reinforced concrete structures, conducted at the Civil Engineering Department of the University of Illinois, Urbana. The research was sponsored by the National Science Foundation under grant PFR-78-16318.

The writers are indebted to the panel of consultants for their advice and criticism. Members of the panel were M.H. Eligator of Weiskopf and Pickworth, A.E. Fiorato of the Portland Cement Association, W.D. Holmes of Rutherford and Chekene, R.G. Johnston of Brandow and Johnston, J. Lefter of Veterans Administration, W.P. Moore, Jr. of Walter P. Moore and Associates, and A. Walser of Sargent and Lundy Engineers.

Special thanks are due to D.P. Abrams and H. Cecen, former research assistants, and J.P. Moehle, research assistant at the University of Illinois, for providing the writers with the results of their experimental studies and for their criticism of the computed results.

Mrs. Sara Cheely, Mrs. Laura Goode, Mrs. Patricia Lane, and Miss Mary Prus are thanked for typing this report.

The IBM-360/75 and CYBER 175 computing systems of the Digital Computer Laboratories of the University of Illinois were used for the development and testing of the analytical models.

This report was based on a doctoral dissertation by M. Saïidi directed by M.A. Sozen.

TABLE OF CONTENTS

CHAPTER		Page
1	INTRODUCTION	1
	1.1 Object and Scope	1
	1.2 Review of Previous Research	2
	1.3 Notation	5
2	ANALYTICAL MODEL	9
	2.1 Introductory Remarks	9
	2.2 Assumptions about Structures and Base Motions	9
	2.3 Force-Deformation Relationship	11
	2.4 Element Stiffness Matrix	16
	2.5 Structural Stiffness Matrix	18
	2.6 Mass Matrix	19
	2.7 Damping Matrix	20
	2.8 Unbalanced Forces	20
	2.9 Gravity Effect	21
	2.10 Differential Equation of Motion	22
	2.11 Solution Technique	23
3	HYSTERESIS MODELS	25
	3.1 Introductory Remarks	25
	3.2 General Comments	25
	3.3 Takeda Hysteresis Model	26
	3.4 Sina Hysteresis Model	27
	3.5 Otani Hysteresis Model	29
	3.6 Simple Bilinear Model	30
	3.7 Q-Hyst Model	30
4	TEST STRUCTURES AND ANALYTICAL STUDY USING MDOF MODEL	32
	4.1 Introductory Remarks	32
	4.2 Test Structures	32
	4.3 Dynamic Tests	33
	4.4 Analytical Procedure	33
	4.5 Analytical Study	35
5	COMPARISON OF MEASURED RESPONSE WITH RESULTS CALCULATED USING THE MDOF MODEL	37
	5.1 Introductory Remarks	37
	5.2 Calculated Response of MF2	37
	5.3 Calculated Response of MF1	38
	5.4 Concluding Remarks	42

	Page
6	DEVELOPMENT OF THE Q-MODEL 44
	6.1 Introductory Remarks 44
	6.2 General Comments 44
	6.3 Q-Model 45
7	ANALYTICAL STUDY USING THE Q-MODEL 50
	7.1 Introductory Remarks 50
	7.2 Structures and Motions 51
	7.3 Equivalent System 52
	7.4 Analytical Results for Different Structures 54
	7.5 Analytical Results for Different Base Motions 56
	7.6 Analytical Results for Repeated Motions 59
8	SUMMARY AND CONCLUSIONS 62
	8.1 Summary 62
	8.2 Observations 64
	8.3 Conclusions 65
	LIST OF REFERENCES 68
	APPENDIX
A	HYSTERESIS MODELS 158
	A.1 General 158
	A.2 Definitions 158
	A.3 Sina Model 158
	A.4 Q-Hyst Model 161
B	COMPUTER PROGRAMS LARZ AND PLARZ 165
C	MAXIMUM ELEMENT RESPONSE BASED ON DIFFERENT HYSTERESIS MODELS 171
D	COMPUTER PROGRAMS LARZAK AND PLARZK 178
E	MOMENTS AND DUCTILITIES FOR STRUCTURE MF1 SUBJECTED TO DIFFERENT EARTHQUAKES 180
F	RESPONSE TO TAFT AND EL CENTRO RECORDS 184

LIST OF TABLES

Table	Page
4.1 LONGITUDINAL REINFORCING SCHEDULES FOR MF1 AND MF2	72
4.2 ASSUMED MATERIAL PROPERTIES FOR MF1 AND MF2	73
4.3 COLUMN AXIAL FORCES DUE TO DEAD LOAD	74
4.4 CALCULATED STIFFNESS PROPERTIES OF CONSTITUENT ELEMENTS OF STRUCTURES MF1 AND MF2	75
4.5 CRACK-CLOSING MOMENTS USED FOR SINA HYSTERESIS MODEL	77
4.6 MEASURED AND CALCULATED MAXIMUM RESPONSE OF MF2 RUN 1	78
4.7 MEASURED AND CALCULATED MAXIMUM RESPONSE OF MF1 USING DIFFERENT HYSTERESIS SYSTEMS	79
7.1 COLUMN AXIAL FORCES FOR STRUCTURES H1, FW1, AND FW2	81
7.2 CALCULATED STIFFNESS PROPERTIES OF CONSTITUENT ELEMENTS OF STRUCTURE H1	82
7.3 CALCULATED STIFFNESS PROPERTIES OF CONSTITUENT ELEMENTS OF STRUCTURE FW1	83
7.4 CALCULATED STIFFNESS PROPERTIES OF CONSTITUENT ELEMENTS OF STRUCTURE FW2	84
7.5 CALCULATED PARAMETERS FOR DIFFERENT STRUCTURES	85
7.6 ASSUMED DEFORMED SHAPES FOR DIFFERENT STRUCTURES	86
7.7 MAXIMUM ABSOLUTE VALUES OF RESPONSE	87
7.8 MAXIMUM RESPONSE OF STRUCTURE MF1 SUBJECTED TO DIFFERENT EARTHQUAKES	89
7.9 MAXIMUM TOP-LEVEL DISPLACEMENTS FOR STRUCTURE MF1 SUBJECTED TO REPEATED MOTIONS	90
7.10 WIRE GAGE CROSS-SECTIONAL PROPERTIES	90
C.1 MAXIMUM RESPONSE OF STRUCTURE MF1 BASED ON TAKEDA MODEL . . .	173
C.2 MAXIMUM RESPONSE OF STRUCTURE MF1 BASED ON SINA MODEL . . .	174
C.3 MAXIMUM RESPONSE OF STRUCTURE MF1 BASED ON OTANI MODEL . . .	175
C.4 MAXIMUM RESPONSE OF STRUCTURE MF1 BASED ON BILINEAR MODEL .	176

Table		Page	Deleted see
C.5	MAXIMUM RESPONSE OF STRUCTURE MF1 BASED ON Q-HYST MODEL . .	177	page 172.a
E.1	MAXIMUM RESPONSE OF STRUCTURE MF1 SUBJECTED TO ORION	181	Deleted
E.2	MAXIMUM RESPONSE OF STRUCTURE MF1 SUBJECTED TO CASTAIC . . .	182	page 180.a
E.3	MAXIMUM RESPONSE OF STRUCTURE MF1 SUBJECTED TO BUCAREST . .	183	

LIST OF FIGURES

Figure	Page
2.1 Idealized Stress-Strain Curve for Concrete	91
2.2 Idealized Stress-Strain Curve for Steel	91
2.3 Idealized Moment-Curvature Diagram for a Member	92
2.4 Moment and Rotation along a Member	92
2.5 Moment-Rotation Diagram for a Member	93
2.6 Rotation due to Bond Slip	93
2.7 Deformed Shape of a Beam Member	94
2.8 Equilibrium of a Rigid-End Portion	94
2.9 Deformed Shape of a Column Member	94
2.10 Biased Curve in Relation to the Specified Force-Deformation Diagram	95
2.11 Treatment of Residual Forces in the Analysis	95
2.12 Equivalent Lateral Load to Account for Gravity Effect . . .	96
3.1 Takeda Hysteresis Model	97
3.2 Small Amplitude Loop in Takeda Model	98
3.3 Comparison of Average Stiffness with and without Pinching for Small Amplitudes	98
3.4 Sina Hysteresis Model	99
3.5 Otani Hysteresis Model	100
3.6 Simple Bilinear Hysteresis System	100
3.7 Q-Hyst Model	101
4.1 Reinforcement Detail and Dimensions of Structures MF1 and MF2	102
4.2 Test Setup for Structure MF1	103
4.3 Measured and Calculated Response for MF2	104
4.4 Measured and Calculated Response for MF1 Using Takeda Hys- teresis Model	107

Figure	Page
4.5 Measured and Calculated Response for MF1 Using Sina Hysteresis Model	110
4.6 Measured and Calculated Response for MF1 Using Otani Hysteresis Model	113
4.7 Measured and Calculated Response for MF1 Using Bilinear Hysteresis Model	116
4.8 Measured and Calculated Response for MF1 Using Q-Hyst Model	119
5.1 Maximum Calculated and Measured Displacements (Single Amplitude) for MF2	122
5.2 Maximum Calculated and Measured Relative Story Displacements for MF2	122
5.3 Maximum Calculated and Measured Displacements (Single Amplitude) for MF1	123
5.4 Maximum Displacements Normalized with Respect to Top Level Displacement	124
5.5 Maximum Calculated (Using Takeda Model) and Measured Relative Story Displacements	125
5.6 Maximum Calculated (Using Sina Model) and Measured Relative Story Displacements	126
5.7 Maximum Calculated (Using Otani Model) and Measured Relative Story Displacements	126
5.8 Maximum Calculated (Using Bilinear Model) and Measured Relative Story Displacements	127
5.9 Maximum Calculated (Using Q-Hyst Model) and Measured Relative Story Displacements	127
6.1 The Q-Model	128
6.2 Static Lateral Loads	129
6.3 Force-Displacement Relationships	130
7.1 Longitudinal Reinforcement Distribution for Structures H1 and H2	131
7.2 Longitudinal Reinforcement Distribution for Structures FW1 and FW2	132
7.3 Normalized Moment-Displacement Diagrams	134

Figure	Page
7.4 Calculated (Solid Line) and Measured (Broken Line) Response for Structure H1	135
7.5 Calculated (Solid Line) and Measured (Broken Line) Response for Structure H2	136
7.6 Calculated (Solid Line) and Measured (Broken Line) Response for Structure MF1	137
7.7 Calculated (Solid Line) and Measured (Broken Line) Response for Structure MF2	138
7.8 Calculated (Solid Line) and Measured (Broken Line) Response for Structure FW1	139
7.9 Calculated (Solid Line) and Measured (Broken Line) Response for Structure FW2	140
7.10 Calculated (Solid Line) and Measured (Broken Line) Response for Structure FW3	141
7.11 Calculated (Solid Line) and Measured (Broken Line) Response for Structure FW4	142
7.12 Maximum Response of Structure H1	143
7.13 Maximum Response of Structure H2	143
7.14 Maximum Response of Structure MF1	144
7.15 Maximum Response of Structure MF2	144
7.16 Maximum Response of Structure FW1	145
7.17 Maximum Response of Structure FW2	145
7.18 Maximum Response of Structure FW3	146
7.19 Maximum Response of Structure FW4	146
7.20 Q-Model (Solid Line) and MDOF Model (Broken Line) Results for Orion Earthquake	147
7.21 Q-Model (Solid Line) and MDOF Model (Broken Line) Results for Castaic Earthquake	148
7.22 Q-Model (Solid Line) and MDOF Model (Broken Line) Results for Bucarest Earthquake	149
7.23 Q-Model (with Increased Frequency; Solid Line) and MDOF Model (Broken Line) Results for Bucarest Earthquake	150

Figure	Page
7.24 Maximum Response for Orion Earthquake	151
7.25 Maximum Response for Castaic Earthquake	151
7.26 Maximum Response for Bucarest Earthquake	152
7.27 Repeated Earthquakes with 0.2g Maximum Acceleration	153
7.28 Repeated Earthquakes with 0.4g Maximum Acceleration	154
7.29 Repeated Earthquakes with 0.8g Maximum Acceleration	155
7.30 Repeated Earthquakes with 1.2g Maximum Acceleration	156
7.31 Repeated Earthquakes with 1.6g Maximum Acceleration	157
A.1 Sina Hysteresis Rules	163
A.2 Q-Hyst Model	164
B.1 Structure with Missing Elements	167
B.2 Block Diagram of Program LARZ	168
B.3 Storage of Structural Stiffness Matrix	169
a&b	
B.3c Storage of Submatrix K_{22}	170
C.1 Element Numbering for Structure MF1	172
D.1 Block Diagram of Program LARZAK	179
F.1 Response for Structure MF1 Subjected to E1 Centro NS	185
F.2 Response for Structure MF1 Subjected to E1 Centro EW	186
F.3 Response for Structure MF1 Subjected to Taft N21E	187
F.4 Response for Structure MF1 Subjected to Taft S69E	188

CHAPTER 1

INTRODUCTION

1.1 Object and Scope

The primary objective of the work reported was to study the possibilities of simplifying the nonlinear analysis of reinforced concrete structures subjected to severe earthquake motions. The study included two distinct parts. One was a microscopic study of one of the particular elements of the analysis, the hysteresis model, and development of simple models leading to acceptable results. The other was a macroscopic study which included the development of a simple model that, with relatively small effort, resulted in a reasonably close estimate of nonlinear response.

The first part was a continuation of the investigation initiated by Otani (26). For this part, a multi-degree nonlinear model (LARZ) was developed to analyze rectangular reinforced concrete frames for given base acceleration records. A special feature of LARZ was that it was capable of accepting a collection of hysteresis systems, some previously used and others developed in the course of the present investigation. The new systems were generally simpler. Chapters Two through Five describe part one of the study.

In the second part, a given structure was viewed as a single-degree-of-freedom system which recognized stiffness changes due to the nonlinearity of material. The model is introduced and examined in Chapters Six and Seven, respectively.

In both parts of this study, to evaluate the reliability of the analytical models, the calculated responses were compared with the

results of dynamic experiments on a group of small-scale ten-story reinforced concrete frames and frame-walls tested on the University of Illinois Earthquake Simulator.

1.2 Review of Previous Research

Several investigators have studied the nonlinear modeling of structures subjected to earthquake motions. The development of high speed digital computers and the availability of numerical techniques have had a substantial contribution to the ease of carrying such studies.

A comprehensive survey of earlier investigations in the area of nonlinear analysis of plane frames is provided by Otani (26). Here, a brief history of more recent studies will be cited in two sections:

a. Complex Models

In a complex model, there is a one-to-one correspondence between the elements of an actual structure and the idealized system. The choice of idealizing assumptions to represent structural members is a crucial one in terms of computational effort and ease of formulating stiffness variations. Giberson studied the possibility of using a one-component element model with two concentrated flexural springs at the ends, and compared the results with the calculated response using a two-component element model (13). The inelastic deformation of a member was assigned to member ends in the former model. It was found that the one-component element was a more efficient model and it resulted in better stiffness characteristics.

Due to relative simplicity, the one-component model attracted considerable attention. Suko and Adams used this model to study a multistory steel frame (33). To determine the location of the inflection

point of each member, a preliminary analysis had to be done. Then the points were assumed to remain stationary for the entire analysis.

Otani used the one-component model to analyze reinforced concrete frames subjected to base accelerations (26). The point of contraflexure for each member was assumed to be fixed at the mid-length of that element. The analytical results were compared with the results of tests on small-scale specimens. The one-component model was also used by Umemura et al (38), Takayanagi and Schnobrich (35), and Emori and Schnobrich (11).

The force-deformation function assigned to a member can have a significant influence on the calculated response. The more dominant the inelastic deformations are, the more sensitive is the response to the hysteresis model used. Therefore, as the research in nonlinear analysis was continued, more attention was paid to the stiffness variation of members. The trend was toward the establishment of more realistic hysteresis functions.

Through several experimental works on reinforced concrete beam-to-column connections, it was realized that the behavior of a reinforced concrete member under cyclic loading is relatively complicated, and that it is not accurate to represent such behavior by a simple bilinear hysteresis function. Clough and Johnston introduced and applied a degrading model which considered reduction of stiffness at load-reversals stages (9).

Takeda examined the experimental results from cyclic loading of a series of reinforced concrete connections, and proposed a hysteresis model which was in agreement with the test results (36). This model, known as the "Takeda Model," was capable of handling different possibilities of unloading and loading at different stages. To accomplish

this task, the model was expectedly complicated. Several investigators have used the "Takeda Model" in its original or modified form, and have concluded that the model represents well the behavior of a reinforced concrete connection in a frame subjected to ground motions (11,26,35).

The Takeda model did not include the "pinching effects" which are observed in many experimental results (18). Takayanagi and Schnobrich considered the pinching action in developing a modified version of Takeda model (35). Later, Emori and Schnobrich used a cubic function to include bar slip effects (11). In both models, the rules for the first quarter of loading were the same with those of Takeda model.

Other more involved systems were constructed by superposing a set of springs with different yield levels. In such systems, the hysteresis function for an individual spring is a simple relationship, however, because each spring yields at a different moment, the overall stiffness of a member changes continuously. Pique examined the multispring model to determine its influence on the calculated response (30).

Anderson and Townsend conducted a study on nonlinear analysis of a ten-story frame using four different hysteresis systems. The models included bilinear and trilinear hysteresis systems (3).

b. Simple Models

Despite the development of sophisticated and efficient digital computers, complex nonlinear models for seismic analysis of structures are involved and costly. Therefore, they impose a limit on the number of alternative configurations and/or ground motions which may be desirable to study, before the final design of a structure is made. As a result, several studies have been aimed at finding less complicated nonlinear models.

Among the earlier work was shear beam representation of structures. The stiffness of each story was assigned to a shear spring which included nonlinear deformations. Aziz used a shear-beam model in the study of ten-story frames, and compared the results with those obtained from complex models (6). It was found that the maxima were in reasonable agreement. A modified shear-beam model was introduced by Aoyama for reinforced concrete structures (4). Tansirikongkol and Pecknold used a bilinear shear model for approximate modal analysis of structures (37).

Pique developed an equivalent single-degree-of-freedom model assuming that structures deform according to their first mode shapes (30). Three different structures with different number of stories were analyzed, and the maxima were compared with the results of the shear-beam and complex models. Reasonable agreement was observed between the maximum response obtained from the single-degree system on one hand, and the maxima obtained from shear-beam and complex models on the other hand.

1.3 Notation

The symbols used in this report are defined where they first appear. A list of symbols are given below for convenient reference.

A_s = area of steel

$[C]$ = damping matrix

D_{max} = maximum deformation attained in loading direction

$D(y)$ = yield deformation

d_b = diameter of the tensile and compressive reinforcement

$d-d'$ = distance between tensile and compressive bars

E = modulus of elasticity

E_s = modulus of elasticity of steel

- e = steel elongation
 F_r = external force at level r
 F_t = total external force
 f = flexibility of rotational spring
 f_c = stress of concrete
 f'_c = measured compressive strength of concrete
 f_s = steel stress
 f_{sy} = yield stress for steel
 g = gravity acceleration
 h_r = height at level r
 I = moment of inertia
 j = number of levels in the original system
 K = stiffness of the original system
 $[K]$ = instantaneous stiffness matrix
 L_{eq} = equivalent height
 l = total length of a member
 l' = length of elastic portion of a member
 l_a = anchorage length
 $[M]$ = mass matrix
 M_c = cracking moment
 M_e = equivalent mass
 M_n = mass at n th degree of freedom
 M_r = mass at level r
 M_t = total mass of the original system
 M_u = ultimate moment
 M_y = yield moment

- ΔM = moment increment at member end
 $\Delta M'$ = moment increment at end of the elastic portion
 P_i = total vertical load at level i
 Q = restoring force
 S'_{cy} = slope of the line connecting yield point to cracking point
 in the opposite direction
 S_γ = slope of unloading for post-yielding segment
 T = time
 Δt = time interval for numerical integration
 u = average bond stress
 V_i = shear force due to gravity load at level i
 X_{max} = maximum residual deformation previously attained
 $\{X\}$ = displacement vector
 \ddot{X}_g = ground acceleration
 $\{\Delta X\}, \{\Delta \dot{X}\}, \{\Delta \ddot{X}\}$ = incremental relative displacement, velocity, and acceleration
 vectors, respectively
 x = distance from the point of contraflexure
 x, \dot{x}, \ddot{x} = relative lateral displacement, velocity, and acceleration
 of the equivalent mass with respect to the ground
 $\ddot{\Delta Y}_g$ = incremental base acceleration vector
 Z = slope of stress-strain curve at $\epsilon_c > \epsilon_0$
 β = constant of the Newmark's β method
 $\Delta \delta$ = incremental lateral displacement
 ϵ_c = strain of concrete
 ϵ_0 = strain at $f'_c = f'_c$
 ϵ_u = ultimate strain of concrete
 θ = rotation due to flexure
 θ' = rotation due to bond slip
 $\Delta \theta$ = incremental rotation at end of the elastic portion

θ_c = rotation at cracking

θ_u = ultimate rotation

θ_y = rotation at yielding

λ = ratio of the length at rigid end to the length of elastic portion

ξ_i = damping factor for i th mode

ϕ = curvature

ϕ_c = cracking curvature

ϕ_r = assumed displacement at level r , normalized with respect to the top level displacement

ϕ_y = yield curvature

$\Delta\phi$ = incremental rotation with respect to vertical axis

ω = circular frequency of single-degree system

ω_i = circular frequency for i th mode

CHAPTER 2

ANALYTICAL MODEL

2.1 Introductory Remarks

An analytical model was developed to study the dynamic response of reinforced concrete frame structures subjected to earthquake motions. Inelastic deformations were considered in the model through hysteresis systems. The model is capable of accepting different hysteresis functions with different levels of complication.

This chapter describes basic principles used for treating the parameters involved in the analysis. It was not the intention of this study to examine different alternative techniques for dealing with such parameters. Therefore, methods were used which have proven to be appropriate and efficient. Similar to several other nonlinear models, this model linearized the problem over a short time step. As a result many assumptions used in an elastic analysis were considered to be valid.

2.2 Assumptions about Structures and Base Motions

Several simplifications were necessary to avoid a complicated and costly solution. Meanwhile, the simplifying assumptions had to assure a relatively realistic representation of the problem. The assumptions were the following:

1. A beam or a column is a massless line element consisting of (a) infinitely rigid portions at ends, (b) a linearly elastic portion in the middle, and (c) two flexural springs connect-

ing the elastic portion to the end portions (Fig. 2.7). The position of each member coincides with its centroidal axis.

2. Axial deformation is neglected in all members. Therefore, at each level, all the joints connected by beams displace equally. Because of this assumption, vertical displacements are not considered in the model.

3. The structure is a plane frame which displaces horizontally in its plane, and rotates about an axis perpendicular to the plane of the structure.

4. Deformations are considered to be sufficiently small to allow the initial configuration of the structure to prevail throughout the analysis.

5. Shear deformations of the members are neglected.

6. Joint cores at beam-to-column connections are infinitely rigid.

7. Stiffness characteristics of the structure remain unchanged over each short time increment.

8. Masses are lumped at locations where the horizontal degrees of freedom are defined. There can be more than one degree of freedom at the same level, if some beams are discontinued.

9. The foundation of the structure is considered infinitely rigid. Columns at the first floor are rigidly connected to this foundation.

10. Gravity effects, usually referred to as "P- Δ effects,"

are taken into account.

11. Base motions occur in the plane of the structure in the horizontal direction.

2.3 Force-Deformation Relationship

Flexural characteristics of structural elements for monotonically increasing loads were calculated based on the measured material properties. To simplify such evaluation it was necessary to make a few idealizations which are explained in the following sections.

a. Stress-Strain Relationships for Concrete and Steel

A function consisting of a parabola and a linear segment, proposed by Hognestad (28), was adopted to idealize stress-strain variation of concrete (Fig. 2.1). The mathematical formulation of the curve is as follows:

$$f_c = f'_c \left[2 \frac{\epsilon_c}{\epsilon_0} - \left(\frac{\epsilon_c}{\epsilon_0} \right)^2 \right] \quad \epsilon_t \leq \epsilon_c \leq \epsilon_0 \quad (2.1)$$

and

$$f_c = f'_c [1 - Z (\epsilon_c - \epsilon_0)] \quad \epsilon_0 < \epsilon_c \quad (2.2)$$

where

f_c = stress of concrete;

f'_c = measured compressive strength of concrete;

ϵ_c = strain of concrete;

ϵ_0 = strain at $f_c = f'_c$;

Z = slope of stress-strain curve at $\epsilon_c > \epsilon_0$.

The idealized stress-strain curve for steel is presented in Fig. 2.2. The curve consists of three segments for linear, plastic, and "strain-hardening" stages.

b. Moment-Curvature Relationship

The primary moment-curvature relationship for an element was idealized as a trilinear curve with two breakpoints at cracking and yielding of the element (Fig. 2.3). Cracking occurs when the tensile stress at the extreme fiber of the concrete under tension is exceeded. Yielding of the section is associated with yielding of the tensile reinforcement.

c. Moment-Rotation Relationship due to Flexure

The idealized primary curve described in Section (b) is used to determine the moment-rotation relationship. Moment was assumed to vary linearly along the member as shown in Fig. 2.4. With the point of contraflexure fixed at the middle of the member, it was possible to specify a relationship between rotation and curvature. This relationship remained invariable during the analysis. The end rotation in terms of curvature is described as follows:

$$\theta = \overline{CD} / \frac{\ell'}{2} = \frac{2}{\ell'} \int_0^{\ell'} [\phi(x)] x dx \quad (2.3)$$

in which

ℓ' = length of elastic portion of a member;

x = distance from the point of contraflexure;

ϕ = curvature

\overline{CD} is in effect the first moment of the area under curvature diagram with respect to the point of contraflexure (Fig. 2.4). Because the variation of the moment along an element is linear and because the skeleton curve was assumed to consist of linear segments, the curvature varies linearly along the element (Fig. 2.4). Hence, the computation is reduced to evaluation of the area moment of a triangular part at the uncracked region of the element and trapezoidal segments in other portions.

Based on the foregoing discussion, the end rotations at cracking, yielding, and ultimate points are calculated as follows:

1. Cracking stage:

$$\theta_c = \frac{l'}{6EI} M_c \quad (2.4)$$

where

EI = elastic flexural stiffness;

M_c = cracking moment.

2. Yielding stage:

$$\theta_y = \frac{l'}{6} [(1-\lambda^3) \phi_y - \lambda^2 \phi_c] \quad (2.5)$$

where

ϕ_c = cracking curvature;

ϕ_y = yield curvature;

$$\lambda = \frac{M_c}{M_y};$$

M_y = yield moment.

3. Ultimate stage:

$$\theta_u = l' \left\{ \left[(2 + \lambda_2)(1 - \lambda_2)(\alpha\lambda_2 + 1 - \lambda_2)/\alpha + \lambda_2(1 + \lambda_2) - 2\lambda_1^3 \right] \frac{\phi_y}{\lambda_2} + 2\lambda_1^2 \phi_c \right\} / 12 \quad (2.6)$$

in which

$$\alpha = \left(\frac{M_u - M_y}{\phi_u - \phi_y} \right) \left(\frac{\phi_y}{M_y} \right)$$

$$\lambda_1 = \frac{M_c}{M_u}$$

$$\lambda_2 = \frac{M_y}{M_u}$$

M_u = ultimate moment

With cracking, yielding, and ultimate breakpoints, the moment rotation curve was idealized into the trilinear curve shown in Fig. 2.5. Because the θ values are proportional to the length of the member, the curve was constructed for only unit length of each member.

d. Rotation Due to Bond Slip

The rotation caused by relative movement between tensile steel and concrete is calculated based on some simplifying assumptions as follows:

1. The anchorage length of the reinforcement is sufficiently long so that no pullout will occur.
2. Steel stress varies linearly from a maximum value at the end of the flexible portion of the beam to zero as shown in Fig. 2.6.
3. The rotation due to bond slip occurs with respect to

the centroid of the compressive reinforcement.

4. The tensile stress in the reinforcement is proportional to the moment.

When the tensile reinforcement is subjected to stress f_s the elongation e can be calculated from (Fig. 2.6)

$$e = \frac{d_b \cdot f_s^2}{8 E_s u} \quad (2.7)$$

in which:

d_b = diameter of the tensile reinforcement;

E_s = modulus of elasticity of steel;

u = average bond stress.

Then the rotation (θ') can be expressed as

$$\theta' = \frac{d_b \cdot f_s^2}{8 E_s u} \times \frac{1}{d-d'} \quad (2.8)$$

where $d-d'$ = distance between tensile and compressive bars.

Assumption (4) can be stated as follows:

$$f_s = f_y \cdot \frac{M}{M_y} \quad (2.9)$$

where f_y = yield stress of steel.

Substituting Eq. 2.9 in Eq. 2.8 will result in a parabolic expression for the rotation in terms of moment:

$$\theta' = \frac{1}{8} \frac{d_b}{E_s u} \times \frac{f_y^2}{d-d'} \left(\frac{M}{M_y} \right)^2 \quad (2.10)$$

From this equation, the rotation due to bond slip is calculated at the breakpoints of the curve in Fig. 2.5, and then, added to

θ_c , θ_y , θ_u values.

2.4 Element Stiffness Matrix

Each element was assumed to consist of (a) an elastic prismatic line member over a length equal to the clear span of the members at the ends, (b) one concentrated rotational spring at each end of the elastic part, and (c) two infinitely rigid parts (Fig. 2.7). The springs were used to account for elastic deformations, and their force-deformation function was governed by a series of hysteresis rules. The rotational spring and the elastic portion of the member behave as two springs in series. The end rotation of the elastic segment at one end is affected by the magnitude of the moment at the other end. However, it was assumed that the rotation in the spring at each end is not influenced by the moment at the other end. As a result the relationship between the incremental end moments and end rotations of a flexible portion of an element, in combination with the flexural springs, can be stated as follows:

$$\begin{Bmatrix} \Delta M'_A \\ \Delta M'_B \end{Bmatrix} = \underbrace{\frac{1}{\left(\frac{l'}{3EI}\right)^2 + (f_A + f_B) \frac{l'}{3EI} + f_A f_B - \left(\frac{l'}{6EI}\right)^2}}_{\text{Stiffness Matrix } [K']} \begin{bmatrix} \frac{l'}{3EI} + f_B & \frac{l'}{6EI} \\ \frac{l'}{6EI} & \frac{l'}{3EI} + f_A \end{bmatrix} \begin{Bmatrix} \Delta \theta_A \\ \Delta \theta_B \end{Bmatrix} \quad (2.11)$$

where

f = flexibility of rotational spring;

$\Delta M'$ = moment increment at end of the elastic portion;

$\Delta \theta$ = incremental rotation at end of the elastic portion.

The stiffness matrix for the entire element, including the rigid end portions, is obtained by appropriate transformation of the stiffness matrix in Eq. 2.11. The transformation matrices were formed by considering the equilibrium of rigid end segments (Fig. 2.8) as

$$\Delta M_A = \Delta M'_A + \lambda_A (\Delta M'_A + \Delta M'_B)$$

or

$$\Delta M_A = (1 + \lambda_A) \Delta M'_A + \lambda_A \Delta M'_B$$

thus

$$\begin{Bmatrix} \Delta M_A \\ \Delta M_B \end{Bmatrix} = \underbrace{\begin{bmatrix} 1 + \lambda_A & \lambda_A \\ \lambda_B & 1 + \lambda_B \end{bmatrix}}_{[E]} \begin{Bmatrix} \Delta M'_A \\ \Delta M'_B \end{Bmatrix} \quad (2.12)$$

where

ΔM = moment increment at member end;

λ = ratio of the length at rigid end to the length of elastic portion

Finally, the element stiffness matrix is formulated in the form

$$[K] = [E]^T [K'] [E] \quad (2.13)$$

which is a 2 by 2 matrix consistent with one rotational degree of freedom at each end. Because no axial deformation is considered for members there are no lateral displacements at beam ends. Therefore, the stiffness matrix in Eq. 2.13 is directly applicable for beams. For columns, however, there are relative

lateral displacements at the ends, consequently the number of degrees of freedom is 2 at each end.

The stiffness matrix for a column can be formulated by inclusion of the effects of lateral displacements. This is accomplished by relating the total rotation and displacement of a column end to the rotation with respect to the axis of the column. The transformation matrix $[T]$ serves the purpose (Fig. 2.9),

$$\begin{Bmatrix} \Delta\theta_A \\ \Delta\theta_B \end{Bmatrix} = [T] \begin{Bmatrix} \Delta\delta_A \\ \Delta\phi_A \\ \Delta\delta_B \\ \Delta\phi_B \end{Bmatrix} \quad (2.14)$$

in which

$$[T] = \begin{bmatrix} -\frac{1}{\ell} & 1 & \frac{1}{\ell} & 0 \\ -\frac{1}{\ell} & 0 & \frac{1}{\ell} & 1 \end{bmatrix} \quad (2.15)$$

where

ℓ = total length of member;

$\Delta\theta$ = incremental rotation at member end with respect to member axis;

$\Delta\phi$ = incremental rotation with respect to vertical axis

$\Delta\delta$ = incremental lateral displacement.

Finally, the column stiffness matrix is expressed in the following form:

$$[K] = [T]^T [K] [T] \quad (2.16)$$

2.5 Structural Stiffness Matrix

By accumulating the contributions of individual element

stiffnesses, the structural stiffness matrix was constructed. First, element indices were developed to relate local degrees of freedom to global. Then, element stiffness matrices were added to the structural stiffness matrix at appropriate locations.

Since axial deformations were neglected, all the joints connected by beams at a level displaced equally in horizontal direction, and introduced one degree of freedom. In addition, each joint between structural elements had one rotational degree of freedom.

The components of the structural stiffness matrix were divided into three categories, and the matrix was partitioned accordingly as described here:

$$\begin{Bmatrix} \Delta P \\ \Delta M \end{Bmatrix} = \begin{bmatrix} K_{11} & K_{12} \\ K_{21} & K_{22} \end{bmatrix} \begin{Bmatrix} \Delta U \\ \Delta \theta \end{Bmatrix} \quad (2.17)$$

Then the structural stiffness matrix was condensed to relate lateral forces to horizontal displacements as

$$\{\Delta P\} = [K]^* \{\Delta U\} \quad (2.18)$$

where $[K]^* = [K_{11}] - [K_{12}] [K_{22}]^{-1} [K_{21}]$ (2.19)

2.6 Mass Matrix

The mass at any level of the structure was considered to be concentrated at that level. As a result, the mass matrix of the system is a diagonal matrix.

$$[M] = \begin{bmatrix} M_1 & & & \\ & M_2 & & \\ & & \ddots & \\ & & & 0 \\ 0 & & & & \ddots & \\ & & & & & & M_n \end{bmatrix} \quad (2.20)$$

No rotational inertia was considered for the masses.

2.7 Damping Matrix

Damping forces were assumed to be proportional to the instantaneous velocities of the points where the degrees of freedom were defined. The damping matrix was considered at structural level, and it was constructed by linear combination of the mass and structural stiffness matrix.

$$[C] = \alpha[M] + \beta[K] \quad (2.21)$$

α and β can be obtained from the following equations:

$$\xi_1 = \frac{1}{2\omega_1} (\alpha + \beta\omega_1^2) \quad (2.22)$$

$$\xi_2 = \frac{1}{2\omega_2} (\alpha + \beta\omega_2^2)$$

in which ξ_1 and ξ_2 = damping factors for the first two modes

It can be seen in Eq. 2.22 that when the damping matrix is proportional only to the mass matrix ($\beta=0$), the damping factor is small for higher frequencies of vibration. On the other hand, if the damping is proportional only to the stiffness matrix ($\alpha=0$), the damping factor is large for higher frequencies. Therefore, the contribution of the higher modes to the response will be less significant.

2.8 Unbalanced Forces

In a structure subjected to motions causing nonlinear deformations the stiffness characteristics change continuously. However, this cannot be reflected directly in a model which uses constant stiffness during a time step. As a result, at the end of each time step there may be residual forces at member ends. If these residual forces are not eliminated, the analysis will converge to erroneous response (Fig. 2.10).

A force-deformation curve, consisting of linear segments, will result in unbalanced forces only at break points; thus, the problem of residual forces is less significant for this case. Nevertheless, the accumulation of these forces will introduce errors in the calculated results.

In the present study, at the end of each time interval the forces were corrected (if necessary), and the new stiffnesses were used for the next time interval (Fig. 2.11). Since the damping matrix is a function of stiffness, there are also unbalanced forces due to change in the damping. But these forces were considered negligible compared with the inaccuracies which existed in the calculated damping forces.

2.9 Gravity Effect

Generally, the inclusion of gravity effect (often known as "P- Δ effect") in the analysis results in softening of the structural model. There have been many reports on the influence of gravity effect on the calculated seismic response. Goel found the effect insignificant when he studied a multistory frame in nonlinear range (14). However, Jennings and Husid in their study of a single-degree-of-freedom system concluded that the P- Δ effect was substantial (16). In the present study, the effect of gravity loads is taken into account.

The resulting additional moment caused by P- Δ effect can be replaced by a restoring force Q at the story level i. The shear force due to the gravity load is (Fig. 2.12):

$$V_i = P_i (X_i - X_{i-1})/h_i \quad (2.23)$$

and for the level $i+1$

$$V_{i+1} = P_{i+1} (X_{i+1} - X_i)/h_{i+1} \quad (2.24)$$

in which P_i is the total vertical load on the column at level i ; and h_i is the height of story i . The net restoring force Q is:

$$Q_i = V_i - V_{i+1} \quad (2.25)$$

It can be seen that, at each level i , Q_i is a function of displacements at level i and the two adjacent levels. Therefore, a banded matrix $[K_p]$ with the band width equal to 3, can be formulated to relate the restoring forces to the story displacements $\{X\}$.

$$\{Q\} = [K_p] \{X\} \quad (2.26)$$

$[K_p]$ can be considered as a stiffness matrix which when subtracted from the structural stiffness matrix, reproduces the softening effect caused by the gravity loads.

2.10 Differential Equation of Motion

By considering the equilibrium of all the forces, the equation of motion can be formulated in an incremental form for a short time step,

$$[M] \{\ddot{\Delta X}\} + [C] \{\dot{\Delta X}\} + [K] \{\Delta X\} = -[M] \{\ddot{\Delta Y}_g\} \quad (2.27)$$

in which

$[M]$ = mass matrix;

$\{\Delta X\}$ = incremental relative acceleration vector;

$[C]$ = instantaneous damping matrix;

$\{\dot{\Delta X}\}$ = incremental relative velocity vector;

- [K] = instantaneous stiffness matrix;
 $\{\Delta X\}$ = incremental relative displacement vector;
 $\{\Delta Y_g\}$ = incremental base acceleration vector.

2.11 Solution Technique

Several explicit and implicit methods are available for integration of the equation of motion. Newmark's β method (23) is one of the most efficient algorithms, and has been widely used for both linear and nonlinear problems. This method was adopted for this analysis.

The value of β was taken equal to 0.25 which corresponds to constant acceleration over the solution time interval. For linear problems $\beta = 0.25$ results in unconditionally stable solutions. However, in a nonlinear problem, the method is unstable if large time steps are used in the analysis (2).

The incremental velocities and displacements over a short time step are calculated from:

$$\Delta \dot{X} = \ddot{X}_n \Delta t + \Delta \ddot{X} \frac{\Delta t}{2} \quad (2.28)$$

$$\Delta X = \dot{X}_n \Delta t + \frac{1}{2} \ddot{X} (\Delta t)^2 + \frac{1}{4} \Delta \ddot{X} (\Delta t)^2 \quad (2.29)$$

From Eq. 2.27 the incremental relative accelerations can be formed

$$\Delta \ddot{X} = \frac{6\Delta X}{(\Delta t)^2} - \frac{6}{\Delta t} \dot{X}_n - 3\ddot{X}_n \quad (2.30)$$

After substituting this equation in Eq. 2.25, $\Delta \dot{X}$ will be in the form:

$$\Delta \dot{X} = \frac{2}{\Delta t} \dot{X}_n - 2\ddot{X}_n \quad (2.31)$$

Substitution of Eqs. 2.28 and 2.29 in the differential equation of motion will result in Eq. 2.32 for relative displacement vector:

$$\{\Delta X\} = [A]^{-1} \{B\} \quad (2.32)$$

in which
$$[A] = \left[\frac{4}{\Delta t^2} [M] + \frac{2}{\Delta t} [C] + [K] \right]$$

and

$$\{B\} = [M] \left\{ \frac{4}{\Delta t} \{X_n^{\dot{\cdot}}\} + 2 \{X_n^{\ddot{\cdot}}\} - \{\Delta \ddot{Y}\} \right\} + 2 [C] \{X_n^{\dot{\cdot}}\}$$

With the values of incremental displacements the incremental velocities and acceleration were calculated from Eq. 2.30. Then, the total values were obtained.

CHAPTER 3

HYSTERESIS MODELS

3.1 Introductory Remarks

In this chapter, general considerations related to hysteresis models are first stated followed by specific explanations about models which had been used before or were developed in the course of this study. Five hysteresis models were used. Two of them have been described in detail elsewhere (25,36). The other three models, which are relatively simpler, are documented in this chapter and in Appendix A.

In the sections on individual hysteresis systems, the degree of complexity as well as the performance of the models for high- and low-amplitude deformations are described. The primary curve in all cases is assumed to be symmetric with respect to the origin.

3.2 General Comments

Since the nonlinear analysis of reinforced concrete structures under cyclic (or dynamic) loading started, special attention was needed to be given to the hysteretic behavior of the members. When experimental results on the cyclic loadings of the reinforced concrete members and joints became available, it was evident that closed-form mathematical formulas did not allow enough versatility to match the measured behavior. Therefore, multisegment hysteresis models consisting of linear portions were developed which could reproduce the experimental results. In this group was the Takeda model (36), which in several cases has proven to lead to satisfactory results. This model is one of the alternative hysteresis systems which can be used by the analytical model developed in this report.

The Takeda model does not include the "pinching" effects (tendency for very low incremental stiffness near the origin followed by a stiffening) which are often observed in the experimental results. And yet, the model is complicated. Therefore, it seemed worthwhile to develop and examine a simpler model which considers the pinching effect. This new model was named "Sina."

Other less complicated hysteresis systems have been used by different investigators. Otani (25) modified the Takeda model to use in conjunction with the original model. Although this model was applied to account for bond slip, it can be regarded as a complete hysteresis system.

Another model, which has been used widely, is a simple bilinear relationship. The analytical model was equipped with the facility to use a bilinear hysteresis.

For unloading and load reversal stages, the bilinear hysteresis system results in incremental stiffness values which are considerably in excess of the corresponding measured values. To obtain closer agreement with test results without complicating the hysteresis system, a new bilinear hysteresis model was developed with softened unloading and load reversal branches. This system (Q-Hyst) along with Otani and the simple bilinear model are the three other alternative hysteresis systems considered in the present study.

3.3 Takeda Hysteresis Model

Based on various experimental results, the Takeda model consists of 16 rules operating on a trilinear primary curve (Fig. 3.1). The primary curve can include additional deformations caused by bond slip. However, the rules do not cover the pinching effect which can also be caused by slip of the reinforcement.

The rules determine different stiffness characteristics at different stages of cracking, yielding, unloading, and reloading in successive cycles. The fact that the model considers cracking as a break-point, results in some energy dissipation under cyclic loads even at pre-yielding stage. This is realistic and desirable. Many of the rules used in Takeda's system are concerned with developing realistic force-displacement relationships during low-amplitude cycles which are within the bounds of large-amplitude cycles previously reached. For example, the force-displacement wave is specified to proceed from X_3 to R_3 (this action requires a special rule) rather than, say, from X_3 to R_2 (which would not have required a special rule, Fig. 3.2).

As it was previously noted, pinching is not included in the Takeda system. As a result, the model ignores the softening that can occur for beam-to-column connections at low amplitudes. This is illustrated in Fig. 3.3. The Takeda rules are presented in full detail in Reference 25.

3.4 Sina Hysteresis Model

This model was developed to account for the pinching effects while it had a fewer number of rules than the Takeda model. The skeleton curve consists of three parts similar to those used by Takeda. Nine rules define this system. A complete description of the rules is presented in Appendix A.

The initial loading and unloading rules are similar to the Takeda rules 1 through 4. The slope of unloading for post-yielding regions (S_1) is assumed to be:

$$S_1 = S_C \cdot Y \cdot \left(\frac{D(Y)}{D_{\max}} \right)^\alpha \quad (3.1)$$

where

$S_{C,Y}$ = slope of a line connecting yield point to cracking point in the opposite direction;

$D(Y)$ = yield deformation;

D_{max} = maximum deformation attained in loading direction;

α = constant (assumed to be 0.5).

When the load is reversed towards the direction previously yielded, a low-slope branch followed by a stiffening part is considered (path $X_1 BU_m$ in Fig. 3.4). The portion X_1B corresponds to the stage when the crack (now in the compressive region) has not been closed, and the moment is resisted only by the reinforcement. When the crack closes (at point B in Fig. 3.4) the compression caused by the moment is resisted by both the compressive steel and the concrete; hence the resistance increases.

The position of the crack-closing point has a significant effect on the stiffness for small amplitudes. Based on the experimental results reported in Reference 18, the following can be stated about the location of this point:

1. For a given section, the value of moment at crack-closing point remains almost constant throughout the loading.
2. If the anchorage condition does not allow any "push-in pull-out" to occur the value of the moment can be calculated from:

$$M = \alpha_1 A_s f_{sy} (d-d') \quad (3.2)$$

in which

α_1 = constant ($\alpha_1 = 0.5$ appears to give a reasonable agreement with the experimental results);

A_s = area of steel;

f_{sy} = yield stress for steel;

$d-d'$ = distance between the centroids of compressive and tensile reinforcement.

Otherwise, the moment is resisted by bond stresses and can be obtained from:

$$M = \pi d_b u \ell_a (d-d') \quad (3.3)$$

where

d_b = diameter of the compressive bar;

u = average bond stress;

ℓ_a = anchorage length.

3. The rotation at which the crack closes depends on the maximum rotation attained in the corresponding direction (Fig. 3.4).

It is assumed that

$$D(B) = \frac{3}{4} (X_{\max}) \quad (3.4)$$

where

X_{\max} = maximum residual deformation previously attained.

3.5 Otani Hysteresis Model

This model, which is a modified version of Takeda system, was originally used to represent the stiffness variation of a joint spring in conjunction with a flexural spring. Because it was simpler than the Takeda model, Otani system was applied here as an independent model.

The primary curve in this system is bilinear with the break-point at yielding of the section (Fig. 3.5). Because the cracking point is not recognized, the rules related to cracking points could be eliminated in this model. There are eleven rules describing the Otani model which are explained in Reference 25. The unloading slope from post-yielding branch was

$$S_1 = S_{OY} \left(\frac{D(Y)}{D_{\max}} \right)^\alpha$$

The general trend for handling of the low amplitude loops is similar to those in the Takeda system. As a result, this model is still complicated.

3.6 Simple Bilinear Model

Because of its simplicity, the bilinear hysteresis system has been extensively used for both steel and reinforced concrete structures. The model can be described by only three rules (Fig. 3.6). There are merely two stiffnesses considered in the model: elastic and yielding stiffnesses. Unloading and load reversal slopes are the same with the slope of the elastic stage.

The general observation in this model is that: (1) large energy dissipation is provided for high amplitude deformations, and (2) in low amplitudes, no hysteretic energy dissipation is considered.

From a crude inspection of the model, it is evident that the stiffness characteristics of the unloading and load reversal stages are substantially different from what is observed in cyclic loading of a reinforced concrete member. However, to obtain a better understanding of the influence of this discrepancy on the calculated response, the bilinear model is examined here.

3.7 Q-Hyst Model

This model was developed as part of the present study. It can be considered as a modified bilinear hysteresis system. The basic purpose of modification was to provide softened branches for unloading and load reversal stages (Fig. 3.7). The model consists of four rules which are described in Appendix A.

Unloading from a point beyond the yield point and reloading in the other direction follows two different slopes:

(1) The slope of the unloading portion ($U_m X_o$) is determined as a function of the displacement U_m and the slope of the initial portion OY in a manner similar to that for Takeda Model (See Appendix A).

(2) The reloading portion has a slope determined by the coordinates of points X_o and U'_m where U'_m represents a point on the primary curve symmetric to U_m with respect to the origin.

This assumption is desirable because: (1) it helps to simplify the model and (2) for low amplitude deformations, provides some softening comparable with pinching effects.

It should be emphasized that this model does not provide any energy dissipation unless the system yields (this deficiency also exists in Otani and simple bilinear models). Consequently, if the load starts with small amplitude deformations below the yield point, the model considers the section elastic. This is unrealistic in view of the fact that nonlinear behavior in a reinforced concrete section starts immediately after the section cracks.

CHAPTER 4

TEST STRUCTURES AND ANALYTICAL STUDY USING MDOF MODEL

4.1 Introductory Remarks

Two test structures were studied using the multi-degree-of-freedom model. First, this chapter briefly describes these structures and the base motions used in the experimental studies. Then, considerations which were given in computing different parameters involved in the analysis are explained. Finally, the analytical program and the calculated results are presented.

4.2 Test Structures

Dynamic behavior of two small-scale ten-story reinforced concrete structures, called MF1 and MF2, was studied. The structures were identical except for (a) the discontinuity of beams at the first floor of MF2, and (b) the first- and second-story column reinforcement which was different for the two structures. Each structure consisted of two identical three-bay frames. In both structures, the first and the tenth stories were longer than each one of the other stories. The overall configuration of the frames is presented in Fig. 4.1.

The mass at each level of each test structure was approximately 465 Kg, except for the first story mass in structure MF2 which was 291 Kg. At each level, the mass was transferred directly to the column centerlines such that each column carried 1/8 of the weight (except for the first floor of MF2).

The structures were designed using the substitute-structure method. The design maximum acceleration was 0.4g. Cross-sectional

dimensions and reinforcement were chosen so that beams would develop major yielding before columns yield. The distribution of longitudinal reinforcement is depicted in Table 4.1 (See also References 15 and 21).

4.3 Dynamic Tests

The tests were conducted using the University of Illinois Earthquake Simulator. In each structure, the frames were placed parallel to each other on the test platform (Fig. 4.2). The direction of motion was parallel to the plane of the frames and in horizontal direction. Each structure was subjected to three simulated motions with increasing intensities (normalized maximum accelerations) in successive runs. In addition, before and after each earthquake simulation, free vibration and steady state tests were carried out to determine damping ratios and changes in natural frequencies of the structures.

The base motion for the three earthquakes was modeled after the measured north-south component of the earthquake at El Centro, California, 1940. Because the structures were in small scale, the time axis of the base motions had to be compressed by a factor of 2.5 to obtain realistic ratios between the earthquake frequency content and natural frequencies of the test structures. For each earthquake motion and steady state test, relative story displacements and total story accelerations in the direction of motion, also total vertical accelerations at the top of two corner columns (one in each frame) were recorded.

4.4 Analytical Procedure

Based on the discussion in Chapter two, a computer program ("LARZ") was developed to analyze reinforced concrete structures

subjected to base motions. Five different hysteresis models (described in Chapter 3) can be assigned to calculate stiffness characteristics of structural elements. A block diagram and some technical information about the program is presented in Appendix B.

a. Flexural Properties of Members

Moment-curvature relationships for members were calculated based on measured material properties and idealized relationships described in Chapter Two. Nominal dimensions of cross section of each member was used in this calculation. No ultimate limit was imposed on strength (or deformation) of a member. The material properties used in the analysis are depicted in Table 4.2.

Axial forces in beams were assumed to be zero. In columns, although the axial forces vary during an earthquake, it was assumed that axial forces remain constant. Consideration of changing axial force would involve complicated hysteresis models. The axial forces due to dead load and the assumed axial forces to calculate moment-curvature relationships of columns are presented in Table 4.3. Moment-rotation relationships were calculated by the computer program using Eq. 2.4 through 2.6.

Rotations due to bond slip were calculated using Eq. 2.10. Values of rotations corresponding to the cracking, yield, and ultimate moment of each member were calculated. Then, they were added to the flexural rotations. The rotations due to bond slip are listed in Table 4.4.

b. Damping

In general, that part of seismic response caused by higher modes of vibration is neither calculated nor measured accurately. To reduce contribution of higher modes to calculated results, a stiffness dependent damping was used in the analysis ($\alpha=0$ in Eq. 2.21). The damping factor (ξ) was taken equal to 2%.

c. Time Step for Numerical Integration

In Newmark's β method (23), the limits on the time step to insure convergence and stability of the solution are functions of natural frequency of the structure. When a structure develops nonlinear deformations, the natural frequencies change as the stiffness changes. Hence, the limits are not directly applicable. Several authors have cited different limits on time step of numerical integration (20,23). In the present study, the time interval was taken approximately equal to one-tenth of the shortest period of the structures. For the structure MF2, $\Delta t=0.0008$ second was used; in analyzing structure MF1, it was found that $\Delta t=0.001$ second led to stable response as well.

Because a piecewise force-deformation relationship is used in the analysis, it is not necessary to vary stiffness in each short time interval. Some investigators have recommended to change the stiffness once at every ten time steps (11). This was adopted in the present study.

4.5 Analytical Study

To observe the performance of the model, structure MF2 was first analyzed subjected to the first six seconds of measured base acceleration in the first earthquake run with the maximum value normalized to 0.38g (design intensity). Takeda hysteresis model was used to govern stiffness

variation. Because the time axis of the input base motion was compressed by a factor of 2.5, the duration of the analysis corresponds to fifteen seconds of the actual earthquake at El Centro. The base motion, used for the analysis, included both large and small amplitudes. The calculated and measured responses are presented in Fig. 4.3.

The measured base moment, base shear, and top story displacement and acceleration are superimposed on the corresponding analytical results to make possible a close comparison of the response. Because the displacements were dominated by the first mode, comparison of the measured and calculated top story displacement is a representative measurement of the quality of the calculated story displacements. The observed and calculated displacements and accelerations at every other level are also depicted in the figure. The maximum response values at all levels are presented in Table 4.6.

Sensitivity of the calculated response to the hysteresis models was studied analyzing structure MF1. The measured base acceleration during the first earthquake run was used as the base motion. This earthquake was comparable with the design motion. The structure was analyzed using the hysteresis models described in Chapter Three. In each case, one hysteresis system was used for all structural elements. The duration of the earthquake in each case was five seconds. This duration was long enough to cover large- and small-amplitude ranges of response. The calculated and measured response are presented in Fig. 4.4 through 4.8. The maximum analytical and observed displacements and accelerations are cited in Table 4.7. Maximum rotational ductilities of member ends are presented in Appendix C.

CHAPTER 5

COMPARISON OF MEASURED RESPONSE WITH RESULTS
CALCULATED USING THE MDOF MODEL5.1 Introductory Remarks

The results obtained from the multi-degree-of-freedom model are discussed in this chapter. First, the calculated values are compared with the test results for structure MF2. In section 5.3, influence of the hysteresis models on the calculated response are described and the performance of each system is studied. Because the waveforms of top-level displacement, base shear, and base moment are similar, only top-level displacement is discussed in detail. To some extent, the discussion is also applicable to top-level acceleration. Note that the displacements are expressed relative to the platform of the earthquake simulator, while the acceleration response represents the total acceleration.

In the following sections, values of T refer to the abscissas in Fig. 4.3 through 4.8. In the discussions of maximum response, absolute values of response are considered.

5.2 Calculated Response of MF2

Measured (broken curves) and calculated (continuous curves) response histories of structure MF2 are presented in Fig. 4.3. The structure was analyzed using the Takeda hysteresis model.

Performance of an analytical model can be evaluated in various aspects. One of the factors of importance is the maximum response. It can be seen in Fig. 4.3 that the measured top level displacement includes two major peaks at $T \approx 1.4$ and $T \approx 2.4$ seconds. Although the analytical model reproduces the first peak very well, it fails to match the second one. The maximum acceleration at Level 10 is calculated reasonably well. In the large-amplitude region, the frequency content and the waveform of the calculated response is very close to

what was measured. In the low-amplitude range, the calculated response has a distinctly alternating character which was not observed in the test results. The difference is even more visible in the acceleration response.

The overall deformed shape of the structure is presented in Fig. 5.1. The numerical values of maxima are listed in Table 4.5. Very close correlation was observed between the measured and calculated shapes. It appears that the analytical model slightly overestimates the displacements at levels one through six.

Relative story displacements are plotted in Fig. 5.2. Between levels five and ten, the calculated values were smaller than those observed. The trend is reversed in lower stories. It is worthwhile to notice that relative story displacements are highly sensitive to slight changes in deformed shape of a structure. Hence, the calculated results may be regarded as being satisfactory.

5.3 Calculated Response of MF1

a. Takeda Model

Figure 4.4 shows the observed and calculated response history of structure MF1 subjected to the base acceleration measured in Run 1. The analytical results were obtained based on the Takeda hysteresis model. Excellent correlation is observed up to $T \approx 3.2$ seconds. During this period, maxima, frequency contents, and waveforms of experimental and analytical results are quite close. This indicates that the overall hysteretic behavior and energy dissipation of the structure were presented well by the Takeda model with $\alpha = 0.5$ (in Eq.3.1)

The calculated response deviates from the measured curve at $T \approx 3.2$ seconds when low-amplitude displacements are experienced. Differences can be seen in amplitudes, waveforms, and frequency contents. In fact, the analytical model results in a response with some visible frequency content while the test results have no clear low-mode frequency content. Such difference signifies that, in

low-amplitude regions, the Takeda hysteresis model resulted in structural stiffnesses larger than the actual stiffness of the structure.

The calculated story displacements along the height of the structure are plotted against observed maxima in Fig. 5.3. The calculated deformed shape of the structure is very close to the measured shape. Some minor differences are observed in lower stories. At the tenth level, the calculated displacement was only 2% smaller than the measured value.

To compare the shape of the structure at the time of maximum response, the maximum story displacements are normalized with respect to the tenth level displacement (Fig. 5.4). The calculated shape is reasonably close to what was measured. It can be seen that the shape obtained from the analytical model is smoother than the observed shape.

For relative story displacements, the difference between the observed and analytical results seem to alternate and no uniform variation can be recognized (Fig. 5.5). The discrepancy is attributed to the sensitivity of relative story displacements to small changes in the deformed shape of the structure.

b. Sina Model

The analytical results based on the Sina hysteresis model are presented in Fig. 4.5. The calculated response seems to be in reasonably good agreement with the measured response up to $T \approx 2$ seconds. Beyond this point and before $T \approx 3.2$ seconds (where low-amplitude response starts), the frequency content of the analytical results is almost the same as that of the test result. However, displacement maxima are overestimated by the model. The fact that three of the four peak points in this range overestimate the response indicate that dissipated energy considered by the Sina model was less than what was experienced by the structure. Consequently, the model had to develop additional displacements to compensate for the difference.

Reasonably close correlation can be seen between low-amplitude response of the measured and the calculated results. The agreement is more pronounced in base shear, base moment, and top level acceleration. Inclusion of pinching effect in Sina model is believed to have resulted in a stiffness close to the actual stiffness of the structure over the low-amplitude region.

The calculated maximum story displacements at all levels are shown in Fig. 5.3. It can be seen that the calculated values consistently overestimate the measured quantities over the height of the structure. The difference at the tenth level is 19%. The deformed shape normalized with respect to the top level displacement (Fig. 5.4) is found to be very close to the shape obtained from the test results. The correlation is more satisfactory at upper levels.

As for relative story displacements, the calculated values are larger than those measured in most stories (Fig. 5.6).

c. Otani Model

The calculated response using Otani model exhibits the same frequency content as the measured response during the period when large-amplitude displacements were obtained (Fig. 4.6). However, the maxima are overestimated at the end of that range. At level ten, the calculated maximum displacement is 33% larger than the observed maximum value. In low-amplitude range of response, the calculated displacement deviates substantially from the observed displacements.

The calculated displacements at other levels are larger than the measured maxima (Fig. 5.3). The difference between the analytical and experimental results is even more pronounced at the fifth and sixth levels. There was considerable difference between calculated and measured normalized shapes between levels three and seven (Fig. 5.4).

Relative story displacements corresponding to maximum displacements are presented in Fig. 5.7. Again, at lower stories, the calculated values are in excess of the measured quantities. The trend is reversed at upper levels.

d. Bilinear Model

Unsatisfactory results were obtained with the simple bilinear hysteresis system. Except for the frequency before $T \approx 1.7$ seconds which is somewhat close to the frequency of the measured response, the calculated results were considerably different from the experimental values in all important aspects. The fact that the response was generally underestimated indicates that the analytical model had dissipated the input energy before it developed displacements comparable to the measured values. Because the hysteresis model is the major source of energy dissipation in a nonlinear structure, it can be concluded that the bilinear hysteresis model has overestimated the energy dissipation. At the top level, the calculated maximum displacement was 14% smaller than the measured value.

Along the height of the structure, at sixth level and below, the calculated maximum displacements were close to the measurements (Fig. 5.3). However, a closer inspection of the deformed shape of the structure reveals that this close correlation is due to inconsistency of the model (Fig. 5.4). It has to be emphasized that even at these levels, the calculated and observed maxima occur at different times.

As it can be expected from almost straight deformed shape of the structure above level six (Fig. 5.3), the calculated relative story displacements were underestimated by the model at these stories (Fig. 5.8).

e. Q-Hyst Model

Reasonably close agreement is observed between the measured and calculated response based on Q-hyst model (Fig. 4.8). The correlation is satisfactory in both large- and small-amplitude ranges. The peak values were overestimated

in most instances. At maximum point of the tenth-story response, the calculated value was 17% larger than the measured response (Fig. 5.3).

Figure 5.4 includes the normalized deformed shape of the structure for the calculations with the Q-hyst model. It can be seen that the calculated shape is reasonably close to the measured shape at all levels except for levels one through three.

Relative story displacements corresponding to the maximum displacements are plotted in Fig. 5.9. Except for the first, ninth, and the tenth stories, the calculated quantities exceeded the test results.

5.4 Concluding Remarks

Different aspects of performance of the hysteresis models for structure MF1 were discussed in sections (a) through (e). In terms of computer memory space and compilation times, the smaller hysteresis models were advantageous. However, the execution time for all the cases was approximately the same, because at each time step only one rule of the hysteresis model is used and whether there are few or many other rules is immaterial. Based on the study reported in sections (a-e) the following conclusions have been reached.

The bilinear model resulted in a response considerably different from the measured response.

Among the four other hysteresis models, the performance of the Otani model was found to be less satisfactory than the others. Considering the fact that two of the other systems (Sina and Q-hyst models) are simpler than Otani system, no advantage was realized in using the Otani model.

The performance of Sina and Q-hyst models appear to be similar. However, between the two, the Q-hyst model is preferred because: (a) Q-hyst system is presented by only four rules as compared with nine rules in Sina model, and (b) in the Q-hyst model, no decision is needed to be made on the location of

crack-closing point which is included in Sina model.

The final comparison is to be made between Q-hyst and Takeda models. Maximum displacements were obtained considerably closer to the measured values when Takeda model was used, although the difference between the results based on Q-hyst model and observed maxima were within acceptable range (17% error). In calculating low-amplitude response, Q-hyst model was more reliable than the Takeda system. Perhaps one of the more important factors is that the Q-hyst model is substantially simpler than the Takeda model. Therefore, this model is easier to understand and apply.

Further study is needed to establish the reliability of the Q-hyst model in representing the hysteretic behavior of connections in a reinforced concrete structure subjected to earthquake motions. Based on this particular study, however, Q-hyst model seems to be preferable to the other hysteresis systems considered, because it is simpler and because it led to satisfactory simulations of the displacement-time records at all levels of the particular test structure analyzed.

CHAPTER 6

DEVELOPMENT OF THE Q-MODEL

6.1 Introductory Remarks

This chapter introduces a single-degree-of-freedom model (Q-Model) for calculating the displacement response of reinforced concrete multistory structures subjected to strong earthquake motions. Nonlinearity of deformations is considered in the model. Using the Q-Model, displacement-histories at all levels of the structure and base moment can be calculated.

In this chapter, "original system" refers to the multi-degree structure to be analyzed.

6.2 General Comments

The key requirement for representing the earthquake response of a multistory structure by a single-degree-of-freedom model is that the deflected shape of the structure remain reasonably constant during an earthquake. Experimental observations of the behavior of multistory reinforced concrete structural systems (1,5,8,15,21) have shown that the deflected shape will tend to remain the same during the large amplitudes of response. For the test structures, this was possible because the columns were proportioned to experience limited yielding during the design earthquake and the displaced shape was not sensitive to the extent of yielding in beams.

For most earthquake motions, the elastic lateral displacement response of multistory structures is dominated by the first mode. The results of experiments mentioned above could be interpreted in terms of moderately damped linear models with some effective stiffnesses smaller than the initial values. In other words, the overall behavior of the test struc-

tures was linear, despite the presence of local nonlinear deformations.

Observing (1) that the nonlinear displacement response of reinforced concrete structures may be interpreted in terms of linear models, (2) that the displacement response is dominated by the lowest mode, and (3) that the deflected shape remains essentially constant during the "design earthquake," it is plausible to use a shape similar to the shape of the first mode in order to develop the characteristics of an equivalent SDOF model for analyzing the nonlinear response of a MDOF system.

For design purposes, lateral displacements caused by an earthquake are of primary importance. Because, for a structure consisting of elements with no abrupt change of stiffness, by controlling the displacements at different levels, the member end forces (and rotations) can be kept below the critical limits.

6.3 Q-Model

The equivalent system is shown in Fig. 6.1. The model consists of a concentrated mass supported by a massless rigid bar. The bar is connected to the ground by a hinge and a nonlinear rotational spring. Damping forces are exerted on the mass by a viscous damper. To define the system, it is necessary to determine the equivalent mass, equivalent height (L_{eq}), stiffness characteristics of the spring, and damping. Damping will be ignored in the discussion which follows immediately, but it will be included after the other parameters are developed.

a. Equivalent Mass

To define the mass of the single-degree model, first the dynamic equilibrium of the system is considered. The differential equation of motion for an undamped equivalent SDOF model representing a MDOF system as derived by

Biggs (7), is:

$$\alpha_m M_t \ddot{x} + \alpha_\ell Kx = \alpha_\ell F_t \quad (6.1)$$

where

F_t = total external force;

M_t = total mass of the original system;

K = stiffness of the original system;

x = relative lateral displacement of the equivalent mass with respect to the ground;

$$\alpha_\ell = \left(\sum_{r=1}^J F_r \phi_r \right) / F_t;$$

$$\alpha_m = \left(\sum_{r=1}^J M_r \phi_r^2 \right) / M_t;$$

F_r = external force at level r ;

j = number of levels in the original system;

M_r = mass at level r ;

ϕ_r = assumed displacement at level r , normalized with respect to the top level displacement (see Section c).

For a structure subjected to an earthquake, the external forces can be expressed as:

$$F_t = -M_t \ddot{X}_g \quad (6.2)$$

where \ddot{X}_g = ground acceleration.

Substitution of F_t from this equation in Eq. 6.1, and then dividing through by α_ℓ results in Eq. 6.3.

$$\left(\alpha_m / \alpha_\ell \right) M_t \ddot{x} + Kx = -M_t \ddot{X}_g \quad (6.3)$$

$$\text{or} \quad M_e \ddot{x} + Kx = -M_t \ddot{X}_g \quad (6.4)$$

in which

$$M_e = \text{equivalent mass} = \left(\alpha_m / \alpha_\ell \right) M_t \quad (6.5)$$

Hence, the equivalent mass is a function of the total mass and the assumed deformed shape of the structure.

b. Stiffness

The stiffness of the single-degree structure is provided by a rotational spring at base (Fig. 6.1). Because the bar connecting the mass to the base is rigid, all elastic and inelastic internal work takes place in the rotational spring. The governing skeleton curve for force-deformation relationship of the spring is directly related to the stiffness characteristics of the multistory structure.

To obtain a representative function of the stiffness of the original system, the structure is analyzed subjected to a set of monotonically increasing static lateral loads at floor levels. The load at each level is proportional to its height from the base of the structure. This part of the analysis results in relationships between base moment and displacements at different levels.

It is also necessary to determine the displacement at the height equal to L_{eq} (L_{eq} = equivalent height; see Section c). If L_{eq} is equal to the height of one of the floor levels, the displacement at this level is directly used. However, if L_{eq} is between the heights of two levels, a linear interpolation is made between the displacements at these levels. The loading is continued until large displacements well beyond the apparent yielding of the structure are developed.

The triangular distribution (Fig. 6.2) is chosen based on the results of the study reported in Reference 30. In this report, it was shown that the triangular, first mode, and RSS distribution led to similar results. Because the triangular distribution is simpler, it is used in the Q-Model.

A typical moment-displacement curve obtained from the static analysis is shown in Fig. 6.3. The vertical axis is normalized with respect to M^* where $M^* = \sum_{r=1}^J (M_r g) h_r$, in which g = gravity acceleration, and h_r = height at level r . The horizontal axis in Fig. 6.3 is normalized with respect to the height of the equivalent system (L_{eq}).

The calculated curve is idealized by two straight broken lines. To obtain the break point, the following procedure is used:

- (a) A tangent to the initial part of the calculated curve is drawn (OT)
- (b) From the horizontal axis at abscissas of 0.002 and 0.003, two lines are drawn parallel to OT
- (c) The break point is assumed to be in between the intersections of these lines with the calculated curve

The slope of the second portion is established by joining the break point to a point on the calculated curve at an abscissa of five times the abscissa of the break point.

The procedure described above is not necessarily a general method. However, for the cases studied here, the procedure yielded reasonable idealizations.

To represent the hysteretic behavior of the spring, Q-Hyst model is used (Appendix A). The model operates on the idealized curve described above. It is assumed that the curve is symmetric with respect to the origin.

c. Deformed Shape of the Structure

During the static analysis of the structure, corresponding to each load increment, the displacements at different levels are obtained. The shape corresponding to the moment equal to M_y (Fig. 6.3) is normalized with respect to the top level displacement and is used as the deformed shape of the struc-

ture (ϕ). This shape is assumed to remain unchanged during the earthquake.

Equivalent height is calculated from

$$L_{eq} = \frac{\sum_{r=1}^j M_r \phi_r h_r}{\sum_{r=1}^j M_r \phi_r} \quad (6.6)$$

After the displacement-history is calculated at this height, the displacements at all levels can be determined based on the assumed deformed shape.

d. Damping

Damping is assumed to be proportional to the relative velocity of the equivalent mass, with respect to the ground. The damping factor is arbitrarily taken equal to 2%. The frequency based on the stiffness of segment OY (Fig. 6.3) is used to determine the damping coefficient (C in Eq. 6.7). Damping coefficient is assumed to remain unchanged during the entire analysis.

e. Equation of Motion

The complete equation of motion is stated as

$$M_e \ddot{x} + C \dot{x} + Kx = -M_t \ddot{X}_g \quad (6.7)$$

where $C = 2\xi\omega M_e$ and ω = circular frequency of the single-degree system based on the slope of the line OY (Fig. 6.3). Newmark's β method (23) with $\beta = 0.25$ is used to integrate the differential equation of motion. This value of β allows the use of relatively large time steps for numerical integration. However, because the Q-Model is simple and small time intervals may be used without a significant increase in computer cost, other values (e.g., $\beta = 1/6$) can also be assigned to β .

CHAPTER 7

ANALYTICAL STUDY USING THE Q-MODEL

7.1 Introductory Remarks

A computer program named "LARZAK" was developed to implement the dynamic part of the analytical procedure described in Chapter Six. The computer cost for each run of this program is only 3% of that of LARZ (Chapter Four), for a ten-story three-bay frame analyzed subjected to six seconds of base acceleration record. A block diagram of the program is presented in Appendix D.

To examine the reliability of the Q-Model, a three-part investigation was conducted. This chapter first describes the test structures which were used in the study. Then the analytical study and the related discussions follow. The first part of the investigation was the analysis of eight different small-scale structures tested using the University of Illinois Earthquake Simulator. The analytical results were compared with the measured responses.

In part two, the performance of the model for different ground motions was studied. For this part, one of the test structures was analyzed subjected to different earthquakes. Because no test results were available for this part, the multi-degree analytical model (Chapters Two and Four) was used to evaluate the results from the Q-Model.

Part three was concerned with the effects of repeated earthquakes on the same structure. Responses of a particular test structure to five different intensities of the same motion was analyzed. In each case the motion was made up of two identical earthquake records separated by a period of no base motion.

In the following sections, comparisons between measured and calculated maxima are made for the absolute values of responses.

7.2 Structures and Motions

a. Test Structures

Eight small-scale, ten-story, three-bay reinforced concrete structures were used for one or more parts of the analytical study. The structures comprised either two frames (Group One), or two frames and a shear wall (Group Two). Structures H1, H2, MF1, and MF2 had no walls. Structures FW1, FW2, FW3, and FW4 had walls. The story mass in all cases was approximately 465 Kg., except for structure MF2 which had a 291-Kg. mass at its first story.

Two of the structures in the first group (MF1 and MF2) were described in Chapter Four. The reinforcement, principal material properties, and the nominal dimensions of the other two structures (H1 and H2) are shown in Fig. 7.1. For these structures, the story height was the same at all stories. The assumed axial forces in columns and the stiffness properties of structural members are tabulated in Tables 7.1 and 7.2. Detailed information about structures H1 and H2 is provided in Reference 8.

In each of the structures of Group Two, a shear wall was centrally located in between the frames. The wall extended along the full height of each structure. The strong axis of the wall was parallel to those of the frames. At each level, the wall was connected to the mass by a hinged link. As a result, the lateral displacements of the wall and the frames were equal at each level. Because the links were hinged, they did not impose any rotational constraint on the wall.

The reinforcement distribution, basic material properties and the

dimensions of the structures of Group Two are shown in Fig. 7.2. Note that each pair of structures FW1 and FW4, also FW2 and FW3 were identical. The assumed axial forces in columns and the stiffness properties for elements are listed in Tables 7.1, 7.3, and 7.4. The complete information on casting and testing of these structures are given in Reference 1.

A conservative amount of shear reinforcement was provided for elements of all structures so that any possible shear failure was prevented with confidence.

b. Base Motion

During the experimental study, each test structure was subjected to three simulated earthquakes (except for H2 which was subjected to seven earthquakes), in addition to free vibration and steady state tests before and after each earthquake run. The base motion for all the structures, except FW3 and FW4, was modeled after the north-south component of the earthquake recorded at El Centro, California, in 1940. The base acceleration for structures FW3 and FW4 was a simulated Taft (N21E component) earthquake.

In all case, the time axes of the earthquakes were compressed by a factor of 2.5, to obtain realistic ratios between the frequencies of the earthquakes and the frequencies of the structures. For example, six-second test duration equals 15 seconds of the original earthquake.

7.3 Equivalent System

To define each structure, force-deformation relationship, deformed shape, equivalent height, and equivalent mass were calculated. These parameters were sufficient to describe the equivalent structural models.

To obtain the moment-displacement curves (described in Chapter Six),

program "LARZ2" which is a static version of the program LARZ (Chapter Four) was used. Assumptions and idealizations made in LARZ2 are similar to those in LARZ. Incremental loads are assumed to be applied at the levels where the degrees of freedom are specified. The stiffness of the structure is a function of previous load history. During each load increment, the stiffness is constant. Considering the fact that different elements yield under a different load set, it is important to apply sufficiently small load increments to allow for gradual yielding of structural elements. In particular, in the vicinity of the apparent yield point of the structure, a large set of load increments may result in an overestimated apparent yield force.

The results of the static analyses are presented in Fig. 7.3. The calculated curves are idealized using the method described in Section 6.3(b). Because the calculated curves for the structures MF1 and MF2 were identical, they were represented by one idealized curve. The ordinates of the break points and the slopes of the idealized curves for different structures are listed in Table 7.5.

It is worthwhile to note that the initial slope of the idealized curve for structure H1 is less than the initial slope for structure MF1. The cross-sectional dimensions for both structures were the same. However, because structure H1 was shorter and had a larger value of reinforcement with higher yield point, structure H1 would have been expected to have a larger lateral stiffness. When the problem was examined more closely, it was noticed that the beam reinforcement in H1 was less than that of MF1 and that, as the lateral load was increased, beams yielded first (beams were designed to yield first). As a result, beam reinforcement played a more important role in choosing the initial stiffness of each structure.

Hence, the structure with lower yield point for beams was idealized to have a lower initial stiffness.

For each structure, the floor displacements corresponding to the break point were normalized with respect to the top-level displacement (Table 7.6). Then, the resulting shape (ϕ) was used to calculate the equivalent mass and height of the structure. The equivalent mass of each structure was obtained using Eq. 6.5. The equivalent height was the geometric centroid of the deformed shape (ϕ). With the stiffness corresponding to the first branch of the idealized curve, the initial frequency of the equivalent system was calculated and used to determine the damping coefficient (C in Eq. 6.6). The values of the equivalent mass, equivalent height, and the initial circular frequency are presented in Table 7.5.

7.4 Analytical Results for Different Structures

The structures were analyzed for the first six seconds of the measured base accelerations during runs corresponding to the "design earthquakes." The first simulated earthquake for all the structures, except H2, had a maximum amplitude approximately equal to that anticipated by the design calculations. For structure H2, the third earthquake run corresponded to the design motion.

Base accelerations, top-level displacements, and base moments are presented in Fig. 7.4 through 7.11. The maximum floor displacements and maximum relative story displacements are depicted in Fig. 7.12 through 7.19. The calculated and measured maxima are listed in Table 7.7.

In all cases, the calculated top-level displacement and base moment had similar waveforms. Because base moment is a less sensitive measure, the difference between the calculated and measured values are distinguished

better in the displacement response. Therefore, comparison will be made between the calculated and measured displacement response histories.

To evaluate the performance of the Q-Model, first the response for structures H1, H2, MF1, and MF2 are considered. The frequency contents of the calculated response, in large-amplitude periods, were quite close to those of the measured response in all four cases. During the period with small amplitude response (from $T \approx 3.3$ to 4.5 seconds), the calculated curve deviated from the measured curve (except for structure MF1). The calculated peak values were reasonably close to the measured values. The absolute value of the maximum top-level displacement was overestimated by 8% for H1, 23% for H2, 19% for MF1, and 27% for MF2.

Comparison of the measured and calculated maximum floor displacements at different levels (Fig. 7.12 through 7.15) showed that the model led to reasonable maxima at all levels. The maximum displacements were generally overestimated except for levels one through three of the structure MF1. Differences were observed between the calculated and the measured maximum relative story displacements. It can be seen that the model overestimated the relative story displacements at lower stories, while it underestimated the response at upper stories.

Results for structures FW1 and FW2 are given in Fig. 7.8 and 7.9. During large-amplitude response, the calculated values were in good agreement with the measured response for each of these two structures. In both cases, the calculated and measured top-level displacement maxima were close. The model underestimated the response of structure FW1 by 8%, but it overestimated the response of structure FW2 by 10%.

The performance of the model was not quite satisfactory during low-amplitude response. In these periods of response, the waveforms were similar but the calculated and measured responses did not match well.

The calculated maximum story displacements at all levels were close to the measured values (Fig. 7.16 and 7.17). No consistent trend was recognized in comparing the measured and calculated maximum relative story displacements.

Calculated and measured responses of the frame-wall structures to a base motion simulating one horizontal component of the Taft 1952 record are shown in Fig. 7.10 and 7.11. For FW3, the test structure with the weaker wall, comparison of the calculated and measured waveforms is seen to be satisfactory throughout the six-second period shown (Fig. 7.10). The same is not true for the results of FW4, the test structure with the stronger wall. The response of the test structure in the first three seconds was considerably less than that calculated. For both structures, the maximum single-amplitude displacement was overestimated by approximately 50%. Despite these discrepancies, the overall success of the model in simulating the nature of the response is acceptable.

7.5 Analytical Results for Different Base Motions

Structure MF1 was analyzed for seven different earthquake records considered in two groups. The first group consisted of three records: Orion NS, San Fernando, 1971; Castaic N21E, California, 1971; and Bucarest NS, 1977. The second group included El Centro NS and EW, 1940; Taft N21E, and S69E, 1952. To have reasonable proportions between the input frequency and the frequency of the structure, the time axis of each record was compressed by 60%.

The maximum accelerations of all the motions were normalized such that nonlinear displacements would be developed. Maximum base acceleration is not necessarily a representative measure of the intensity of an earthquake. Many authors consider Housner's spectrum intensity as a better

index (10). However, it was not the intention of this study to compare the response caused by different motions; rather, the objective was to assess the performance of the Q-Model for each individual earthquake.

For the first group, the analysis was conducted using both the Q-Model and the MDOF system (Chapter Two). Takeda hysteresis rules were used for the MDOF analysis. The response-histories for top-level displacements and base moments are presented in Fig. 7.20 through 7.26. The maximum absolute values of the response are listed in Table 7.8. Maximum element ductilities, obtained from the MDOF analysis, are presented in Appendix E.

Earthquake records in the second group were similar to the simulated motions described in Section 7.3. Therefore, results based on these records were studied only qualitatively. No MDOF analysis was performed for this group. The results and relating discussions are cited in Appendix F.

For the Orion and Castaic records, the Q-Model resulted in responses comparable to the results of MDOF model (Fig. 7.20 and 7.21). The frequency of the response from the two models were close, and most of the peaks occurred at the same time. In both cases, the maximum top-level displacements from the Q-Model were larger than those of MDOF system. Along the height of the structure, for the Orion record, the results from both models were quite close at first to fourth level (Fig. 7.24). At other floors, the Q-Model results in larger values. Similarly, for the Castaic record (Fig. 7.25), larger values were calculated using the Q-Model. In Fig. 7.24 and 7.25 it can be seen that the Q-Model resulted in maximum relative story displacements equal or larger than those calculated using the MDOF model.

The Q-Model led to a top-level maximum displacement considerably larger than that of the MDOF system, when the Bucarest earthquake record was used (Fig. 7.22). Study of the response revealed that the period of the structure, as assumed by the Q-Model, was close to the period of the input acceleration between $T \approx 1.2$ to $T \approx 1.8$ seconds. Therefore, the structure was in a state of near resonance during this interval. As a result, large displacement was developed.

The MDOF model regarded the structure with a shorter period than the period considered by the Q-Model. Hence, considerably smaller maximum displacement was calculated using the MDOF model. To examine the validity of the above observation, the initial period of the single-degree structure was reduced by 10%. It was seen that, under the new condition, the Q-Model resulted in a response comparable to the response from the MDOF model (Fig. 7.23). In addition, maximum floor displacements and relative story displacements along the height of the structure were in good agreement for the two models (Fig. 7.26).

It should be noted that the period of the SDOF system between $T \approx 1.2$ and 1.8 seconds is considerably different from the initial period (associated with the slope of OY in Fig. 6.4). However, the initial period has an effect on the period of the structure, at least, immediately after yield displacements are developed. Therefore, a 10% reduction in the initial period has reduced the apparent period between $T \approx 1.2$ and 1.8 seconds enough so that resonance did not occur.

The difference between the results from MDOF model and the first solution using the Q-Model can be explained as follows: In the MDOF model, because the stiffness of the uncracked section was recognized in moment-rotation relationships, hysteretic energy dissipation started with low

amplitudes of response. The Q-Model, using a bilinear moment-rotation curve, did not dissipate any energy through hysteresis during low-amplitude responses. Therefore, the Q-Model resulted in relatively larger displacements (at $T \approx 1.4$ seconds in Fig. 7.22). Because of the large displacement, the stiffness of the structure was reduced causing an increase in the apparent period of the structure so that, in this particular case, the new apparent period was close to that of the input acceleration. Hence, the single-degree structure was in a state of resonance.

The Q-Model resulted in responses reasonably close to the responses from the MDOF model, for different motions. The results for Bucarest earthquake records, which was not a typical motion, showed that the results from the Q-Model need careful interpretation if the period of the input acceleration is close to the apparent period of the system. However, for more probable earthquakes the performance of the Q-Model was quite satisfactory.

7.6 Analytical Results for Repeated Motions

In Reference 8, it is reported that structure H2 experienced almost the same displacement history, when it was subjected to two identical motions strong enough to cause inelastic deformations. In this study, after the first motion, the structure was allowed to come to rest before the second motion started. To determine if such behavior can be simulated using the Q-Model, structure MF1 was subjected to five motions, each comprising two identical earthquake records. The base acceleration used was the north-south component of El Centro, 1940.

At each case, the record consisted of two motions with the same maximum acceleration. The maximum acceleration was normalized to values ranging

from 0.2 g to 1.6 g. The input acceleration in each case consisted of two six-second durations and a 0.4-second quiet period in between. The quiet period was included to separate the records. During the quiet period, any free vibration was eliminated by setting the displacement, velocity, and acceleration of the equivalent mass equal to zero. As a result, when the second motion started, the structure was at rest, but with stiffness characteristics the same with those at the end of the first motion.

The base accelerations, top-level displacements, and the base moments are presented in Fig. 7.27 through 7.31. In each case, the response for the second motion (between $T = 6.4$ to 12.4 seconds) is shown by broken line and superimposed on the response for the first motion. The displacement maxima are listed in Table 7.9. Because in some cases there was a permanent drift, one-half of double-amplitude displacements were cited.

For the case with 0.2 g maximum acceleration (Fig. 7.27), the apparent frequency of the response for the second motion was smaller than that of the first one. This showed a reduction in the structural stiffness from the first earthquake to the second. During the first motion, major non-linear displacement was not developed until $T \approx 2.4$ seconds. Beyond this point, the structure had a smaller stiffness and longer average period. This was seen more clearly during the first 2.4 seconds of the response for motion two. During this period, larger displacements were developed resulting in further period elongation. The maximum double-amplitude displacement for the second motion was 14% larger than that of the first one.

In the run with 0.4 g maximum acceleration (Fig. 7.28), the response for the two motions coincided most of the time. The nonlinear displacement started before $T \approx 1.0$ second of the first motion. So the structure lost part of its stiffness early during the motion, and had an increased period for the rest of the time. When the second motion started, differences were

seen between the two displacement responses before $T = 1.0$ second. The difference is attributed to the change in the stiffness characteristics of the structure. Beyond $T \approx 1.0$ second, the response for the two motions coincided. At maxima, the double-amplitude displacement of the second response was 4% larger than that of the first one.

The above observation also applies to the cases with 0.8 g and 1.2 g maximum accelerations (Fig. 7.29 and 7.30). The maximum double-amplitude displacement, for motion two with 0.8 g, was 13% larger than that of the first motion. For the case with 1.2 g, the maximum displacement was increased by 8% in the second earthquake. Here (Fig. 7.30), the second response exhibited some shift with respect to the time axis.

The frequency contents of the two displacement responses, obtained from the two records with 1.6 g maximum acceleration, were close (Fig. 7.31). However, the peak values were increased in the second response. The double-amplitude maximum displacement of the second curve was 20% larger than that of the first curve.

The findings in Reference 8 and the above observations suggest that if a reinforced concrete structure has developed nonlinear deformations (associated with the cracking of concrete and the yielding of reinforcement) as a result of an earthquake, structural repair is not a necessity if there are no bond slip or shear failure, and if a stronger earthquake is not expected to occur during the service life of the structure.

In each of the five cases studied in this section, the Q-Model resulted in similar responses for two consecutive records. This behavior is in agreement with the experimental results on structure H2 which was subjected to two identical motions (third and fourth simulated earthquakes, Reference 8).

CHAPTER 8

SUMMARY AND CONCLUSIONS

8.1 Summary

This study consisted of two parts. The first part was aimed at determining the sensitivity of calculated seismic response of reinforced concrete structures to the hysteresis models used in the analysis. This part included the development of a multi-degree analytical model for nonlinear analysis of rectangular plane frames subjected to base excitations. In addition, two new hysteresis systems were introduced which compensated for some of the shortcomings, with respect to realistic response, of previously proposed systems. The analytical model was formed so that it was able to work in conjunction with the new hysteresis systems as well as three of the systems used in earlier studies.

The previously proposed models were Takeda system (36), Otani model (25), and the bilinear system. Takeda model (Fig. 3.1), which is relatively complicated, was proposed based on experimental results on reinforced concrete joints. Otani model was a simplified version of Takeda system (Fig. 3.5). The bilinear model is a simple system which has been used extensively, despite its poor correlation with experimental results (Fig. 3.6).

The two systems developed in the course of this study were Sina and Q-Hyst models. Sina model was a version of Takeda model modified by adding pinching effect (tendency for small incremental stiffness upon load reversal), and simplified by eliminating some of the rules (Fig. 3.4). Q-Hyst system was, in effect, a modified bilinear model which took into account: (1) reduction in stiffness during unloading from the post-yielding segment of primary

moment-rotation curve, (2) dependence of such reduction on the maximum rotation experienced, and (3) reduction of stiffness at load reversal stage (Fig. 3.7).

To study the influence of the hysteresis systems on the calculated response of structures and to determine the system which best represented the hysteretic behavior of the test frames, the multi-degree model was used to analyze the small-scale ten-story three-bay structure tested by T. J. Healey (15) using the University of Illinois Earthquake Simulator. The results from the analytical model were evaluated assuming that the experimental results provided a standard.

The objective of the second part of the study was the development of a simple economical model to be used as an efficient tool for estimating the overall seismic behavior of reinforced concrete structures undergoing inelastic deformations. The available results of tests on numerous physical specimens (1,5,8,15,21) served to develop and test the model. A very simple model was introduced which treated each structure as a nonlinear "single-degree" system (Q-Model) consisting of a mass, a viscous damper, a massless rigid bar, and a rotational spring (Fig. 6.1). The properties of the single-degree model were related to those of the structure by assuming for the structure a deflected shape corresponding to a linear lateral force distribution. The backbone curve for the nonlinear spring of the Q-Model was based on the calculated static force-displacement response for the structure. Using the Q-Model, response histories for displacements at all levels and base moment response are obtained. Computer cost for Q-Model analysis of a

ten-story three-bay structure was approximately 3% of the cost for the MDOF analysis. The proposed model was tested for a collection of eight different test specimens including frames and walls (Fig. 4.1, 7.1 and 7.2), seven different ground motions (Fig. 7.20 through 7.26 and F.1 through F.4), and five repeated earthquake records (Fig. 7.27 through 7.31). The results were compared with experimental results where available. Otherwise, the complex model developed for the first part of the study was used to evaluate responses calculated using the Q-Model.

8.2 Observations

a. Part One

(1) The experimental results and the response calculated based on Takeda hysteresis model were in excellent agreement during the high-amplitude displacement response. The correlation was not close during the low-amplitude response.

(2) The inclusion of "pinching" (Fig. 3.4) in the hysteresis model improved the response during the small-amplitude period, while it resulted in a larger maximum displacement.

(3) The Q-Hyst system, which is a simple hysteresis model comprising only four rules (Fig. 3.7), resulted in an acceptable waveform for the entire response. The calculated maximum top-level displacement was 17% larger than the corresponding measured value (Fig. 4.8).

(4) The simple bilinear model (Fig. 3.6) resulted in a waveform different from the measured response. The results from this model were considered to be unsatisfactory (Fig. 4.7).

b. Part Two

(1) The displacement and base moment responses of the eight different test structures, calculated using the Q-Model, had waveforms and frequency contents similar to those of the measured responses (Fig. 7.4 through 7.19). For all but two structures, the calculated and measured displacement maxima were reasonably close. This was also true for the maximum displacements at different levels of each structure. The agreement between the measured and calculated maximum base moments was even closer. Despite the overestimated maxima for two cases, the overall performance of the Q-Model was satisfactory.

(2) The Q-Model resulted in reasonable responses for different earthquake records. It was found that, for exceptional earthquake records similar to Bucarest 1977, the Q-Model may view the structure at a state of near resonance and hence, result in excessive displacements (Fig. 7.20 through 7.26).

(3) When the same structure was analyzed for repeated earthquake records with the same maximum accelerations, the response did not change significantly from the first motion to the second. Differences were observed only in low-amplitude-response range occurring at the beginning of the run (Fig. 7.27 through 7.31). This was in agreement with the observations reported in Reference 8.

8.3 Conclusions

Based on the results of the study in this report the following conclusions were reached:

a. Part One

(1) Several stiffness characteristics may be included in a hysteresis model (e.g., reduction in stiffness upon unloading from post-yielding portion

of the primary curve, pinching effect, etc.). The extent to which the inclusion of these factors affect the response may differ from large- to small-amplitude responses. For example the inclusion of the pinching effect may alter the low-amplitude response significantly, while it has relatively small effect on high-amplitude response. Therefore, to evaluate the influence of hysteresis models used for the analysis of a structure, the calculation has to be extended over both the large- and small-amplitude periods of response history.

(2) The assumed hysteretic behavior can have a significant effect on the calculated maxima, waveform, and the apparent frequency of the response of a structure subjected to base motions. If large-amplitude displacements are developed early during the motion, the first one or two cycles are insensitive to the particular hysteresis rules used.

(3) Observed response can be simulated faithfully by using more realistic (and correspondingly more complicated) hysteresis models. However, a reasonable estimate of the response waveform can be obtained by using simpler models which represent the overall energy dissipation in the joints of a structure.

b. Part Two

(1) The displacement and base moment waveforms of a multistory reinforced concrete structure with columns proportioned to develop limited yielding, subjected to earthquake motions causing inelastic deformations, was evaluated with acceptable accuracy, using the simple model introduced in Chapter Six.

(2) Local inelastic rotation requirements in a reinforced concrete structure may be controlled satisfactorily by controlling the lateral displacement as a function of the height of the building, provided the individual elements do not have abrupt changes in stiffness. Therefore, determination of the lateral displacements may be adequate to check the overall performance of a structure subjected to a given earthquake.

(3) For design, a simple and inexpensive model is highly desirable because by using such a model

- (a) several preliminary designs with varying parameters can be examined before the final design is reached, and
- (b) the performance of a given structure can be evaluated using a wide range of ground motions.

LIST OF REFERENCES

1. Abrams, D.P., and M.A. Sozen, "Experimental Study of Frame-Wall Interaction in Reinforced Concrete Structures Subjected to Strong Earthquake Motions," Civil Engineering Studies, Structural Research Series No. 460, University of Illinois, Urbana, May 1979.
2. Adeli, H., J.M. Gere, and W. Weaver, "Algorithms for Nonlinear Structural Dynamics," Journal of Structural Division, ASCE, Vol. 104, ST 2, February 1978, p. 274.
3. Anderson, J.C. and W.H. Townsend, "Models for RC Frames with Degrading Stiffness," Journal of Structural Division, ASCE, Vol. 103, ST 12, December 1977, pp. 2361-2376.
4. Aoyama, H., "Simple Nonlinear Models for the Seismic Response of Reinforced Concrete Buildings," U.S.-Japan Cooperative Research Program in Earthquake Engineering with Emphasis on the Safety of School Buildings, August 1975, pp. 291-309.
5. Aristizabal-Ochoa, J.D., and M.A. Sozen, "Behavior of Ten-Story Reinforced Concrete Walls Subjected to Earthquake Motion," Civil Engineering Studies, Structural Research Series No. 431, University of Illinois, Urbana, October 1976.
6. Aziz, T.S., "Inelastic Dynamic Analysis of Building Frames," Publication No. R76-37, Department of Civil Engineering, Massachusetts Institute of Technology, Cambridge, August 1976.
7. Biggs, J.M., Introduction to Structural Dynamics, McGraw-Hill Book Co., 1964, pp. 202-205.
8. Cecen, H.M., "Response of Ten-Story Reinforced Concrete Frames to Simulated Earthquakes," Doctoral Dissertation, Graduate College, University of Illinois, Urbana, May 1979.
9. Clough, R.W. and S.B. Johnston, "Effect of Stiffness Degradation on Earthquake Ductility Requirements," Proceedings, Japan Earthquake Engineering Symposium, Tokyo, October 1966, pp. 195-198.
10. Clough, R.W., J. Penzien, Dynamics of Structures, McGraw-Hill Book Company, 1975, pp. 227-232.
11. Emori, K., and W.C. Schnobrich, "Analysis of Reinforced Concrete Frame-Wall Structures for Strong Motion Earthquakes," Civil Engineering Studies, Structural Research Series No. 457, University of Illinois, Urbana, December 1978.
12. Gavlin, N., "Bond Characteristics of Model Reinforcement," Civil Engineering Studies, Structural Research Series No. 427, University of Illinois, Urbana, April 1976.

13. Giberson, M.F., "The Response of Nonlinear Multistory Structures to Earthquake Excitation," Earthquake Engineering Research Laboratory, California Institute of Technology, Pasadena, California, May 1967.
14. Goel, S.C., and G.V. Berg, "Inelastic Earthquake Response of Tall Steel Frames," Journal of Structural Division, ASCE, Vol. 94, ST 8, August 1968, pp. 1693-1711.
15. Healey, T.J., and M.A. Sozen, "Experimental Study of the Dynamic Response of Ten-Story Reinforced Concrete Frame with a Tall First Story," Civil Engineering Studies, Structural Research Series No. 450, University of Illinois, Urbana, August 1978.
16. Jennings, P.C. and R. Husid, "Collapse of Yielding Structures During Earthquakes," Journal of Engineering Mechanics Division, ASCE, Vol. 94, EM 5, October 1968, pp. 1045-1065.
17. Kanaan, A.E., G.H. Powell, "General Purpose Computer Program for Inelastic Dynamic Response of Plane Structures," EERC 73-6, University of California, Berkeley, April 1973.
18. Kreger, M.E., and D.P. Abrams, "Measured Hysteresis Relationships for Small-Scale Beam-Column Joints," Civil Engineering Studies, Structural Research Series No. 453, University of Illinois, Urbana, August 1978.
19. Livesley, R.K., Matrix Method of Structural Analysis, Pergamon Press, New York, 1964, pp. 106-116.
20. McNamara, J.F., "Solution Schemes for Problems of Nonlinear Structural Dynamics," Transactions of the ASME, Pressure Vessels and Piping Division, May 1974, pp. 96-102.
21. Moehle, J.P., and M.A. Sozen, "Earthquake-Simulation Tests of a Ten-Story Reinforced Concrete Frame with a Discontinued First-Level Beam," Civil Engineering Studies, Structural Research Series, No. 451, University of Illinois, Urbana, August 1978.
22. Mondkar, D.P., and G.H. Powell, "ANSR-1, General Purpose Program for Analysis of Nonlinear Structural Response," EERC No. 75-73, University of California, Berkeley, December 1975.
23. Newmark, N.M., "A Method of Computation for Structural Dynamics," Journal of Engineering Mechanics Division, ASCE, Vol. 85, EM3, July 1959, pp. 69-86.
24. Newmark, N.M., and E. Rosenbluth, Fundamentals of Earthquake Engineering, Prentice-Hall, Inc., 1971, pp. 321-364.
25. Otani, S., "SAKE-A Computer Program for Inelastic Response of R/C Frames to Earthquake," Civil Engineering Studies, Structural Research Series No. 413, University of Illinois, Urbana, November 1975.

26. Otani, S., and M. A. Sozen, "Behavior of Multistory Reinforced Concrete Frames During Earthquakes," Civil Engineering Studies, Structural Research Series No. 392, University of Illinois, Urbana, November 1972.
27. Otani, S., and M.A. Sozen, "Simulated Earthquake Tests of R/C Frames," Journal of Structural Division, ASCE, Vol. 100, No. ST 3, March 1974, pp. 687-701.
28. Park, R., and T. Paulay, Reinforced Concrete Structures, John Wiley and Sons, Inc., 1975, pp. 11-15 and 312-411.
29. Perry, E. S., and N. Jundi, "Pullout Bond Stress Distribution Under Static and Dynamic Repeated Loadings," ACI Journal, May 1969, pp. 377-380.
30. Pique, J. R., "On the Use of Simple Models in Nonlinear Dynamic Analysis," Publication R76-43, Department of Civil Engineering, Massachusetts Institute of Technology, Cambridge, September 1976.
31. Powell, G. H., and D. G. Row, "Influence of Analysis and Design Assumptions on Computed Inelastic Response of Moderately Tall Frames," EERC 76-11, University of California, Berkeley, April 1976.
32. Sozen, M. A., "Hysteresis in Structural Elements," Applied Mechanics in Earthquake Engineering, ASME, MMD-Vol. 8, November 1974, pp. 63-73.
33. Suko, M. and P. F. Adams, "Dynamic Analysis of Multibay Multistory Frames," Journal of Structural Division, ASCE, Vol. 97, ST 10, October 1971, pp. 2519-2533.
34. Tada, T., T. Takeda, Y. Takemoto, "Research on Reinforcement of Beam-Column Joint Panel for Seismic Resistant Reinforced Concrete Frame (Part 1)," (in Japanese), Report of the Technical Research Institute, OHBAYASHI-GUMI, LTD., No. 12, 1976, pp. 33-37.
35. Takayangi, T., and W. C. Schnobrich, "Computed Behavior of Reinforced Concrete Coupled Shear Walls," Civil Engineering Studies, Structural Research Series No. 434, University of Illinois, Urbana, December 1976.
36. Takeda, T., M. A. Sozen, and N. N. Nielsen, "Reinforced Concrete Response to Simulated Earthquake," Journal of Structural Division, ASCE, Vol. 96, ST12, December 1970, pp. 2557-2573.
37. Tansirikongkol, V. and D. A. Pecknold, "Approximate Modal Analysis of Bilinear MDF Systems Subjected to Earthquake Motions," Civil Engineering Studies, Structural Research Series, No. 449, University of Illinois, Urbana, August 1978.

38. Umemura, H., H. Aoyama, and H. Takizawa, "Analysis of the Behavior of Reinforced Concrete Structures During Strong Earthquakes Based on Empirical Estimation of Inelastic Restoring Force Characteristics of Members," Proceedings, Fifth World Conference on Earthquake Engineering, Rome, Italy, June 1973, pp. 2201-2210.
39. Walpole, W. R., and R. Shepherd, "Elasto-Plastic Seismic Response of Reinforced Concrete Frame," Journal of Structural Division, Vol. 95, ST 10, October 1969, pp. 2031-2055.

TABLE 4.1 LONGITUDINAL REINFORCING SCHEDULES FOR MF1 AND MF2

Level	Number of No. 13 g Wires Per Face					
	Test Structure MF1		Test Structure MF2			
	Beams	Interior Columns	Exterior Columns	Beams	Interior Columns	Exterior Columns
10	2	2	2	2	2	2
9	2	2	2	2	2	2
8	2	2	2	2	2	2
7	3	3	3	3	3	3
6	3	3	3	3	3	3
5	3	3	3	3	3	3
4	3	3	3	3	3	3
3	3	3	3	3	3	3
2	3	3	3	3	3	3
1	3	3	3	3	3	3

TABLE 4.2 ASSUMED MATERIAL PROPERTIES FOR
MF1 and MF2

Concrete

f'_c = Compressive strength	38.0 MPA
f_t = Tensile strength	3.4 MPA
ϵ_o = Strain at f'_c	0.003
ϵ_u = Strain at ultimate point	0.004
E_c = Young's Modulus	20,000 MPA

Steel

f_{sy} = Yield stress	358 MPA
E_s = Young's Modulus	200,000 MPA
ϵ_{sh} = Strain at strain hardening	0.0018
f_{su} = Ultimate strength	372 MPA
ϵ_{su} = Ultimate strain	0.03

TABLE 4.3 COLUMN AXIAL FORCES DUE TO DEAD LOAD

Level	Nominal Force (kN)	Assumed Force (kN)
10	0.57	1.0
9	1.14	"
8	1.70	"
7	2.27	"
6	2.84	3.2
5	3.41	"
4	3.98	"
3	4.55	"
2	5.12	5.2
1	5.70	5.2

TABLE 4.4 CALCULATED STIFFNESS PROPERTIES OF
CONSTITUENT ELEMENTS OF STRUCTURES MF1 and MF2

1. BEAMS AND THIRD TO TENTH STORY COLUMNS

Member (Level)	$(EI)_{uncracked}^*$ (kN-M ²)	M_c (kN-M)	M_y (kN-M)	S_2^{**} (kN-M ²)	S_3^{**} (kN-M ²)	θ_c^{\dagger} Rad	θ_y^{\dagger} Rad	θ_u^{\dagger} Rad
Beams (1-7)	3.48	0.027	0.119	1.31	0.039	0.0002	0.0033	0.0045
Beams (8-10)	3.48	0.027	0.082	0.96	0.033	0.0004	0.0033	0.0052
Columns (3-6)	8.40	0.079	0.179	2.84	0.045	0.0004	0.0021	0.0026
Columns (7-10)	8.40	0.061	0.136	2.35	0.040	0.0004	0.0021	0.0029

75

* Effect of reinforcement not included

** See Fig. 2.3

† Rotations due to bond slip

θ_u^{\dagger} = Rotation corresponding to moment at $\epsilon_c = 0.004$

TABLE 4.4 CALCULATED STIFFNESS PROPERTIES OF CONSTITUENT ELEMENTS OF STRUCTURES MF1 AND MF2 (Continued)

2. COLUMNS (Levels 1 and 2)

Structure	Level	$(EI)^*$ uncracked (kN-M^2)	M_c (kN-M)	M_y (kN-M)	S_2^{**} (kN-M^2)	S_3^{**} (kN-M^2)	θ_c^{\dagger} (Rad)	θ_y^{\dagger} (Rad)	θ_u^{\dagger} (Rad)
MF1	Ext. 2	8.40	0.079	0.179	2.84	0.045	0.0004	0.0021	0.0026
	Ext. 1	"	0.088	0.268	3.06	0.066	0.0002	"	0.0024
	Int. 2	"	"	"	"	"	"	"	"
	Int. 1	"	"	"	"	"	"	"	"
MF2	Ext. 2	"	"	0.321	4.52	0.076	0.0002	"	"
	Ext. 1	"	"	"	"	"	"	"	"
	Int. 2	"	0.079	0.179	2.84	0.045	0.0004	"	0.0026
	Int. 1	"	0.088	0.321	4.52	0.076	0.0002	"	0.0024

* Effect of reinforcement not considered

** Slopes of cracked and yielded section (Fig. 2.3)

+ Rotations due to bond slip

θ_u^{\dagger} = Rotation corresponding to $\epsilon_c = 0.004$

TABLE 4.5 CRACK-CLOSING MOMENTS
USED FOR SINA HYSTERESIS
MODEL

Unit = kN-M

1-BEAMS

Levels	Moment	
	Exterior End	Interior End
1-7	0.050	0.016
8-10	0.033	0.010

2-COLUMNS

	Moment
Columns with 3 bars/face	0.160
Columns with 2 bars/face (levels 2-10)	0.107

TABLE 4.6 MEASURED AND CALCULATED MAXIMUM
RESPONSE OF MF2 RUN 1

Level	Displacement (mm)		Acceleration (g)	
	Measured	Calculated	Measured	Calculated
10	24.4	24.1	0.59	0.57
9	23.4	23.4	0.48	0.49
8	22.8	22.7	0.43	0.45
7	21.6	21.7	0.39	0.44
6	19.7	20.3	0.38	0.48
5	17.3	18.5	0.35	0.44
4	14.3	15.7	0.39	0.40
3	12.1	12.4	0.43	0.49
2	7.4	8.5	0.40	0.53
1	3.8	4.2	0.34	0.39
Base	-	-	0.38	-

Base Moment
(kN-M) Measured = 22.0
Calculated = 21.5

Base Shear
(kN) Measured = 13.0
Calculated = 14.0

TABLE 4.7 MEASURED AND CALCULATED MAXIMUM RESPONSE
OF MF1 USING DIFFERENT HYSTERESIS SYSTEMS

1. DISPLACEMENTS (mm)

Level	Measured	Takeda	Sina*	Otani*	Bilinear	Q-hyst
10	23.6	23.1	28.2	31.4	20.7	27.8
9	22.8	22.5	27.3	30.9	20.3	27.0
8	21.3	21.7	26.3	30.0	19.7	25.9
7	20.7	20.6	24.8	28.9	19.2	24.2
6	18.6	19.1	22.0	27.4	18.5	22.0
5	16.7	17.1	19.1	25.4	17.0	19.3
4	14.4	14.3	16.1	21.7	14.4	15.8
3	12.3	10.9	12.1	16.4	10.9	11.8
2	8.3	7.1	8.0	10.5	7.1	7.6
1	4.8	3.5	4.0	5.1	3.4	3.6
Base Moment (kN-M)	20.8	21.6	22.1	21.4	20.0	22.0

*Measured and calculated maxima occur at different times

TABLE 4.7 MEASURED AND CALCULATED MAXIMUM RESPONSE OF MF1
USING DIFFERENT HYSTERESIS SYSTEMS (Continued)

2. ACCELERATIONS (g)

Level	Measured	Takeda	Sina	Calculated Otani	Bilinear	Q-hyst
10	0.76	0.62	0.68	0.61	0.60	0.56
9	0.60	0.49	0.50	0.46	0.47	0.51
8	0.51	0.46	0.48	0.47	0.53	0.49
7	0.49	0.50	0.51	0.48	0.48	0.43
6	0.41	0.48	0.51	0.43	0.48	0.42
5	0.40	0.41	0.44	0.38	0.46	0.40
4	0.43	0.51	0.54	0.50	0.37	0.48
3	0.46	0.56	0.53	0.56	0.45	0.49
2	0.50	0.45	0.37	0.41	0.48	0.33
1	0.40	0.35	0.35	0.35	0.43	0.30
Base Shear (kN)	15.6	14.2	14.3	13.6	12.8	13.0

TABLE 7.1 COLUMN AXIAL FORCES FOR
STRUCTURES H1, FW1, AND FW2

Unit = kN

Level	Nominal Dead Load	Assumed Axial Force	
		H1	FW1 & FW2
10	0.57	1.2	0.0
9	1.14	1.2	0.0
8	1.70	1.2	2.2
7	2.27	1.2	2.2
6	2.84	1.2	2.2
5	3.41	1.2	2.2
4	3.98	4.5	4.5
3	4.55	4.5	4.5
2	5.12	4.5	4.5
1	5.70	4.5	4.5

TABLE 7.2 CALCULATED STIFFNESS PROPERTIES OF
CONSTITUENT ELEMENTS OF STRUCTURE H1

Member (Level)	$(EI^*)_{\text{uncracked}}$ (kN-M ²)	M_c (kN-M)	M_y (kN-M)	[†] S_2 (kN-M ²)	[†] S_3 (kN-M ²)
Beams (1→4)	3.48	0.027	0.107	0.90	0.027
Beams (5→10)	3.48	0.027	0.078	0.70	0.023
Ext. Columns (1→4)	8.40	0.072	0.628	6.04	0.103
Ext. Columns (5→10)	8.40	0.054	0.357	3.92	0.052
Int. Columns (1→4)	8.40	0.073	0.530	5.25	0.087
Int. Columns (5→10)	8.40	0.055	0.190	2.32	0.033

* Effect of reinforcement not included

† See Fig. 2.3

TABLE 7.3 CALCULATED STIFFNESS PROPERTIES OF
CONSTITUENT ELEMENTS OF STRUCTURE FW1

Member (Level)	$(EI)_{\text{uncracked}}^*$ (kN-M ²)	M_c (kN-M)	M_y (kN-M)	S_2^+ (kN-M ²)	S_3^+ (kN-M ²)
Beams (1→4)	3.35	0.026	0.080	0.89	0.029
Beams (5→9)	3.35	0.026	0.116	1.29	0.032
Beams (10)	3.35	0.026	0.080	0.89	0.029
Ext.&Int. Columns (1→4)	8.11	0.085	0.199	2.84	0.047
Ext.&Int. Columns (5→8)	8.11	0.067	0.159	2.65	0.038
Ext. Columns (9→10)	8.11	0.047	0.117	2.09	0.037
Int. Columns (9→10)	8.11	0.047	0.171	2.90	0.042
Wall (1→4)	520.	0.76	13.7	515.	10.4
Wall (5→6)	520.	0.76	7.93	460.	5.59
Wall (7→10)	520.	0.76	4.24	350.	2.73

* Effect of reinforcement not included

† See Fig. 2.3

TABLE 7.4 CALCULATED STIFFNESS PROPERTIES OF
CONSTITUENT ELEMENTS OF STRUCTURE FW2

Member (Level)	$(EI)^*_{\text{uncracked}}$ (kN-M ²)	M_c (kN-M)	M_y (kN-M)	S_2^+ (kN-M ²)	S_3^+ (kN-M ²)
Beams (1→2)	4.00	0.029	0.088	0.99	0.031
Beams (3→7)	4.00	0.029	0.118	1.31	0.040
Beams (8→10)	4.00	0.029	0.088	0.99	0.031
Ext. Column (1→3)	9.66	0.090	0.202	3.21	0.050
Int. Columns (1→3)	9.66	0.090	0.255	3.92	0.061
Ext.&Int. Col. (4→8)	9.66	0.072	0.162	2.75	0.041
Ext.&Int. Col. (9→10)	9.66	0.053	0.118	2.19	0.036
Wall (1→10)	731.1	0.85	4.23	350.	2.67

* Effect of reinforcement not included

† See Fig. 2.3

TABLE 7.5 CALCULATED PARAMETERS FOR DIFFERENT STRUCTURES

Structure	Equivalent Mass (kN/g)	Equivalent Height (M)	$(\frac{M}{M^*}) \times 10^2$ at break point	S ₁	S ₂	Frequency (cycle/sec.)
H1 & H2	3.69	1.58	25.	48.	9.	17.
MF1	3.68	1.59	29.	64.	8.	20.
MF2	3.60	1.59	29.	64.	8.	20.
FW1 & FW4	3.36	1.64	33.	113.	29.	27.
FW2 & FW3	3.36	1.63	38.	93.	12.	25.

TABLE 7.6 ASSUMED DEFORMED SHAPES FOR DIFFERENT STRUCTURES

Level	H1 & H2	MF1	MF2	FW1 & FW4	FW2 & FW3
10	1.0	1.0	1.0	1.0	1.0
9	0.98	0.97	0.97	0.93	0.92
8	0.95	0.92	0.92	0.85	0.83
7	0.88	0.86	0.87	0.75	0.74
6	0.79	0.79	0.79	0.64	0.63
5	0.66	0.69	0.70	0.51	0.51
4	0.52	0.57	0.59	0.37	0.39
3	0.37	0.43	0.46	0.24	0.26
2	0.22	0.27	0.29	0.12	0.15
1	0.08	0.13	0.13	0.03	0.05

TABLE 7.7 MAXIMUM ABSOLUTE VALUES OF RESPONSE

Displacement Unit = mm

Level	H1 RUN 1		H2 RUN 3		MF1 RUN 1		MF2 RUN 1	
	Measured	Calculated	Measured	Calculated	Measured	Calculated	Measured	Calculated
10	29.2	31.7	24.5	30.1	23.6	28.1	24.4	31.1
9	29.0	31.1	24.7	29.5	22.8	27.3	23.4	30.2
8	26.0	30.1	22.2	28.6	21.3	25.8	22.8	28.6
7	24.3	27.9	20.8	26.5	20.7	24.2	21.6	27.1
6	21.2	25.0	17.5	23.8	18.6	22.2	19.7	24.6
5	17.2	20.9	13.2	19.9	16.7	19.4	17.3	21.8
4	13.7	16.5	10.1	15.7	14.4	16.0	14.3	18.3
3	9.0	11.7	7.0	11.1	12.3	12.1	12.1	14.3
2	5.3	7.0	4.2	6.6	8.3	7.6	7.4	9.0
1	2.0	2.5	1.7	2.4	4.8	3.7	3.8	3.8

TABLE 7.7 (CONTD.) MAXIMUM ABSOLUTE VALUES OF RESPONSE

Displacement Unit = mm

Level	FW1 RUN 1		FW2 RUN 1		FW3 RUN 1		RW4 RUN 1	
	Measured	Calculated	Measured	Calculated	Measured	Calculated	Measured	Calculated
10	28.2	26.0	28.4	31.2	18.7	27.0	21.5	34.1
9	26.5	24.2	25.6	28.7	17.4	24.8	19.7	31.7
8	23.8	22.1	23.6	25.9	15.0	22.4	17.2	29.0
7	20.5	19.5	20.6	23.1	13.0	20.0	15.0	25.6
6	17.0	16.6	17.3	19.7	10.8	17.0	12.3	21.8
5	13.5	13.3	14.2	15.9	8.8	13.8	9.8	17.4
4	9.5	9.6	10.7	12.2	6.8	10.5	7.1	12.6
3	7.1	6.2	8.3	8.1	4.8	7.0	4.9	8.2
2	4.1	3.1	5.1	4.7	3.0	4.0	2.8	4.1
1	2.0	0.8	2.3	1.6	1.4	1.3	1.2	1.0

TABLE 7.8 MAXIMUM RESPONSE OF STRUCTURE MF1
SUBJECTED TO DIFFERENT EARTHQUAKES

Unit = mm

Level	Orion		Castaic N21E 71		Bucarest 77		
	MDOF	Q-Model	MDOF	Q-Model	MDOF	Original Frequency	Q-Model Increased Frequency
10	13.5	17.3	10.8	14.2	16.9	30.7	18.7
9	13.2	16.8	10.5	13.8	16.6	29.8	18.1
8	12.8	15.9	10.1	13.1	16.2	28.2	17.2
7	12.3	15.0	9.6	12.2	15.7	26.7	16.3
6	11.7	13.6	8.9	11.2	14.9	24.3	14.8
5	11.0	11.9	7.8	9.8	13.7	21.2	12.9
4	9.0	9.8	6.4	8.1	11.9	17.5	10.7
3	7.0	7.4	4.7	6.1	9.5	13.2	8.0
2	4.7	4.7	3.0	3.8	6.6	8.3	5.0
1	2.3	2.3	1.4	1.8	3.4	4.0	2.4

TABLE 7.9 MAXIMUM TOP-LEVEL DISPLACEMENTS* FOR
STRUCTURE MF1 SUBJECTED TO REPEATED MOTIONS

Unit = mm

Max. Base Acceleration	Displacement		Difference	Disp./Height	
	Motion 1	Motion 2		Motion 1	Motion 2
0.2 g	13.5	15.4	+14%	0.6%	0.6%
0.4 g	21.4	22.2	+ 4%	0.9%	0.9%
0.8 g	37.2	42.0	+13%	1.6%	1.8%
1.2 g	64.9	70.0	+ 8%	2.7%	2.9%
1.6 g	94.0	112.0	+20%	3.9%	4.7%

* (Double Amplitude)/2

TABLE 7.10 WIRE GAGE CROSS-SECTIONAL PROPERTIES

Gage No.	Diameter (mm)	Cross-Section Area (mm ²)
2	6.67	34.92
7	4.50	15.87
8	4.11	13.30
10	3.43	9.23
13	2.32	4.24
16	1.59	1.98

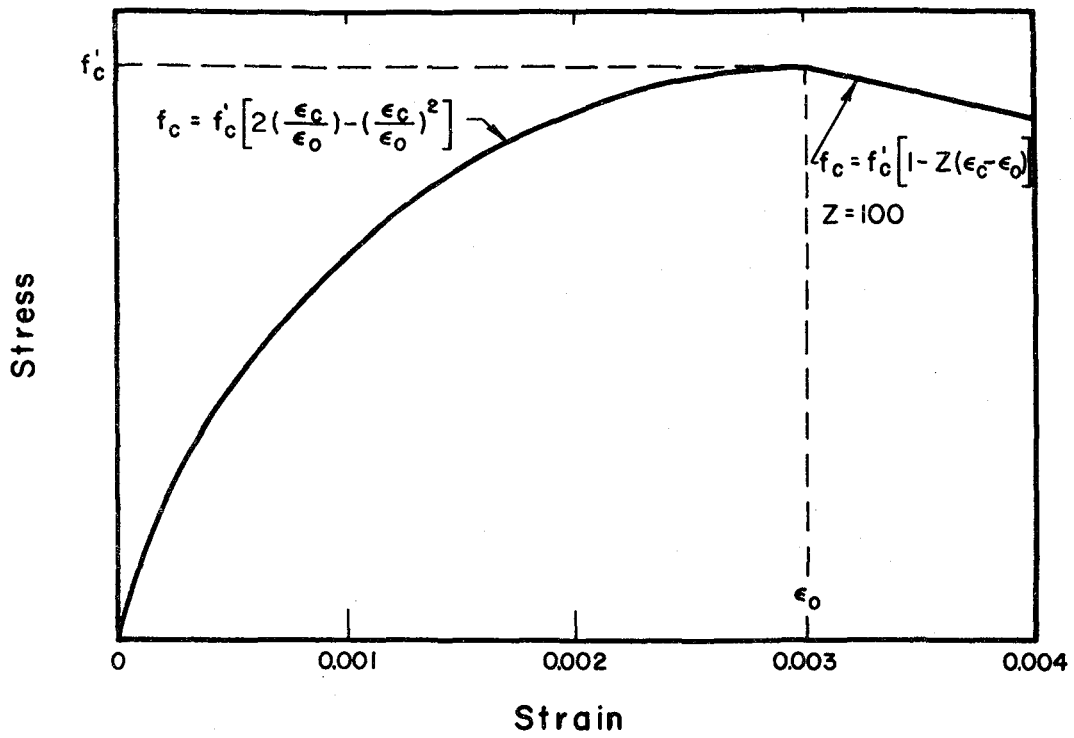


Fig. 2.1 Idealized Stress-Strain Curve for Concrete

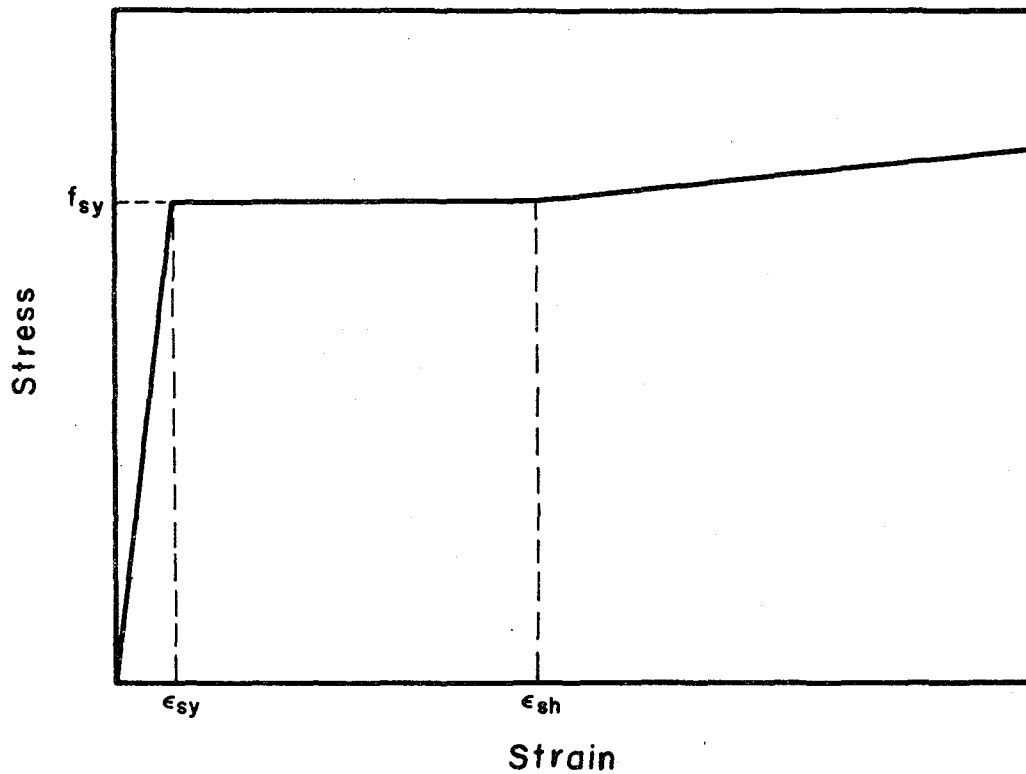


Fig. 2.2 Idealized Stress-Strain Curve for Steel

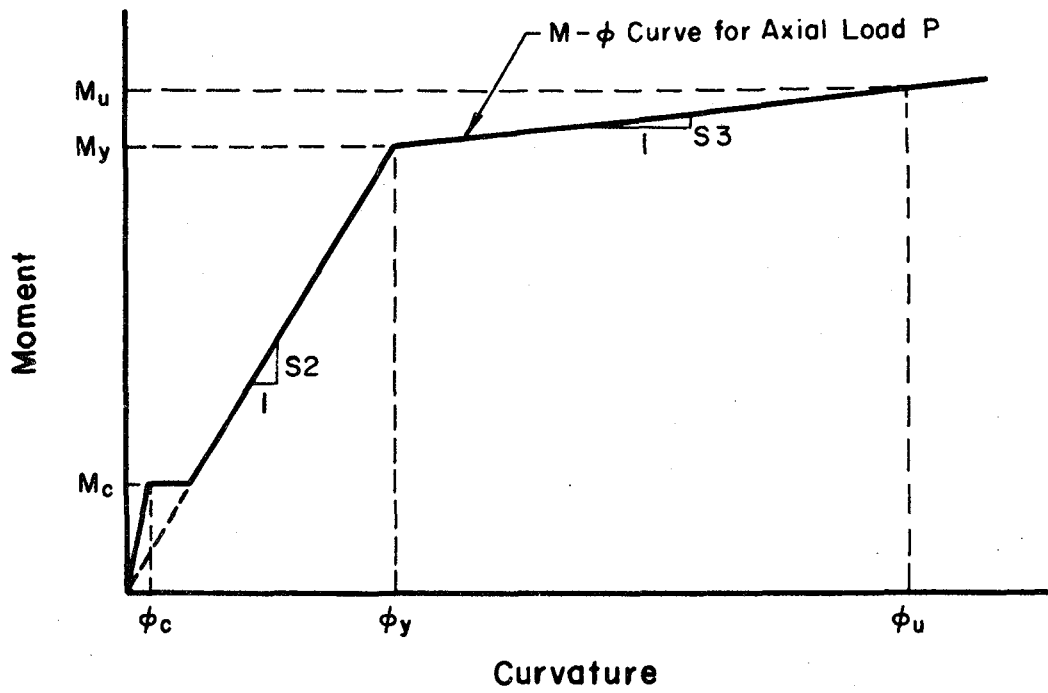


Fig. 2.3 Idealized Moment-Curvature Diagram for a Member

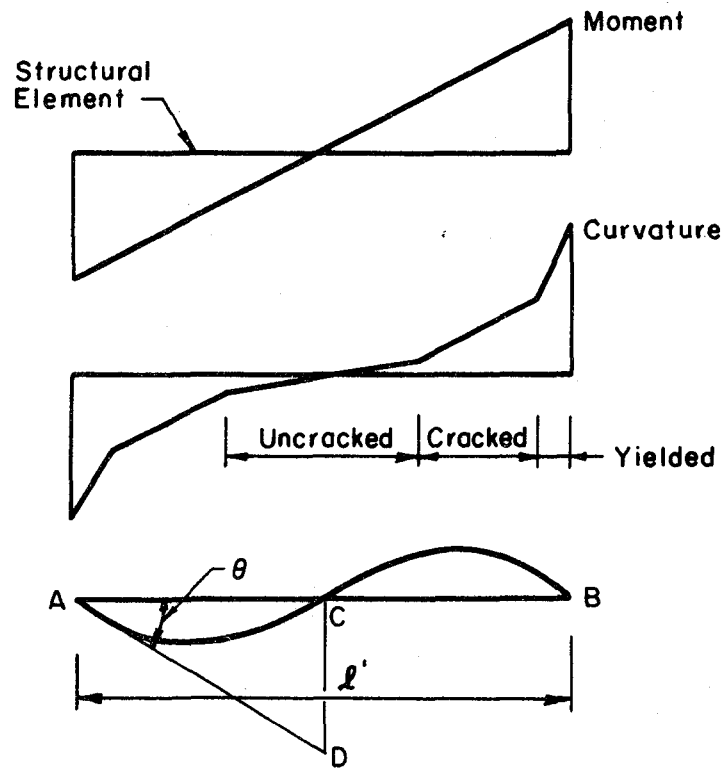


Fig. 2.4 Moment and Rotation along a Member

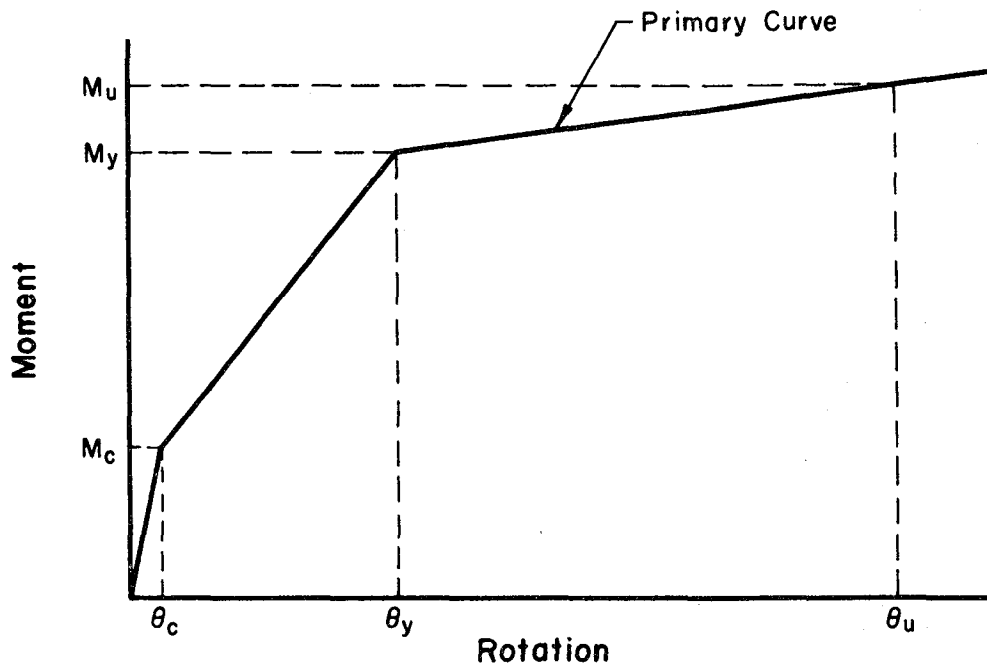


Fig. 2.5 Moment-Rotation Diagram for a Member

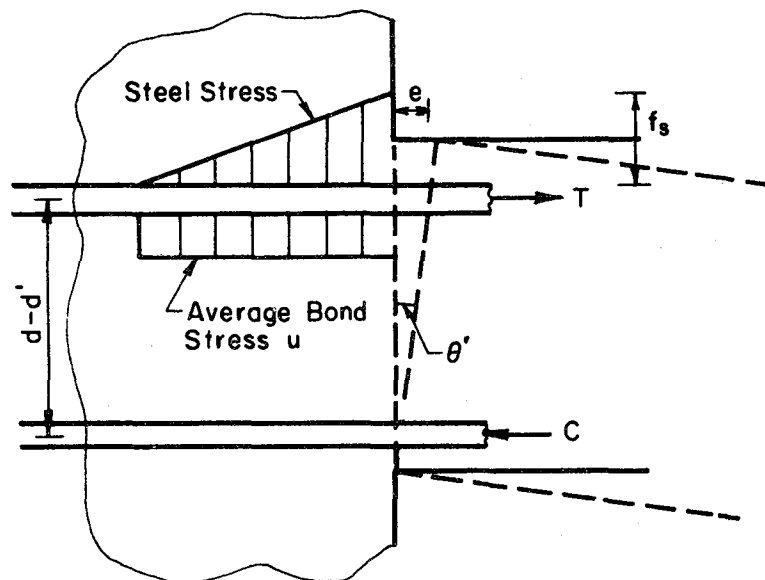


Fig. 2.6 Rotation due to Bond Slip

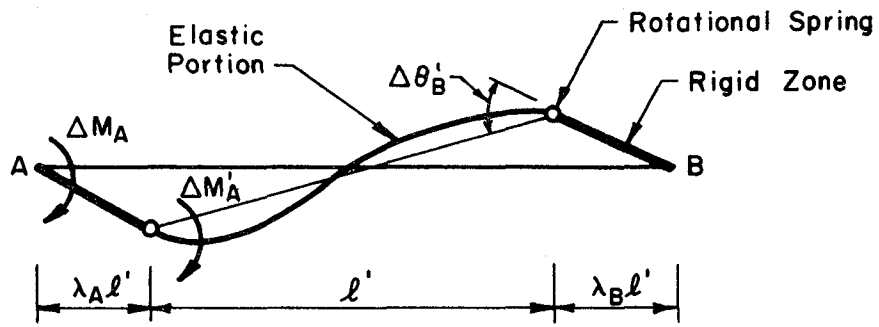


Fig. 2.7 Deformed Shape of a Beam Member

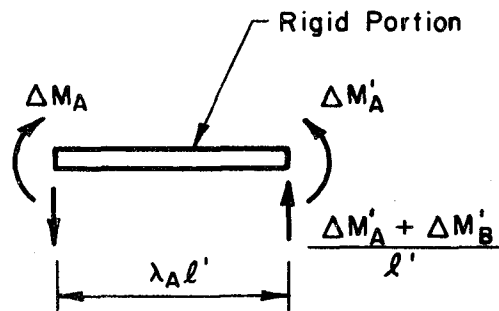


Fig. 2.8 Equilibrium of a Rigid-End Portion

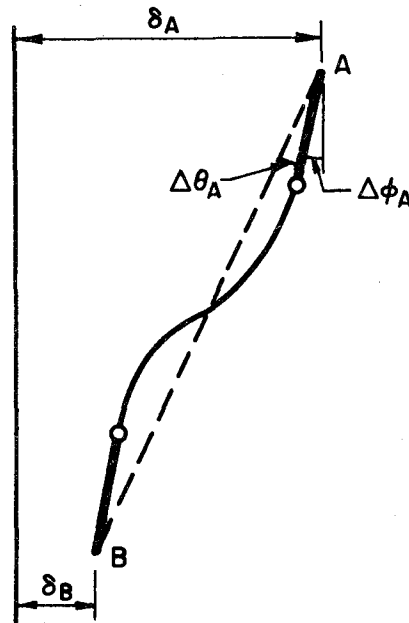


Fig. 2.9 Deformed Shape of a Column Member

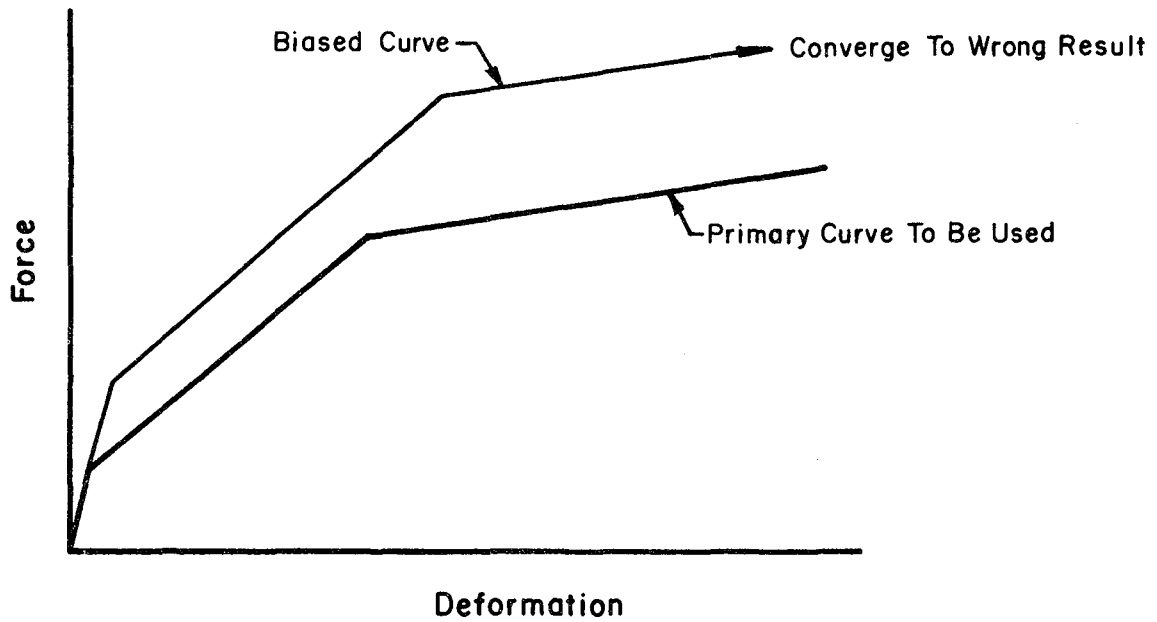


Fig. 2.10 Biased Curve in Relation to the Specified Force-Deformation Diagram

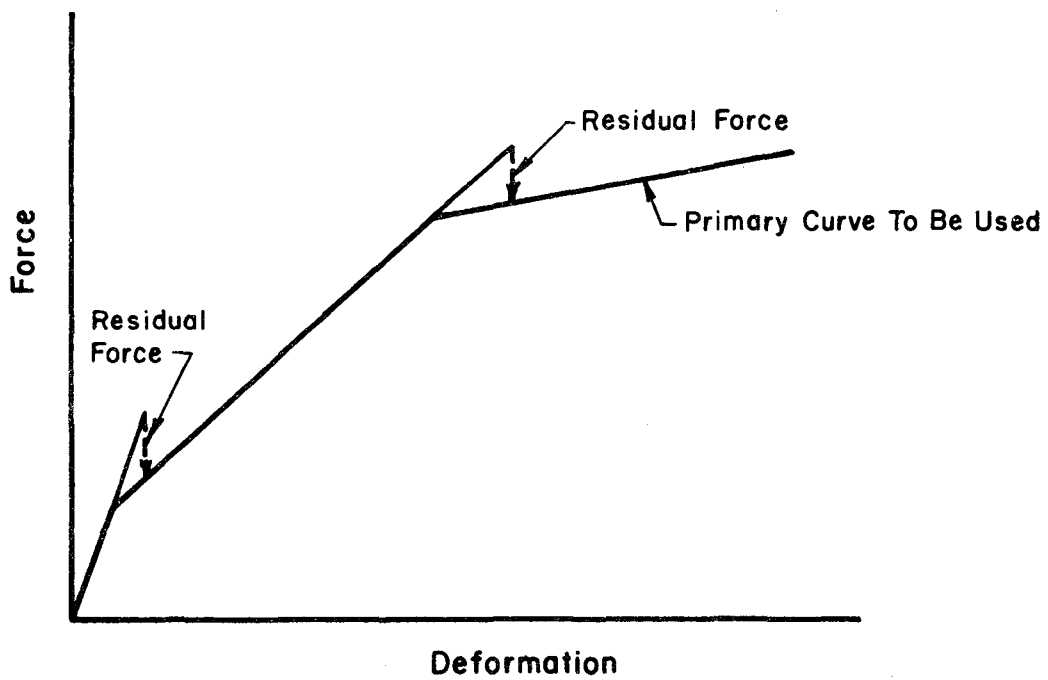


Fig. 2.11 Treatment of Residual Forces in the Analysis

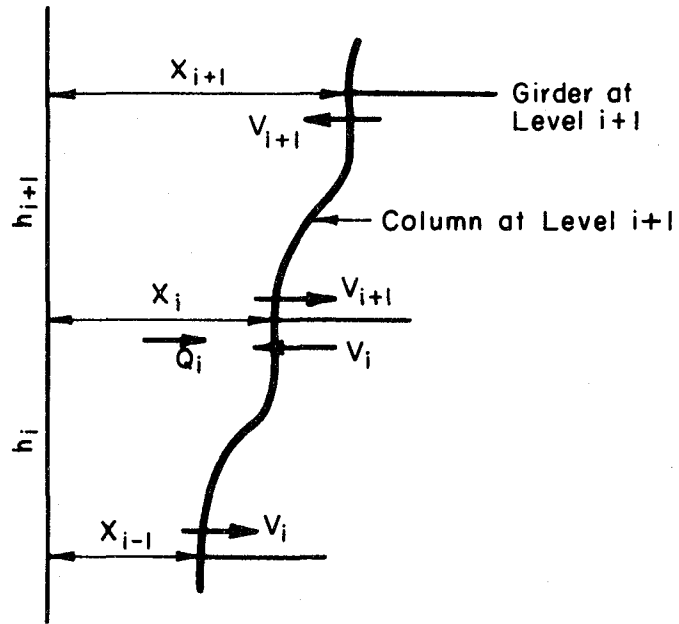


Fig. 2.12 Equivalent Lateral Load to Account for Gravity Effect

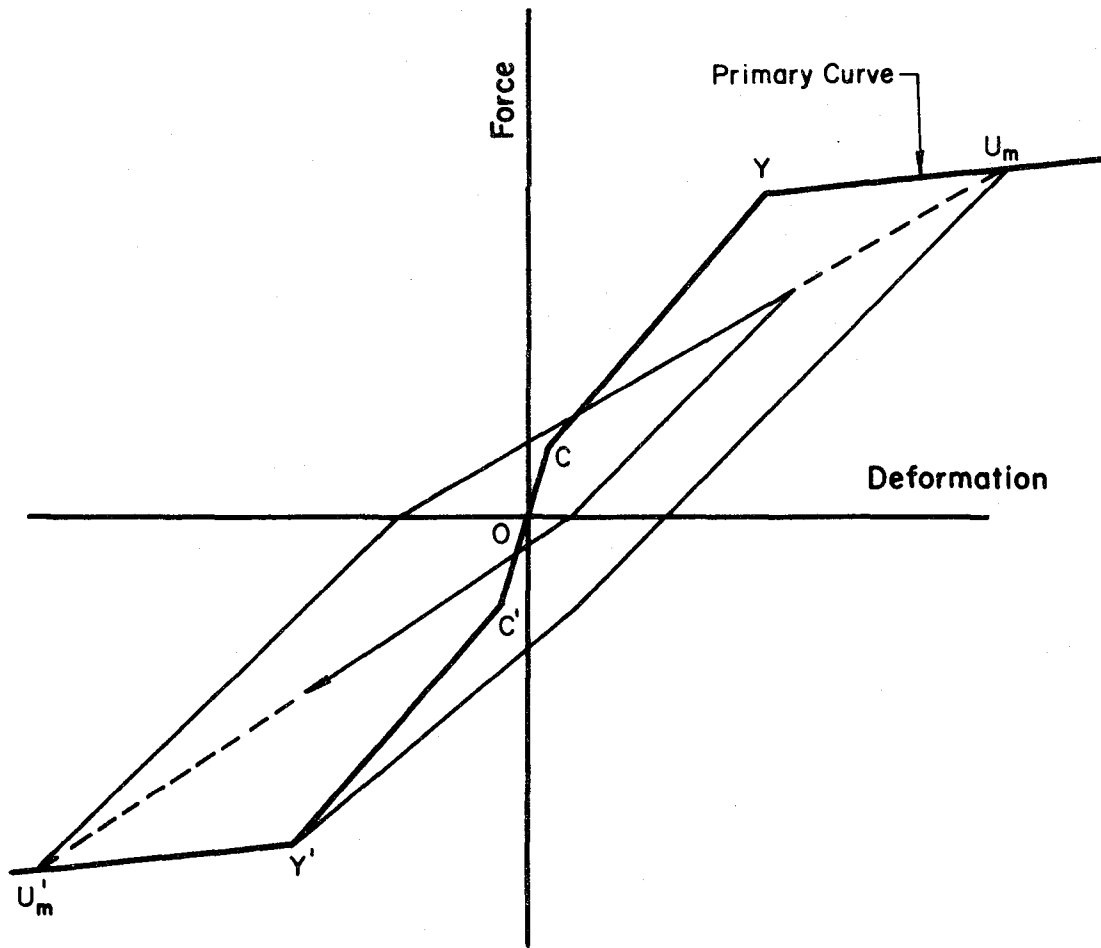


Fig. 3.1 Takeda Hysteresis Model

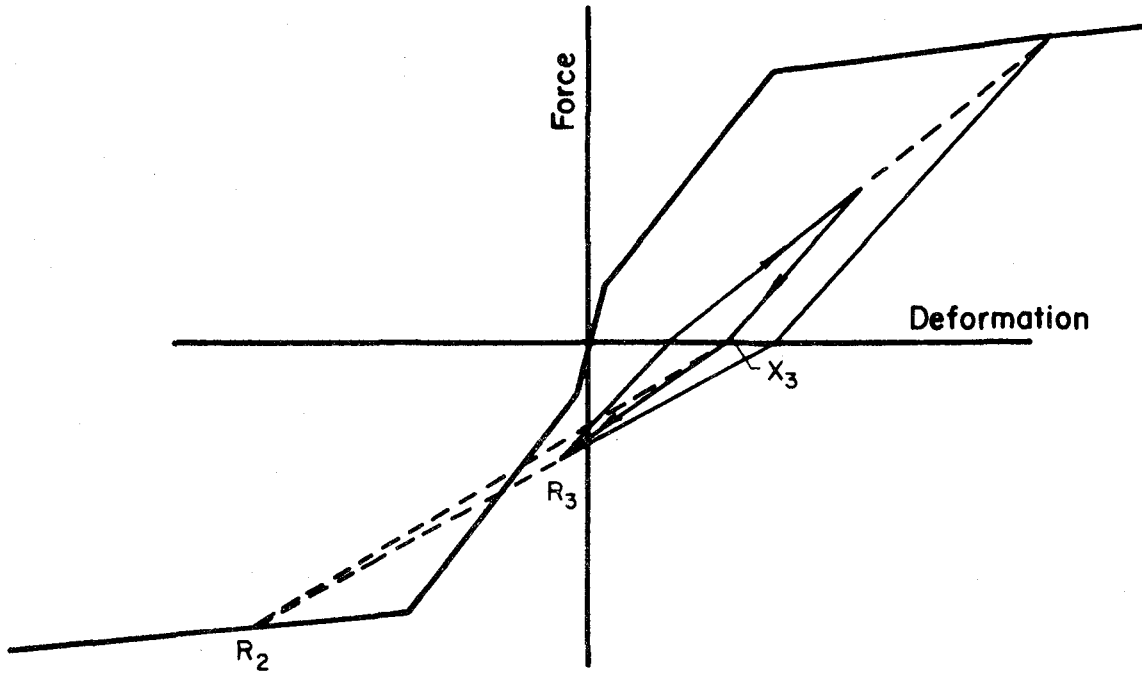


Fig. 3.2 Small Amplitude Loop in Takeda Model

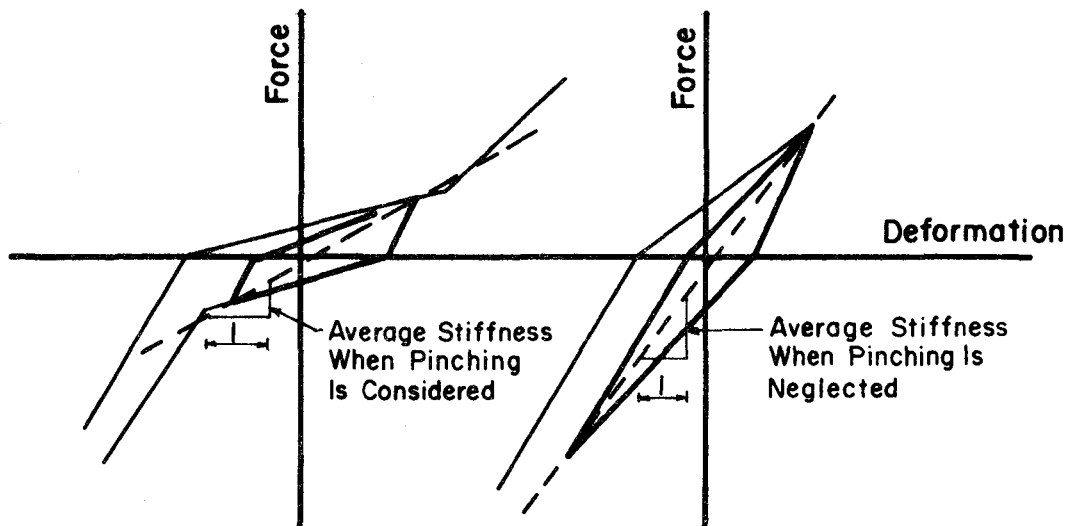


Fig. 3.3 Comparison of Average Stiffness with and without Pinching for Small Amplitudes

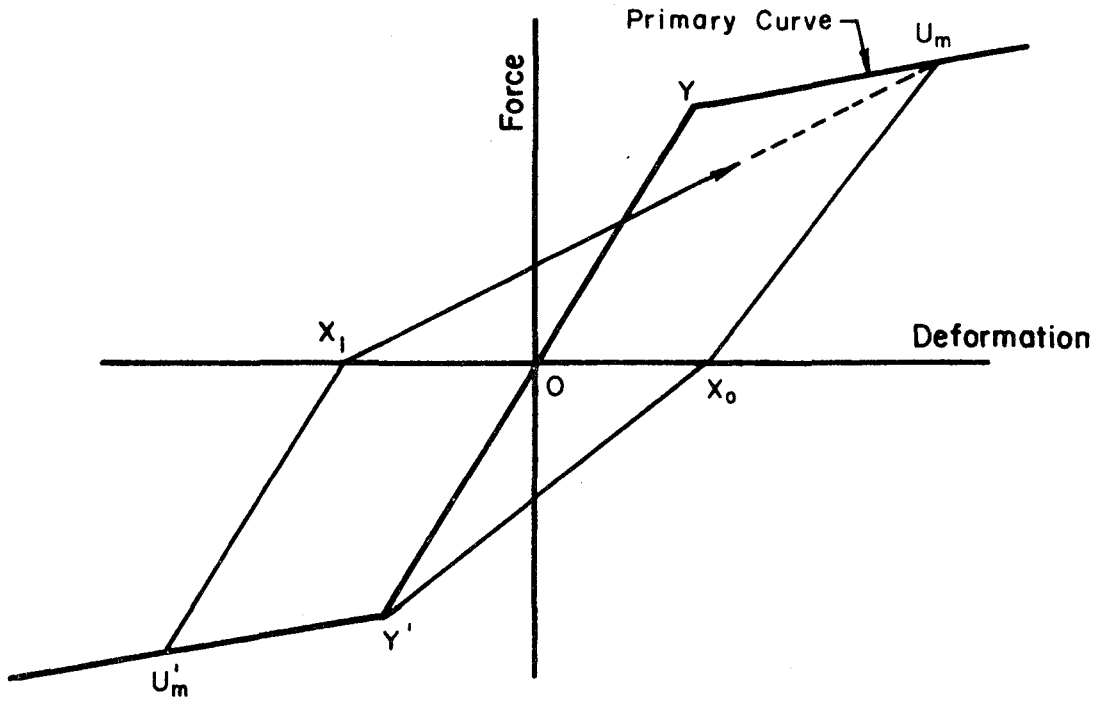


Fig. 3.5 Otani Hysteresis Model

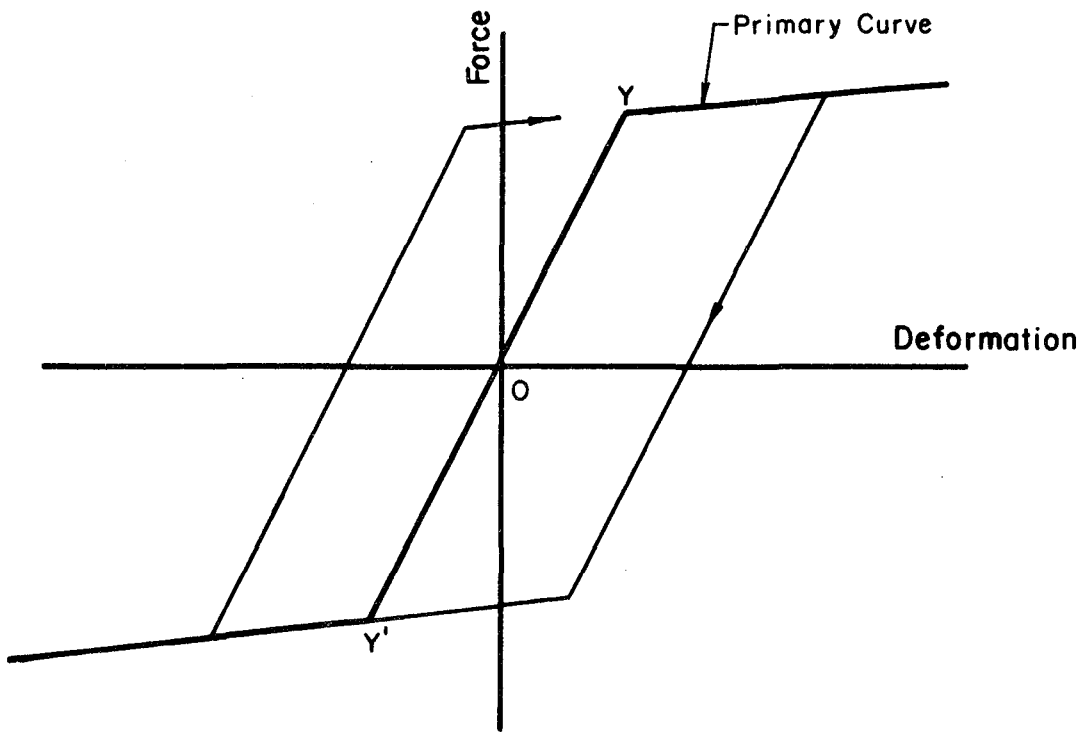


Fig. 3.6 Simple Bilinear Hysteresis System

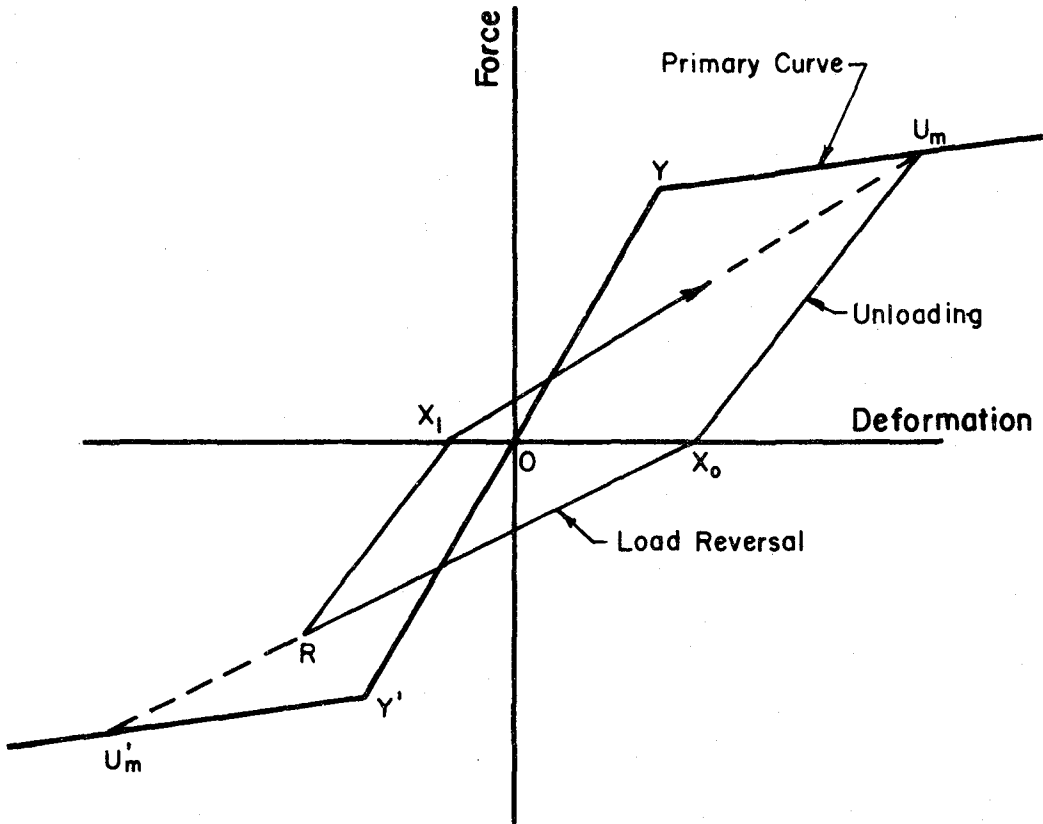


Fig. 3.7 Q-Hyst Model

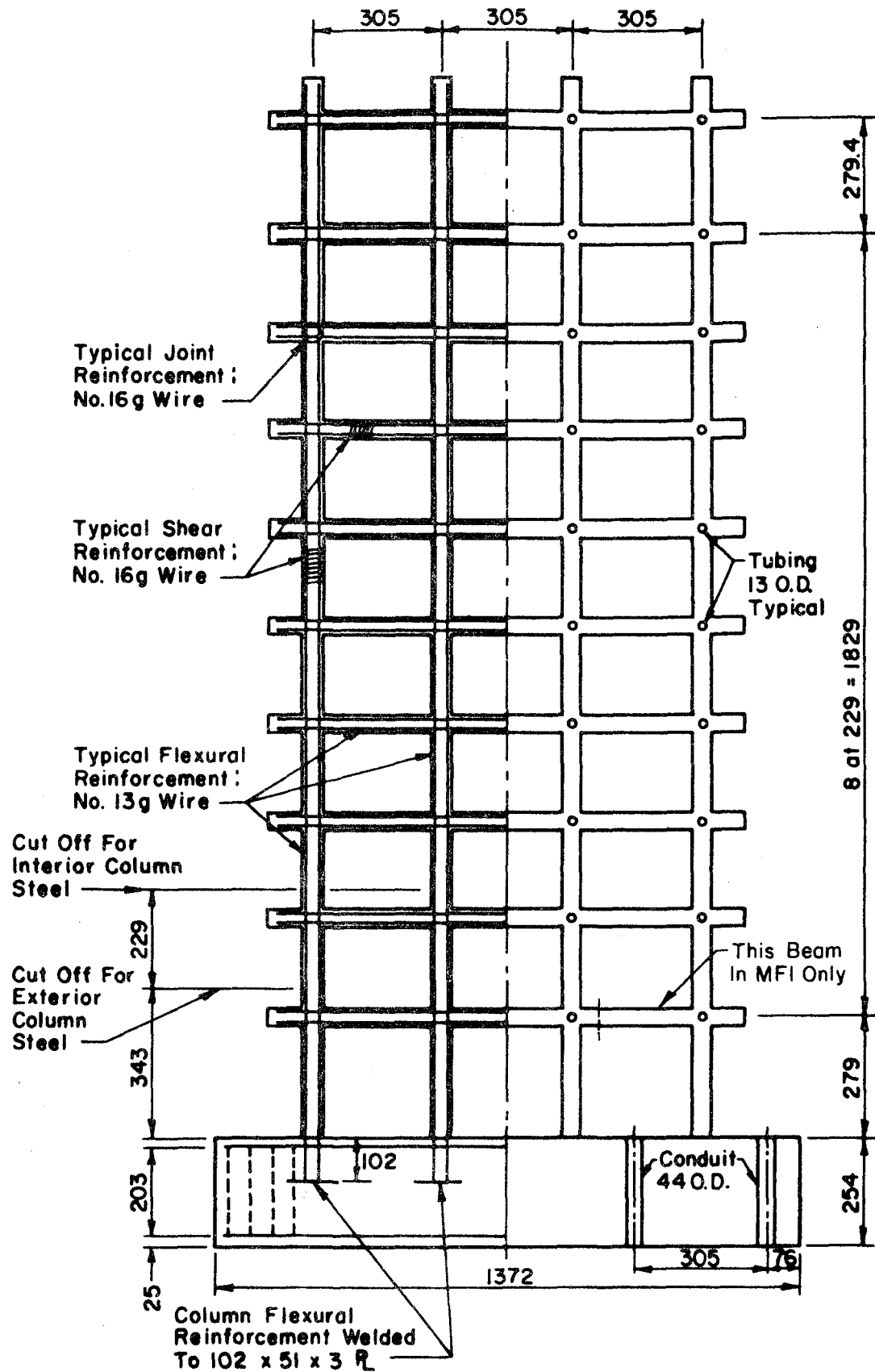


Fig. 4.1 Reinforcement Detail and Dimensions of Structures MF1 and MF2

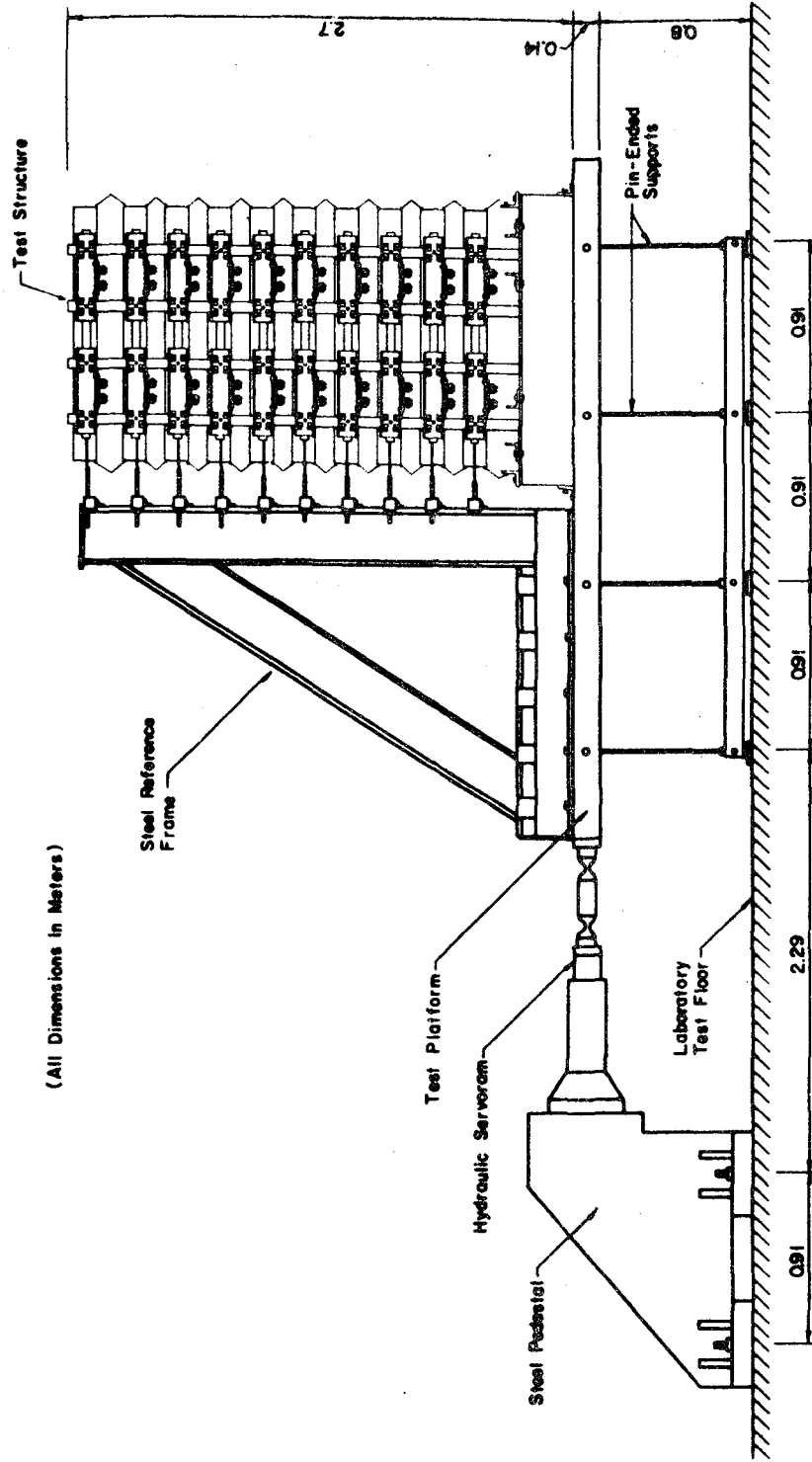


Fig. 4.2 Test Setup for Structure MF1

MF2. RUN 1

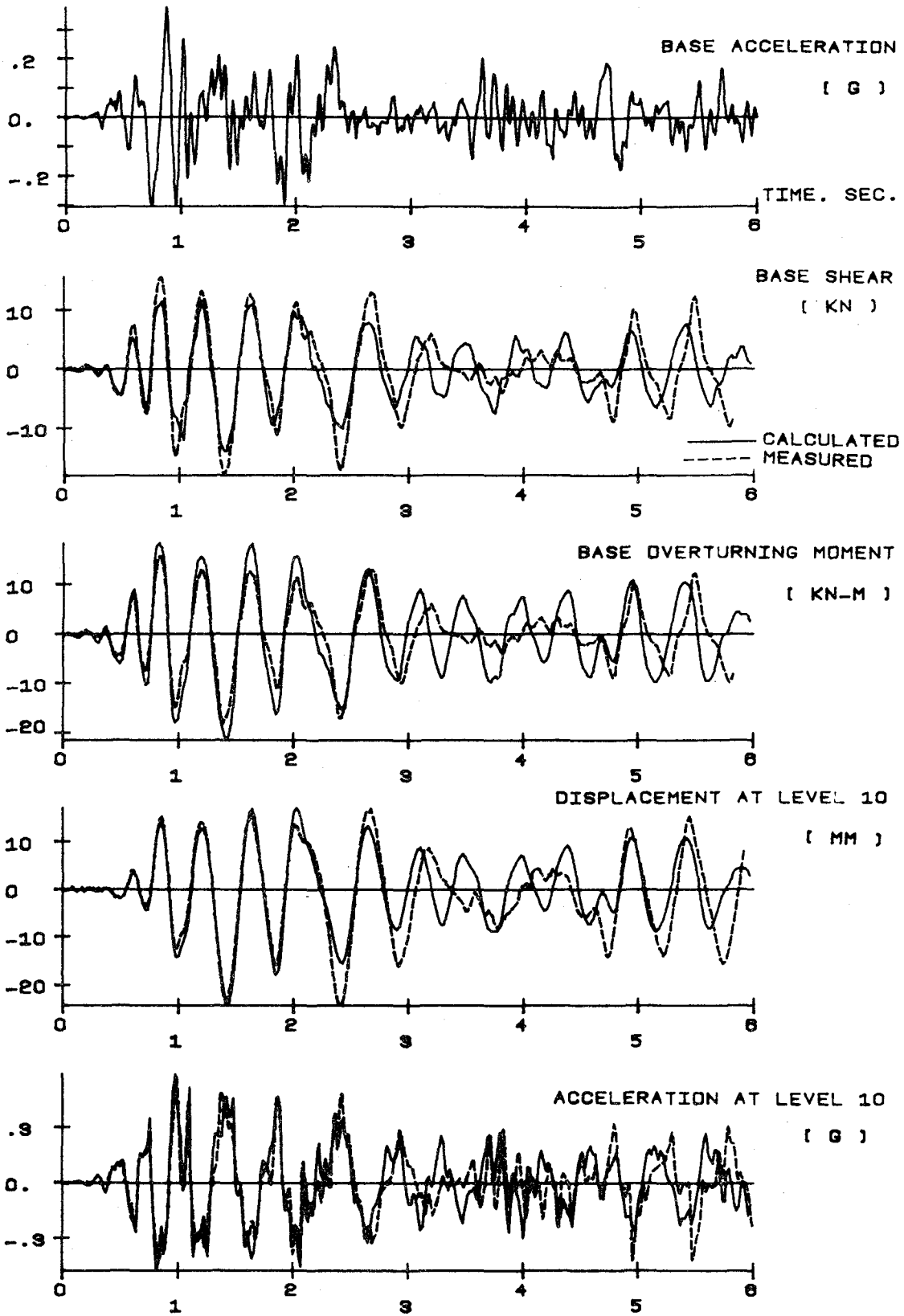


Fig. 4.3 Measured and Calculated Response for MF2

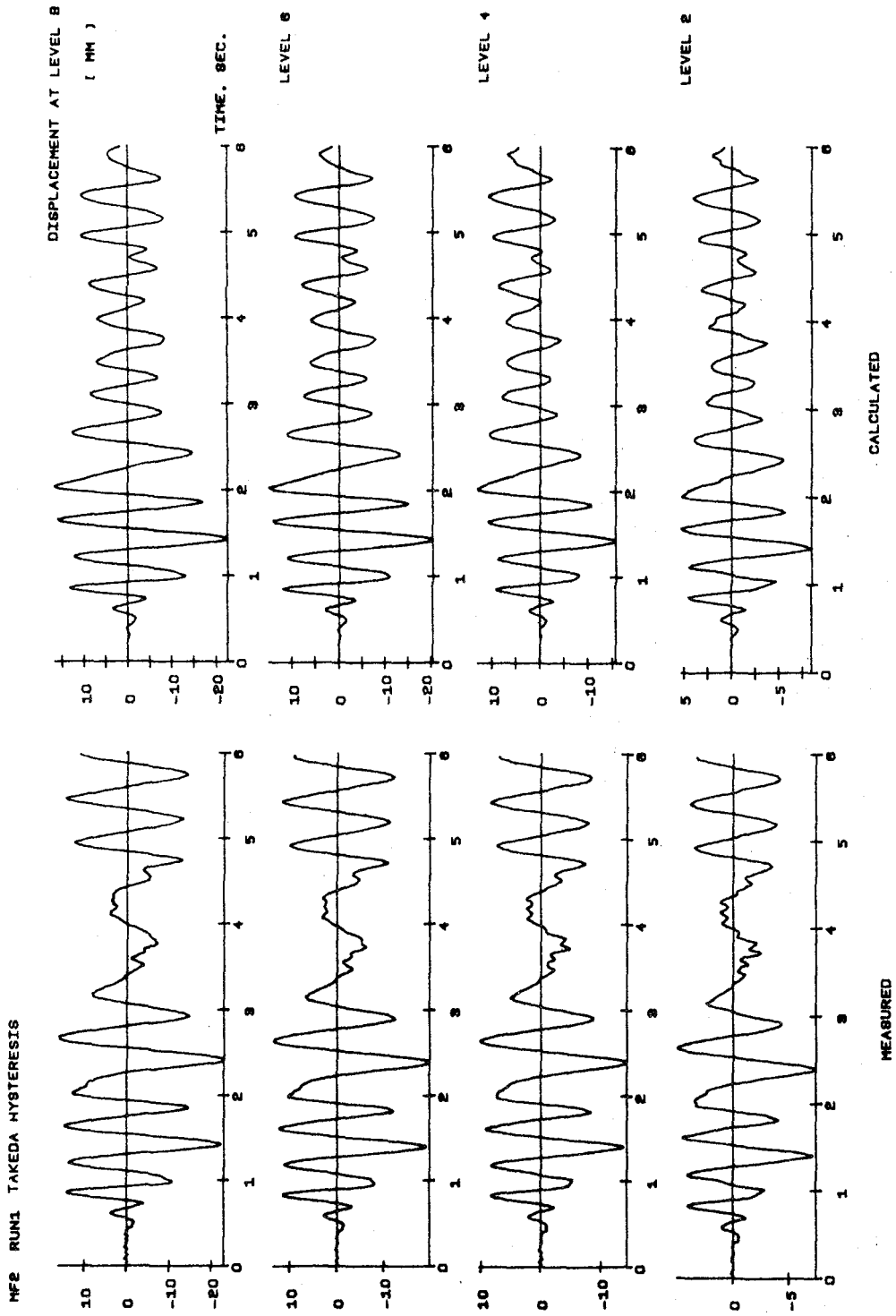


Fig. 4.3 (cont'd). Measured and Calculated Response for MF2

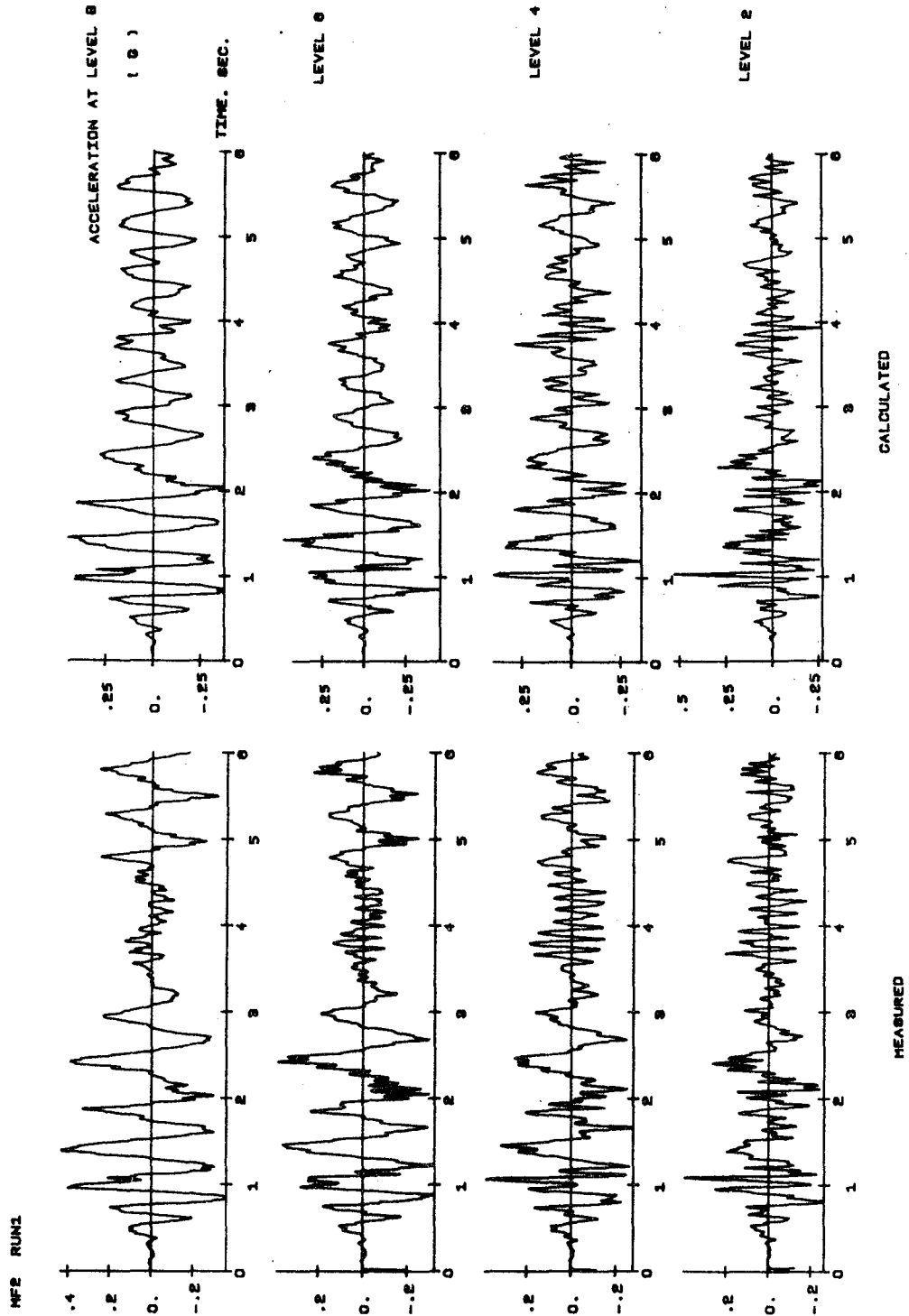


Fig. 4.3 (cont'd). Measured and Calculated Response for MF2

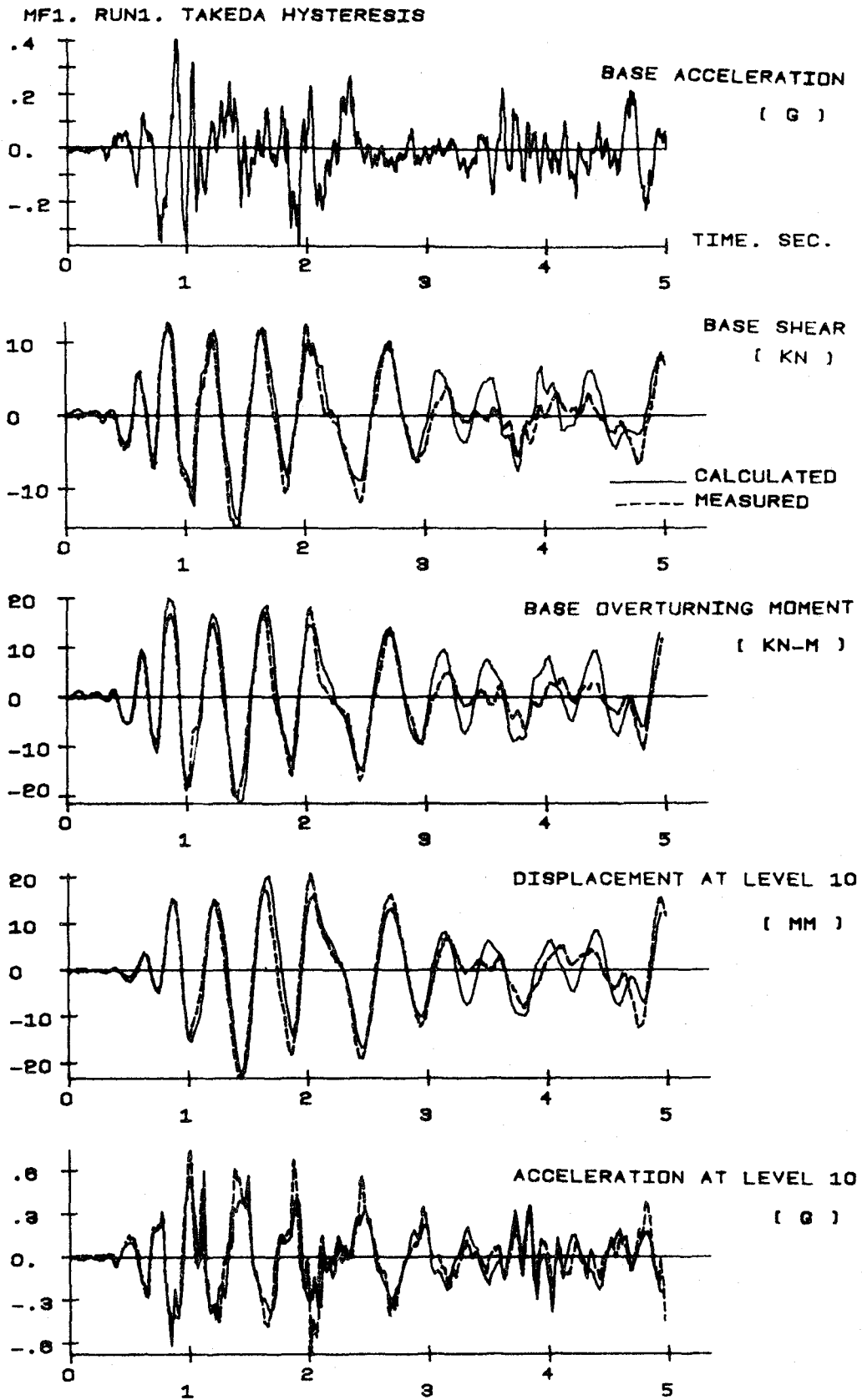


Fig. 4.4 Measured and Calculated Response for MF1 Using Takeda Hysteretic Model

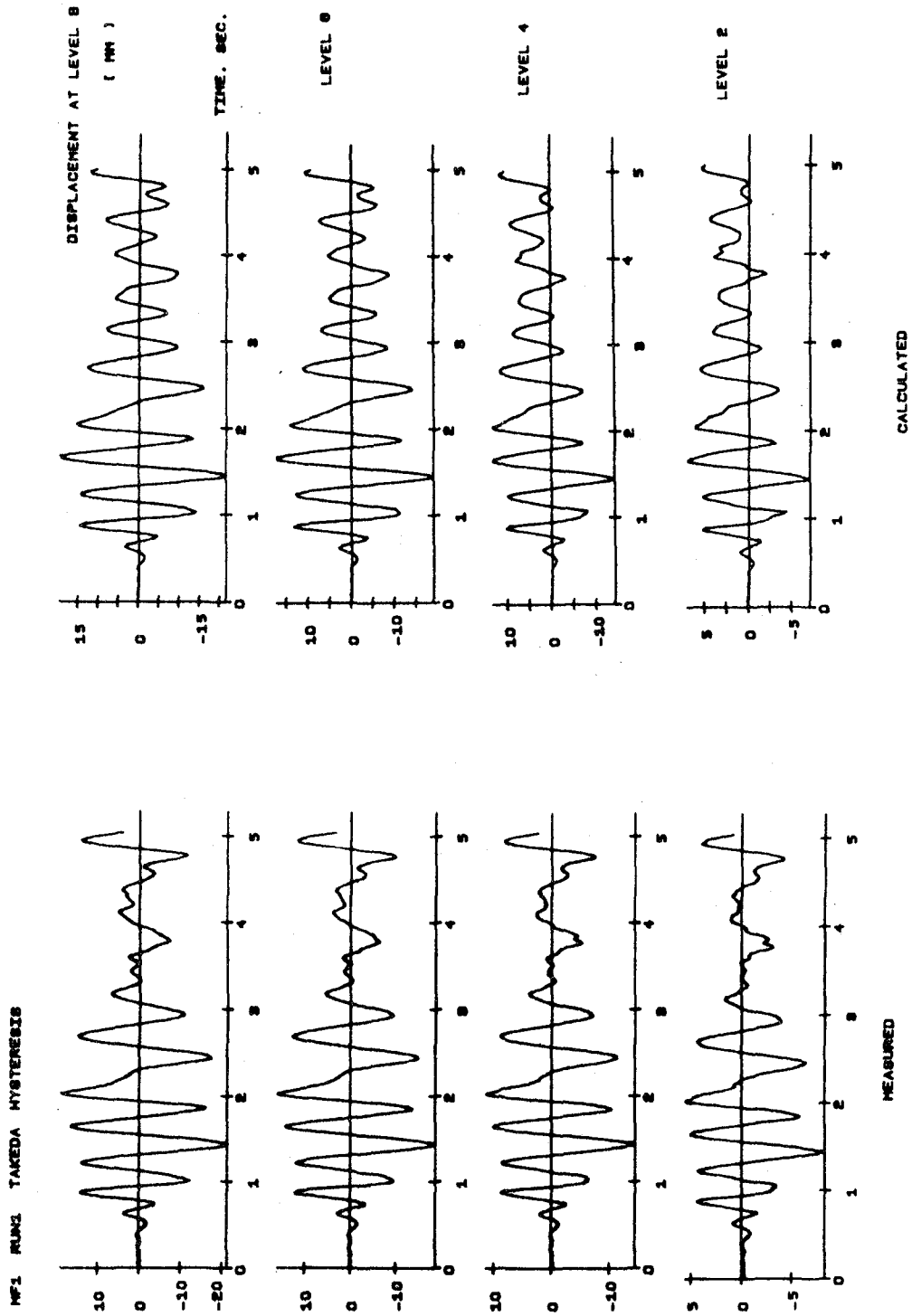


Fig. 4.4 (cont'd). Measured and Calculated Response for MFI Using Takeda Hysterisis Model

MF1 RUN1 TAKEDA HYSTERESIS

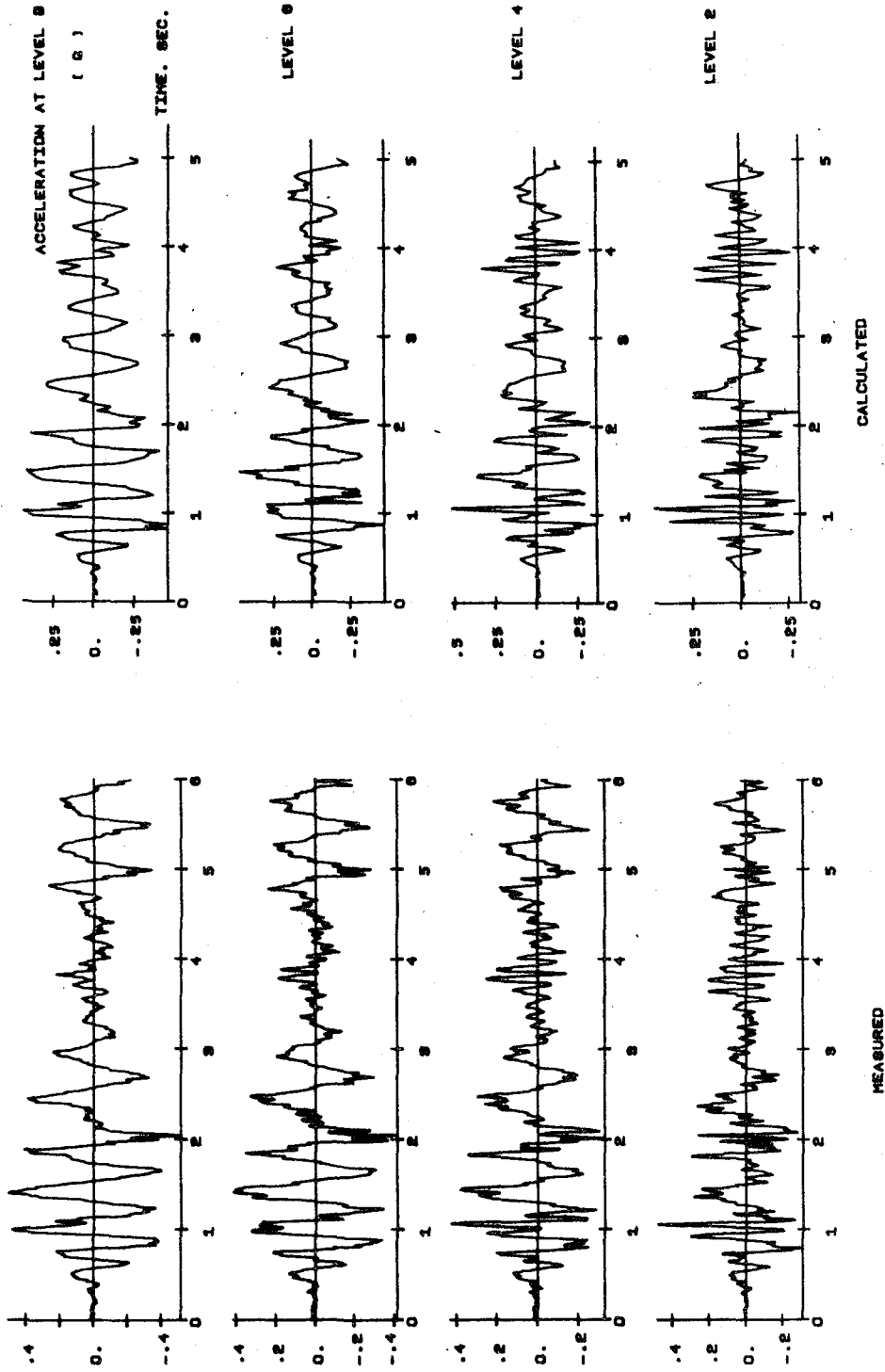


Fig. 4.4 (cont'd). Measured and Calculated Response for MF1 Using Takeda Hysterisis Model

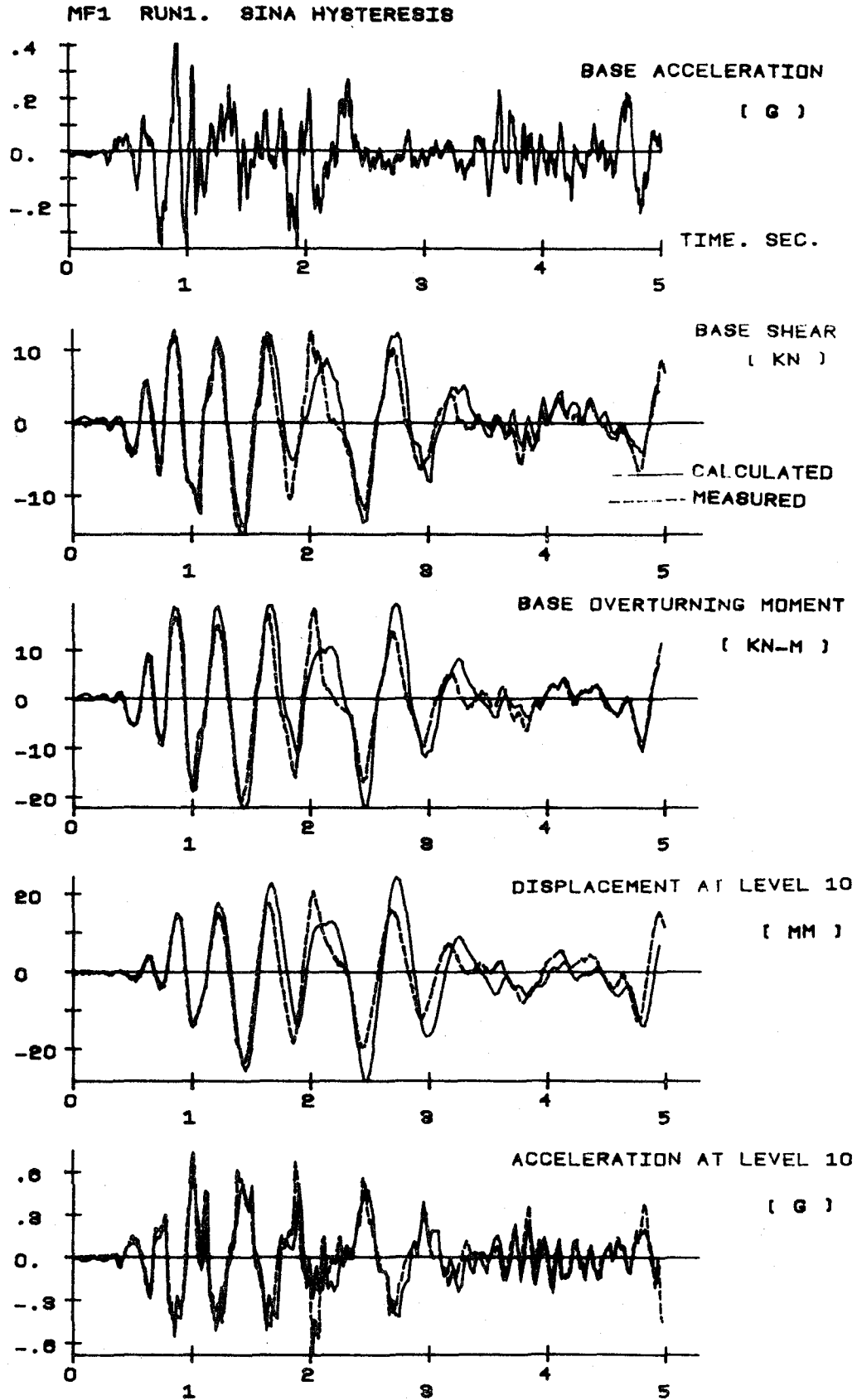


Fig. 4.5 Measured and Calculated Response for MF1 Using Sina Hysteresis Model

MF1 RUN1 SINA HYSTERESIS

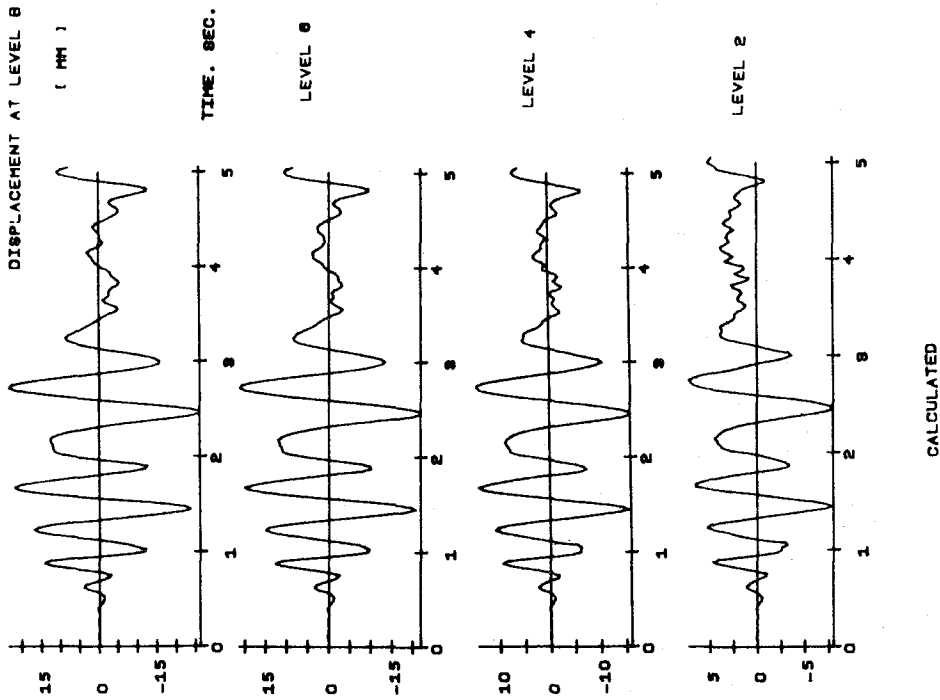
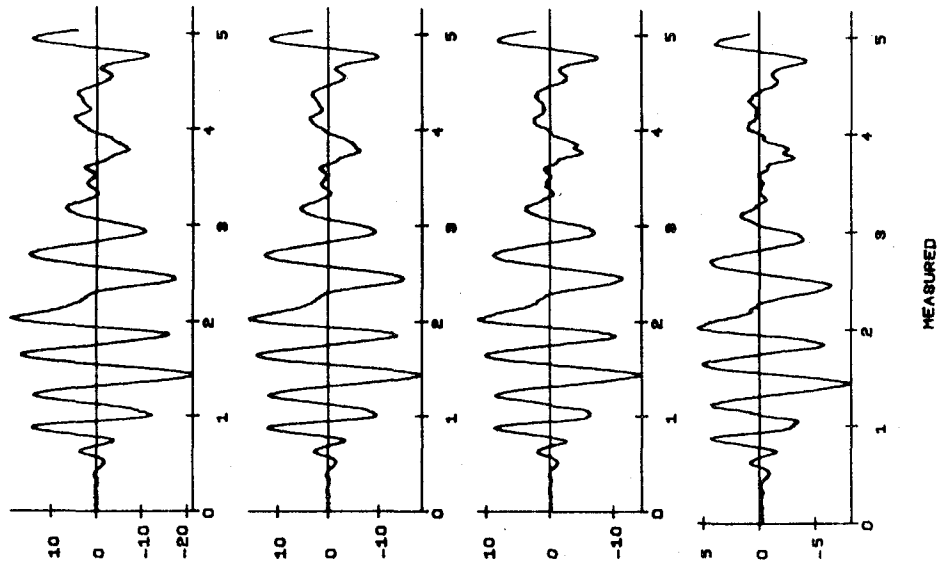


Fig. 4.5 (cont'd). Measured and Calculated Response for MF1 Using Sina Hysteresis Model

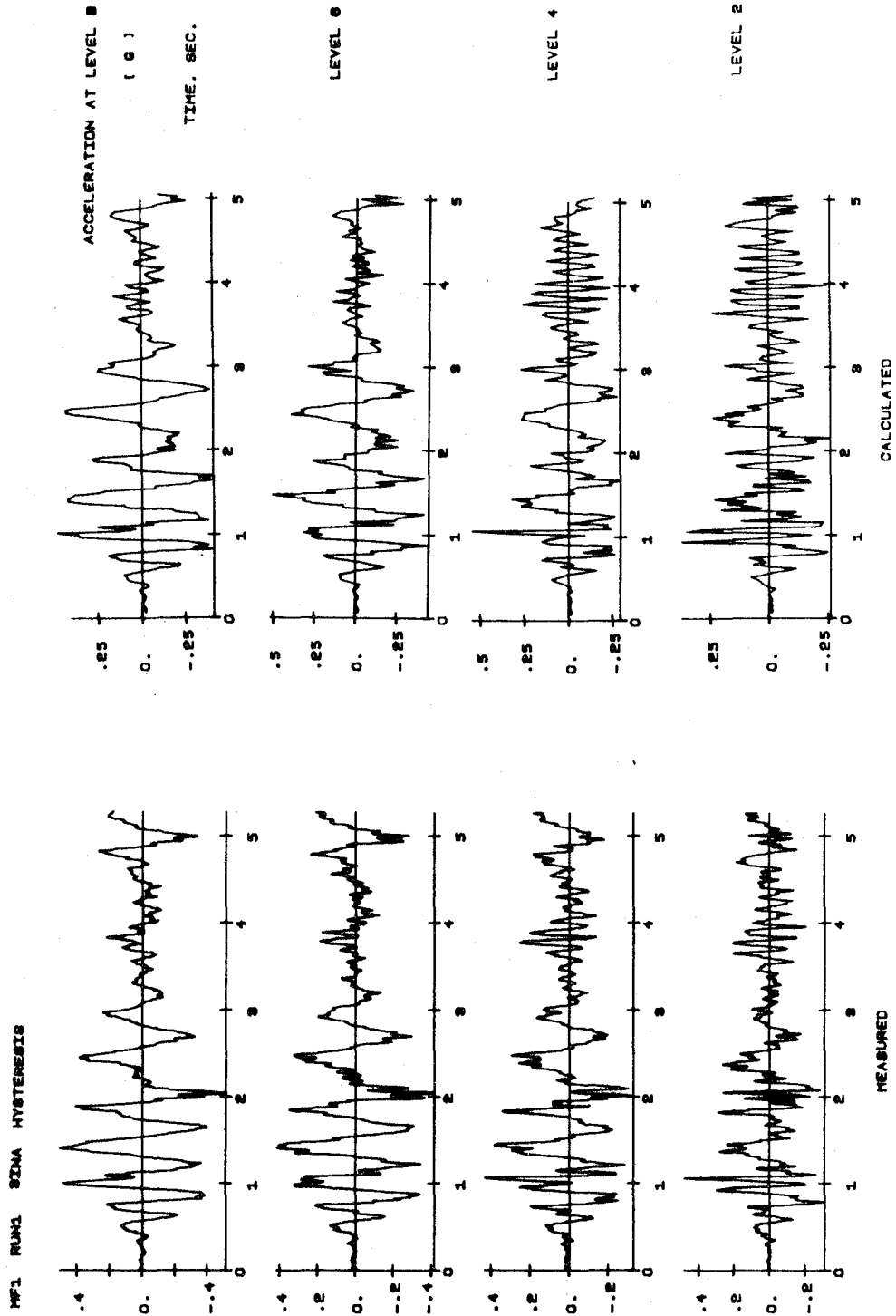


Fig. 4.5 (cont'd). Measured and Calculated Response for MF1 Using Sina Hysteresis Model

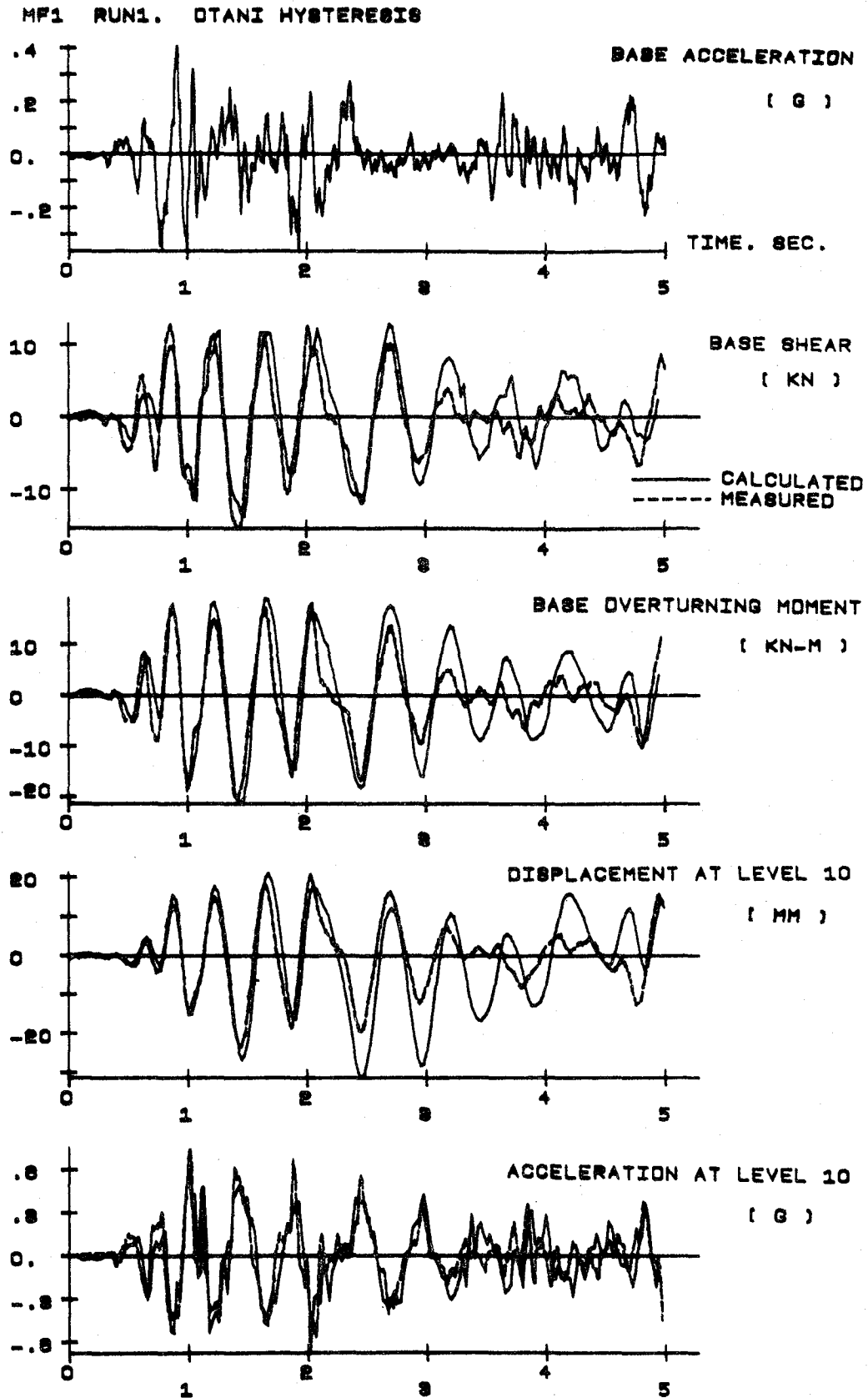


Fig. 4.6 Measured and Calculated Response for MF1 Using Otani Hysteresis Model

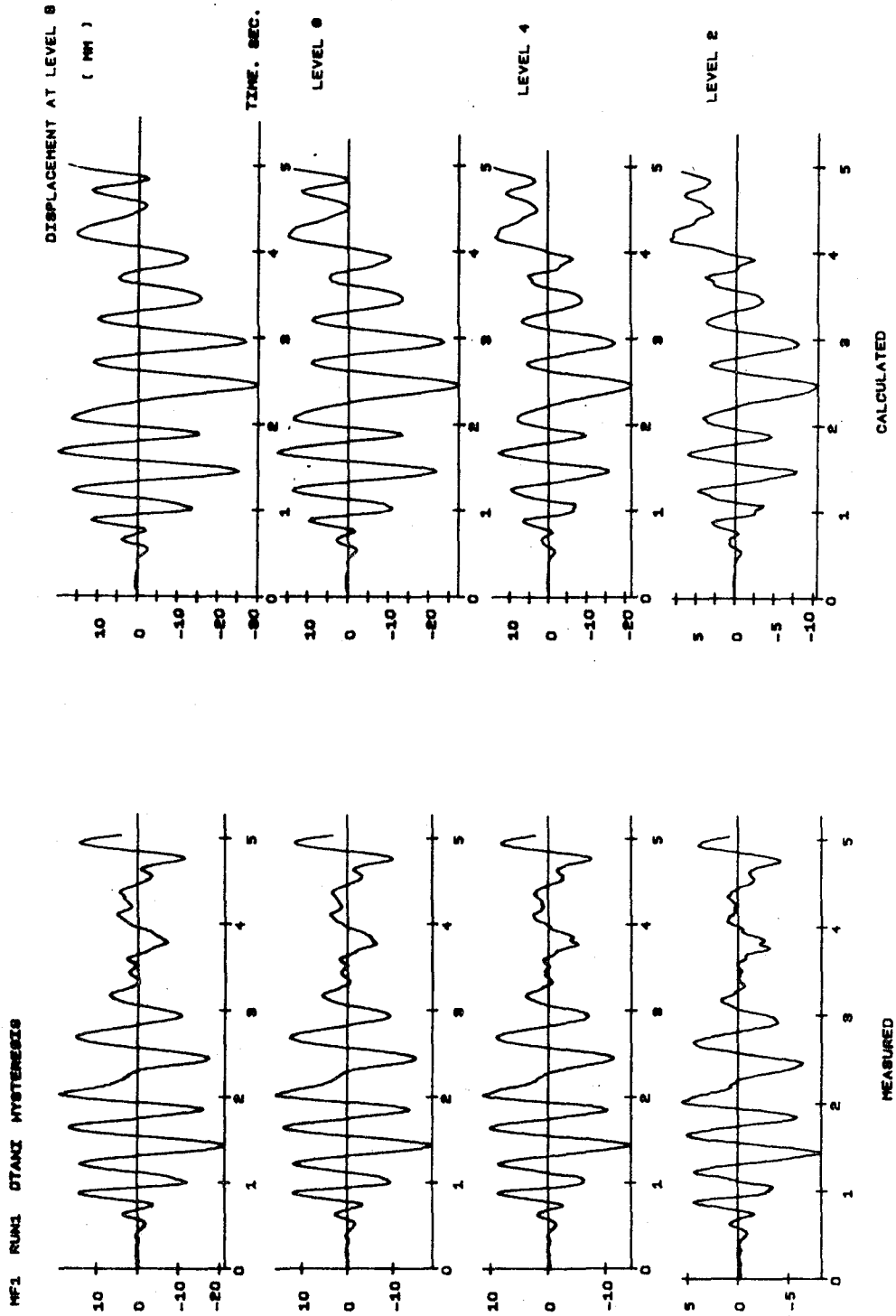


Fig. 4.6 (cont'd). Measured and Calculated Response for MF1 Using Otani Hysteresis Model

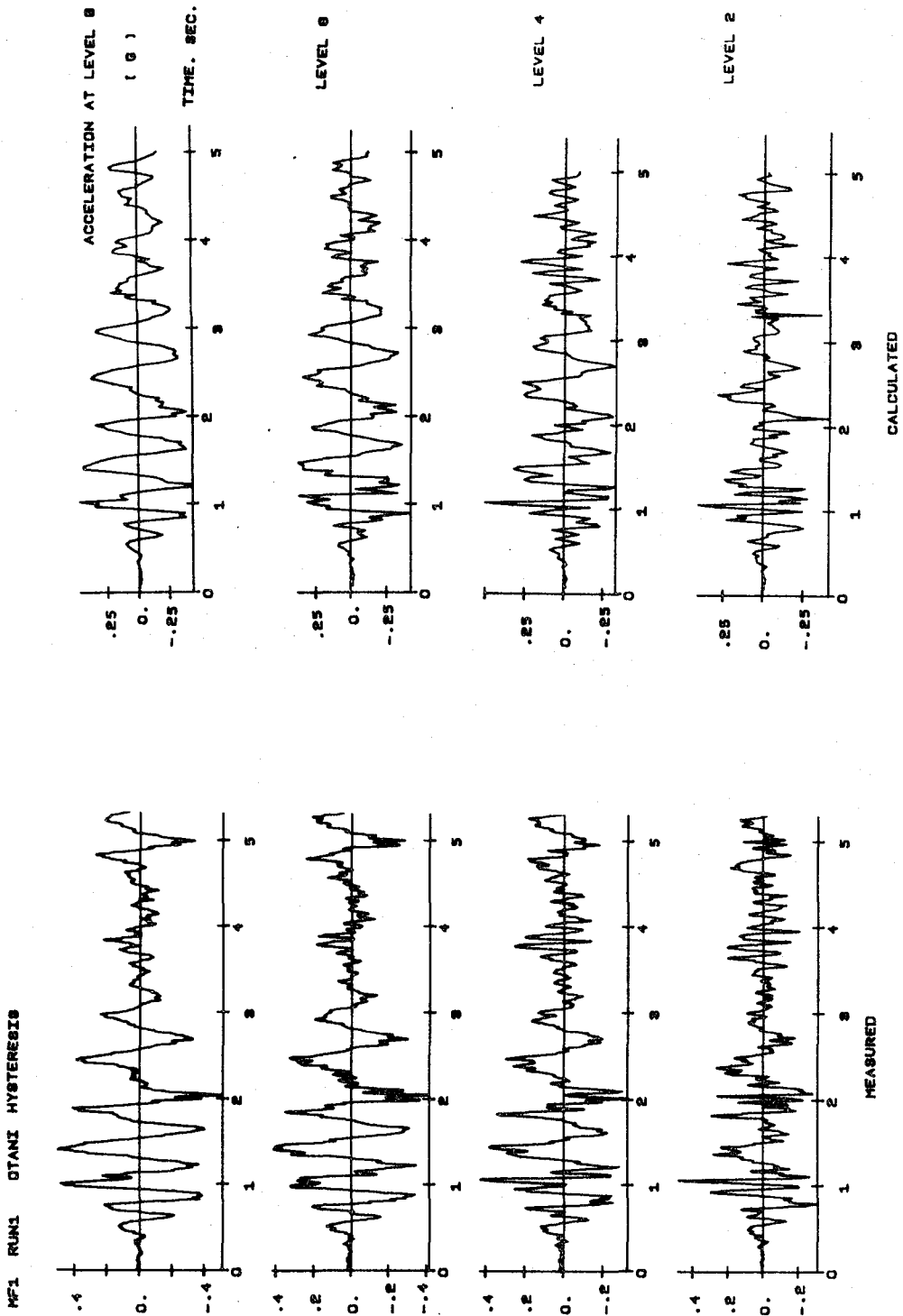


Fig. 4.6 (cont'd). Measured and Calculated Response for MF1 Using Otani Hysteresis Model

MF1 RUN1. BILINEAR HYSTERESIS

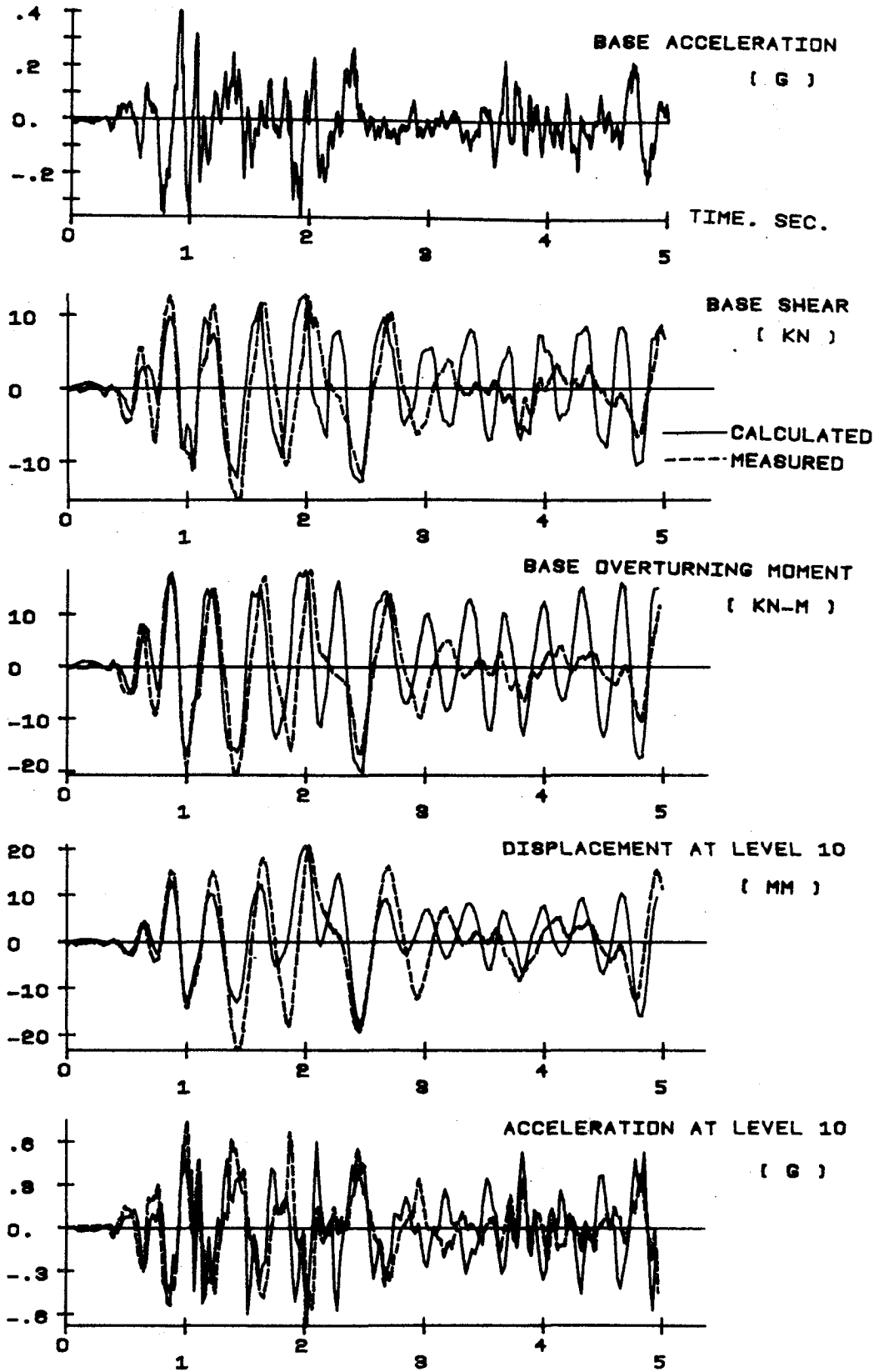


Fig. 4.7 Measured and Calculated Response for MF1 Using Bilinear Hysteresis Model

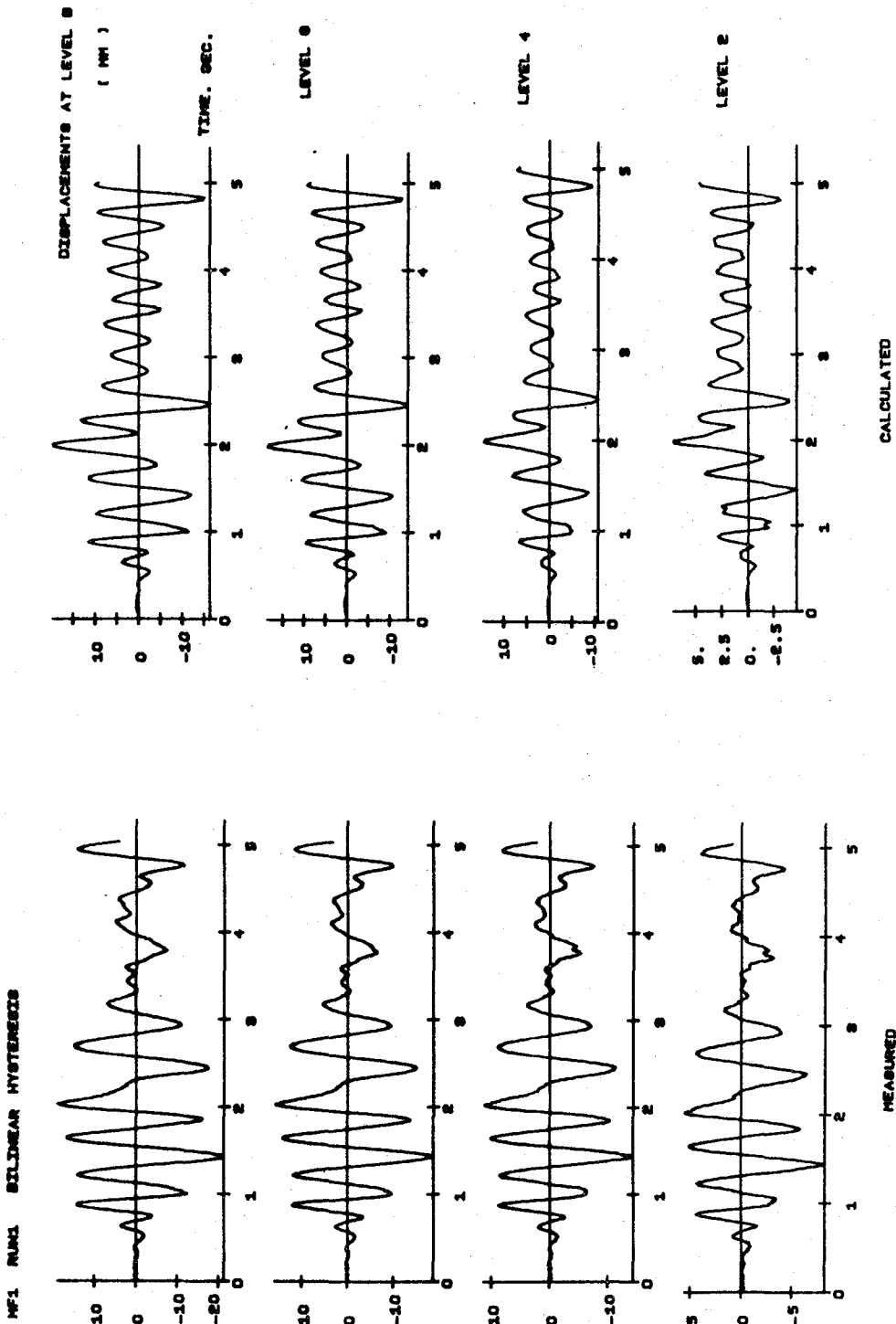


Fig. 4.7 (cont'd). Measured and Calculated Response for MF1 Using Bilinear Hysteresis Model

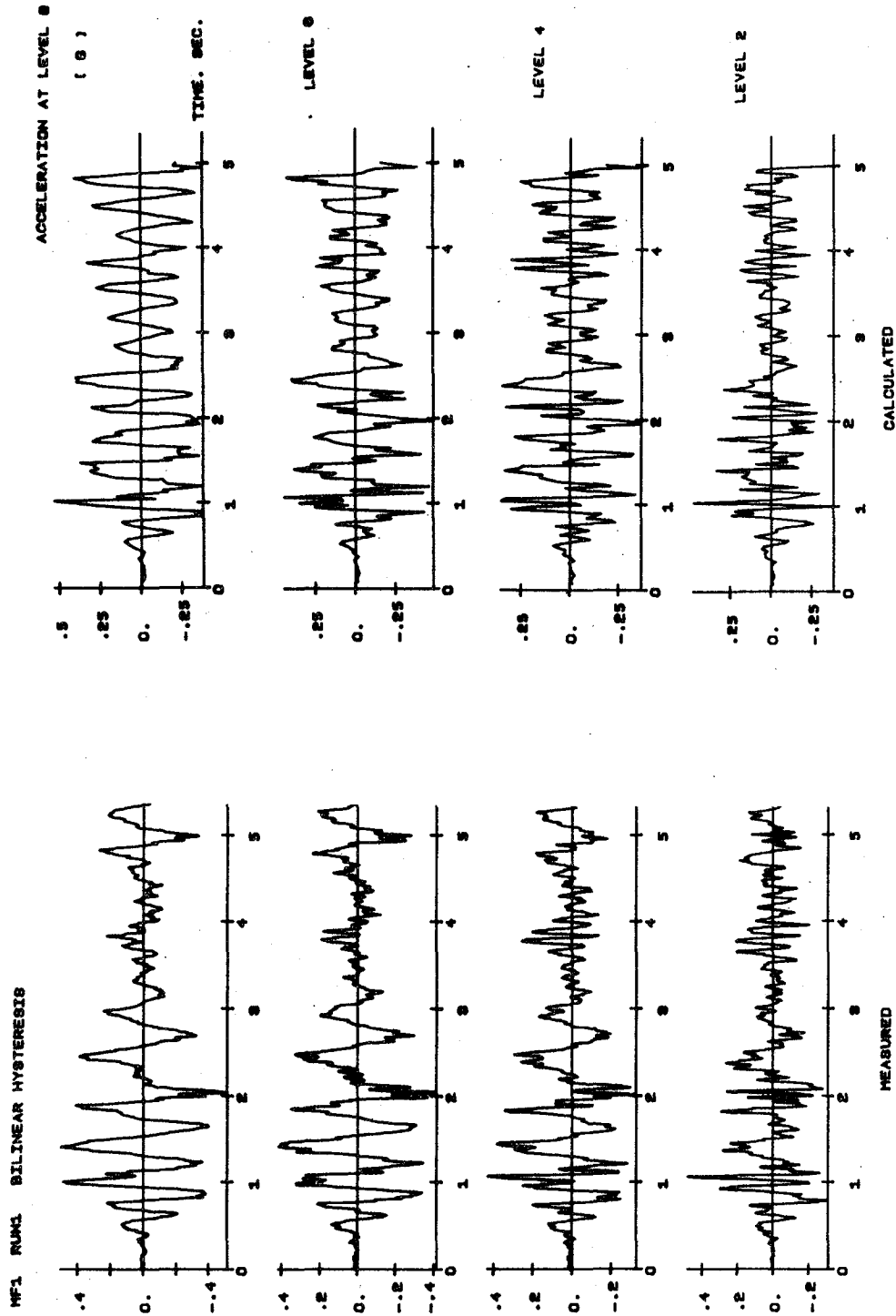


Fig. 4.7 (cont'd). Measured and Calculated Response for MFI Using Bilinear Hysteresis Model

MF1 RUN1. Q-HYST HYSTERESIS

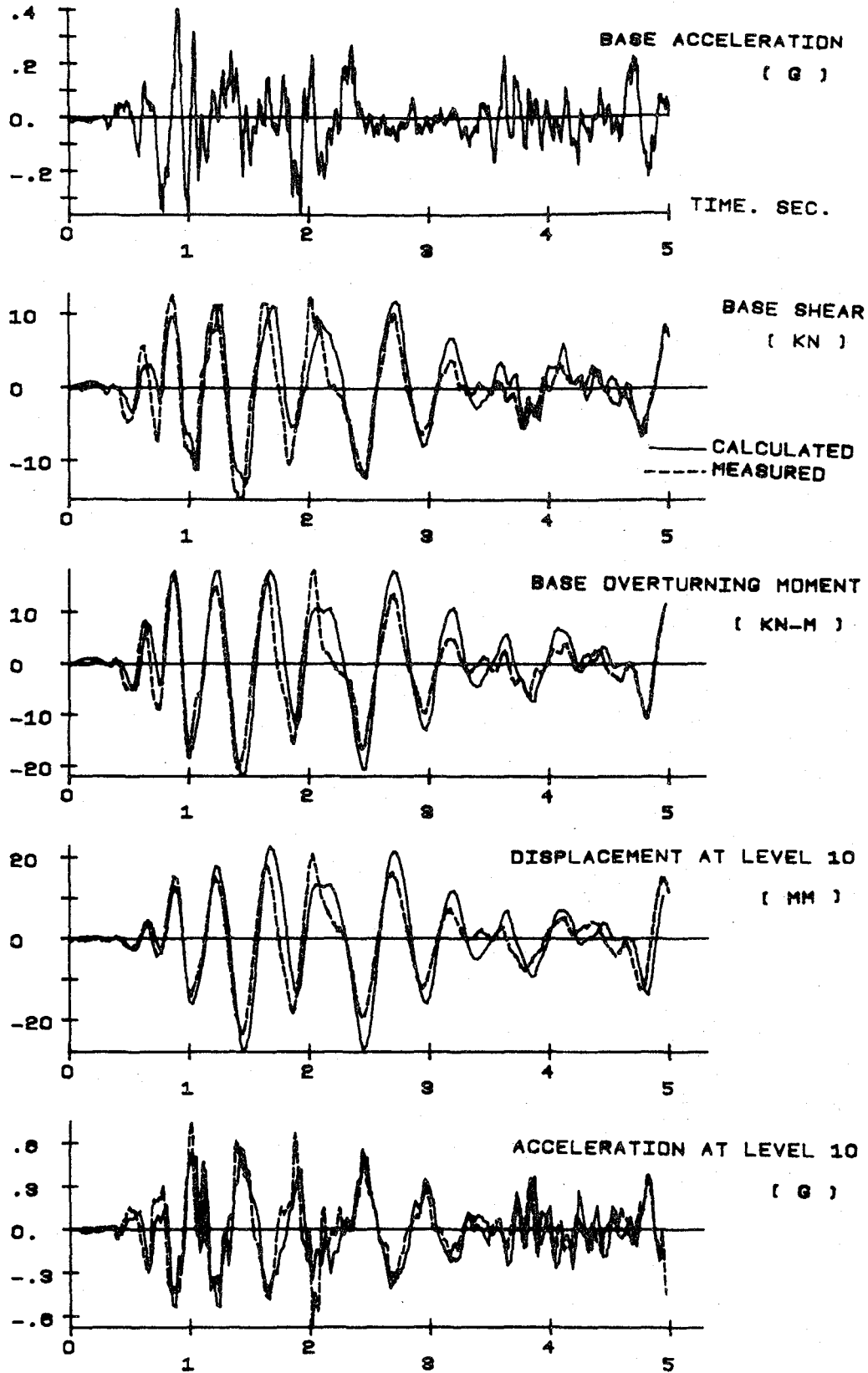


Fig. 4.8 Measured and Calculated Response for MF1 Using Q-Hyst Model

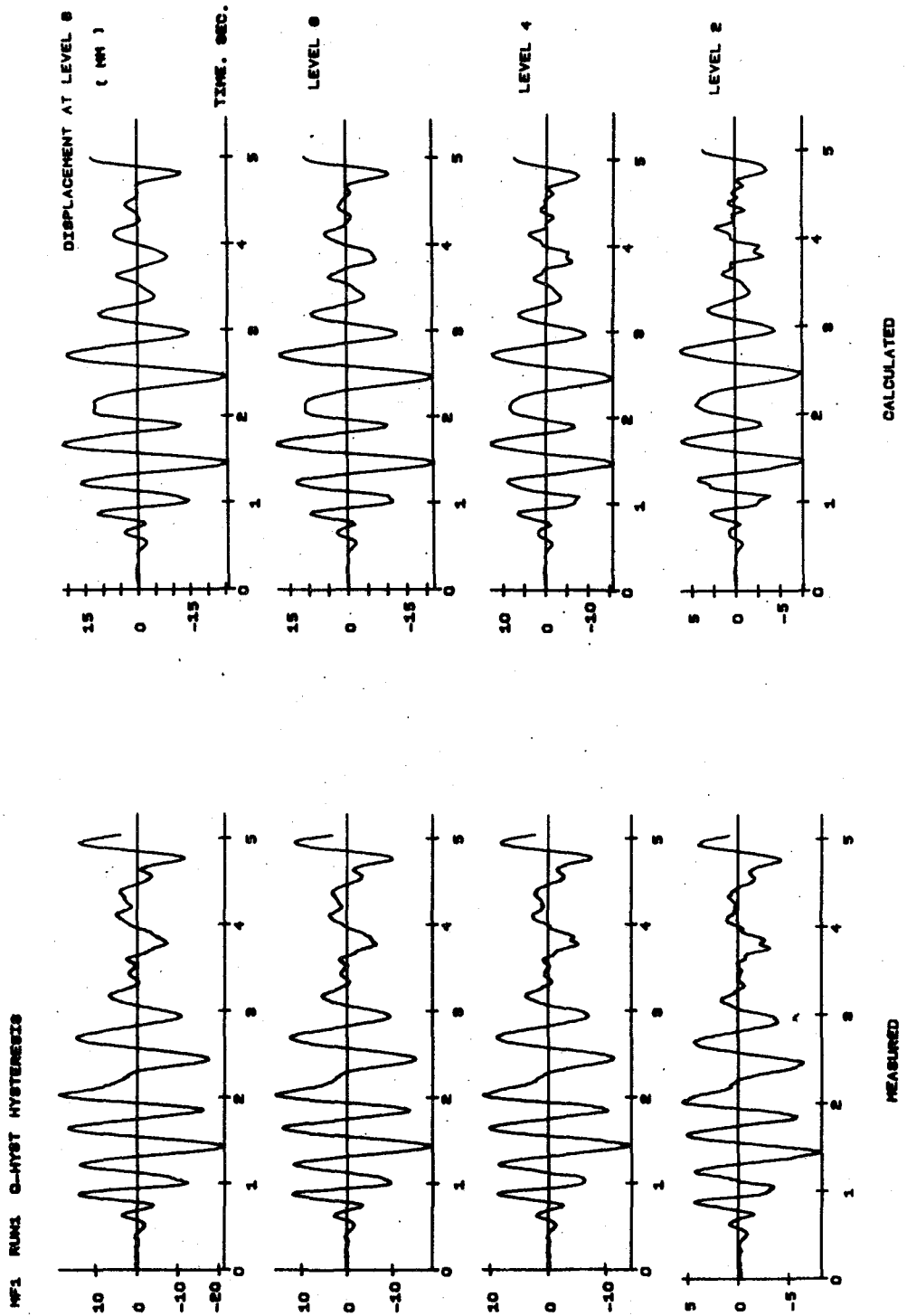


Fig. 4.8 (cont'd). Measured and Calculated Response for MF1 Using Q-Hyst Model

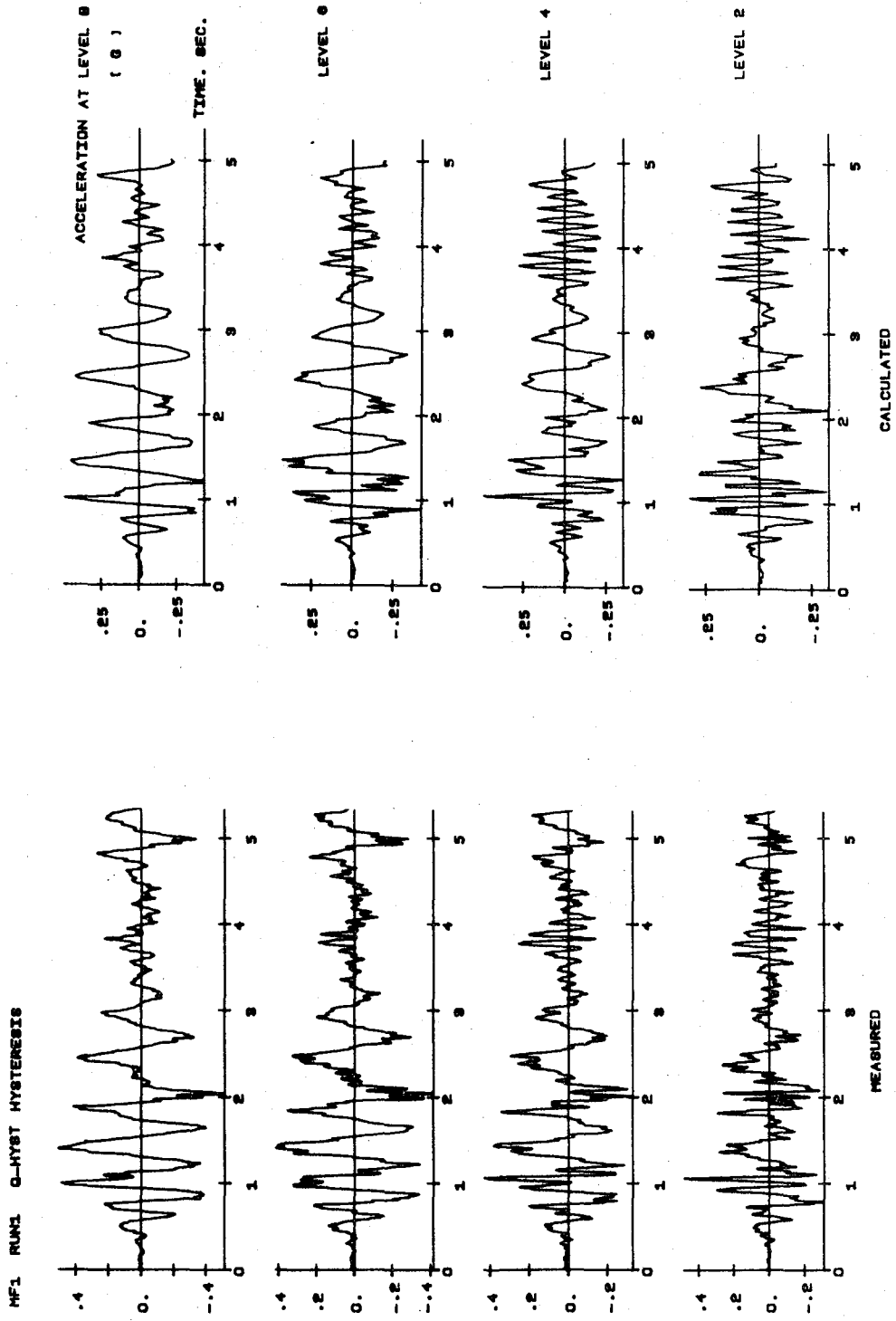


Fig. 4.8 (cont'd). Measured and Calculated Response for MF1 Using Q-Hyst Model

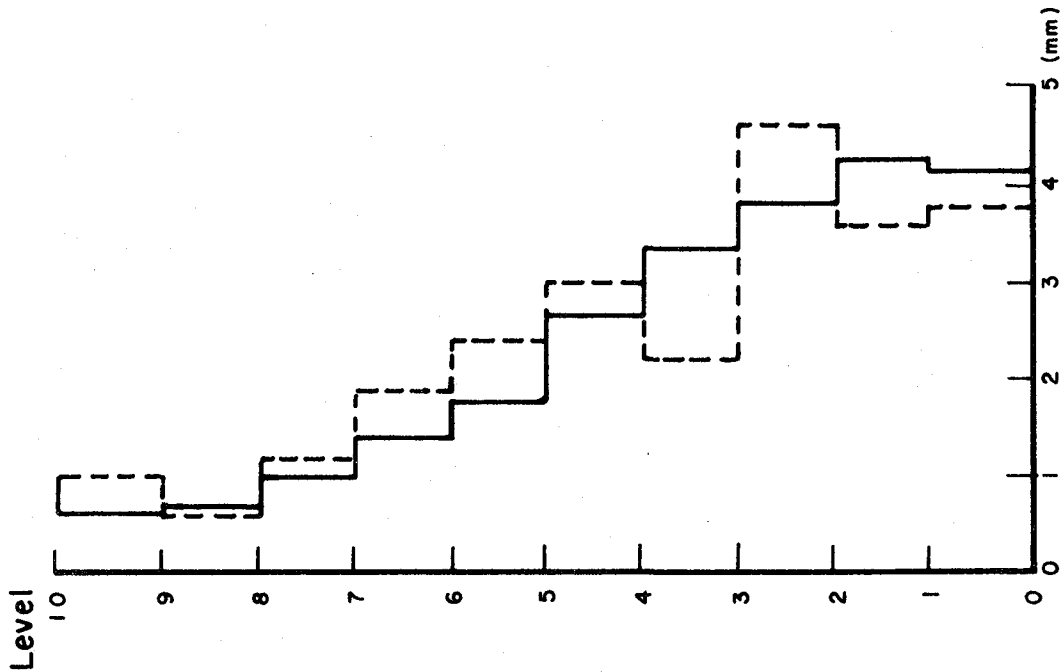


Fig. 5.2 Maximum Calculated and Measured Relative Story Displacements for MF2

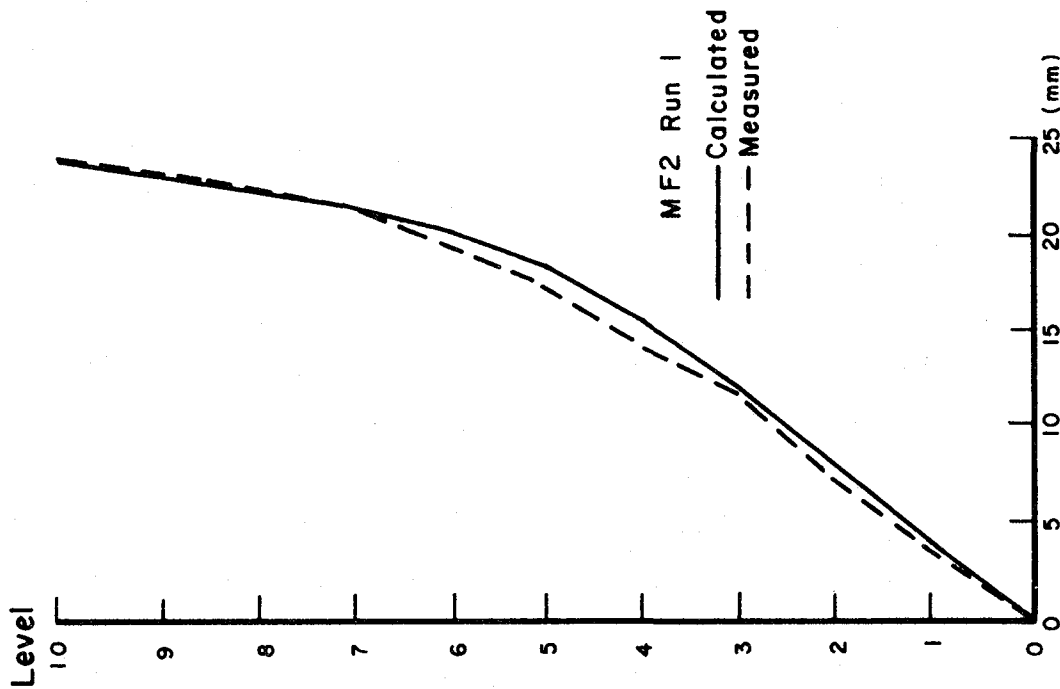


Fig. 5.1 Maximum Calculated and Measured Displacements (Single Amplitude) for MF2

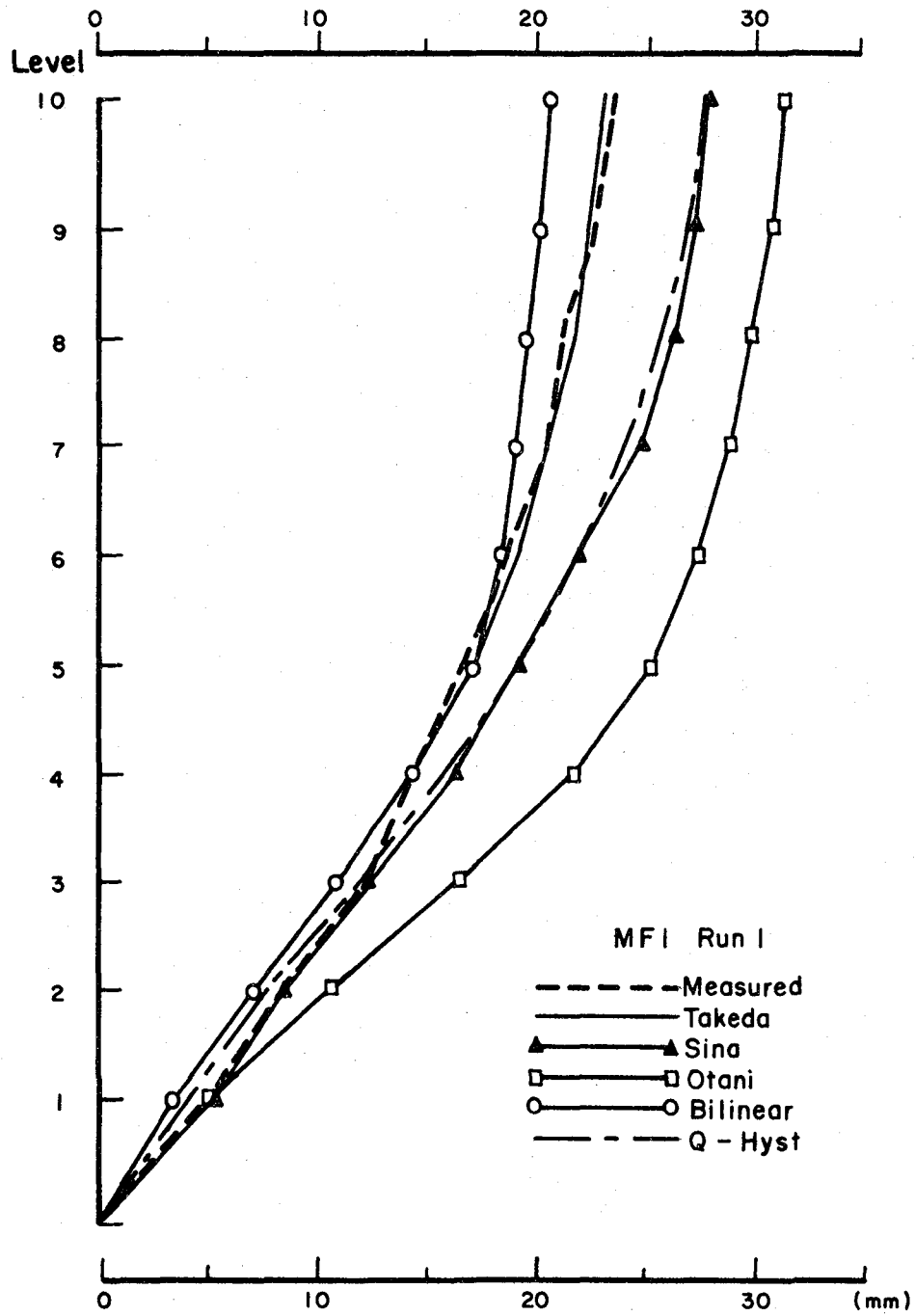


Fig. 5.3 Maximum Calculated and Measured Displacements (Single Amplitude) for MF1

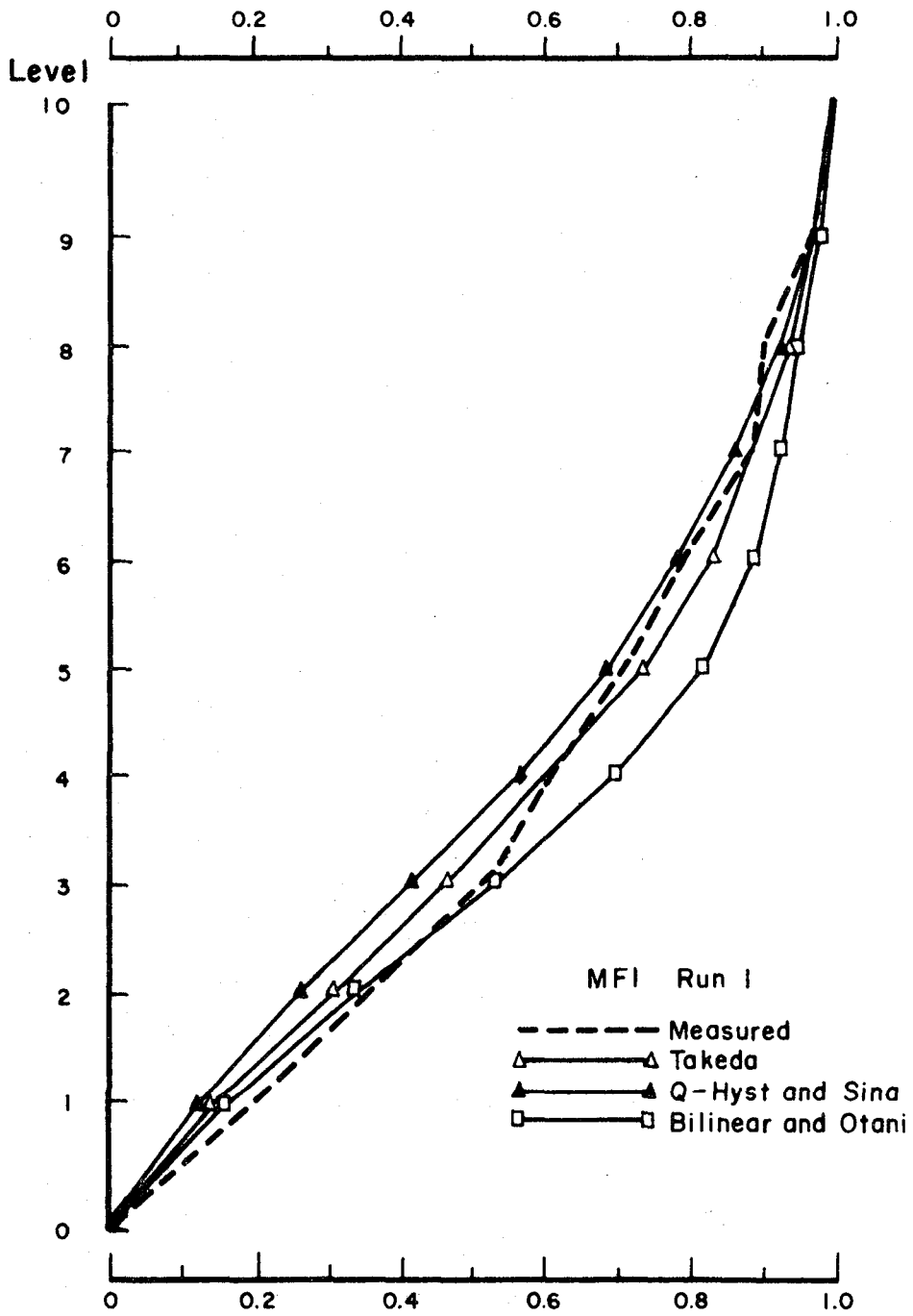


Fig. 5.4 Maximum Displacements Normalized with Respect to Top Level Displacement

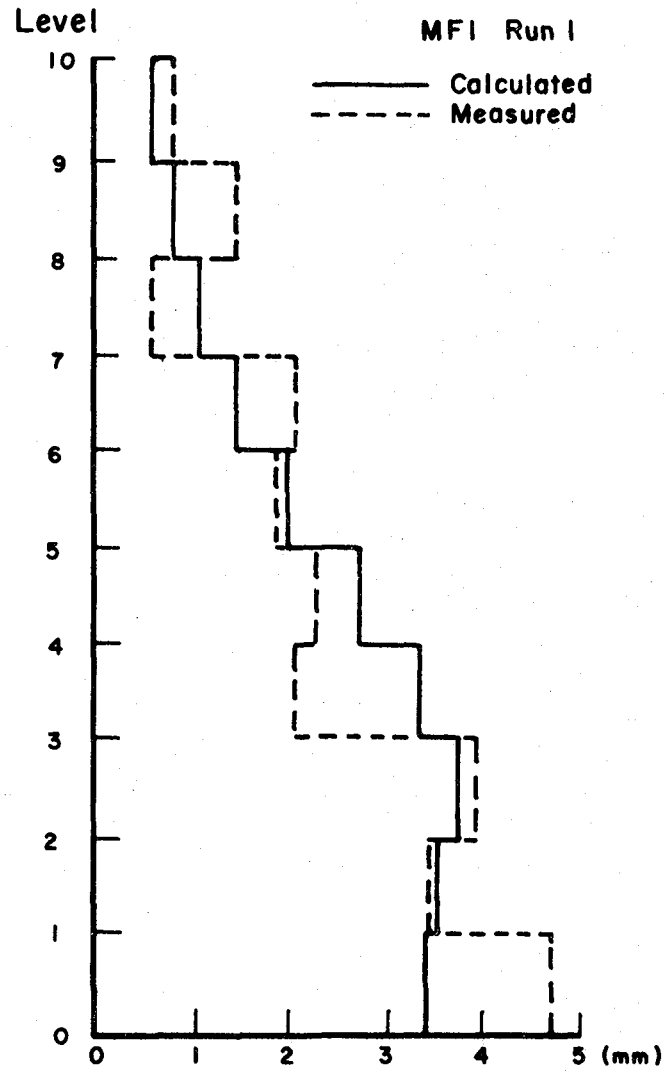


Fig. 5.5 Maximum Calculated (Using Takeda Model) and Measured Relative Story Displacements

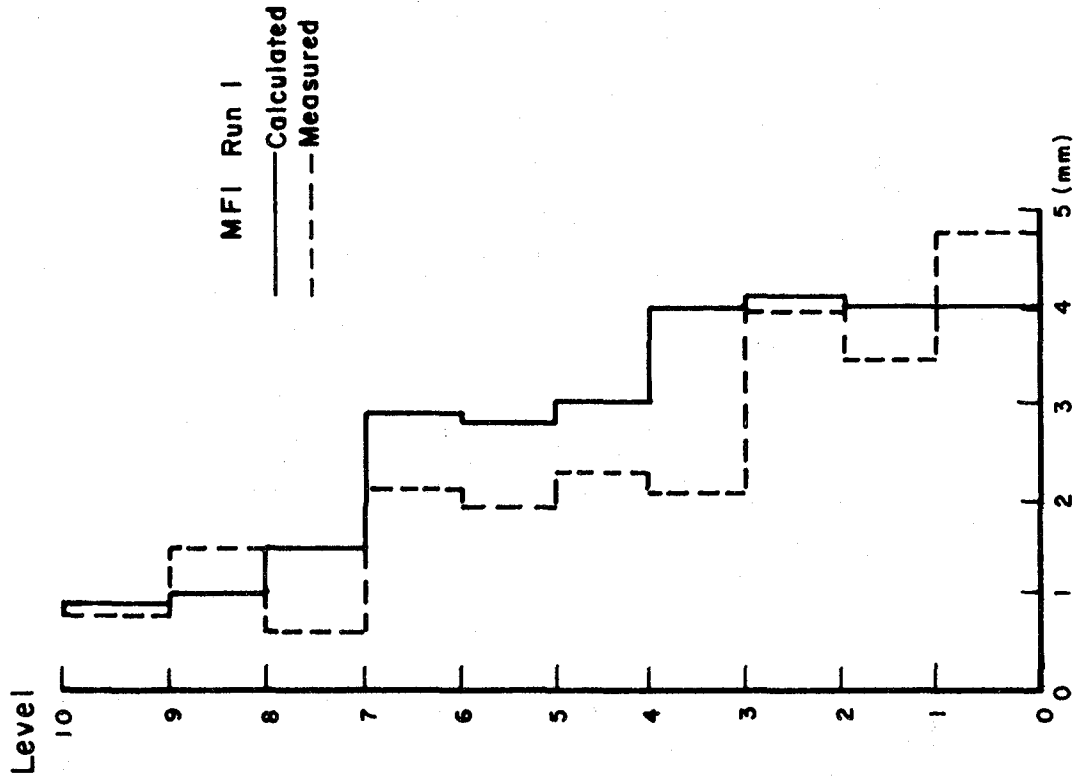
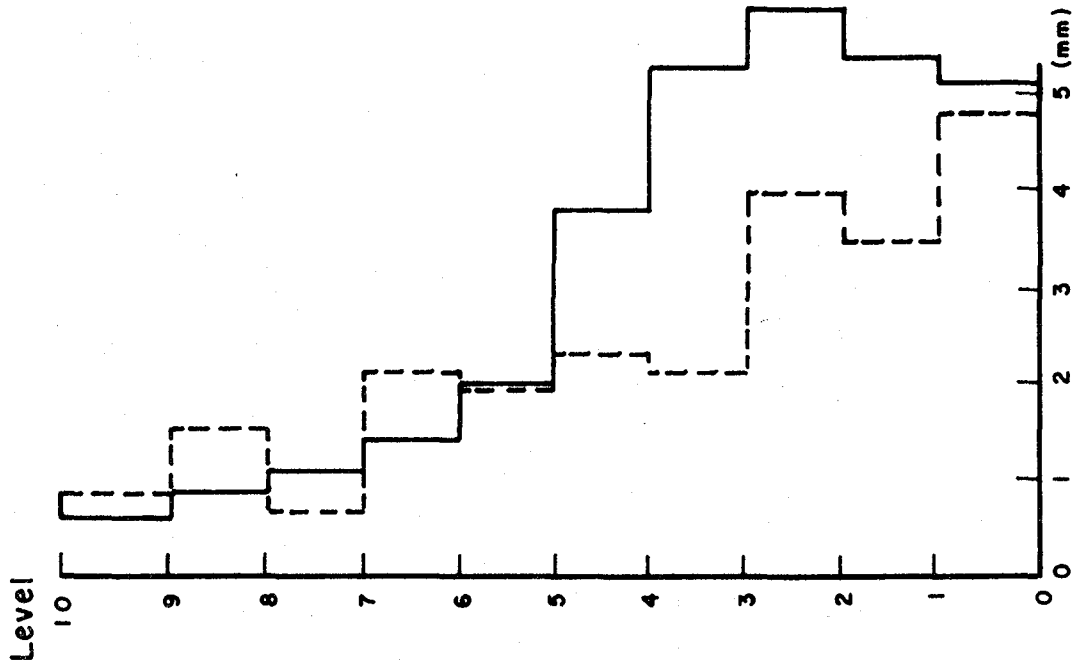


Fig. 5.6 Maximum Calculated (Using Sina Model) and Measured Relative Story Displacements

Fig. 5.7 Maximum Calculated (Using Otani Model) and Measured Relative Story Displacements

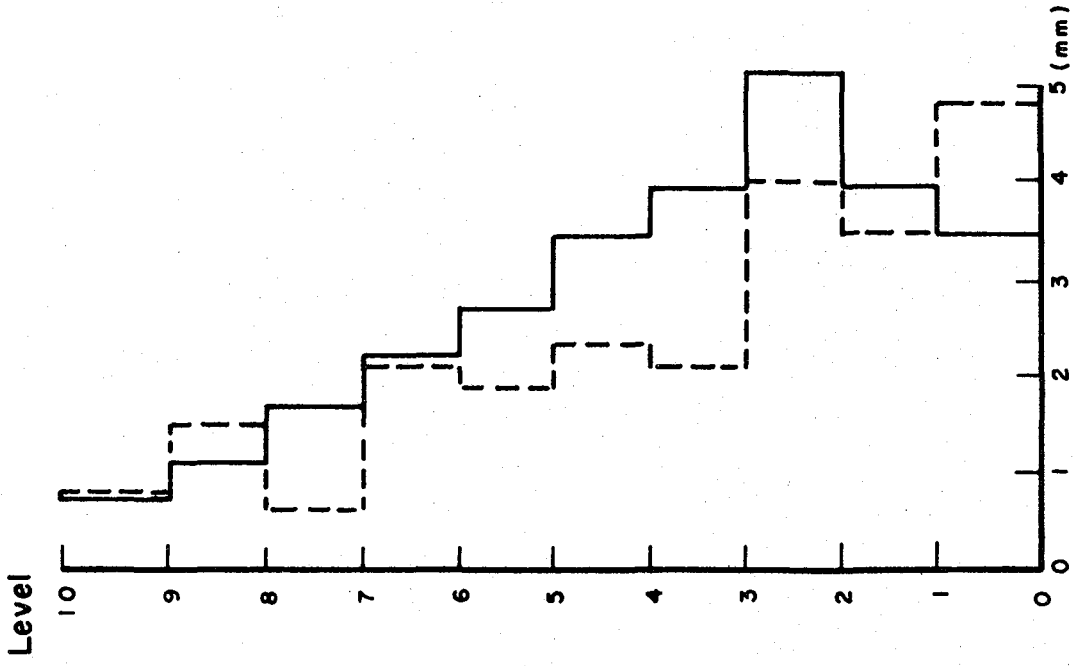


Fig. 5.9 Maximum Calculated (Using Q-hyst Model) and Measured Relative Story Displacements

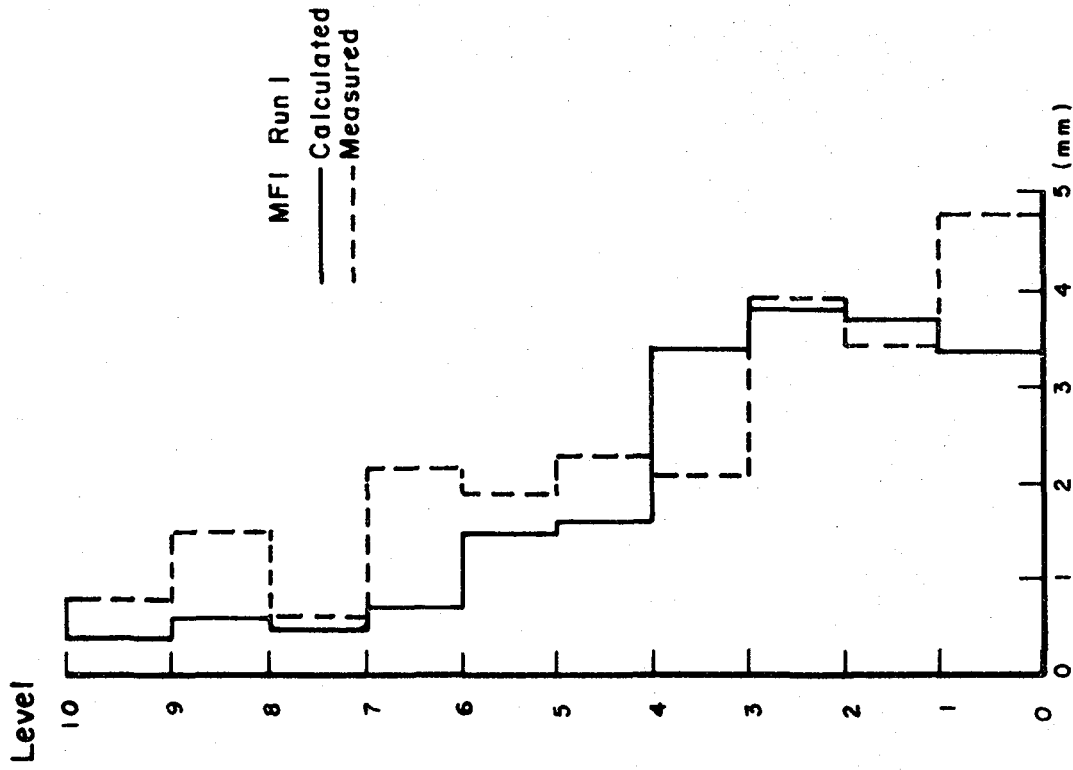


Fig. 5.8 Maximum Calculated (Using Bilinear Model) and Measured Relative Story Displacements

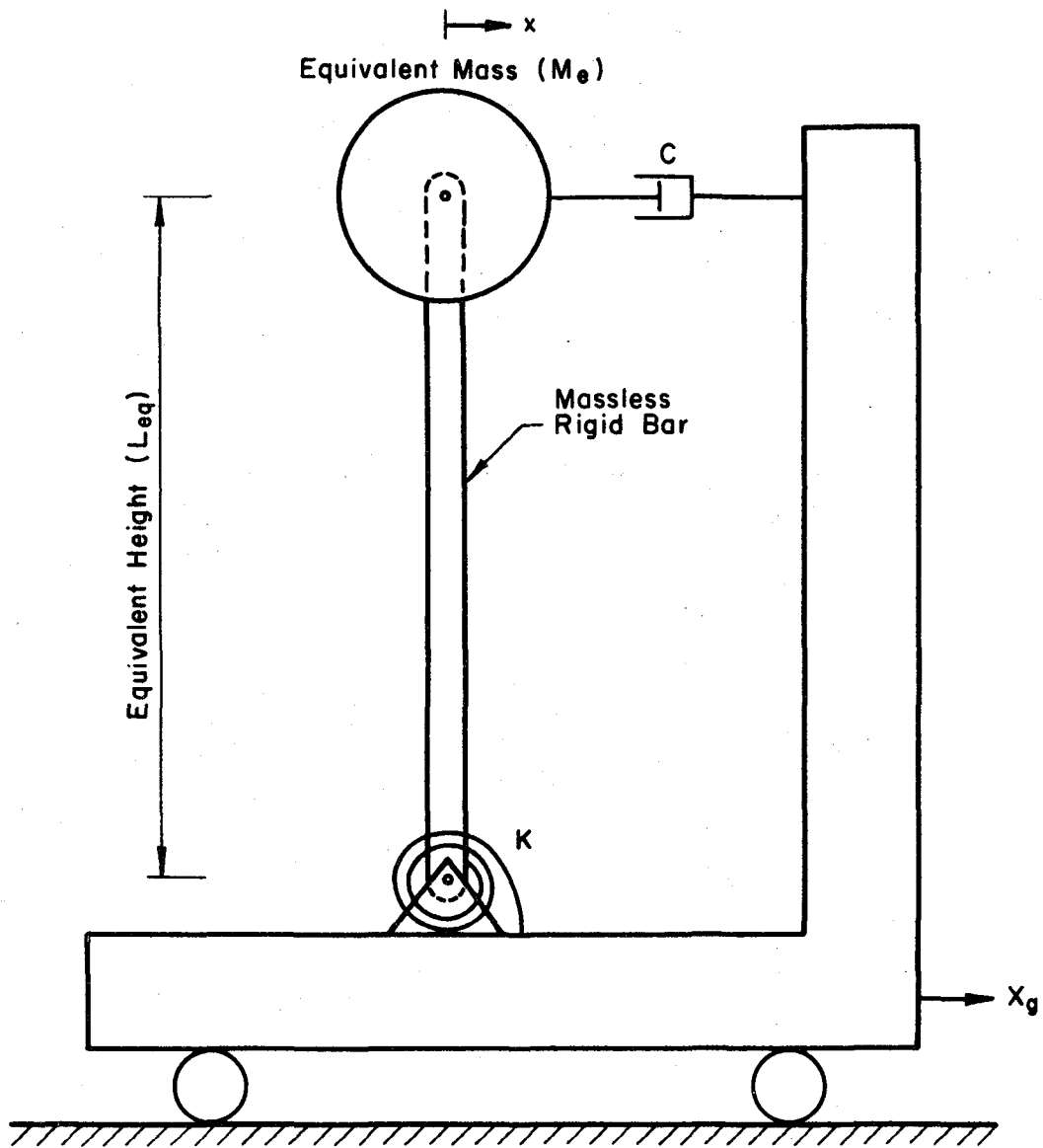


Fig. 6.1 The Q-Model

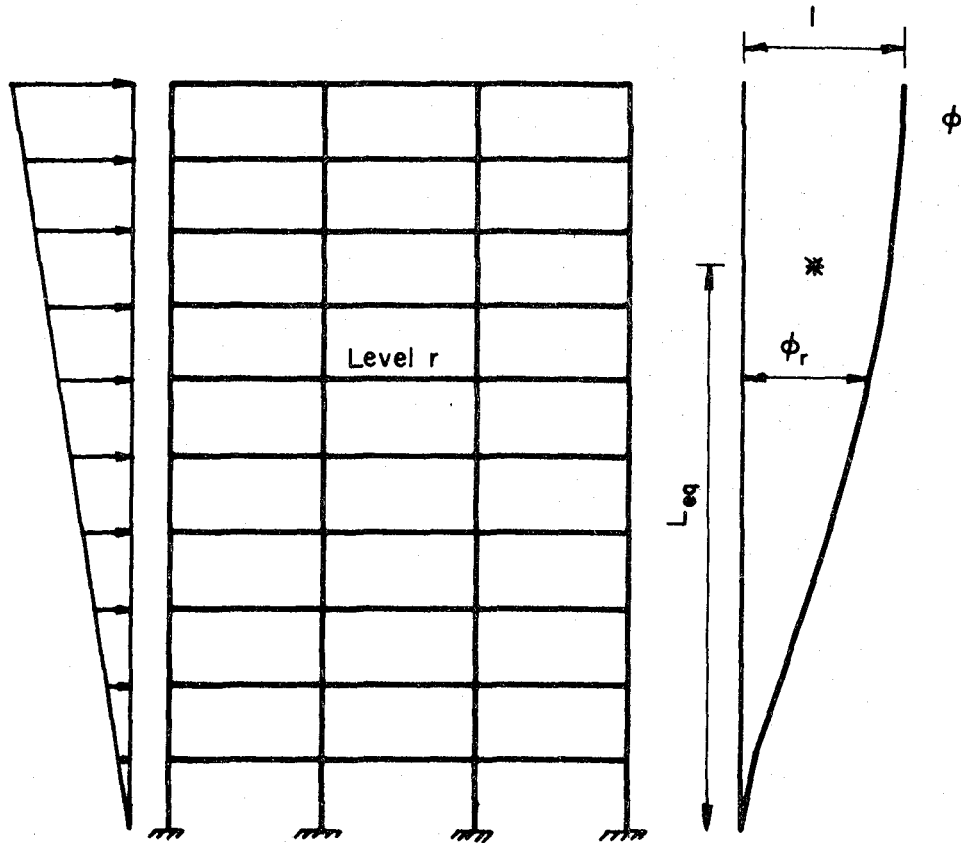


Fig. 6.2 Static Lateral Loads

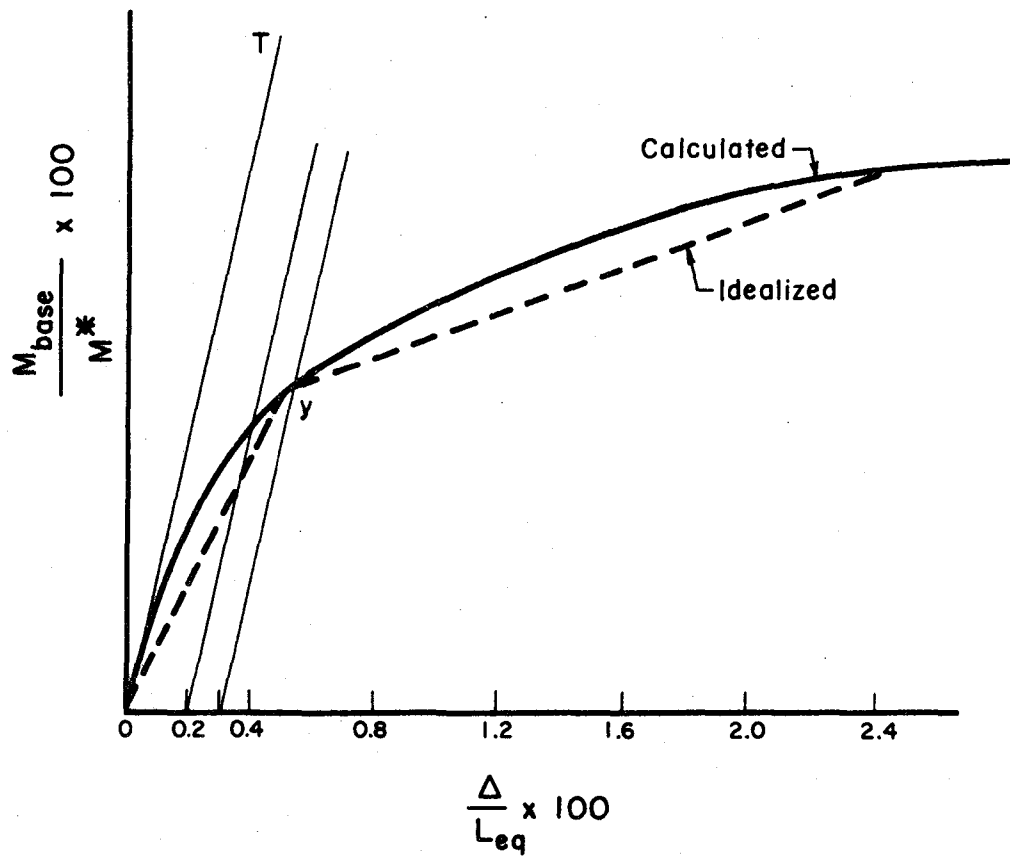
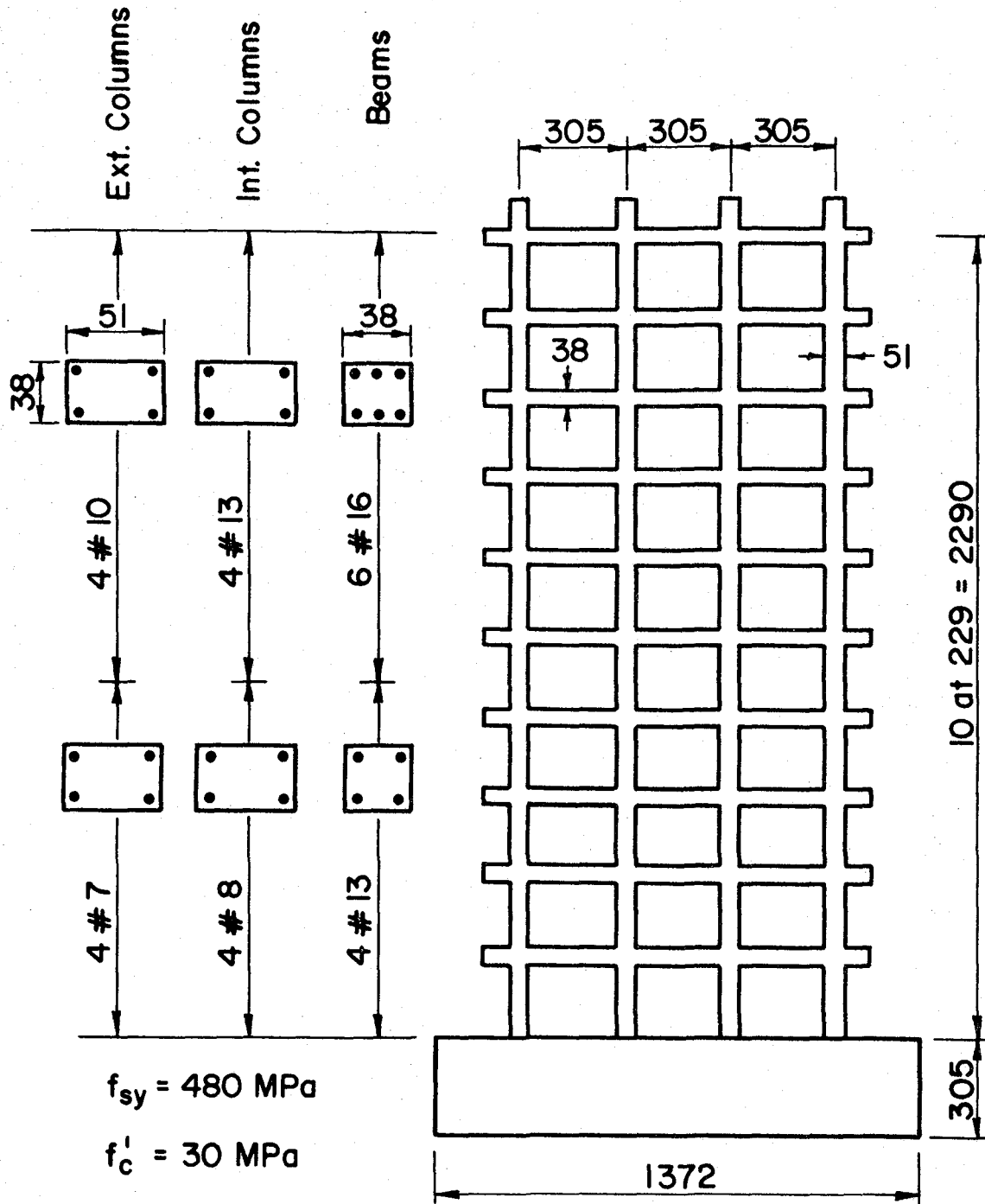


Fig. 6.3 Force-Displacement Relationships



indicate gage wire number (see Table 7.10)

Fig. 7.1 Longitudinal Reinforcement Distribution for Structures H1 and H2

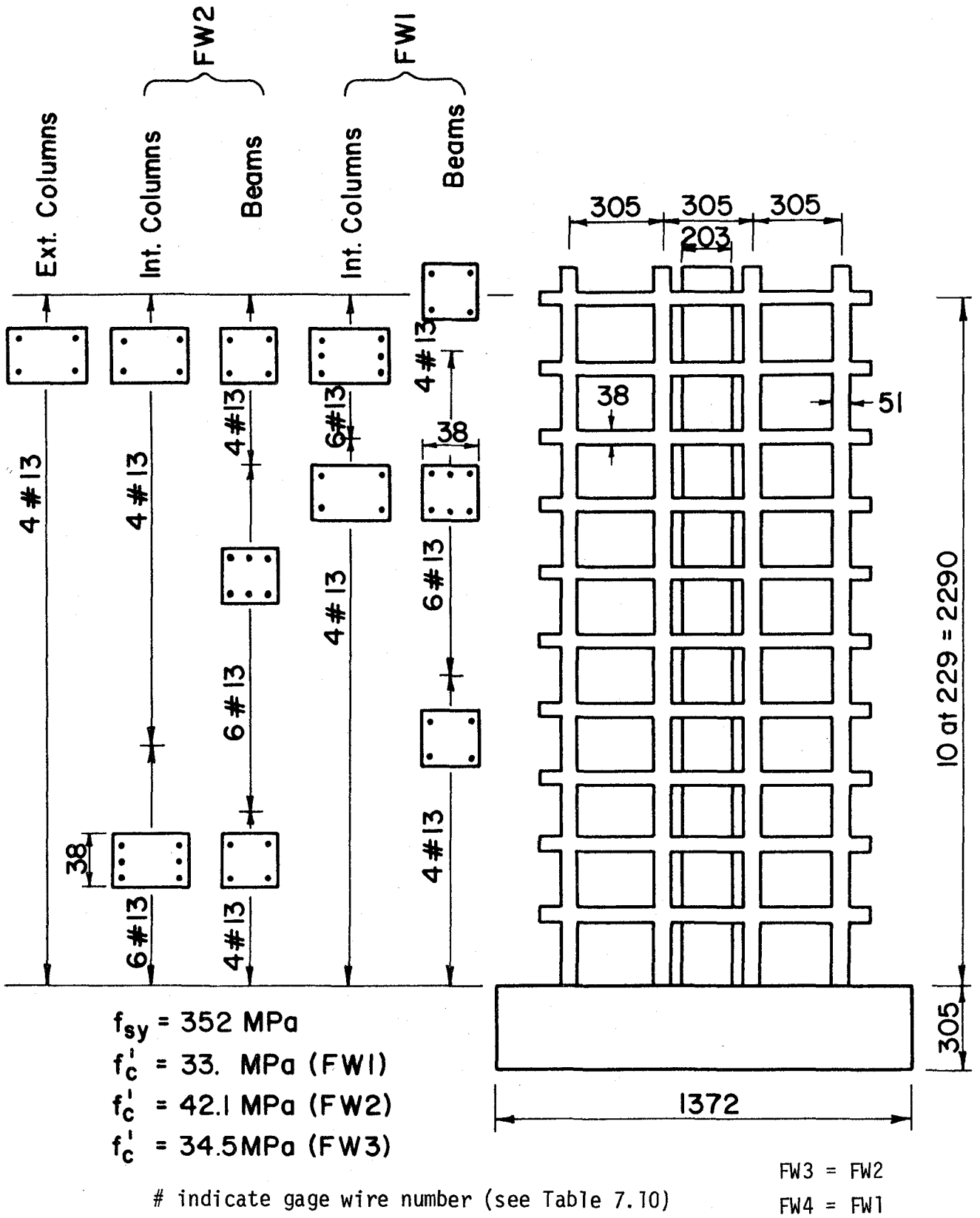
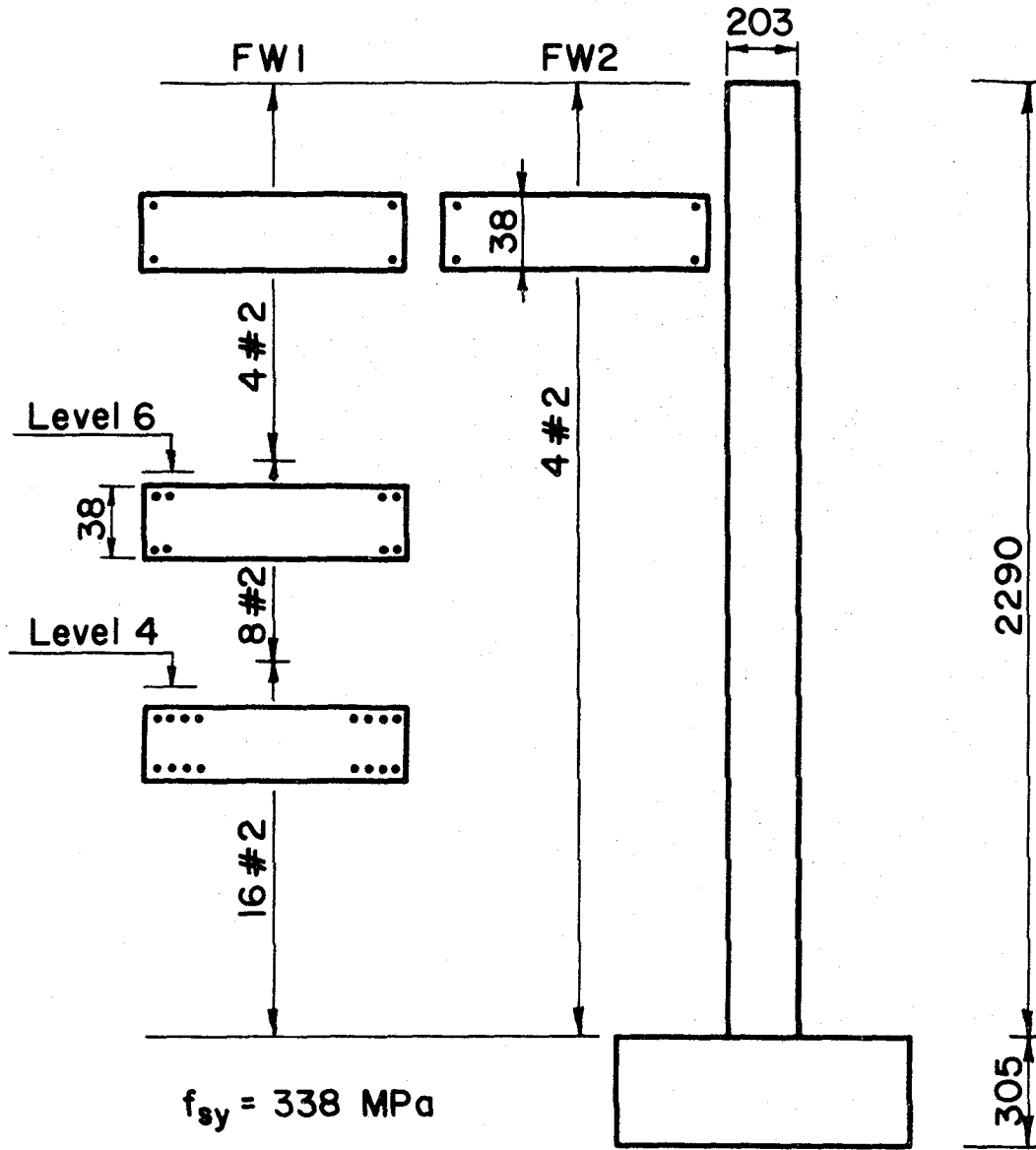


Fig. 7.2 Longitudinal Reinforcement Distribution for Structures FW1 and FW2



indicate gage wire number (see Table 7.10)

Fig. 7.2 (cont'd) Longitudinal Distribution for Structures FW1 and FW2

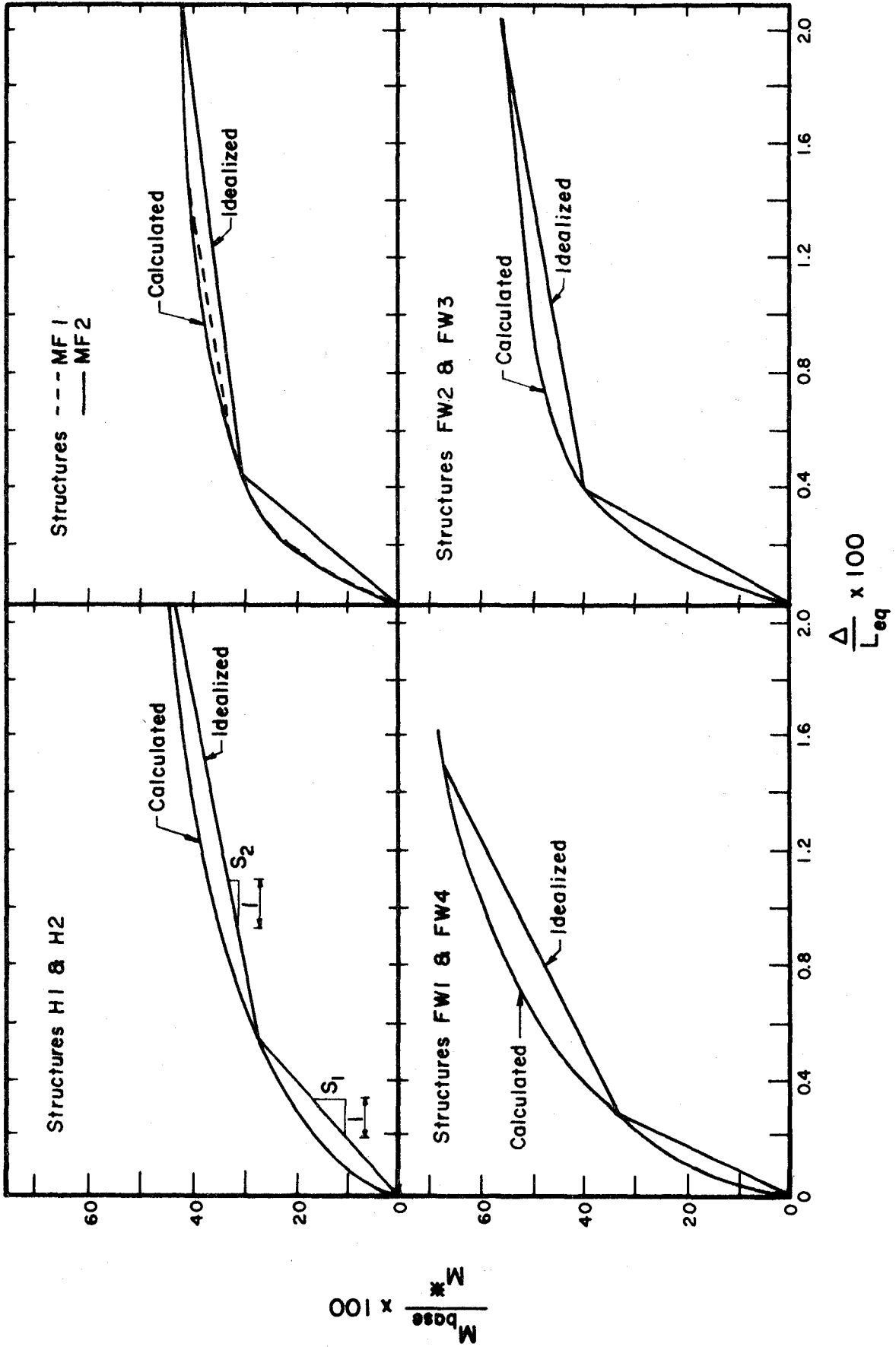
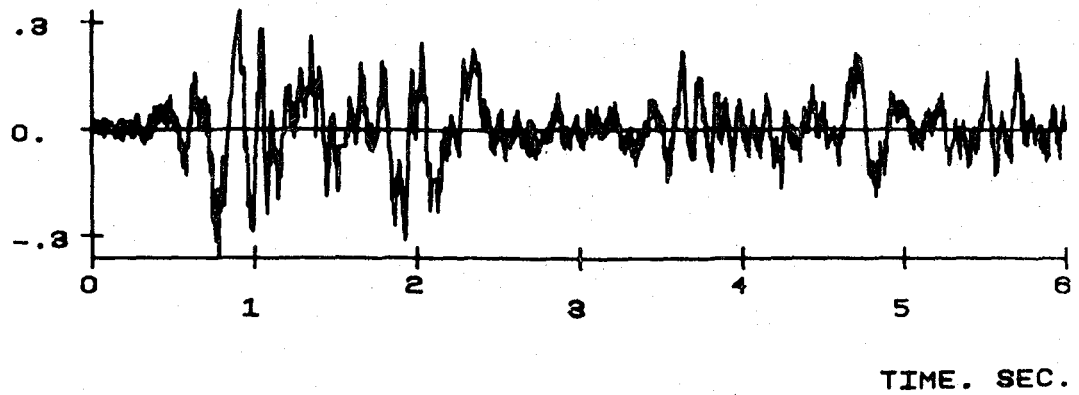


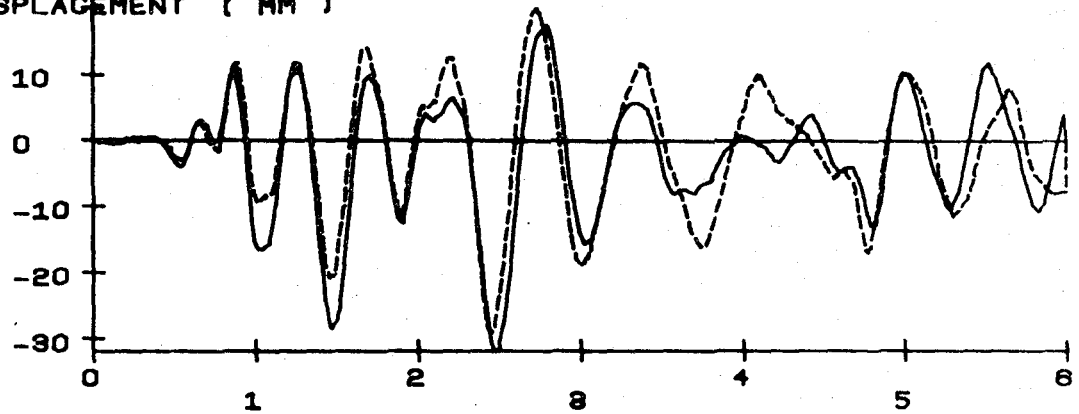
Fig. 7.3 Normalized Moment-Displacement Diagrams

H1 RUN 1

BASE ACCELERATION (G)



DISPLACEMENT (MM)



BASE OVERTURNING MOMENT (KN-M)

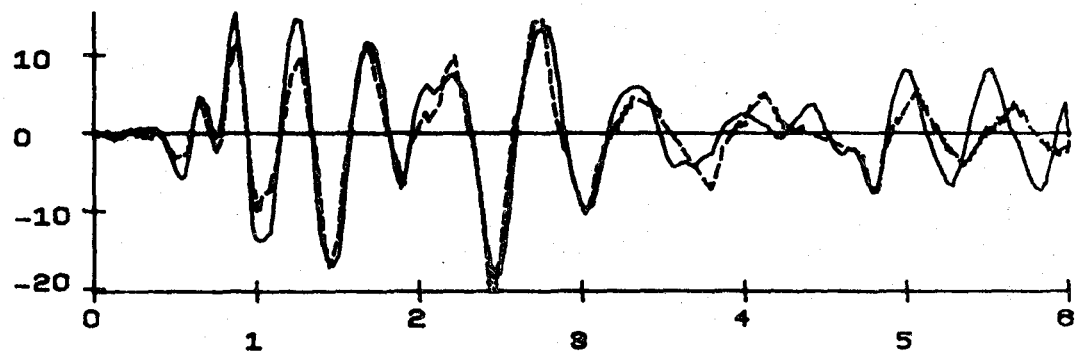


Fig. 7.4 Calculated (Solid Line) and Measured (Broken Line) Response for Structure H1

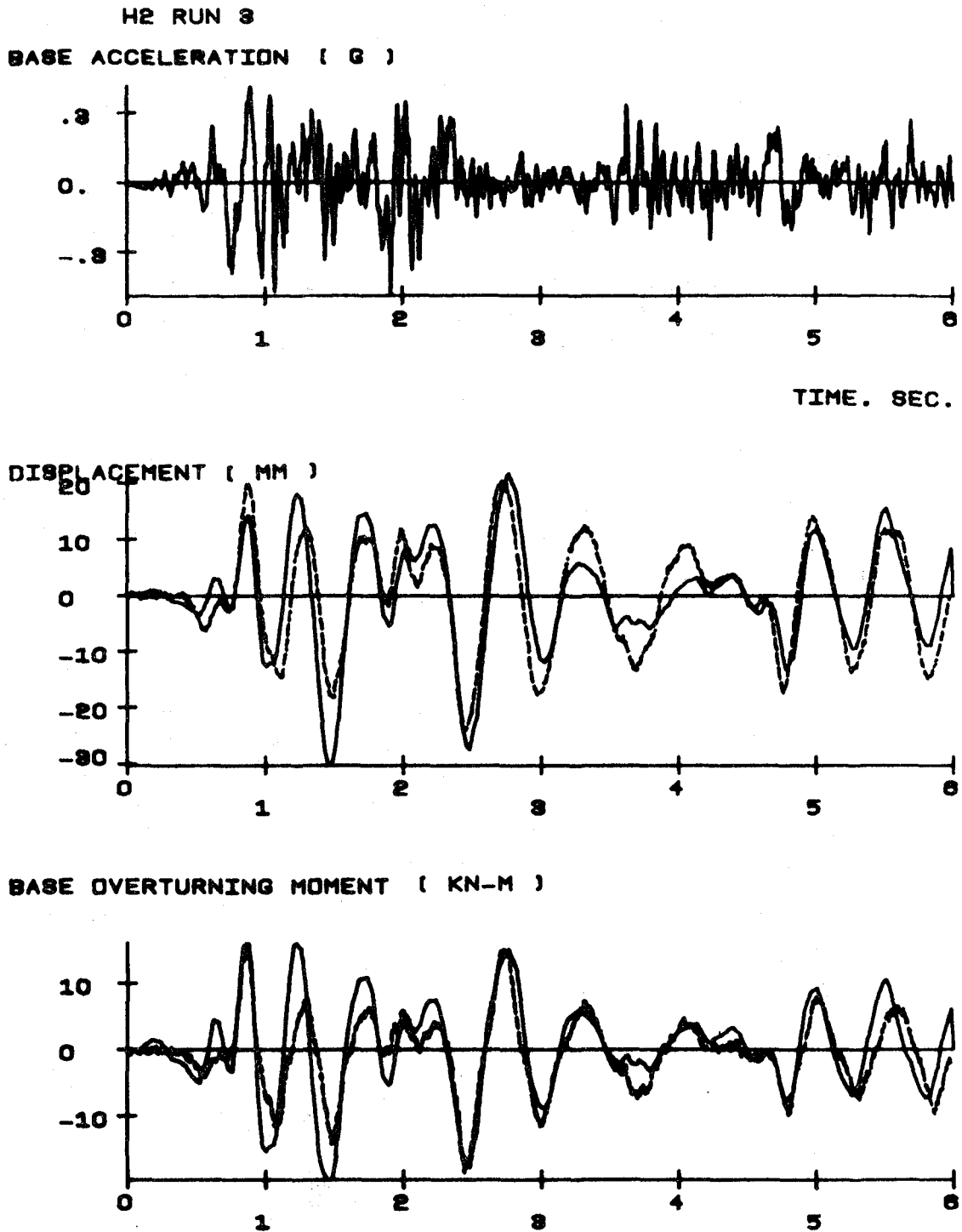
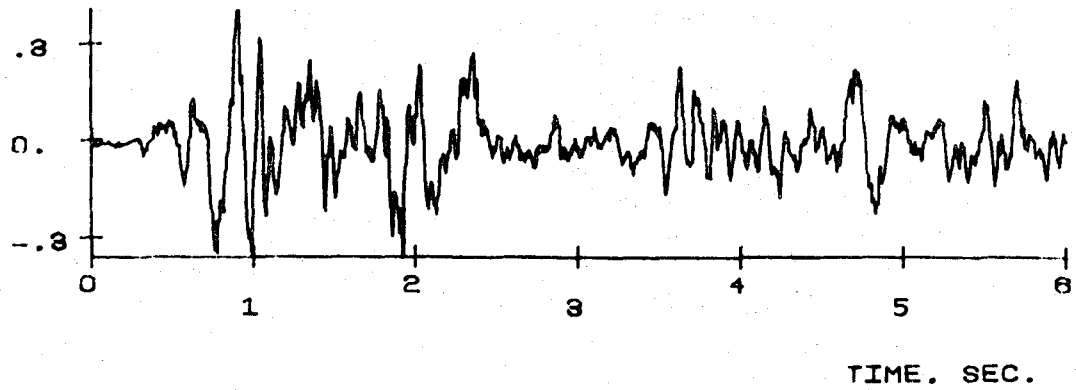


Fig. 7.5 Calculated (Solid Line) and Measured (Broken Line) Response for Structure H2

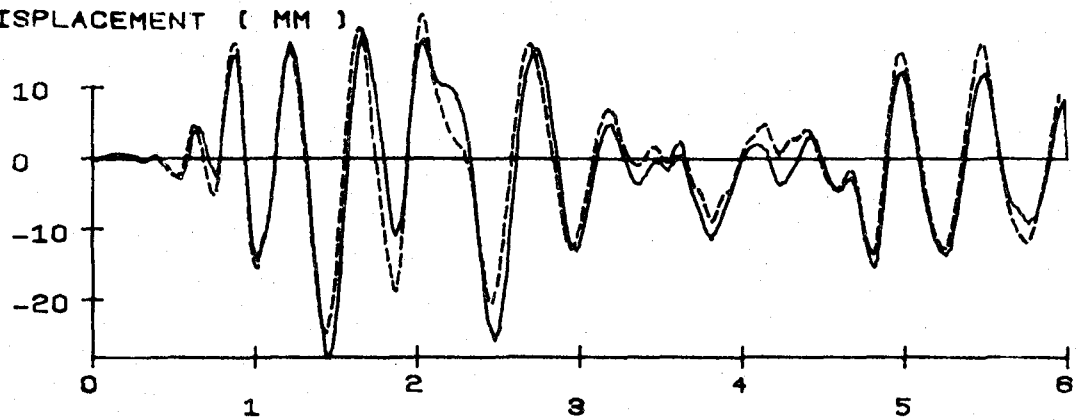
SDOF MODEL MF1 RUN 1

SIMULATED ELCENTRO 1940 NS RUN 1

BASE ACCELERATION (G)



DISPLACEMENT (MM)



BASE OVERTURNING MOMENT (KN-M)

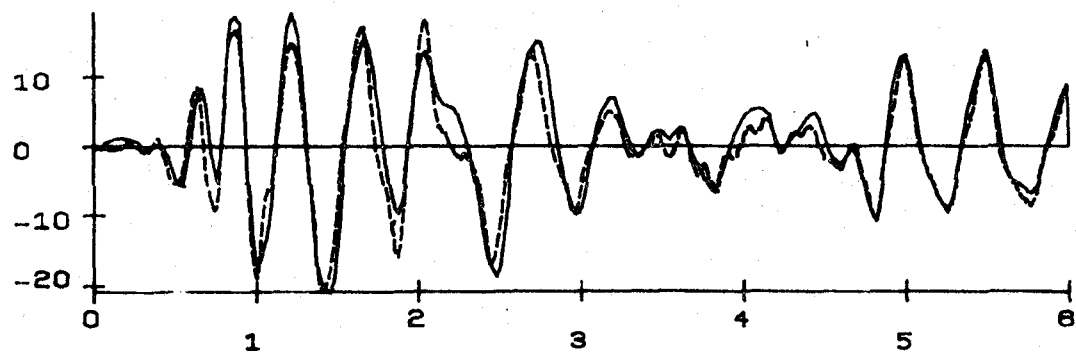
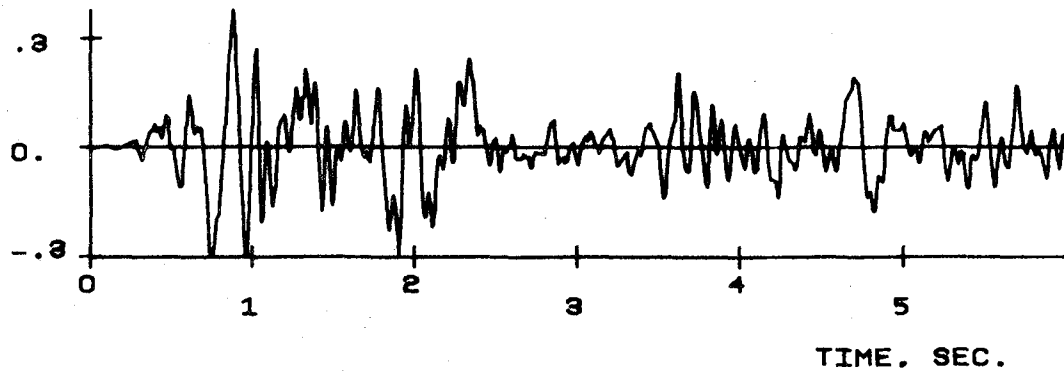


Fig. 7.6 Calculated (Solid Line) and Measured (Broken Line) Response for Structure MF1

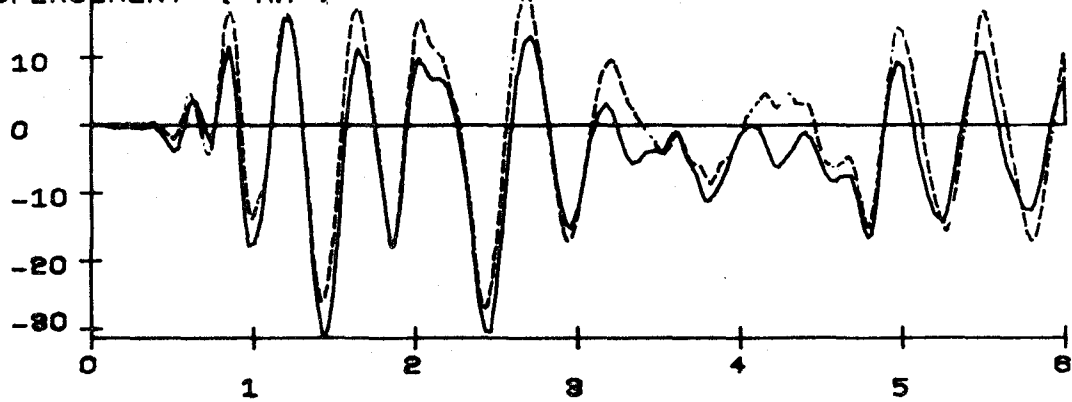
SDOF MODEL MF2 RUN 1

SIMULATED ELCENTRO 1940 NS RUN 1

BASE ACCELERATION (G)



DISPLACEMENT (MM)



BASE OVERTURNING MOMENT (KN-M)

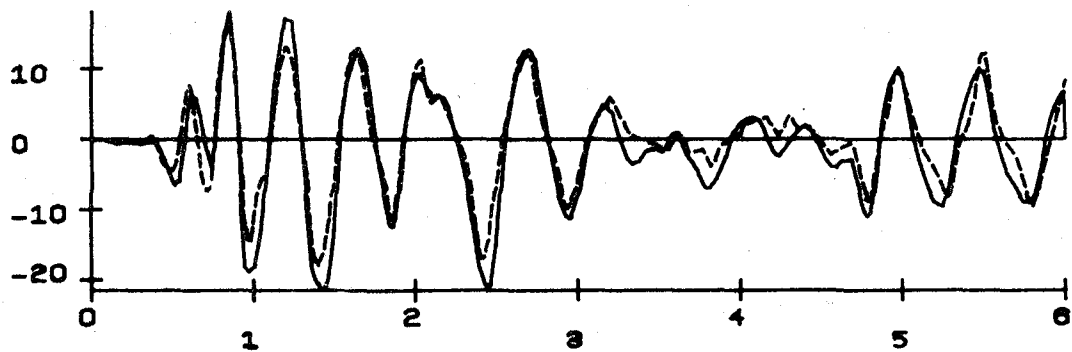
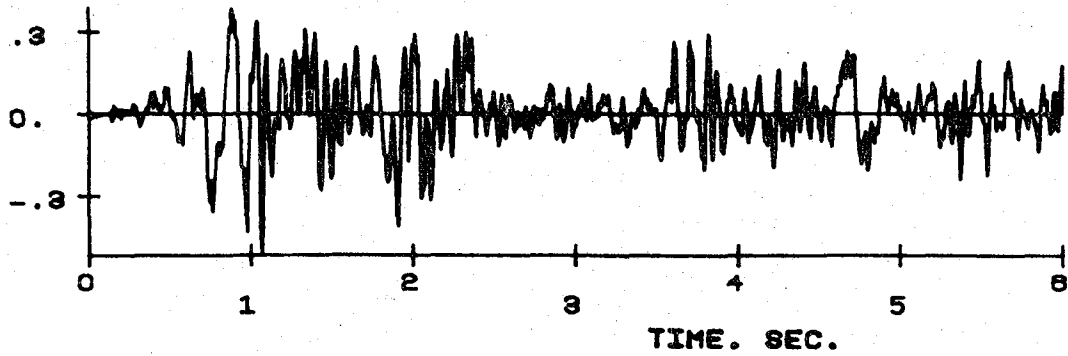


Fig. 7.7 Calculated (Solid Line) and Measured (Broken Line) Response for Structure MF2

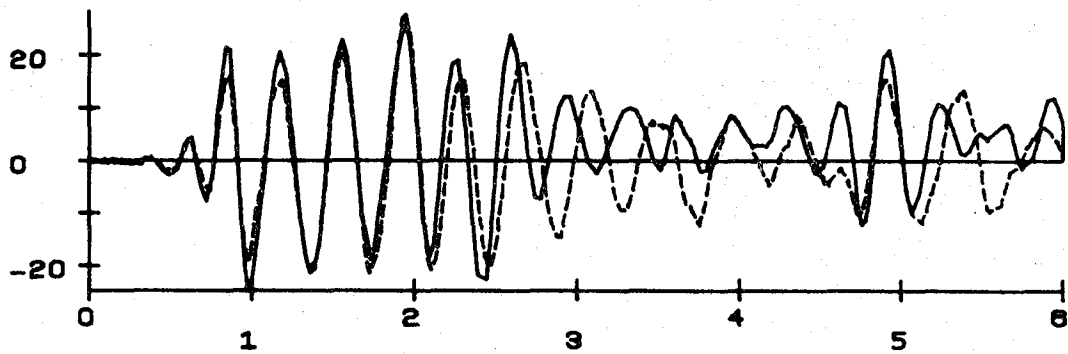
SDOF MODEL FW1 RUN 1

SIMULATED ELCENTRO 1940 NS RUN 1

BASE ACCELERATION (G)



DISPLACEMENT (MM)



BASE OVERTURNING MOMENT (KN-M)

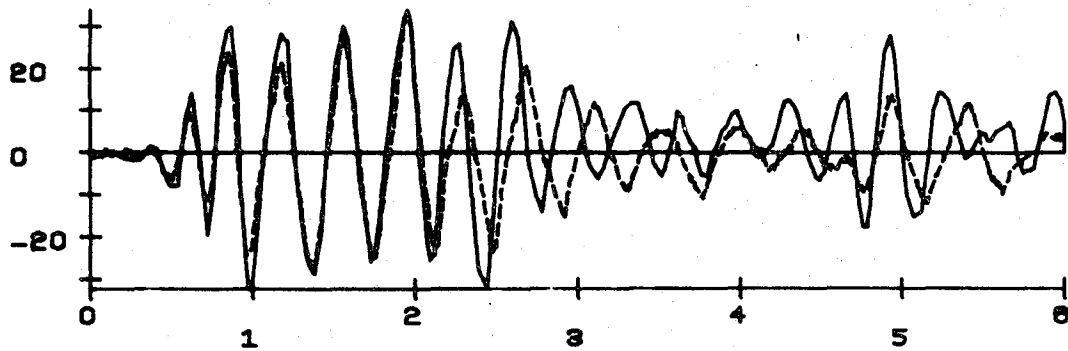
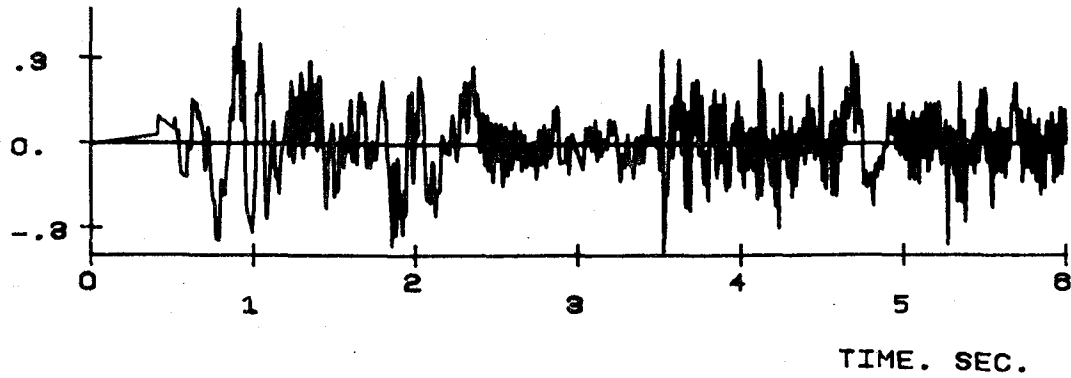


Fig. 7.8 Calculated (Solid Line) and Measured (Broken Line) Response for Structure FW1

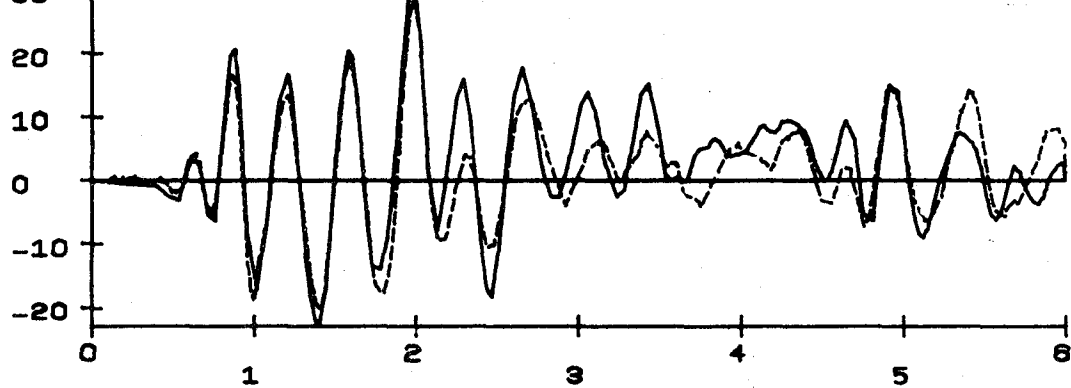
SDOF MODEL FW2 RUN 1

SIMULATED ELCENTRO 1940 NS RUN 1

BASE ACCELERATION (G)



DISPLACEMENT (MM)



BASE OVERTURNING MOMENT (KN-M)

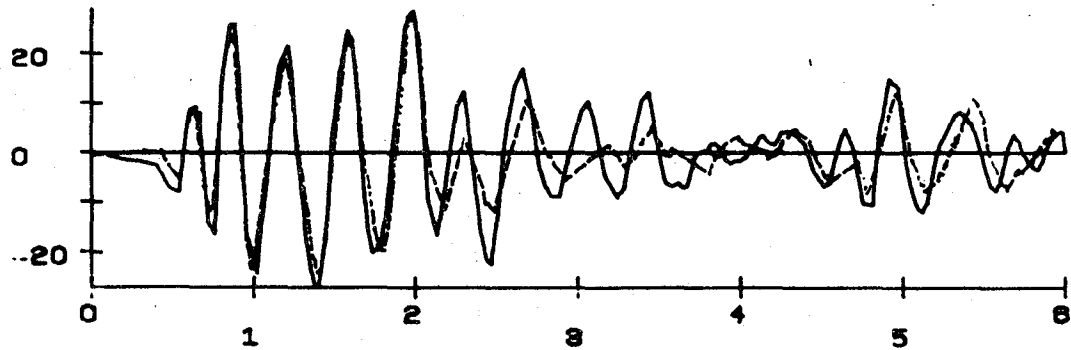
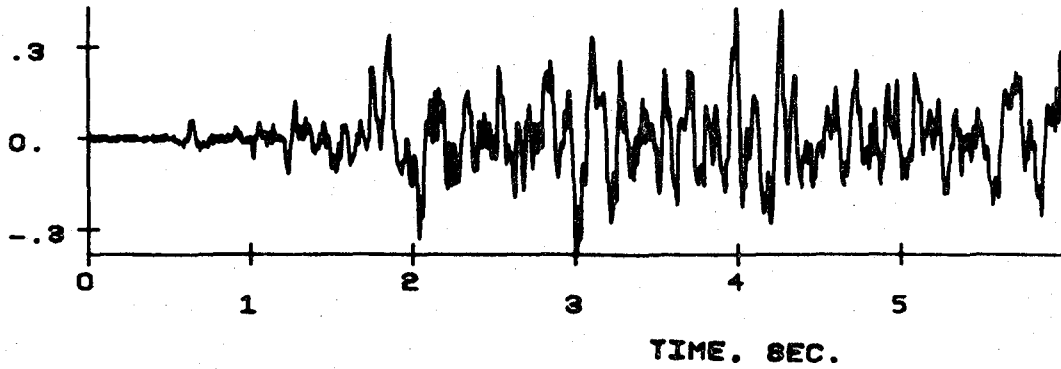


Fig. 7.9 Calculated (Solid Line) and Measured (Broken Line) Response for Structure FW2

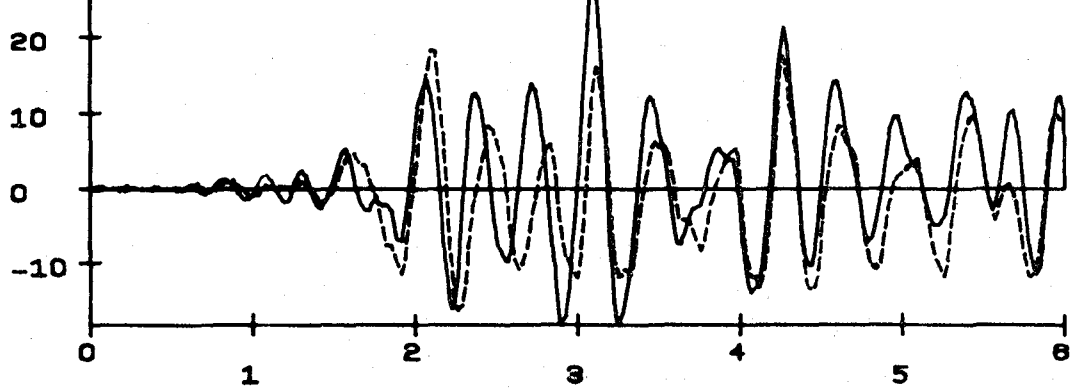
SDOF MODEL FW3 RUN 1

SIMULATED TAFT N21E RUN 1

BASE ACCELERATION (G)



DISPLACEMENT (MM)



BASE OVERTURNING MOMENT (KN-M)

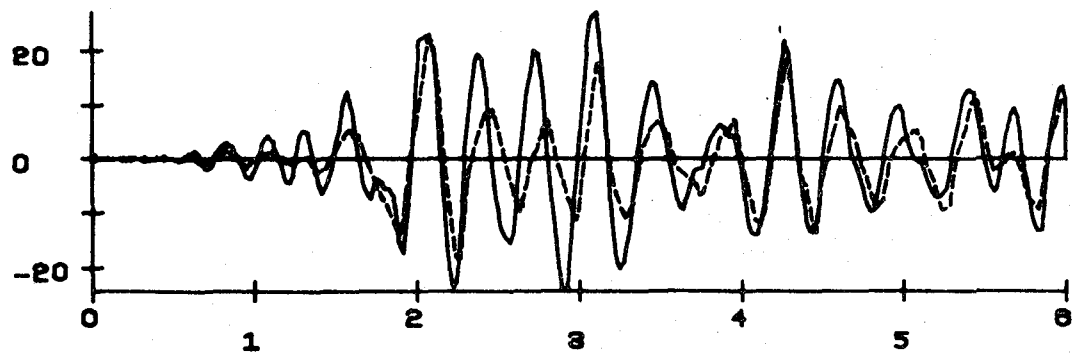
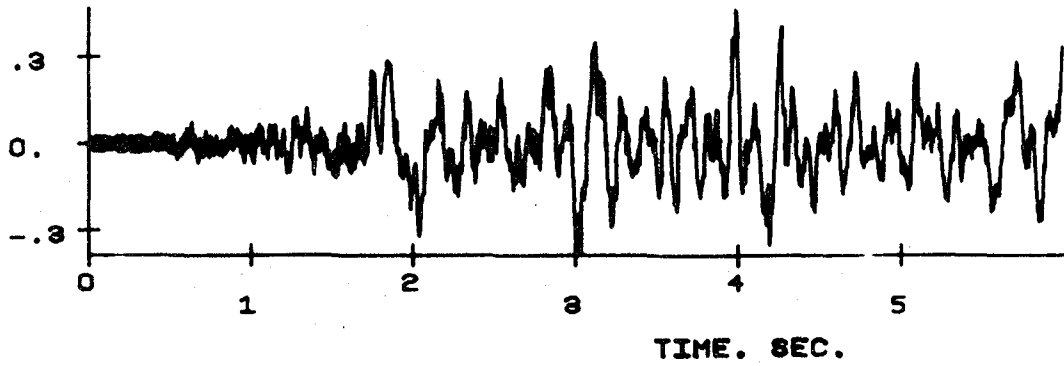


Fig. 7.10 Calculated (Solid Line) and Measured (Broken Line) Response for Structure FW3

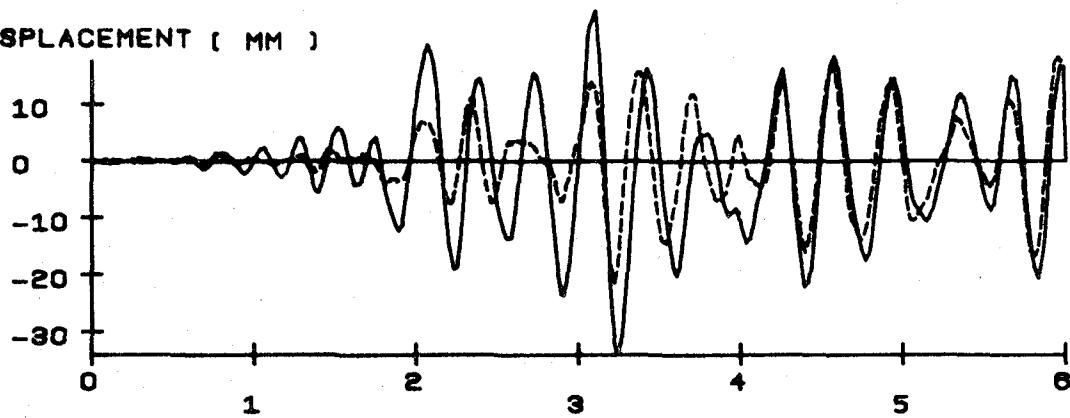
SDOF MODEL FW4 RUN 1

SIMULATED TAFT N21E RUN 1

BASE ACCELERATION (G)



DISPLACEMENT (MM)



BASE OVERTURNING MOMENT (KN-M)

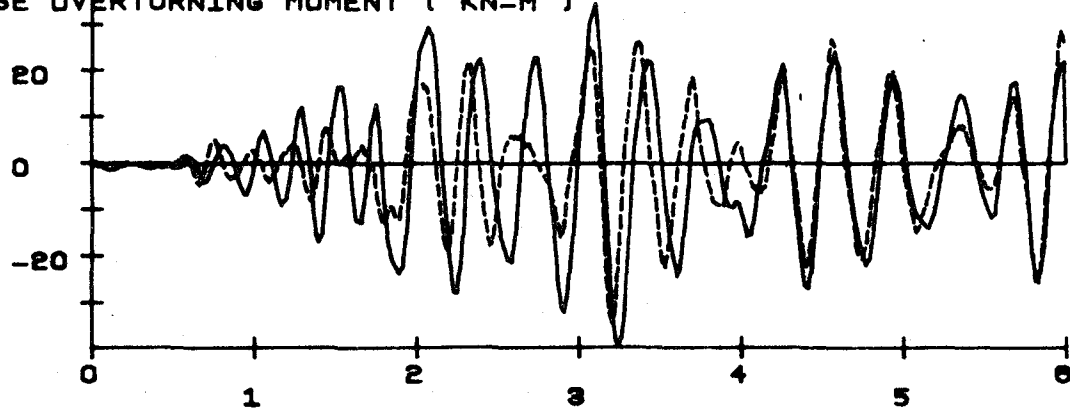


Fig. 7.11 Calculated (Solid Line) and Measured (Broken Line) Response for Structure FW4

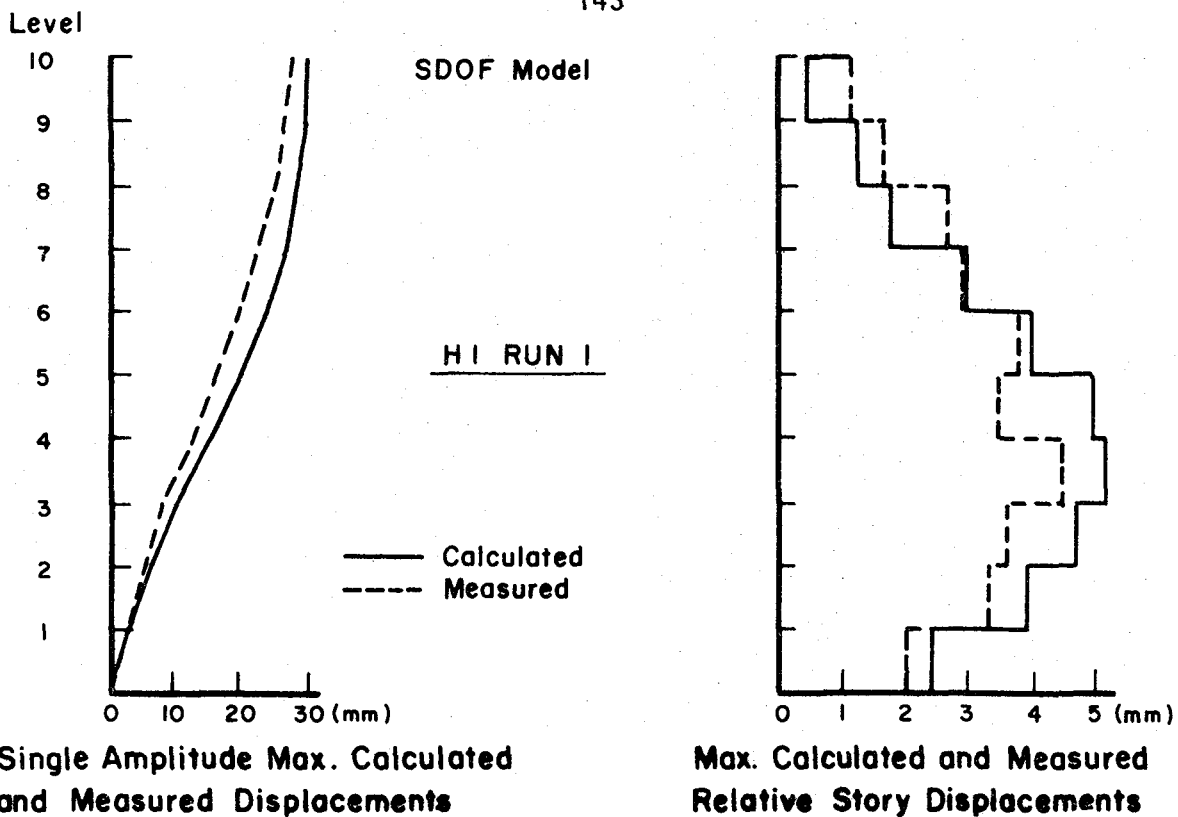


Fig. 7.12 Maximum Response of Structure H1

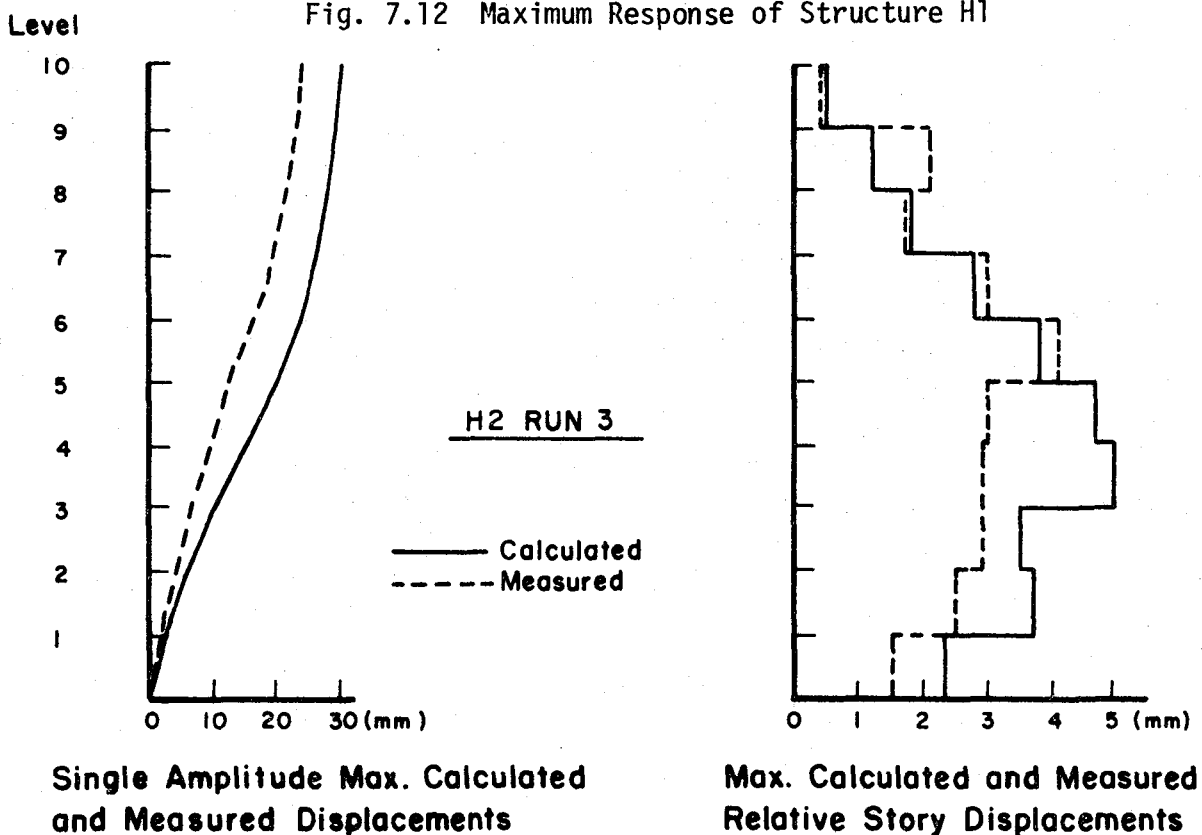


Fig. 7.13 Maximum Response of Structure H2

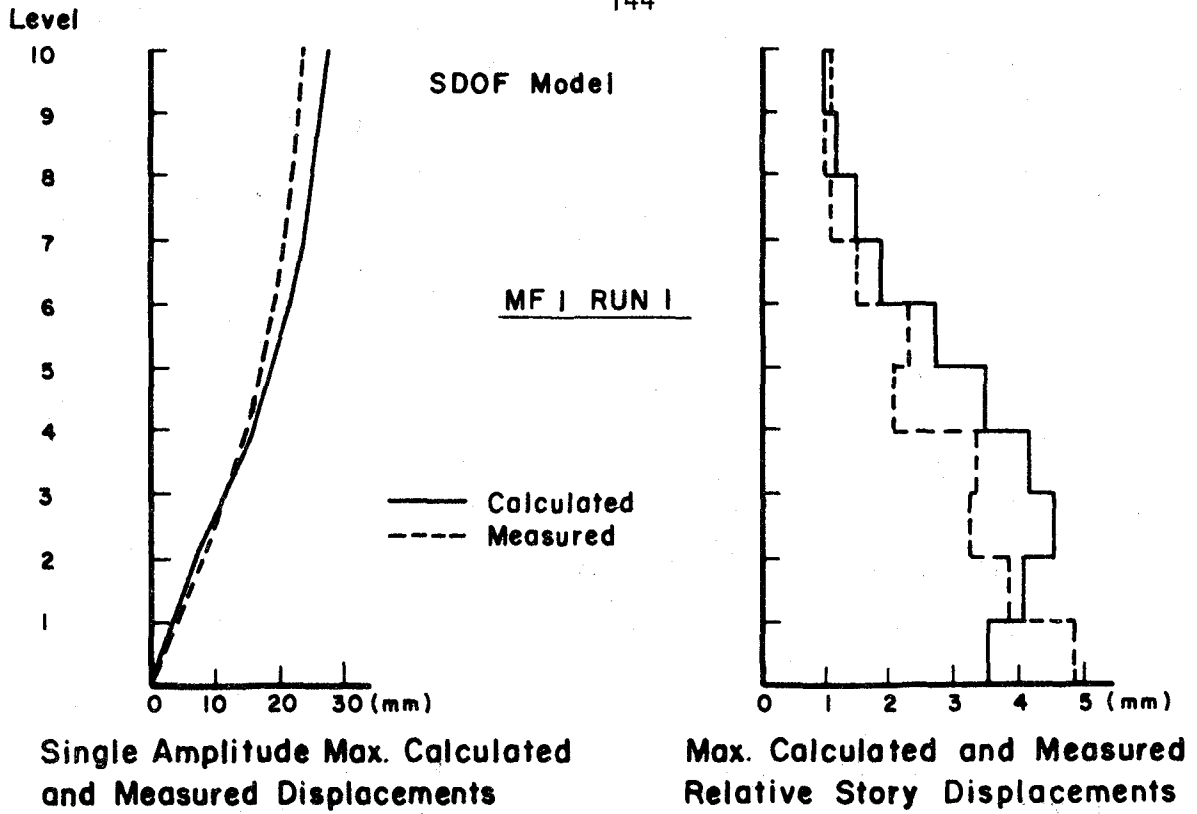


Fig. 7.14 Maximum Response of Structure MF1

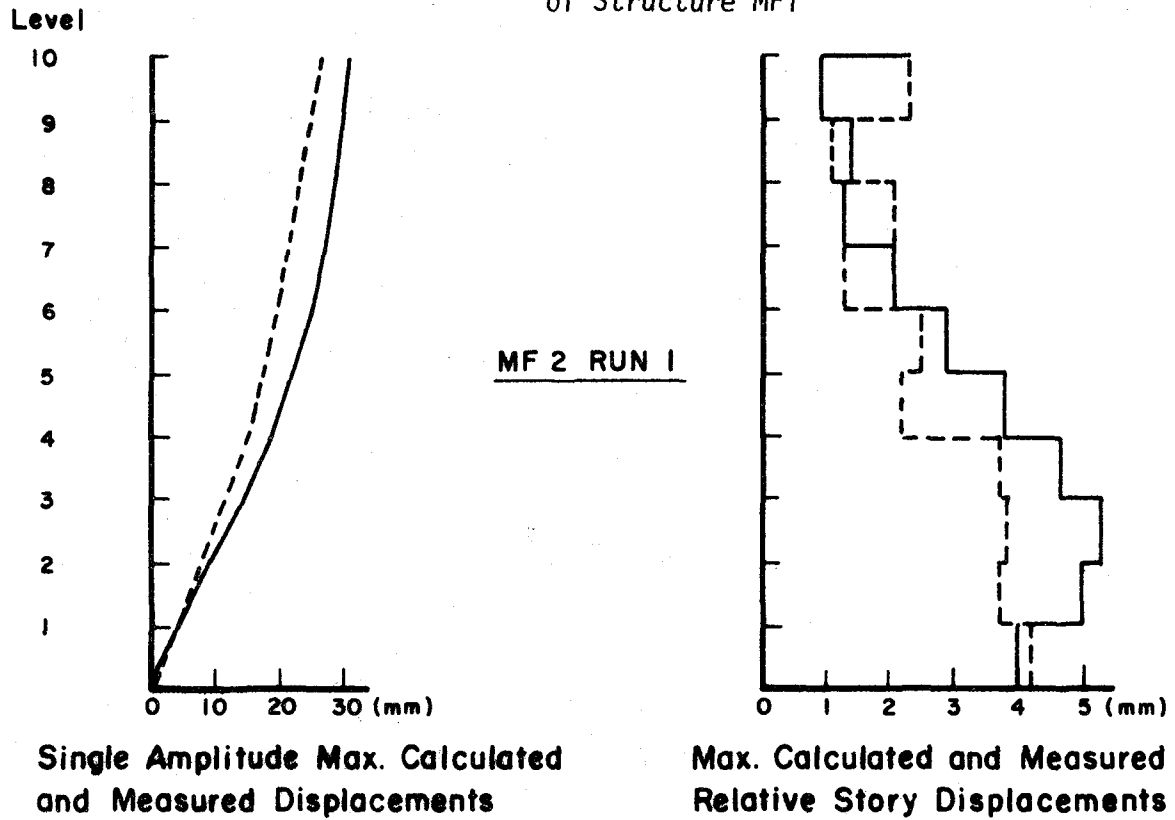


Fig. 7.15 Maximum Response of Structure MF2

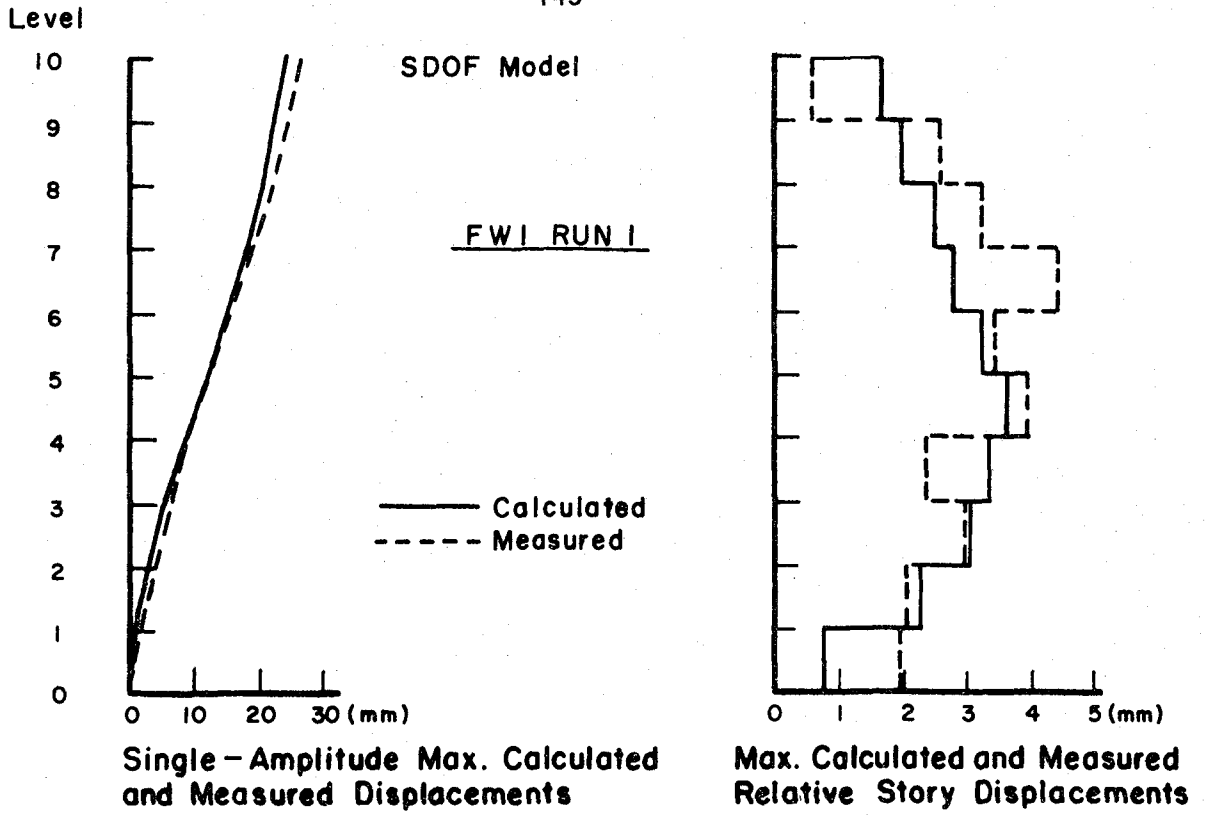


Fig. 7.16 Maximum Response of Structure FW1

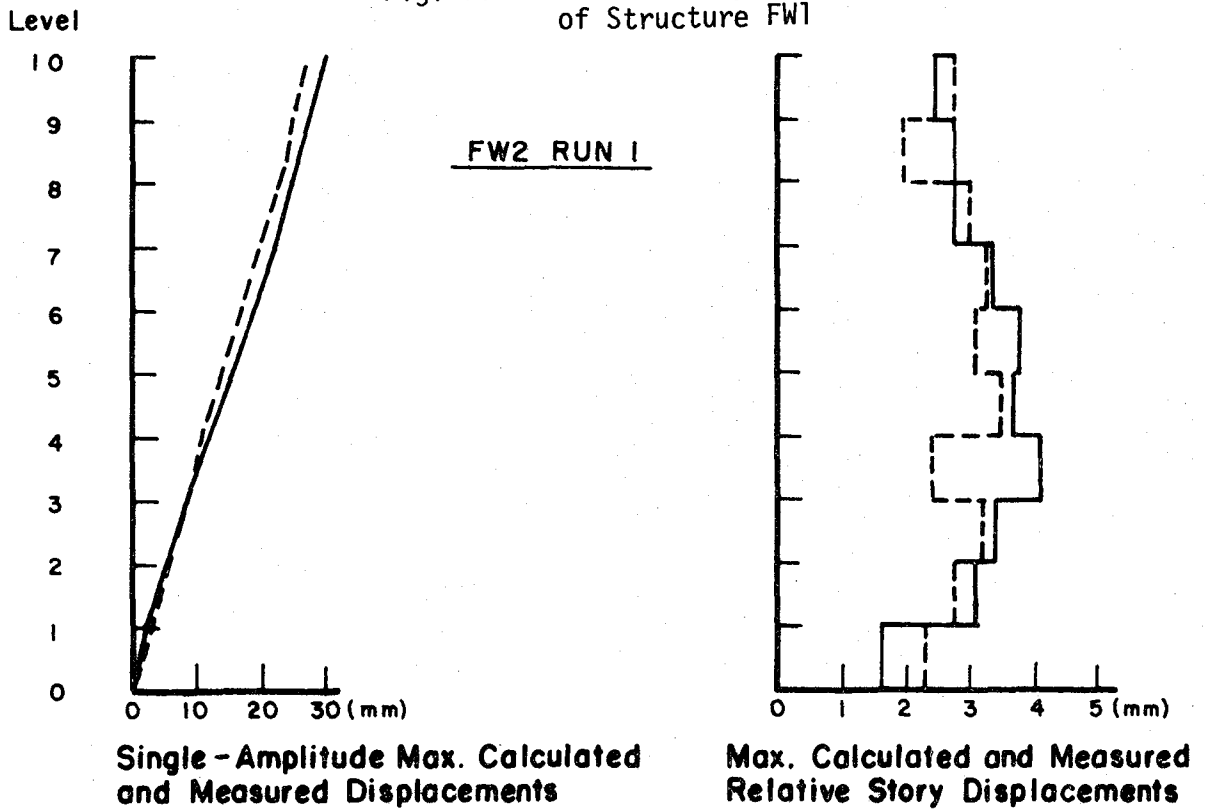


Fig. 7.17 Maximum Response of Structure FW2

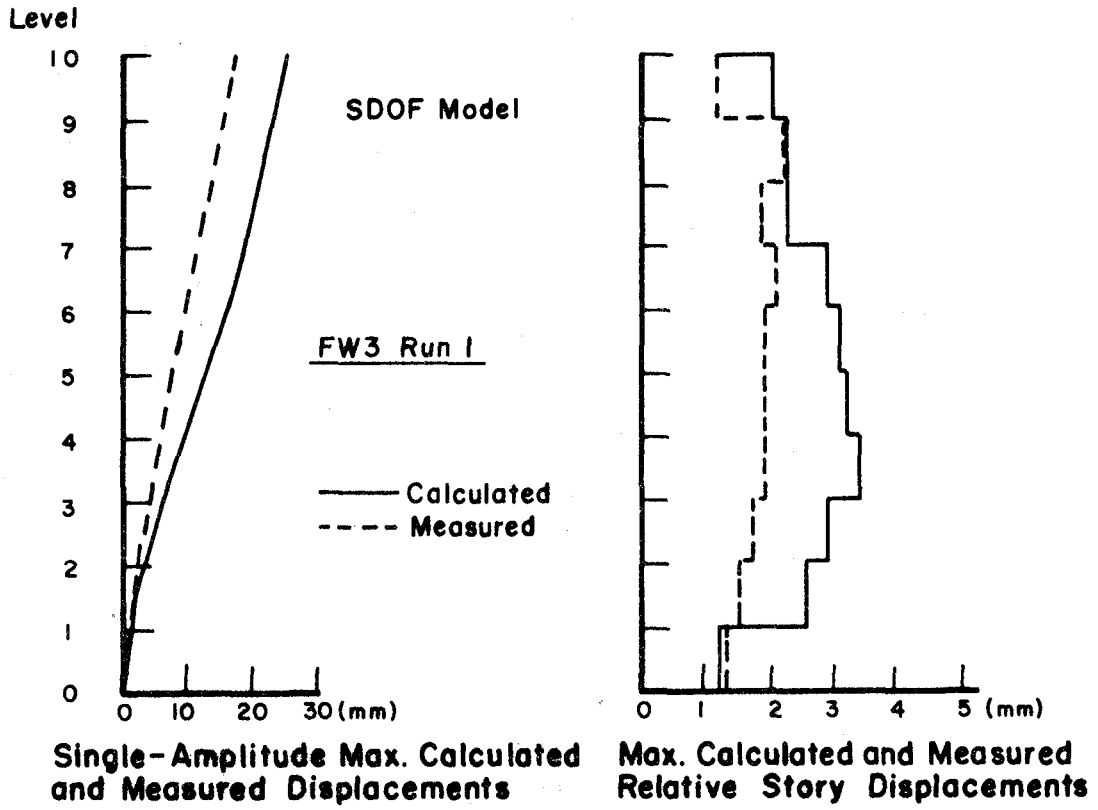


Fig. 7.18 Maximum Response of Structure FW3

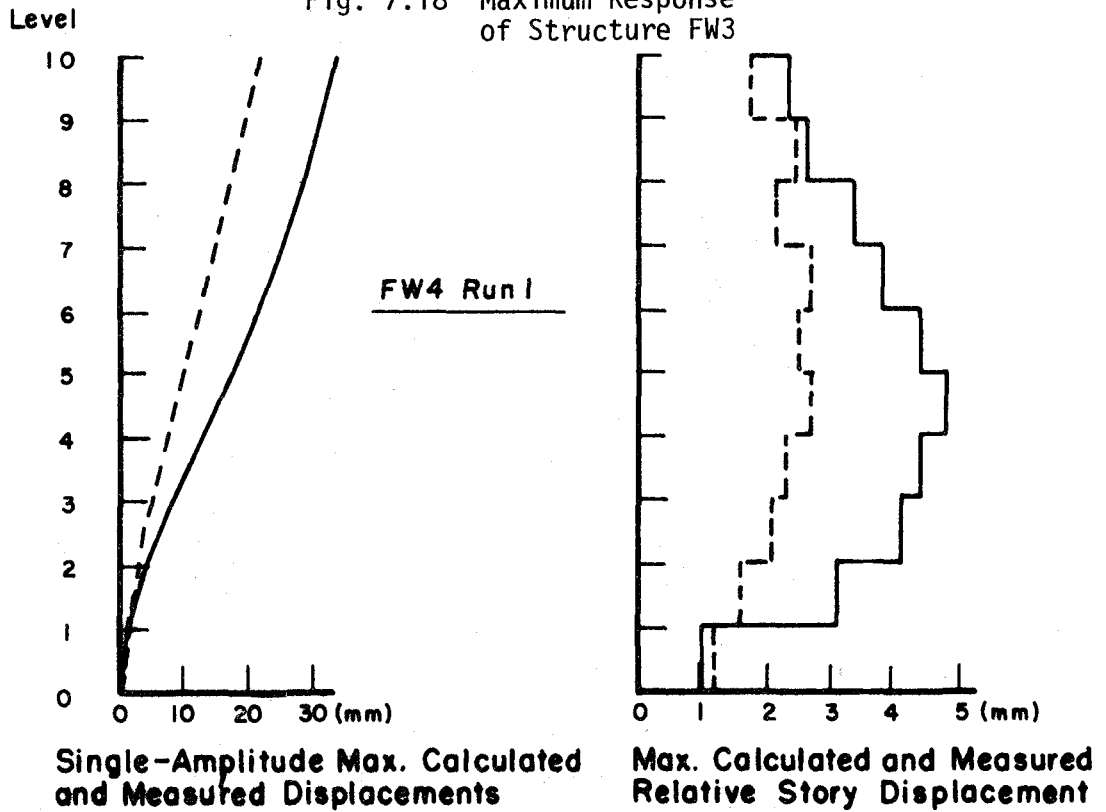
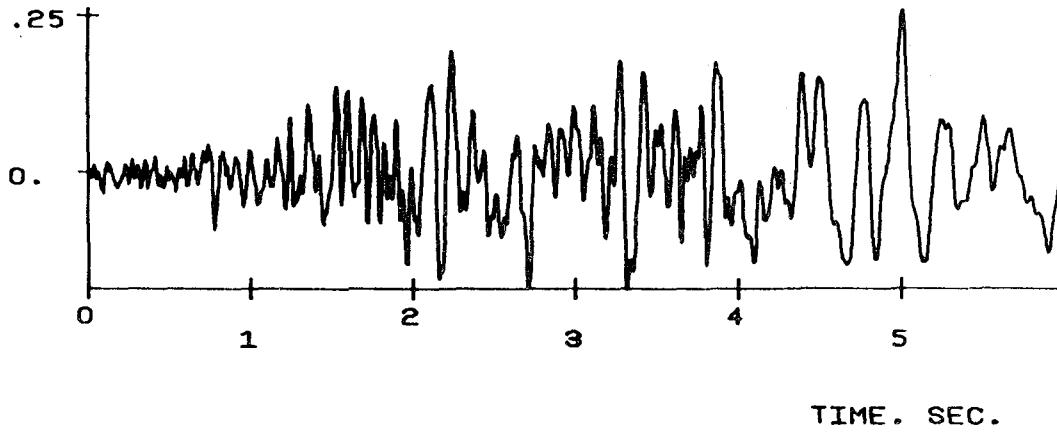


Fig. 7.19 Maximum Response of Structure FW4

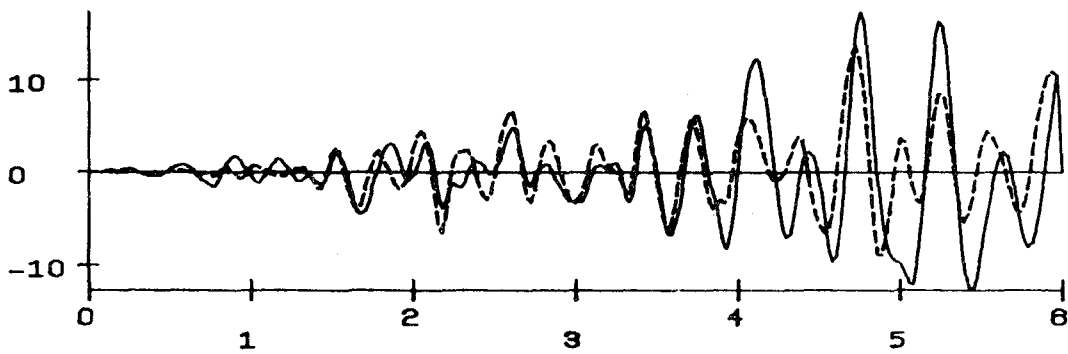
SDOF MODEL MF1

HOLIDAY INN

BASE ACCELERATION (G)



DISPLACEMENT (MM)



BASE OVERTURNING MOMENT (KN-M)

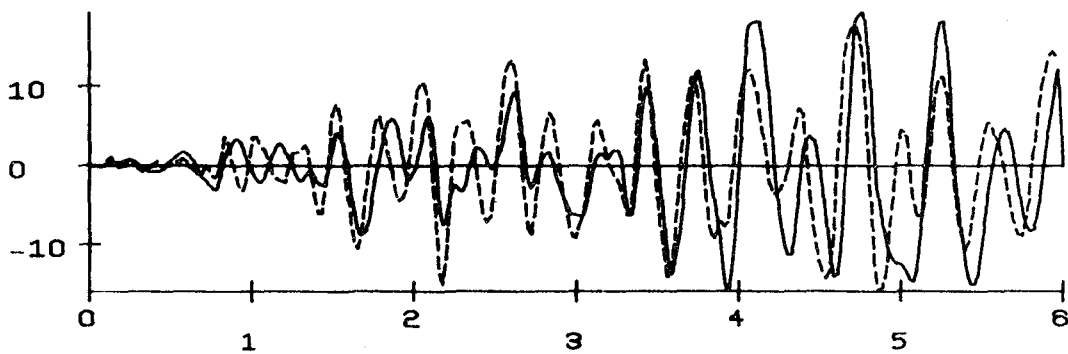
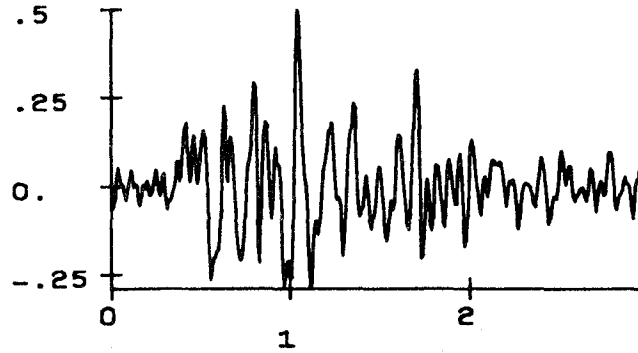


Fig. 7.20 Q-Model (Solid Line) and MDOF Model (Broken Line)
Results for Orion Earthquake

SDOF MODEL MF1

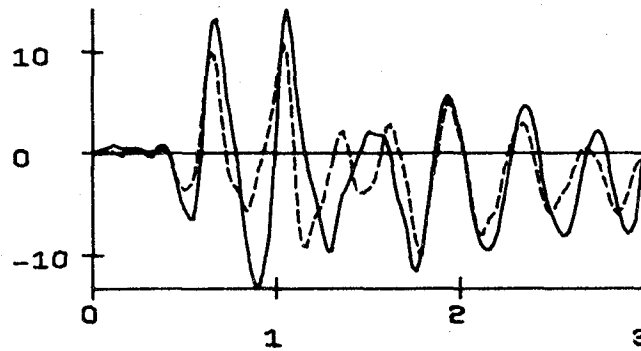
CASTAIC N21E 1971

BASE ACCELERATION (G)



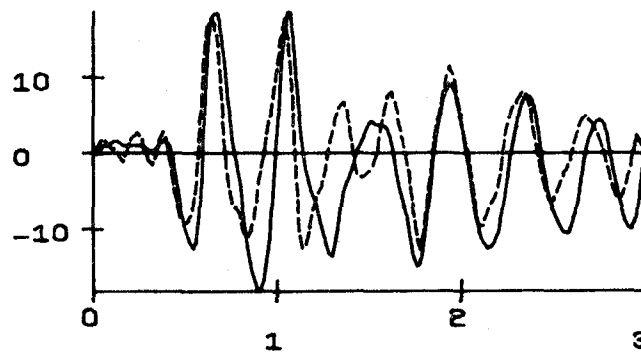
TIME. SEC.

DISPLACEMENT (MM)



TIME. SEC.

BASE OVERTURNING MOMENT (KN-M)



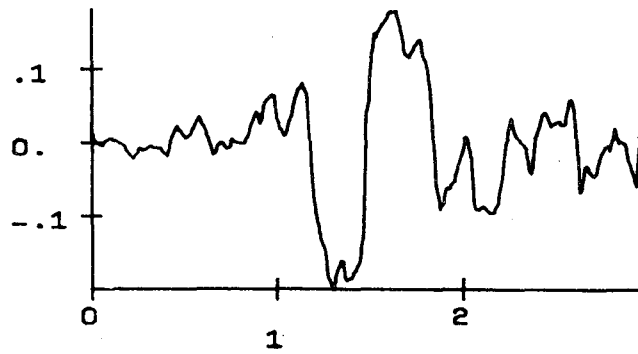
TIME. SEC.

Fig. 7.21 Q-Model (Solid Line) and MDOF Model (Broken Line) Results for Castaic Earthquake

SDOF MODEL MF1

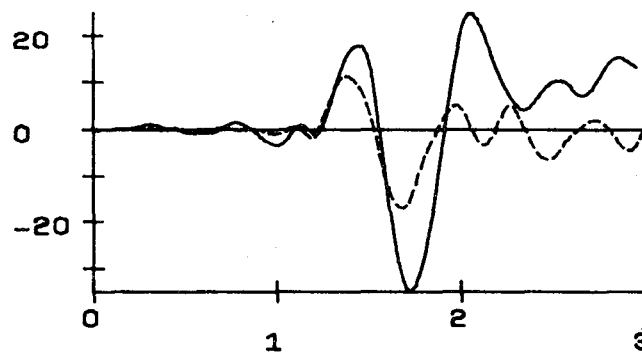
BUCAREST NS 1977

BASE ACCELERATION [G]



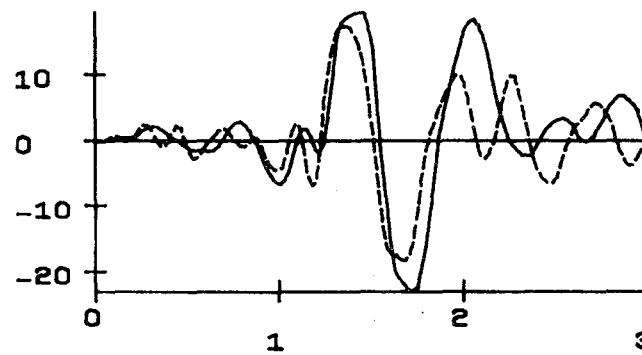
TIME. SEC.

DISPLACEMENT [MM]



TIME. SEC.

BASE OVERTURNING MOMENT [KN-M]



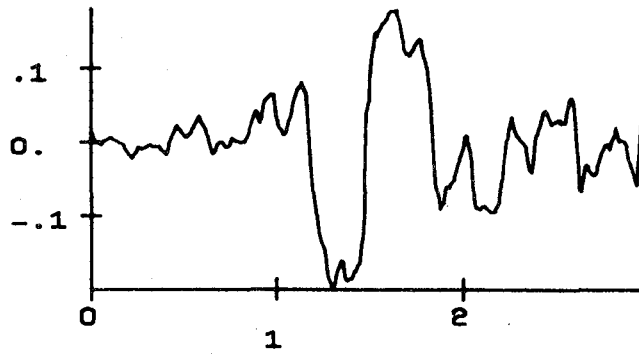
TIME. SEC.

Fig. 7.22 Q-Model (Solid Line) and MDOF Model (Broken Line)
Results for Bucarest Earthquake

SDOF MODEL MF1

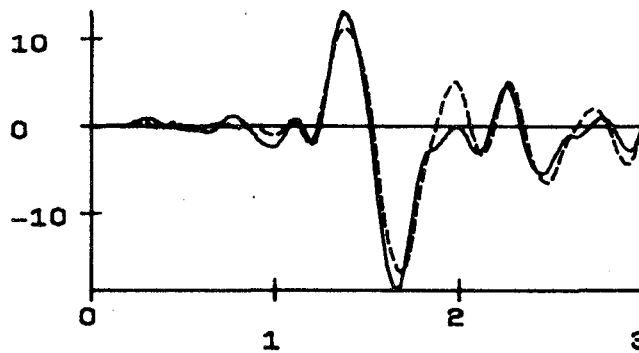
BUCAREST NS 1977

BASE ACCELERATION (G)



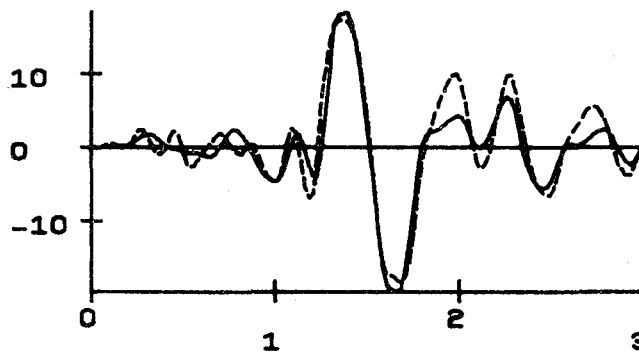
TIME. SEC.

DISPLACEMENT (MM)



TIME. SEC.

BASE OVERTURNING MOMENT (KN-M)



TIME. SEC.

Fig. 7.23 Q-Model (with Increased Frequency; Solid Line) and MDOF Model (Broken Line) Results for Bucarest Earthquake

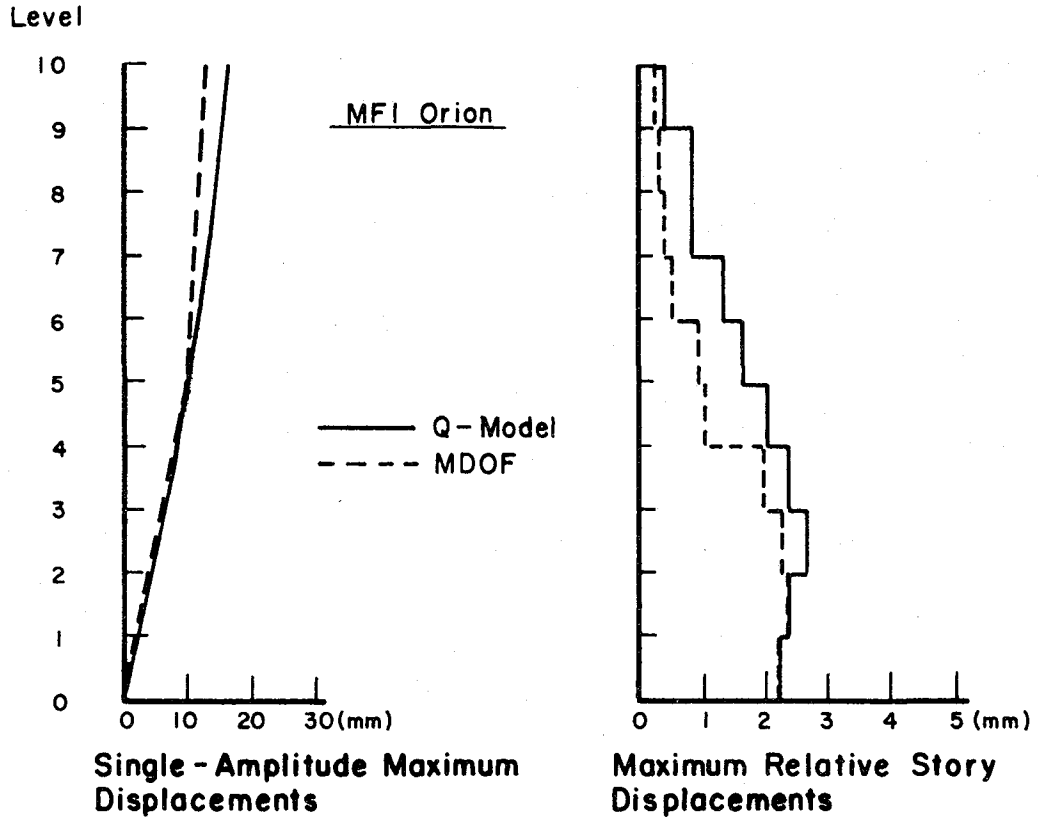


Fig. 7.24 Maximum Response for Orion Earthquake

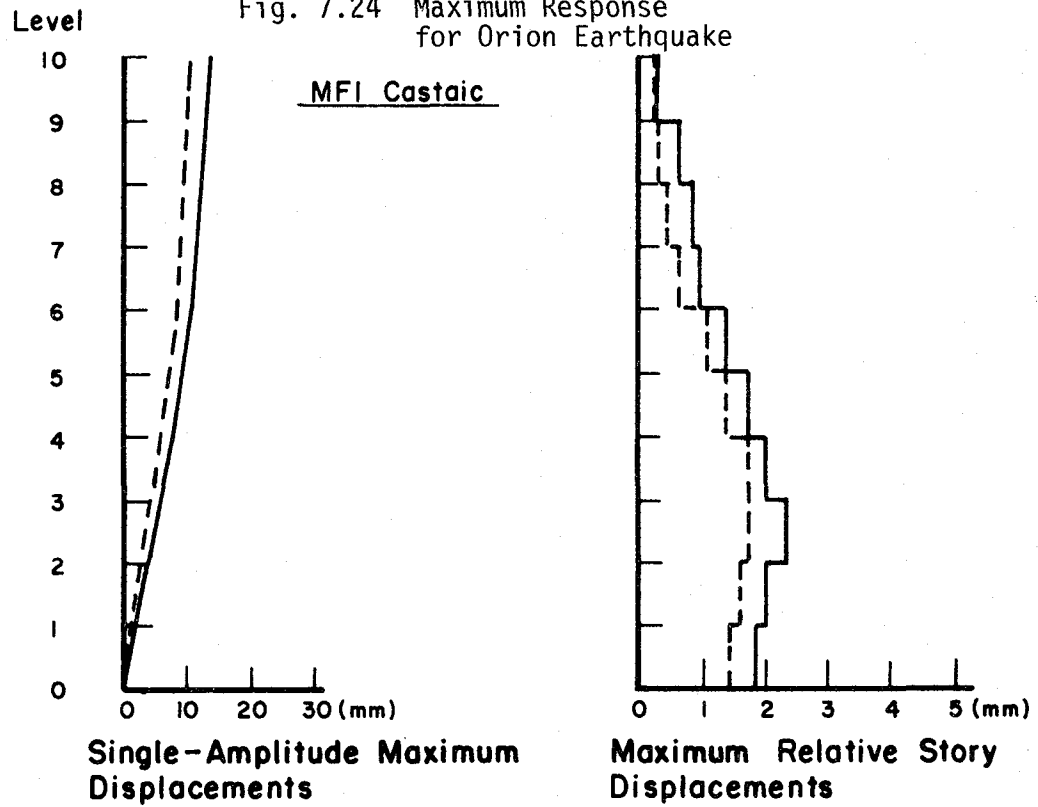


Fig. 7.25 Maximum Response for Castaic Earthquake

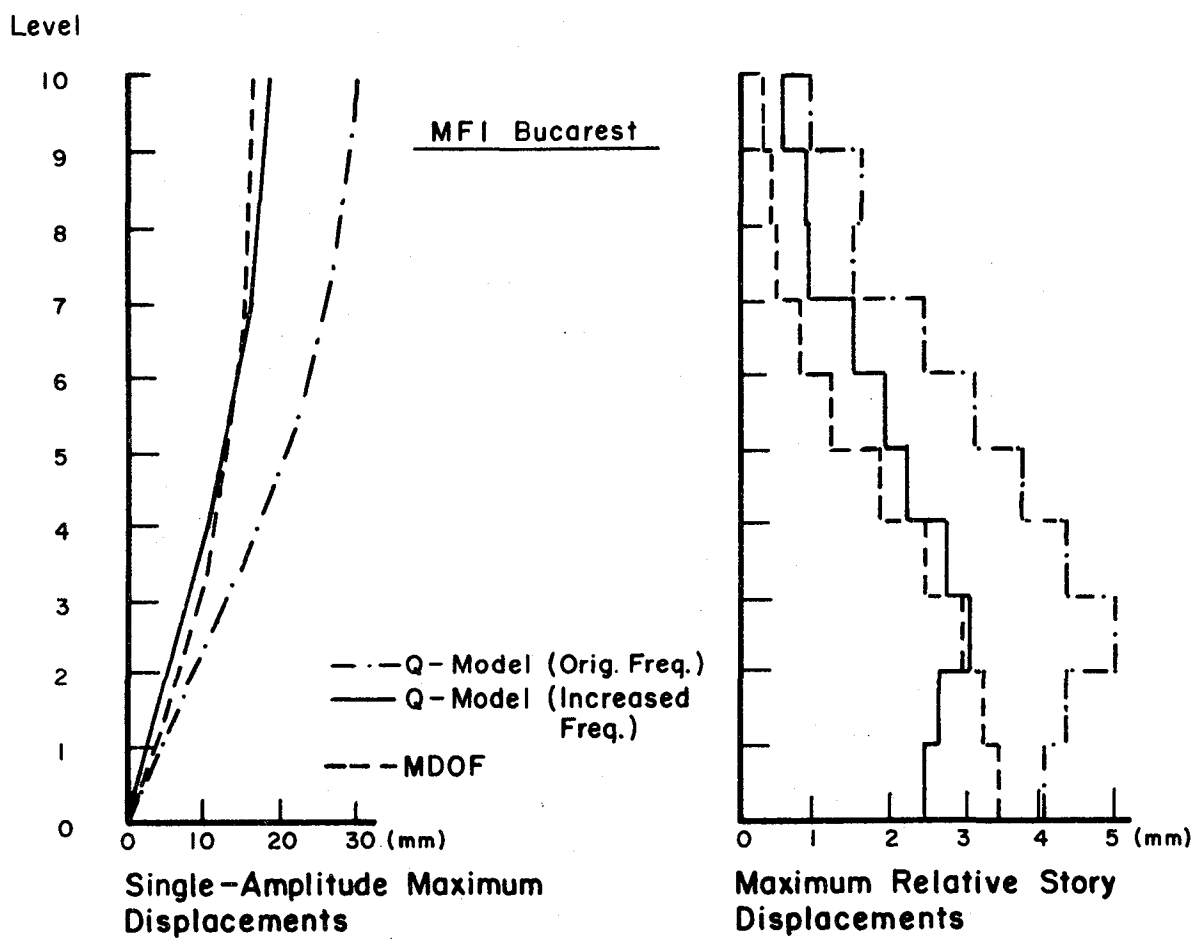


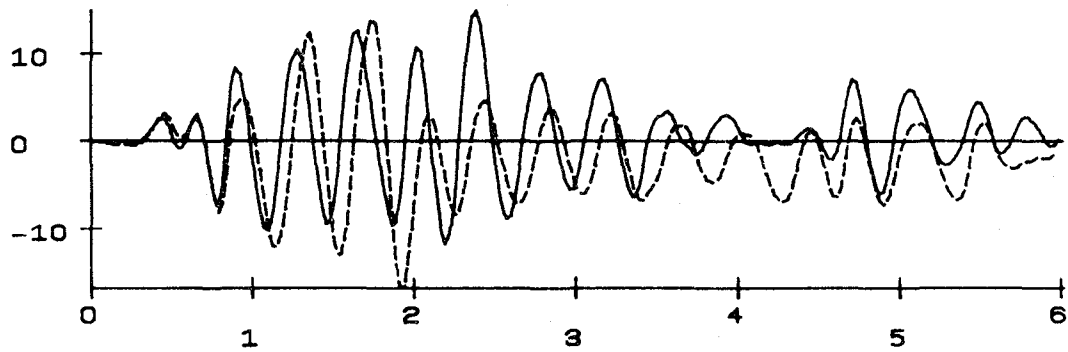
Fig. 7.26 Maximum Response for Bucarest Earthquake

SDOF MODEL MF1

ELCENTRO 1940 NS .2G



DISPLACEMENT (MM)



BASE OVERTURNING MOMENT (KN-M)

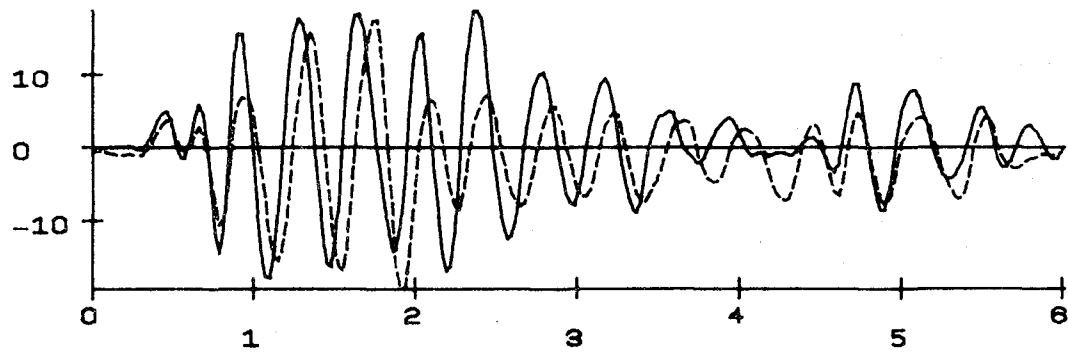


Fig. 7.27 Repeated Earthquakes with 0.2g Maximum Acceleration

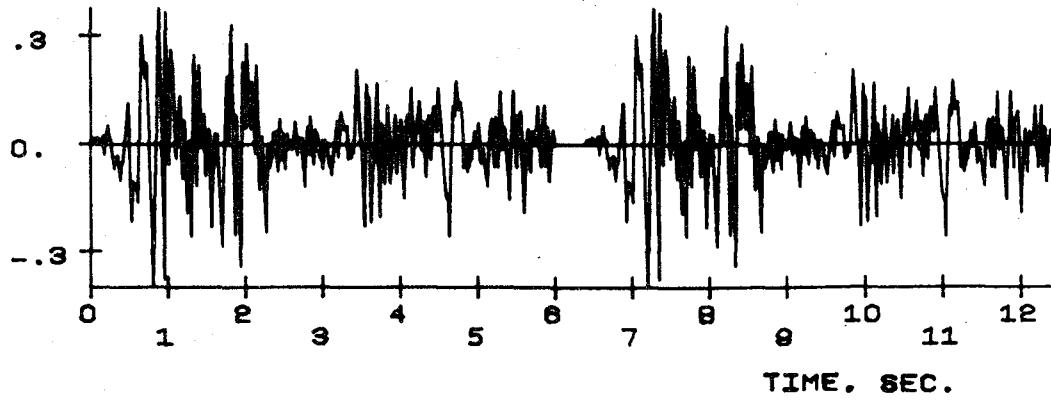
SDOF MODEL MF1

ELCENTRO 1940 NS .4G

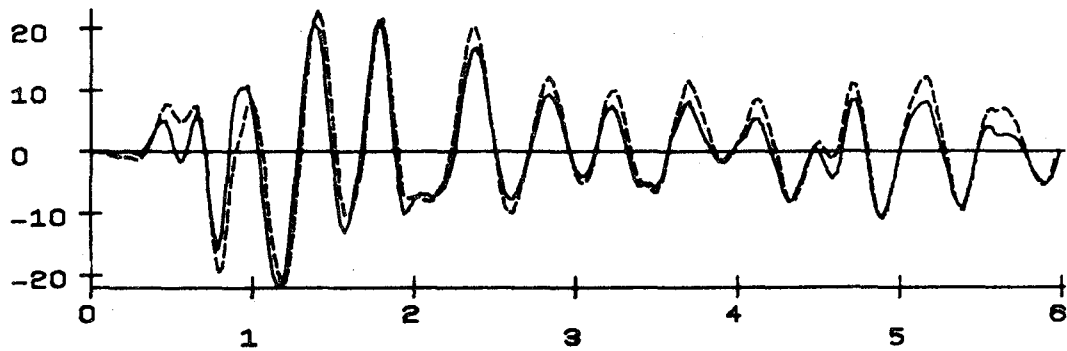
SOLID LINE , MOTION 1

BASE ACCELERATION (G)

BROKEN LINE , MOTION 2



DISPLACEMENT (MM)



BASE OVERTURNING MOMENT (KN-M)

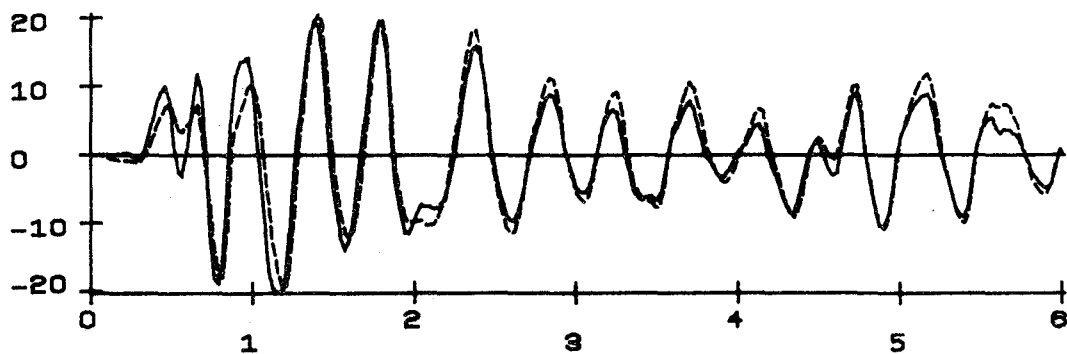
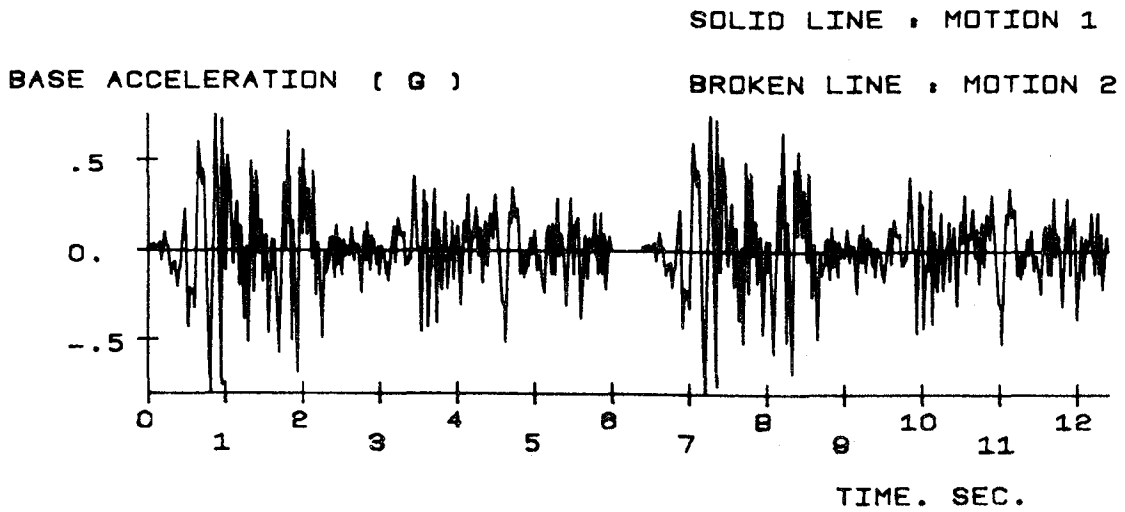


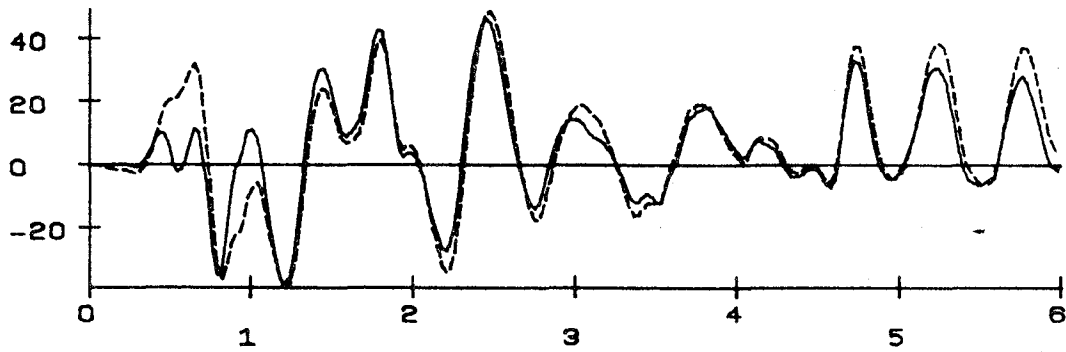
Fig. 7.28 Repeated Earthquakes with 0.4g Maximum Acceleration

SDOF MODEL MF1

ELCENTRO 1940 NS .8G



DISPLACEMENT (MM)



BASE OVERTURNING MOMENT (KN-M)

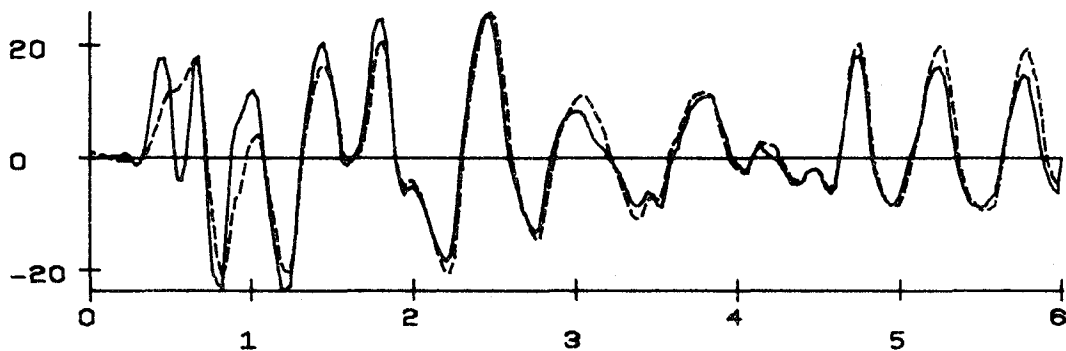


Fig. 7.29 Repeated Earthquakes with 0.8g Maximum Acceleration

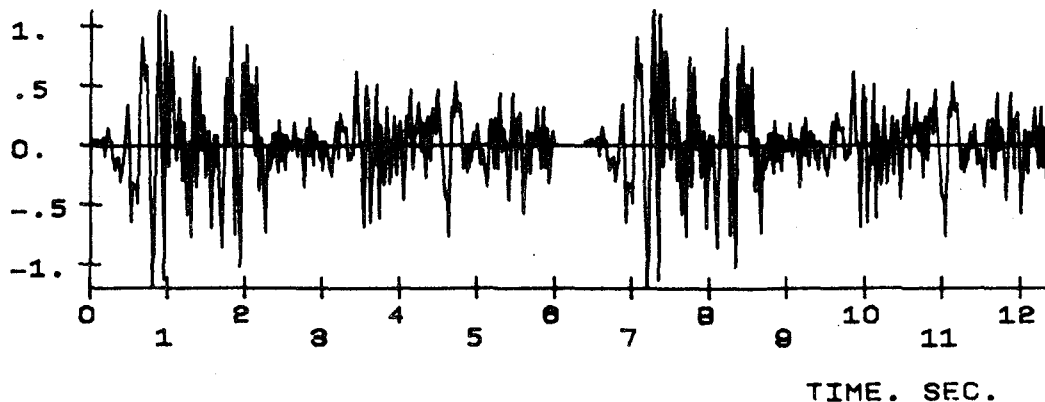
SDOF MODEL MF1

ELCENTRO 1940 NS 1.2G

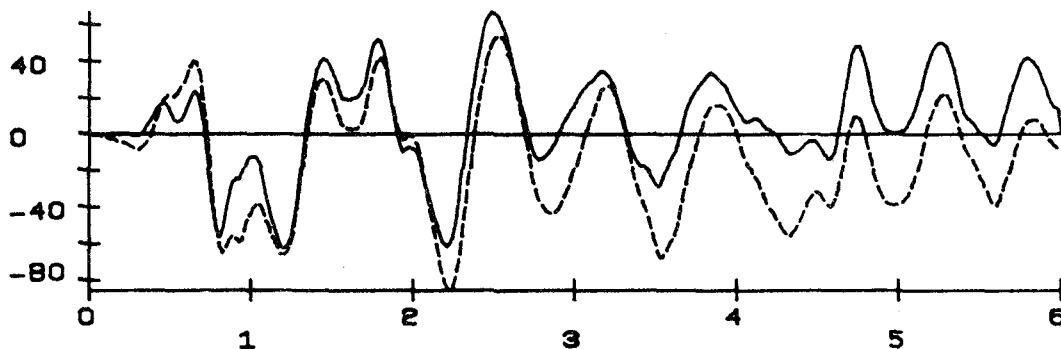
SOLID LINE , MOTION 1

BASE ACCELERATION (G)

BROKEN LINE , MOTION 2



DISPLACEMENT (MM)



BASE OVERTURNING MOMENT (KN-M)

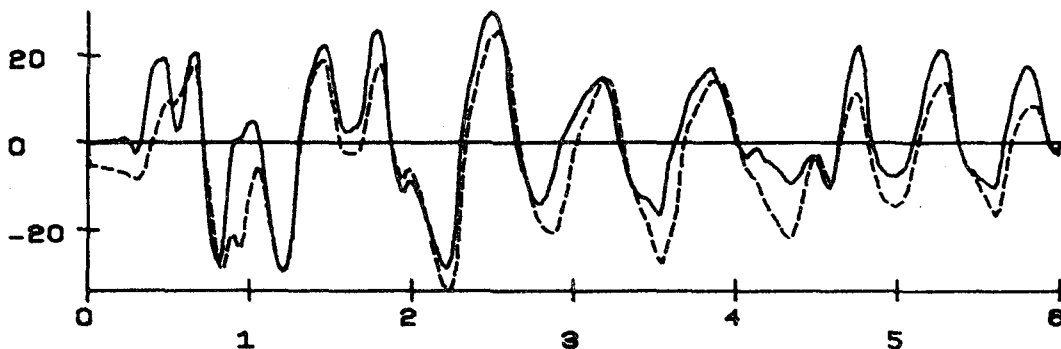


Fig. 7.30 Repeated Earthquakes with 1.2g Maximum Acceleration

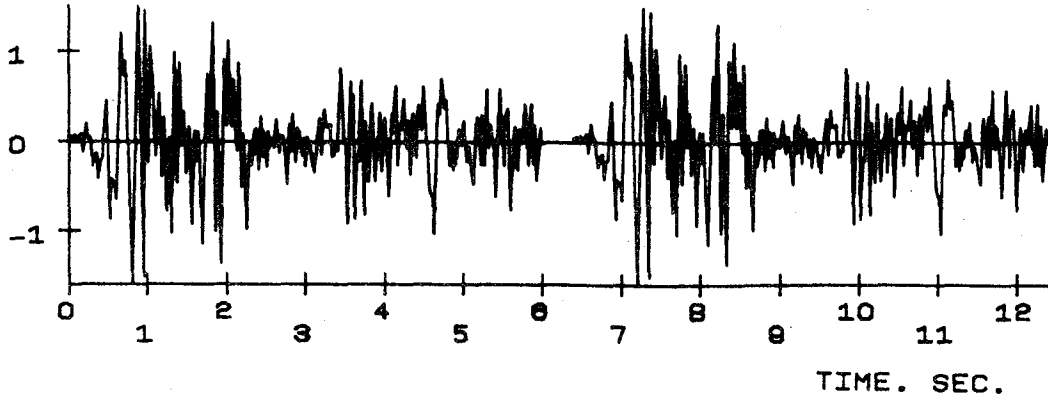
SDOF MODEL MF1

ELCENTRO 1940 NS 1.6G

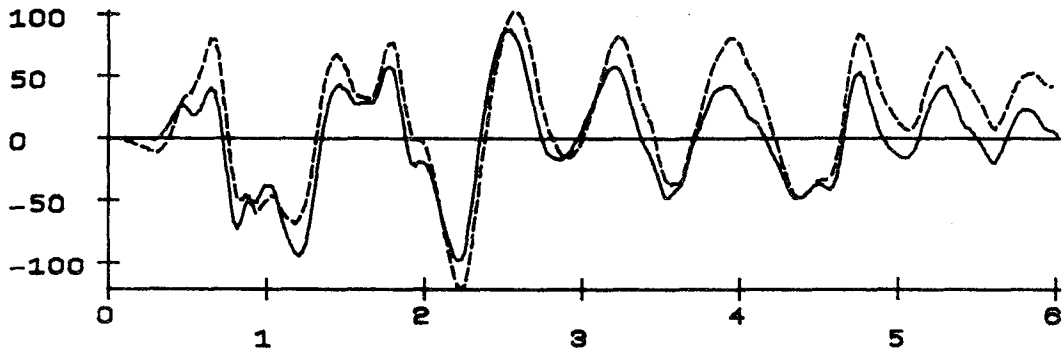
SOLID LINE , MOTION 1

BASE ACCELERATION (G)

BROKEN LINE , MOTION 2



DISPLACEMENT (MM)



BASE OVERTURNING MOMENT (KN-M)

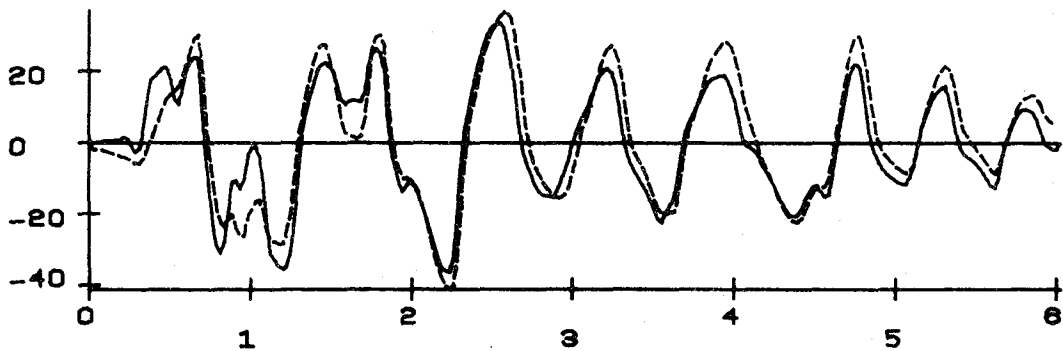


Fig. 7.31 Repeated Earthquakes with 1.6g Maximum Acceleration

APPENDIX A
HYSTERESIS MODELS

A.1 General

The rules of the following models apply to both positive and negative ranges of forces. If the current force is negative, it has to be compared with corresponding forces at break-points in negative region. In this case, the absolute value of the current force is compared with the absolute value of the force at break-point. For example, in Section 1.1 of Sina model it is stated:

1.1 Loading:

$$F(P) \leq F(C) \dots$$

In negative range this rule should be read as:

1.1 Loading:

$$|F(P)| \leq |F(C')| \dots$$

A.2 Definitions

Loading: Increasing the force in one direction

Unloading: Decreasing the force in one direction

Load Reversal: Changing the force and its sign at the same step

A.3 Sina Model

There are 9 rules in Sina hysteresis system as follows (Fig. A.1)

Rule 1: Elastic stage

1.1 Loading:

$$F(P) \leq F(C) \quad K = \text{stiffness} = \text{slope of OC}; \\ \text{go to rule 1}$$

$$F(P) > F(C) \quad K = \text{slope of CY}; \text{ go to rule 2}$$

Rule 2: Current point on CY

2.1 Loading:

$F(P) \leq F(Y)$ $K = \text{slope of CY}; \text{ go to rule 2}$

$F(P) > F(Y)$ $K = \text{slope of YU}; \text{ go to rule 3}$

2.2 Unloading:

$K = \text{slope of PC}'; \text{ go to rule 5}$

Rule 3: Current point on YU

3.1 Loading:

$K = \text{slope of YU}; \text{ go to rule 3}$

3.2 Unloading:

$S_1 = \text{slope of CY} * \left(\frac{D(Y)}{D_{\max}}\right)^{0.5}$

$K = S_1$

where D_{\max} = maximum deformation
attained in loading
direction

Rule 4: Current point on unloading branch from YU

4.1 Loading:

$F(P) \leq F(U_m)$ $K = S_1; \text{ go to rule 4}$

$F(P) > F(U_m)$ $K = \text{slope of YU}; \text{ go to rule 3}$

4.2 Unloading:

$K = S_1; \text{ go to rule 4}$

4.3 Load reversal:

1. If not yielded previously $K = \text{slope of } X_0Y';$
go to rule 07

2. If formerly yielded $K = \text{smaller of the slope}$
of X_0B' and $X_2U_m';$
go to rule 6

Rule 5: Current point on R_0C' (R_0 = Unloading point from CY)

5.1 Loading:

$F(P) \leq F(R_0)$ $K = \text{slope of } R_0C'$; go to rule 5

$F(P) > F(R_0)$ $K = \text{slope of CY}$; go to rule 2

5.2 Unloading:

$K = \text{slope of } R_0C'$; go to rule 5

5.3 Load reversal:

the same as 4.3

Rule 6: Current point on branch reaching crack-closing point

6.1 Loading:

$F(P) \leq F(B)$ $K = \text{slope of } X_1B$; go to rule 6

$F(P) > F(B)$ $K = \text{slope of } BU_m$; go to rule 7

6.2 Unloading: (name the unloading point R_3)

$K = S_1$; go to rule 9

Rule 7: Current point on branch pointing towards U_m

If the section has not yielded previously, U_m is assumed to be at Y.

7.1 Loading:

$F(P) \leq F(U_m)$ $K = \text{slope of } X_1U_m$ (or BU_m); go to rule 7

$F(P) > F(U_m)$ $K = \text{slope of } YU$; go to rule 3

7.2 Unloading:

$K = S_1$; go to rule 8

Rule 8: Current point on unloading from branch of rule 7

8.1 Loading:

$F(P) \leq F(U'_m)$ $K = S_1$; go to rule 8

$F(P) > F(U'_m)$ $K = \text{slope of } X_0Y$ (or BU'_m); go to rule 7

8.2 Unloading:

$K = S_1$; go to rule 8

8.3 Load reversal:

the same as 4.3.2

Rule 9: Current point on unloading branch X_1B

9.1 Loading:

$F(P) \leq F(R_3)$ $K = S_1$; go to rule 9

$F(P) > F(R_3)$ $K = \text{slope of } X_1B$; go to rule 6

9.2 Unloading:

$K = S_1$; go to rule 9

9.3 Load reversal:

the same as 4.3.2

A.4 Q-Hyst Model

There are four rules in Q-Hyst model as follows (Fig. A.2):

Rule 1:

1.1 Loading: if $F(P) \leq F(Y)$ $K = \text{slope of } OY$; go to rule 1

if $F(P) > F(Y)$ $K = \text{slope of } YU$; go to rule 2

1.2 Unloading: $K = \text{slope of } OU$; go to rule 1

1.3 Load reversal: $K = \text{slope of } OY$; go to rule 1

Rule 2:

2.1 Loading: $K = \text{slope of } YU$; go to rule 2

2.2 Unloading: $K = S_1 = (\text{slope of } OY) \times \left(\frac{D(Y)}{D_{\max}}\right)^\alpha$;
go to rule 3

$\alpha = 0.5$ in MDOF model
 0.4 in SDOF model

Rule 3:

- 3.1 Loading: 1. If last unloading point on YU, go to 3.1.2
 if $F(P) \leq F(R)$ $K = S_1$; go to rule 3
 if $F(P) > F(R)$ $K = (\text{Slope of } X_0U'_m)$;
 go to rule 4
2. If $F(P) \leq F(U_m)$ $K = S_1$; go to rule 3
 if $F(P) > F(U_m)$ $K = \text{slope of } YU$;
 go to rule 2
- 3.2 Unloading: $K = S_1$; go to rule 3
- 3.3 Load reversal: $K = \text{slope of } X_0U'_m$;
 go to rule 4

Rule 4:

- 4.1 Loading: If $F(P) \leq F(U'_m)$ $K = \text{slope of } X_0U'_m$; go to rule 4
 if $F(P) > F(U'_m)$ $K = \text{slope of } Y'U'$; go to rule 2
- 4.2 Unloading: $K = S_1$; go to rule 3
 (name the unloading point R)

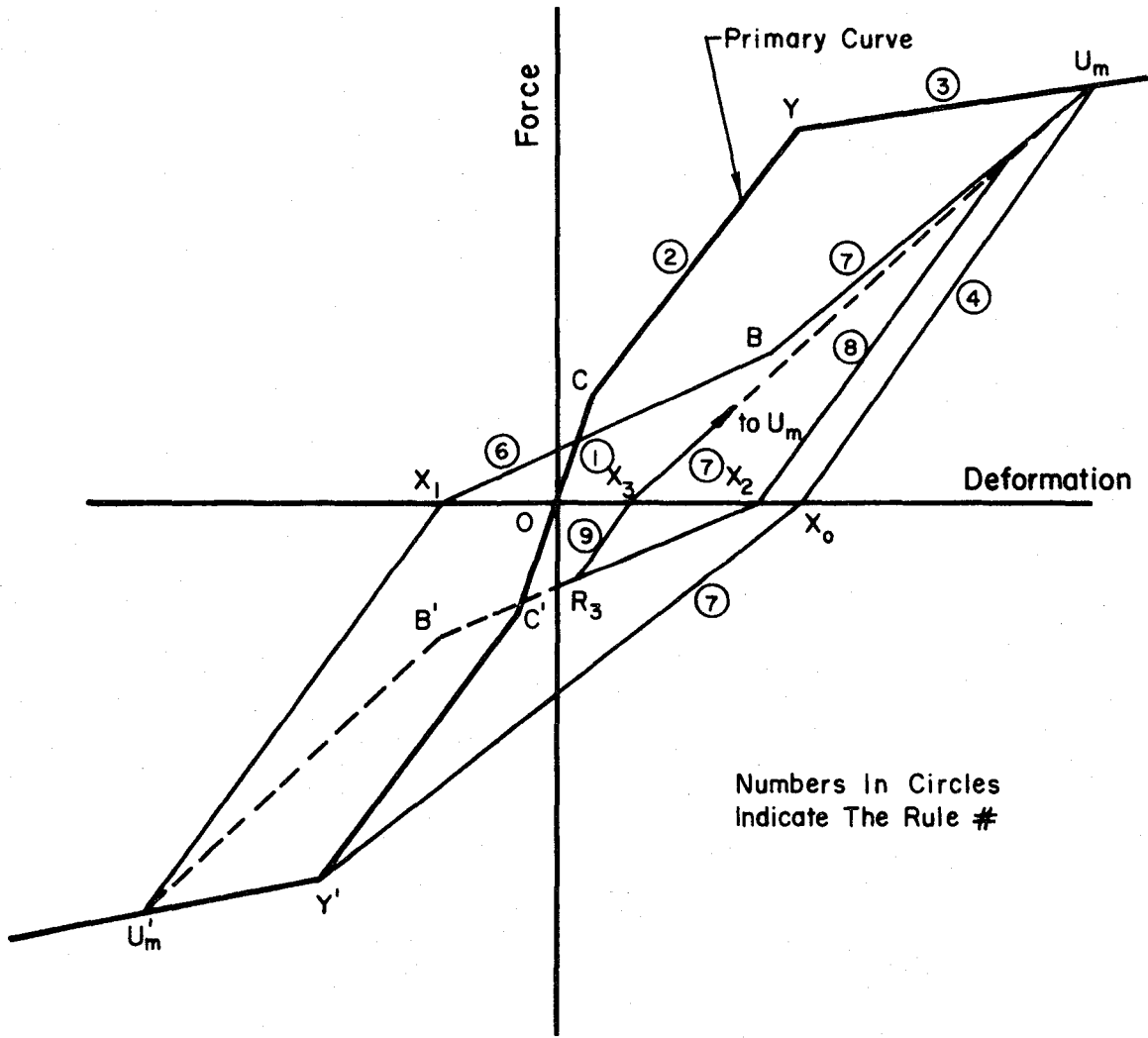
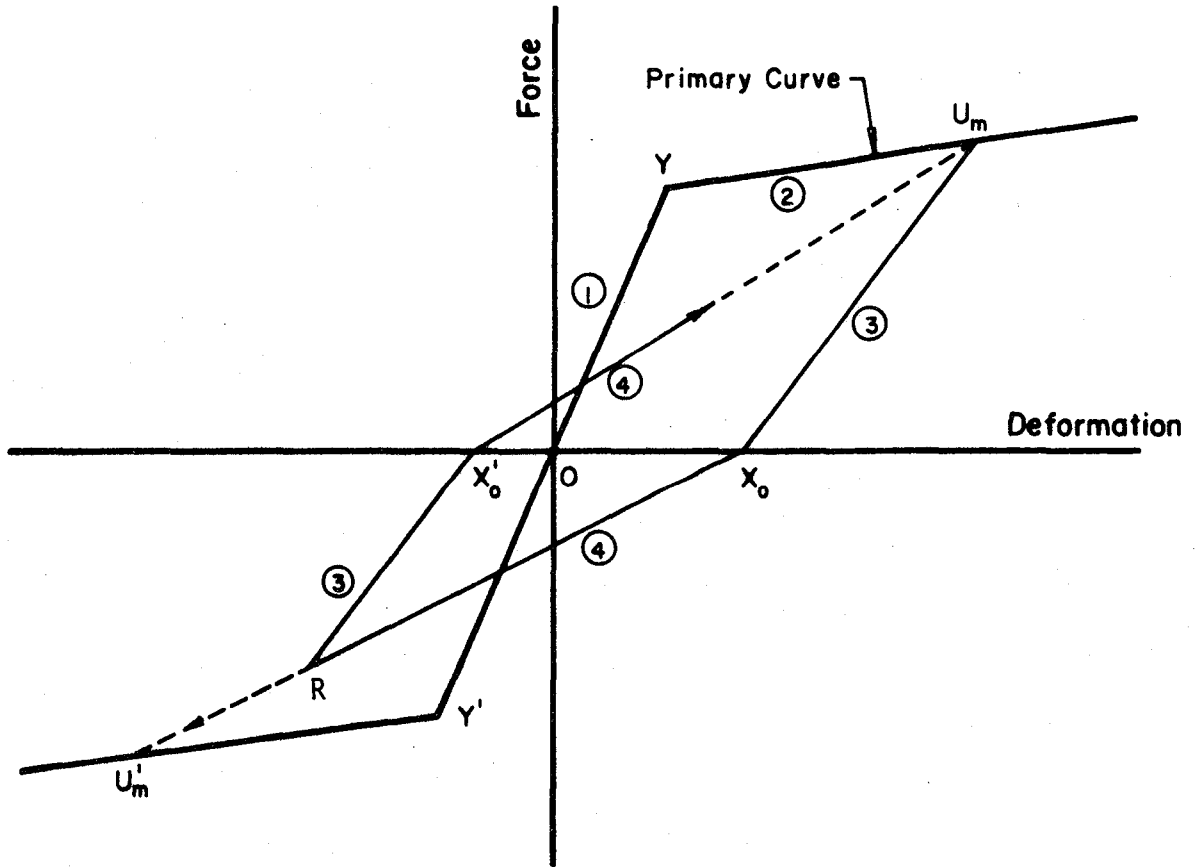


Fig. A.1 Sina Hysteresis Rules



- ① Rule 1
- ② Rule 2
- ③ Rule 3
- ④ Rule 4

Fig. A.2 Q-Hyst Model

APPENDIX B

COMPUTER PROGRAMS LARZ AND PLARZ

A special purpose computer program was developed to study the seismic response of reinforced concrete rectangular frames subjected to earthquake motions (LARZ). To plot response histories, a small program (PLARZ) was written to be used in conjunction with LARZ. The computer language of the programs is FORTRAN IV. The Cyber 175 computer system at Digital Computer Laboratory of the University of Illinois was used to develop the programs.

In LARZ, two subroutines from IMSL computer library for matrix inversion (LINIPB) and for solution of simultaneous equations of equilibrium (LEQIS) have been used. For plotting purposes, the graphic routines from GCS library have been applied.

Irregular frames similar to the one shown in Fig. B.1 can be analyzed by program LARZ. There can be more than one horizontal degree of freedom at the same level. A special feature of the program is that it can accept different hysteresis systems (models presently implemented are those described in Chapter Three). In fact, LARZ can be used to study steel frames using the bilinear hysteresis system if this system is considered appropriate.

A block diagram of the program LARZ is presented in Fig. B.2.

a. Storage of Stiffness Matrix

The structural stiffness matrix is divided into three sub-matrices as shown in Fig. B.3. All matrix operations are performed in main core.

Because $[K_{11}]$ is a symmetric matrix, only its lower half is stored. No particular disadvantage is realized in storing the matrix row-wise, so it is stored as a row-wise array. $[K_{12}]$ is stored completely. However, the location of non-zero elements are stored using pointer arrays {ITK} and {JTK} as shown in Fig. B.3. Only non-zero elements of $[K_{12}]$ enter in matrix operations.

$[K_{22}]$ is a symmetric banded matrix, hence, only half of the banded portion needs to be stored. By the requirement of subroutine LINIPB, the lower half of this matrix is stored in a two-dimensional array as shown in Fig. B.3.

b. Response-History Data

Secondary memory is used to store calculated response history. Upon the execution of LARZ, if response plots are desired, the generated data are written on three sequential files. At later stage, these data are read by the program PLARZ, and plotted according to the scale specified by the user. The response plots can be obtained in different scales without a need to re-execute LARZ.

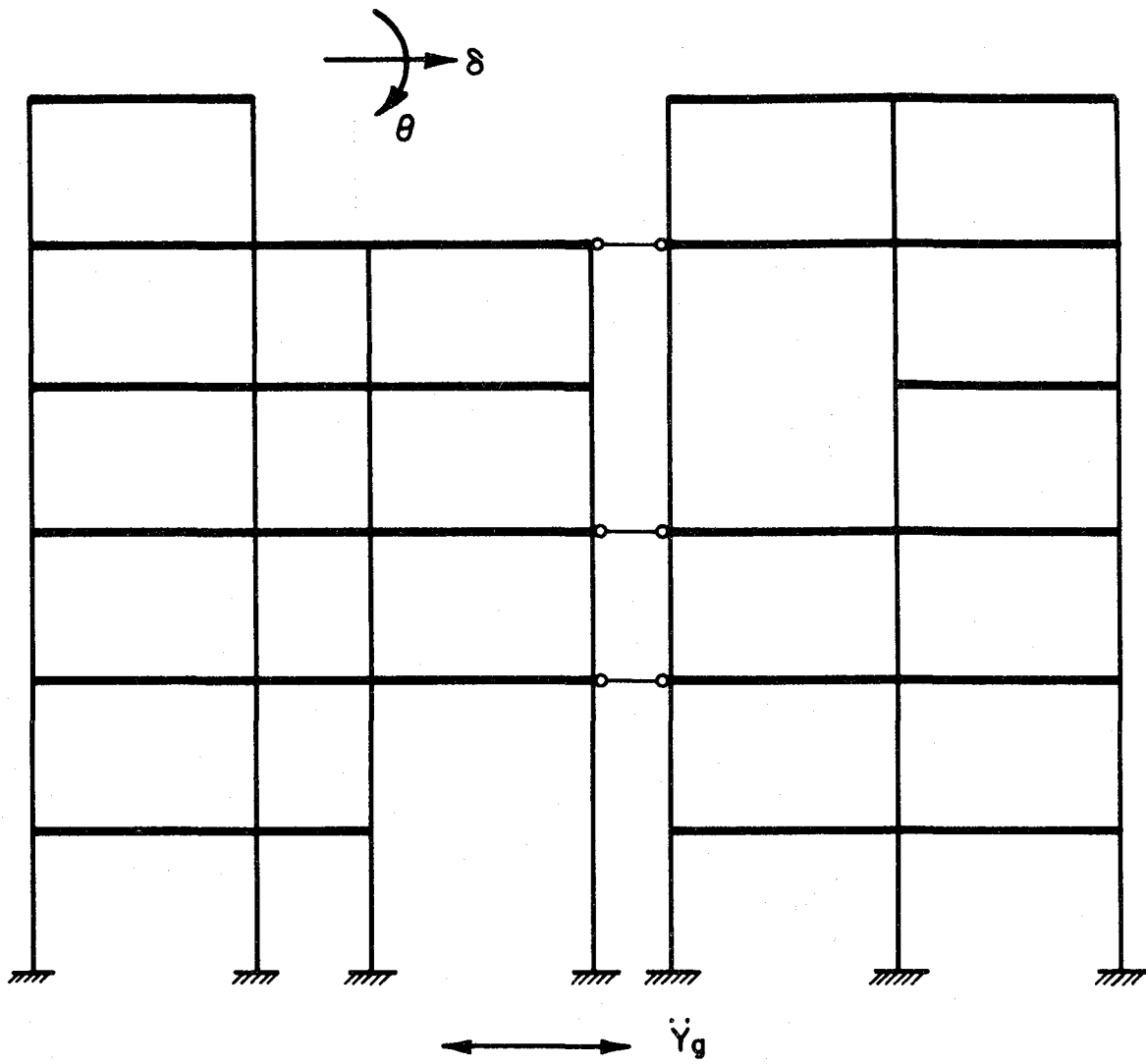


Fig. B.1 Structure with Missing Elements

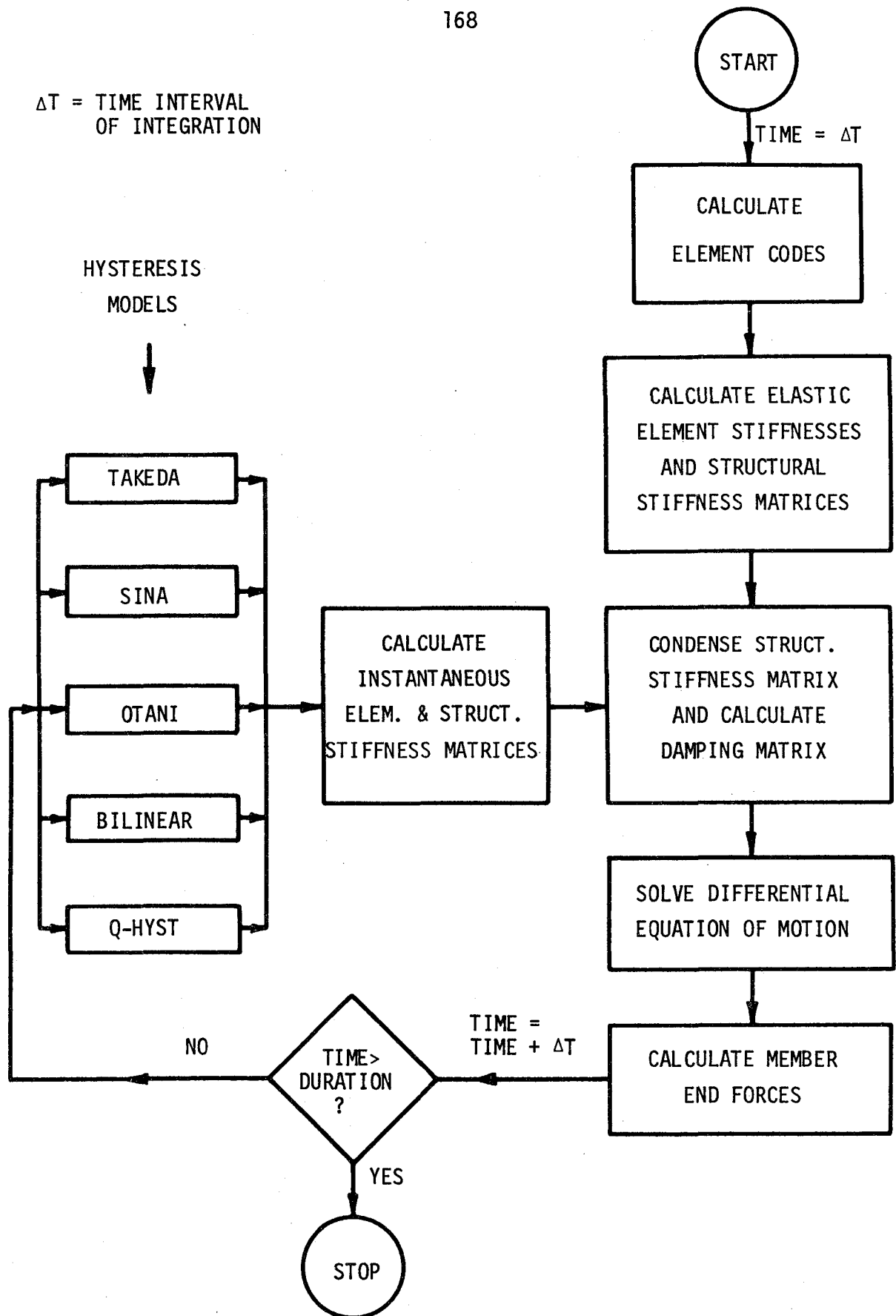


Fig. B.2 Block Diagram of Program LARZ

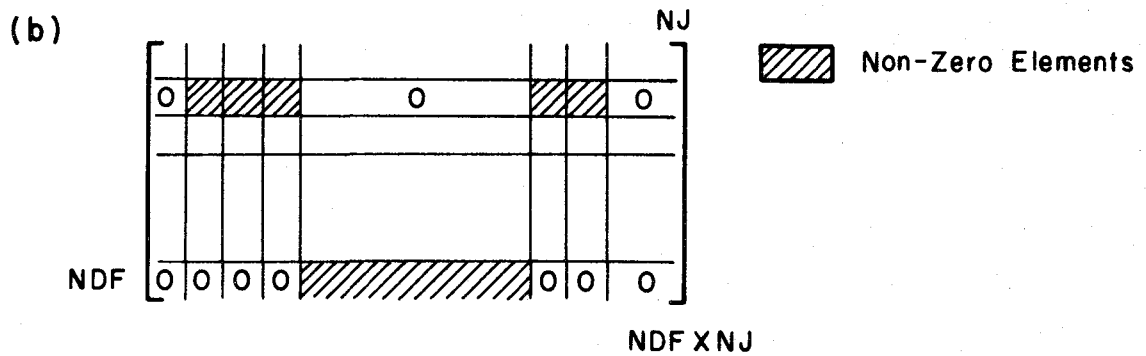
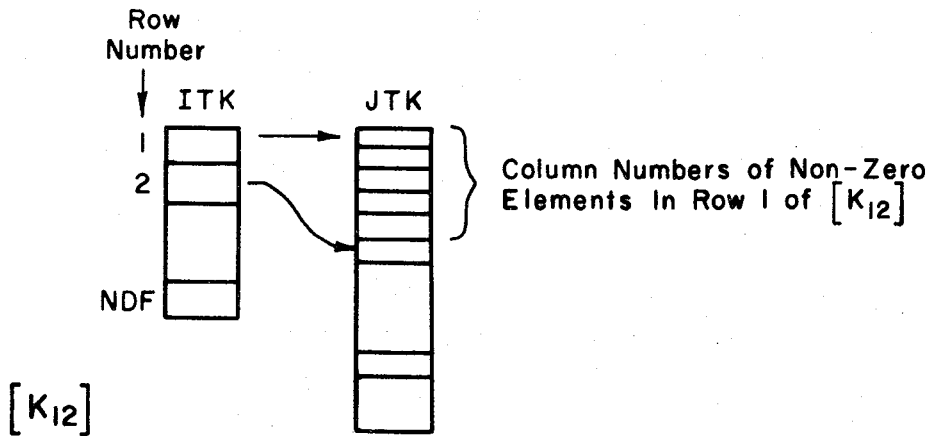
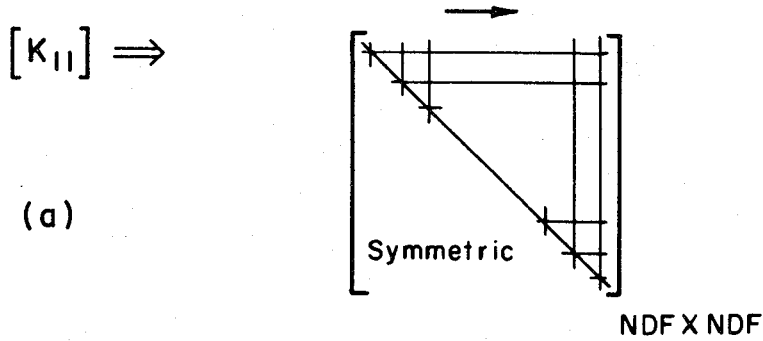
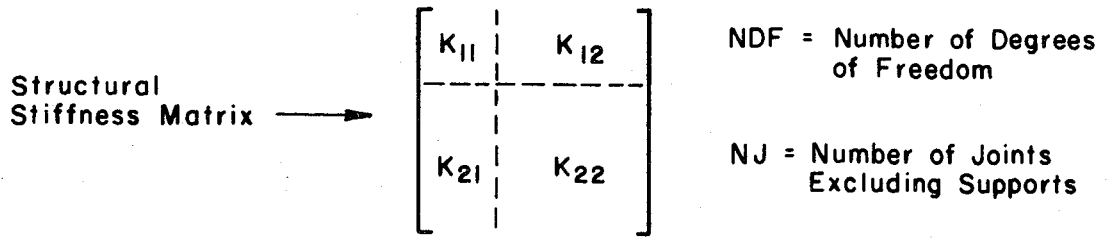
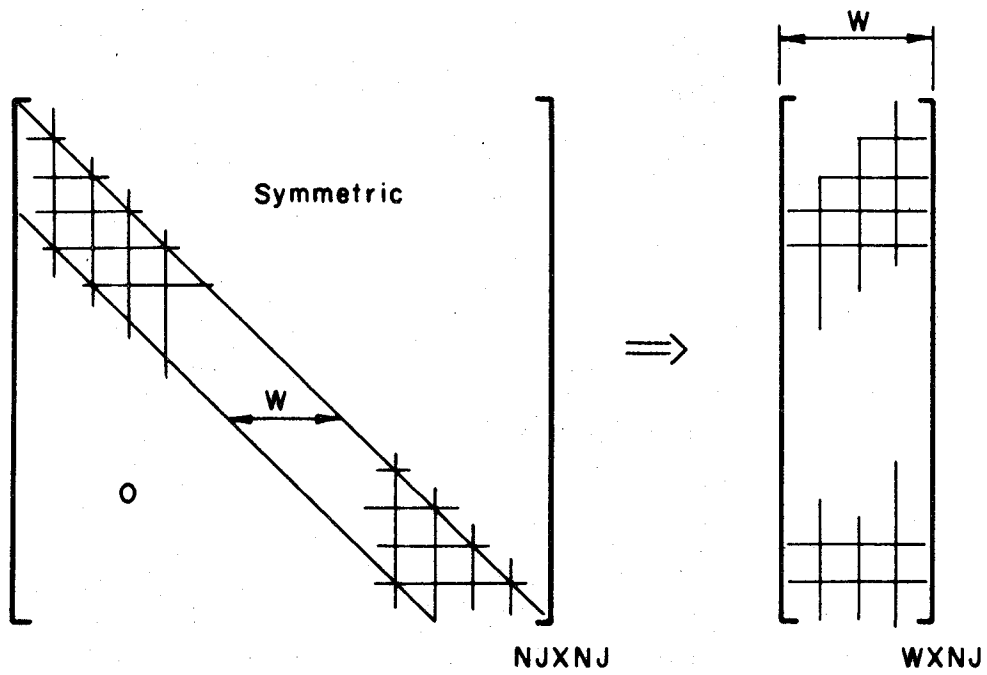


Fig. B.3a & b Storage of Structural Stiffness Matrix

$[K_{22}]$ Fig. B.3c Storage of Submatrix K_{22}

APPENDIX C

MAXIMUM ELEMENT RESPONSE BASED ON DIFFERENT
HYSTERESIS MODELS

The maximum moments and ductilities at the ends of flexible portions of members, calculated based on different hysteresis models, are presented in Tables C.1 through C.5. Element numbering is shown in Fig. C.1. The rotations are for unit length of each member. Ductility at a member end is defined as the ratio of maximum rotation to the yield rotation.

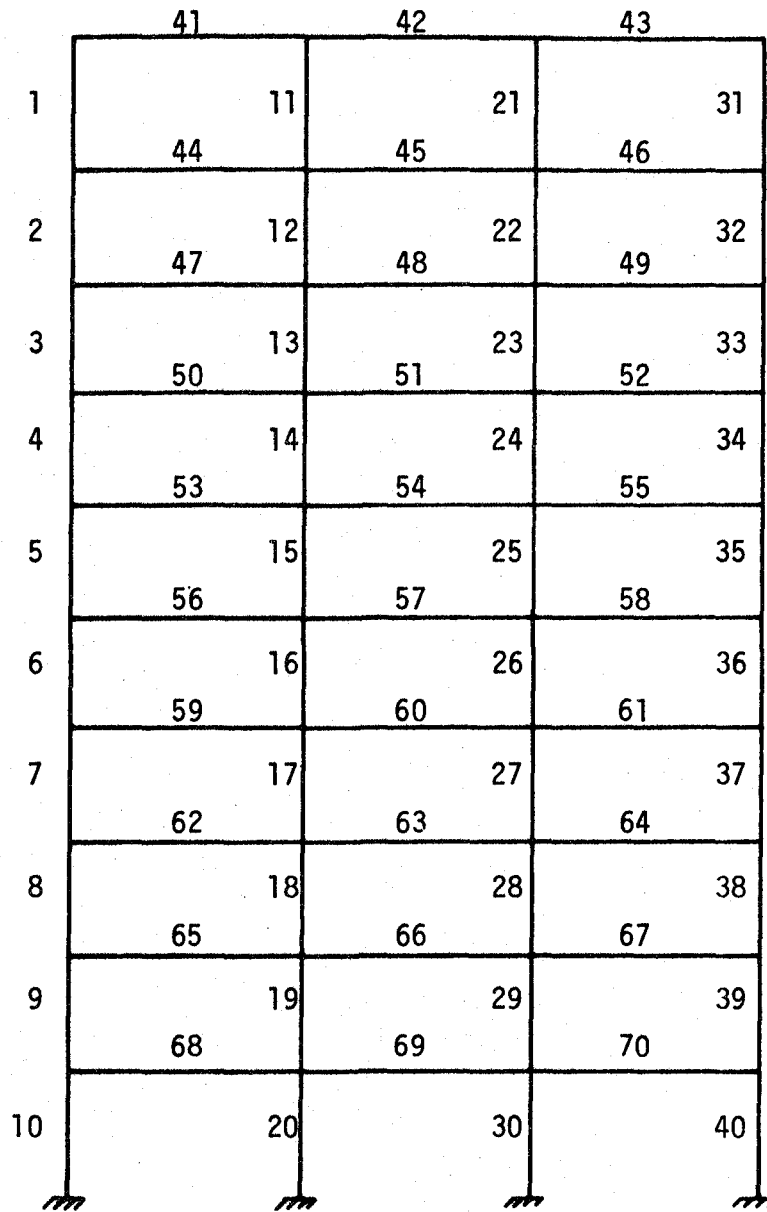


Fig. C.1 Element Numbering for Structure MF1

Pages 173-177 have been removed.

Due to legibility problems, the following computer printouts have been omitted: "Table C.1 Maximum Response of Structure MF1 Based on Takeda Model;" "Table C.2 Maximum Response of Structure MF1 Based on Sina Model;" "Table C.3 Maximum Response of Structure MF1 Based on Otani Model;" "Table C.4 Maximum Response of Structure MF1 Based on Bilinear Model;" and "Table C.5 Maximum Response of Structure MF1 Based on Q-Hyst Model."*

*For information concerning these pages contact Mete A. Sozen, University of Illinois at Urbana-Champaign, Department of Civil Engineering, Urbana, IL 61801.



APPENDIX D

COMPUTER PROGRAMS LARZAK AND PLARZK

A special purpose computer program was developed to calculate the seismic response of a single-degree system consisting of a mass mounted on a massless rigid bar connected to the ground by a hinge support and a nonlinear rotational spring. The input base acceleration and the response histories of displacement of the mass and the base moment are stored on temporary tapes. A plotting program (PLARZK) was developed to read the data and plot the response histories. The programs were written in Fortran IV, using Cyber 175 computer at the University of Illinois. Plotting routines from GCS library were used to plot the response histories. To obtain hard copies of the plots, the Calcomp plotter at Digital Computer Laboratories of the University of Illinois was used.

A block diagram of program LARZAK is presented in Fig. D.1.

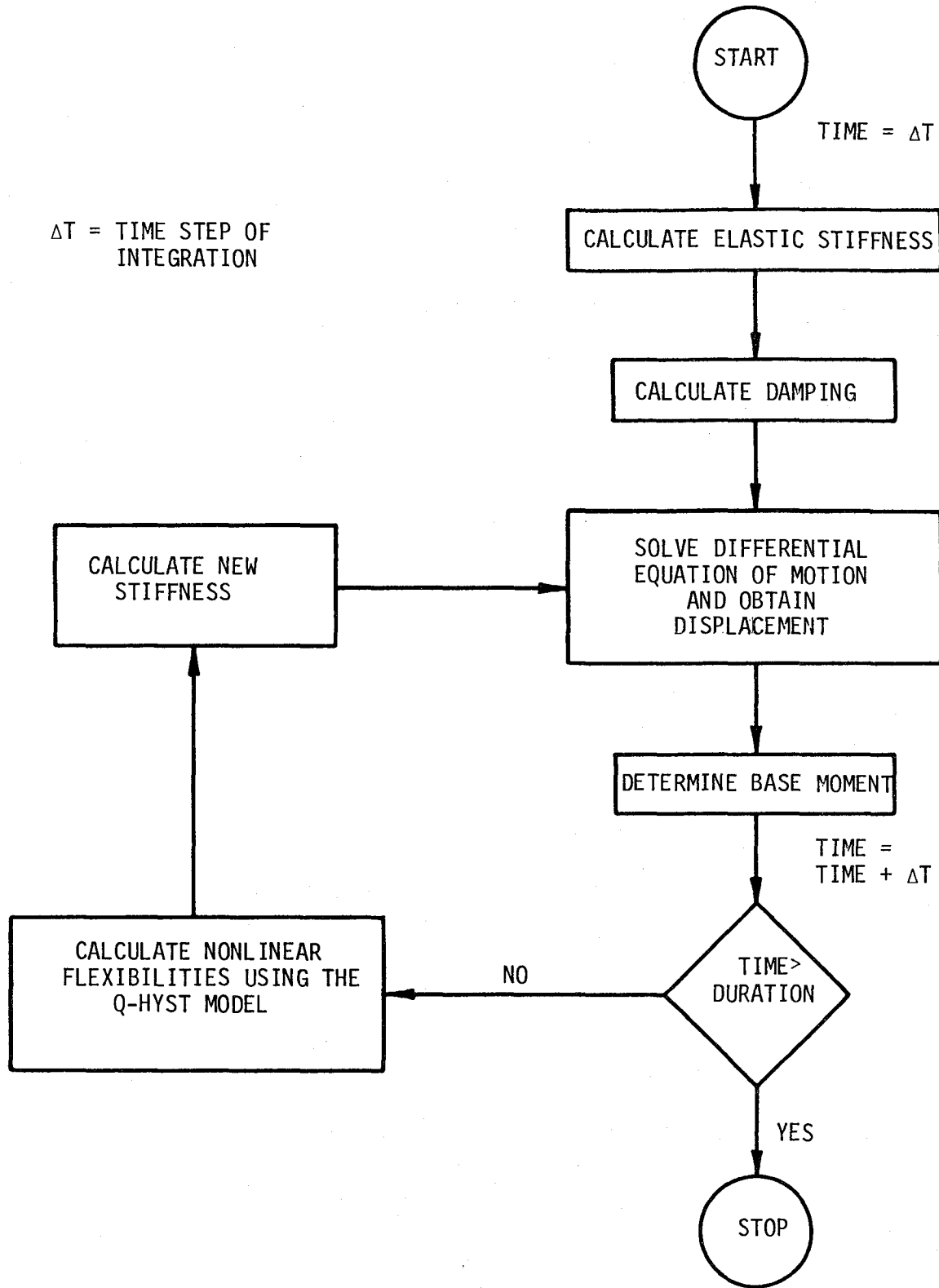


Fig. D.1 Block Diagram of Program LARZAK

APPENDIX E

MOMENTS AND DUCTILITIES FOR STRUCTURE MF1 SUBJECTED
TO DIFFERENT EARTHQUAKES

Tables E.1 through E.3 present the maximum moments and ductilities at the ends of flexible portions of the elements of structure MF1 subjected to Orion, Castaic, and Bucarest earthquakes. The results were obtained using the program LARZ, which treated the structure as multi-degree model. Element numbering is shown in Fig. C.1. In the tables, the rotations are for the unit length of each member. Ductility is defined as the ratio of rotation to the yield rotation.

Pages 181-183 have been removed.

Due to legibility problems, the following computer printouts have been removed: "Table E.1 Maximum Response of Structure MF1 Subjected to Orion;" "Table E.2 Maximum Response of Structure MF1 Subjected to Castaic;" and "Table E.3 Maximum Response of Structure MF1 Subjected to Bucarest".*

*For information concerning these pages contact Mete A. Sozen, University of Illinois at Urbana-Champaign, Department of Civil Engineering, Urbana, IL 61801.



APPENDIX F
RESPONSE TO TAFT AND EL CENTRO RECORDS

Structure MF1 was analyzed for the measured records of El Centro NS, El Centro EW, Taft N21E, and Taft S69W, using the Q-Model. In each case, the structure was subjected to 15 seconds of the original record. The time axes of the records were compressed by a factor of 2.5. The maximum acceleration for each earthquake was normalized to 0.4g which was the design intensity for structure MF1. The base acceleration, top-level displacement and base moment responses are presented in Fig. F.1 through F.4.

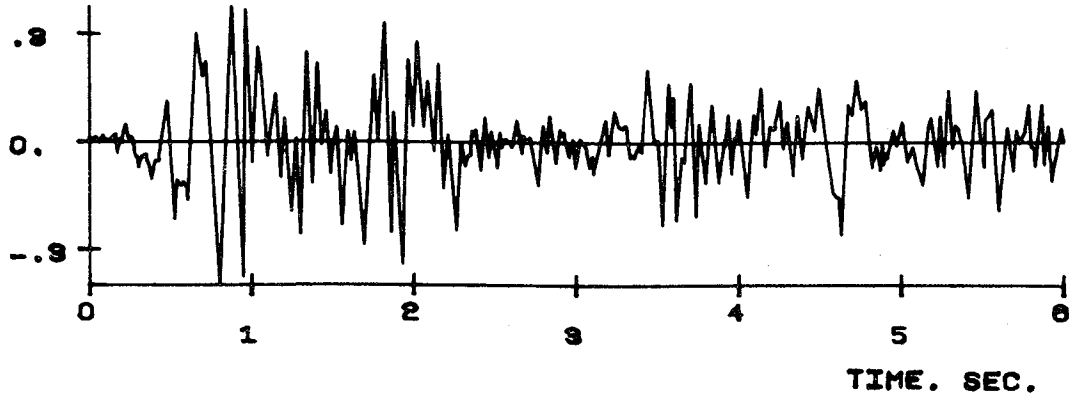
Except for the north-south component of El Centro, which was simulated in the laboratory, no test results were available for structure MF1 subjected to the above records. Considering the fact that the Q-Model was successful in simulating the measured response for structure MF1 subjected to a simulated north-south component of El Centro (Sec. 7.4), and noting that the other three motions were similar to El Centro NS, the calculated responses were judged based on their overall appearance in relation to the measured response for the simulated El Centro, NS.

The waveform in all cases (Fig. F.1 and F.4) seemed reasonable; i.e., no unusual response was seen. The maximum absolute value of the single-amplitude top-level displacement varied from 16.7mm (for Taft N21E) to 33 mm (for El Centro EW). These values were in the same order of magnitude of that from the experimental results (23.6mm). It is therefore possible to conclude that the Q-Model yielded reasonable overall responses for the earthquake records considered.

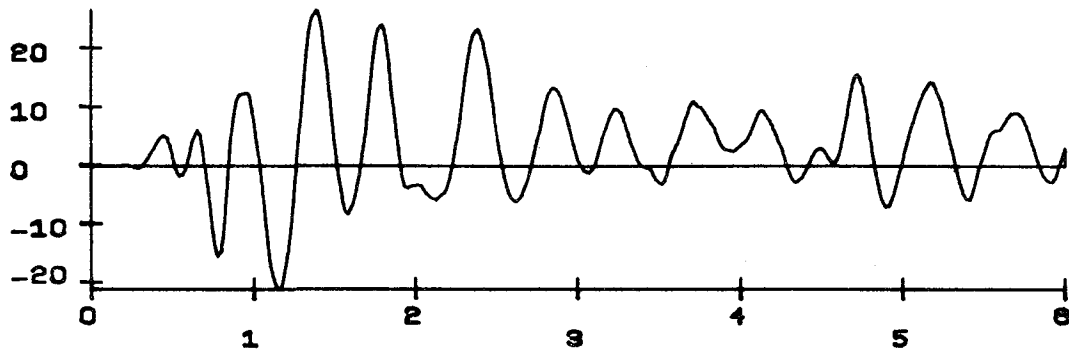
SDOF MODEL MF1

ELCENTRO 1940 NS .4G

BASE ACCELERATION (G)



DISPLACEMENT (MM)



BASE OVERTURNING MOMENT (KN-M)

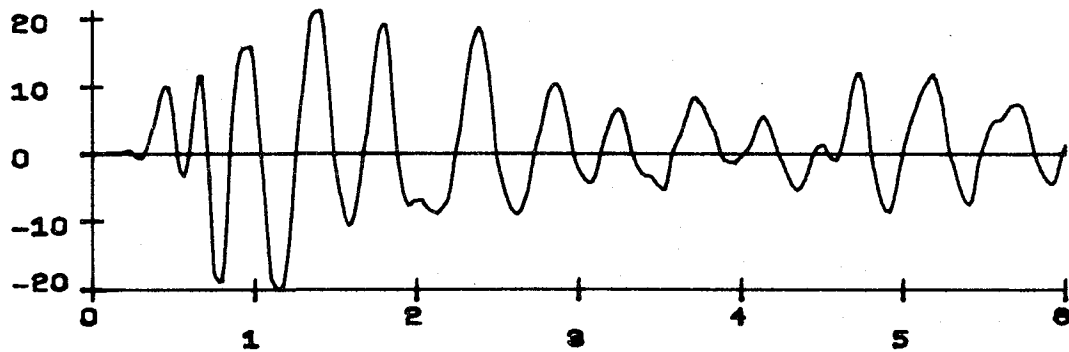
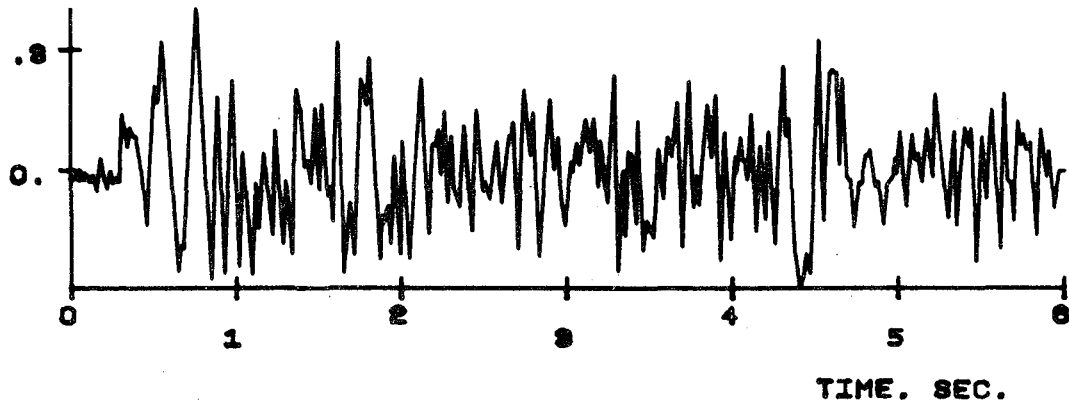


Fig. F.1 Response for Structure MF1 Subjected to El Centro NS

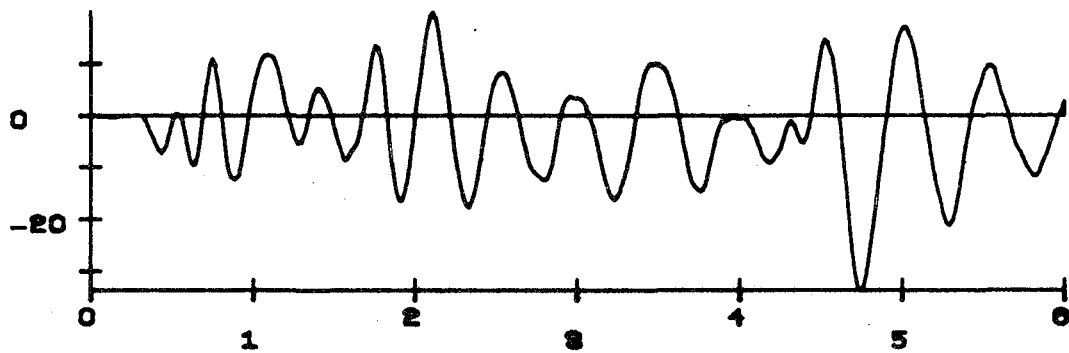
SDOF MODEL MF1

EL CENTRO 1940 EW

BASE ACCELERATION (G)



DISPLACEMENT (MM)



BASE OVERTURNING MOMENT (KN-M)

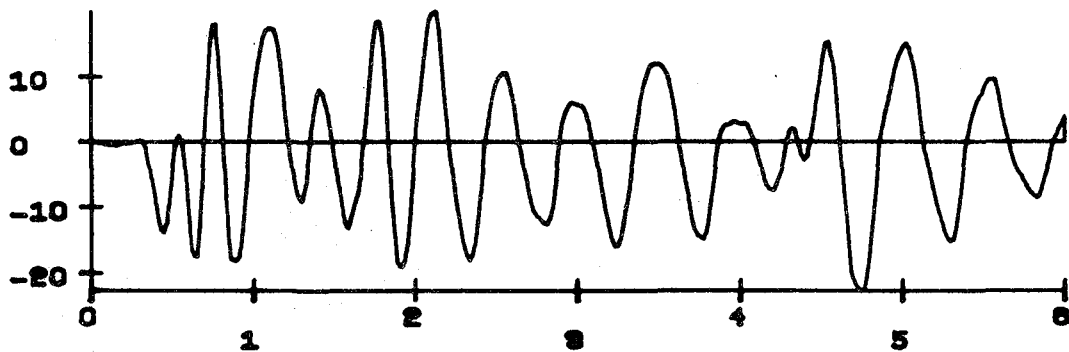
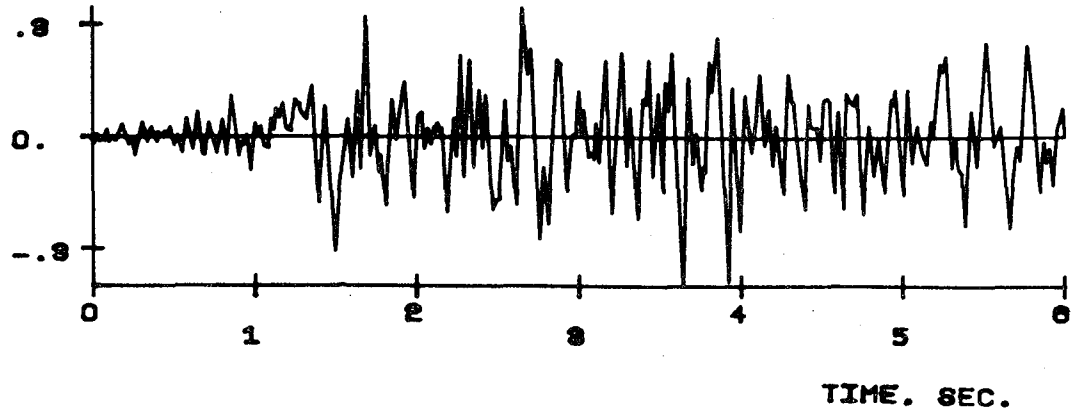


Fig. F.2 Response for Structure MF1 Subjected to El Centro EW

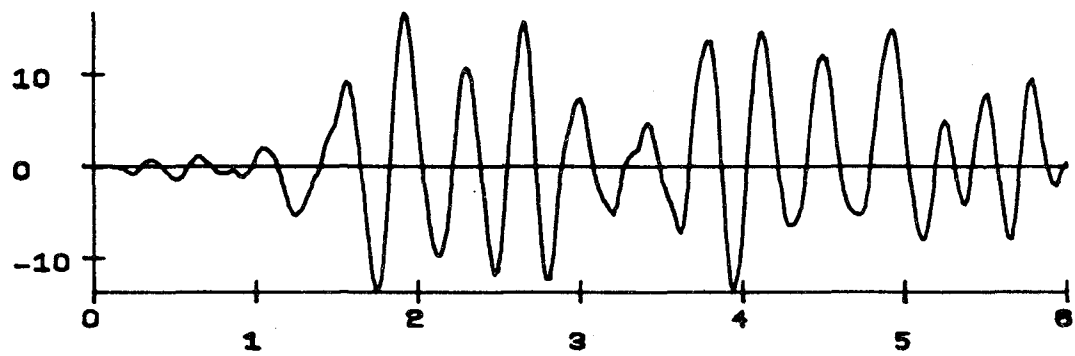
SDOF MODEL MF1

TAFT 1952 (N21E)

BASE ACCELERATION (G)



DISPLACEMENT (MM)



BASE OVERTURNING MOMENT (KN-M)

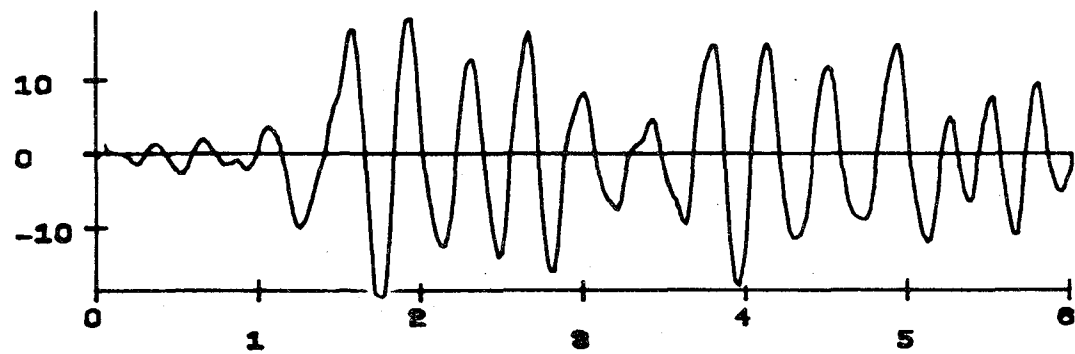
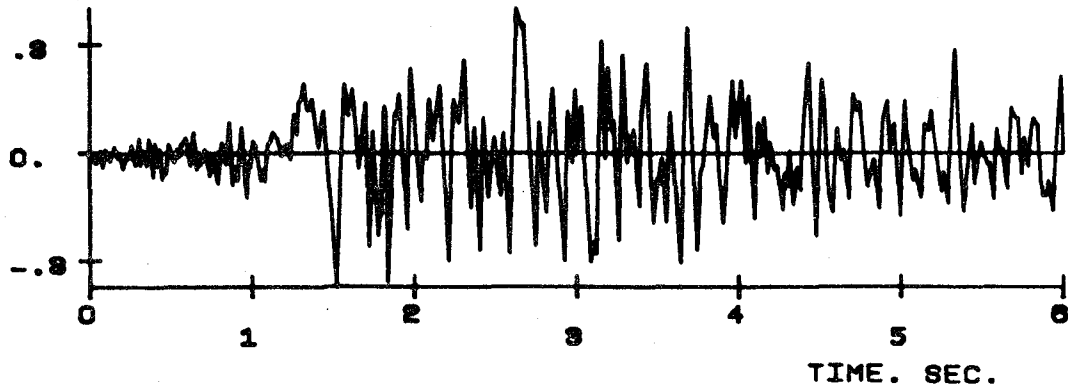


Fig. F.3 Response for Structure MF1 Subjected to Taft N21E

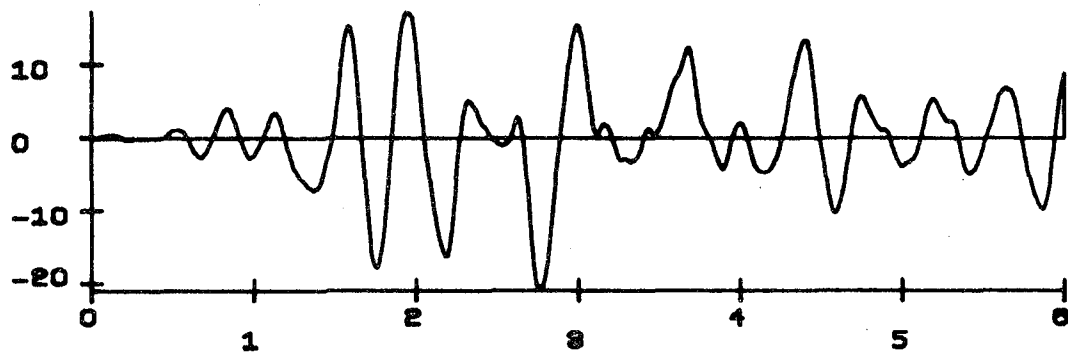
SDOF MODEL MF1

TAFT S69E .4G

BASE ACCELERATION (G)



DISPLACEMENT (MM)



BASE OVERTURNING MOMENT (KN-M)

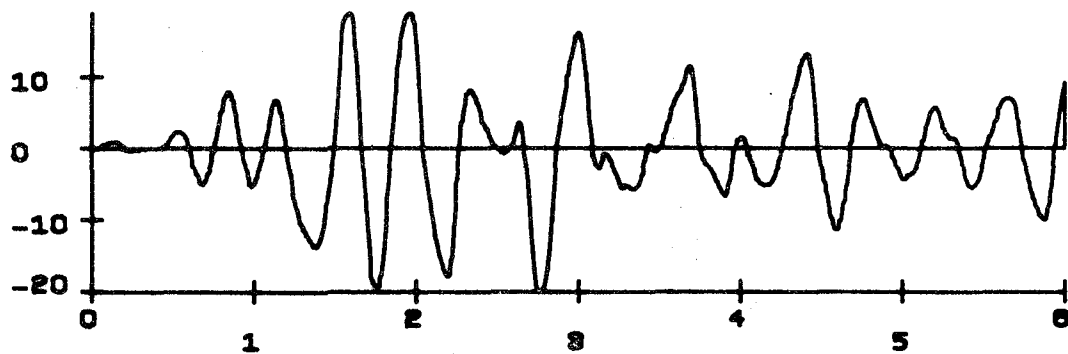


Fig. F.4 Response for Structure MF1 Subjected to Taft S69E

